WADC TECHNICAL REPORT 54-313

A DESIGN MANUAL FOR THERMAL ANTI-ICING SYSTEMS

HAROLD H. SOGIN

ILLINOIS INSTITUTE OF TECHNOLOGY

DECEMBER 1954

WRIGHT AIR DEVELOPMENT CENTER

NOTICES

When Government drawings, specifications, or other data are used for any purpose other than in connection with a definitely related Government procurement operation, the United States Government thereby incurs no responsibility nor any obligation whatsoever; and the fact that the Government may have formulated, furnished, or in any way supplied the said drawings, specifications, or other data, is not to be regarded by implication or otherwise as in any manner licensing the holder or any other person or corporation, or conveying any rights or permission to manufacture, use, or sell any patented invention that may in any way be related thereto.

- - - - -

Copies of WADC Technical Reports and Technical Notes should not be returned to the Wright Air Development Center unless return is required by security considerations, contractual obligations, or notice on a specific document.

WADC TECHNICAL REPORT 54-313

A DESIGN MANUAL FOR THERMAL ANTI-ICING SYSTEMS

HAROLD H. SOGIN

ILLINOIS INSTITUTE OF TECHNOLOGY

DECEMBER 1954

IIT PROJECT No. 6066
CONTRACT No. AF 33(616)-444

WRIGHT AIR DEVELOPMENT CENTER
AIR RESEARCH AND DEVELOPMENT COMMAND
UNITED STATES AIR FORCE
WRIGHT-PATTERSON AIR FORCE BASE, OHIO

Carpenter Litho & Prtg. Co., Springfield,O.
500 - April 1956

FOREWORD

This report was prepared by Dr. Harold H. Sogin on Air Force Contract AF 33(616)-444. The work was performed with the assistance of Mr. Frederick Salzberg and Dr. Shi-ming Yang and was directed by Dr. Max Jakob, Director, Heat Transfer Laboratory, all of the Department of Mechanical Engineering of Illinois Institute of Technology, Chicago, Illinois. The contract was administered by the Equipment Laboratory, Wright Air Development Center, Mr. L. V. Larson acting as project engineer.

The cooperation and information obtained from several individuals and airframe manufacturers are gratefully acknowledged. These are Dr. M. Tribus; Mr. D. M. Patterson of Aeronautical Icing Research Laboratories; Messrs. F. L. Boeke, R. A. Paselk, F. Weiner, and G. Feuerman of NORTH AMERICAN; Messrs. N. A. Baird and W. W. Reaser of DOUGLAS, Santa Monica; Mr. F. E. Lenherr of NORTHROP; Mr. V. Hudson of CONVAIR; and Mr. T. H. Grieger of MARTIN. Also, thanks are due to BOEING and GRUMMAN for their kind responses.

We are particularly grateful to Mr. Larson, who read various drafts and the final manuscript, and provided many valuable suggestions.

ABSTRACT

This manual deals with the thermal anti-icing of aircraft wing and tail surfaces which are protected by double-skin heaters. After a brief introduction, reference material is presented for pressure drop of duct components, water impingement on airfoils, and coefficients of heat and mass transfer by convection. The last parts of the manual are devoted to mass and heat balances on airfoils and to a design procedure presented from the viewpoint of performance analysis.

PUBLICATION REVIEW

This report has been reviewed and is approved.

FOR THE COMMANDER:

W T Hamilton for

S.T. SMITH
Colonel, USAF
Chief, Equipment Laboratory

TABLE OF CONTENTS

LIST OF TABLES

LIST OF ILLUSTRATIONS

NOMENCLATURE

Note 1: The symbol lb is used for pound force and lb_m for pound mass. However, in many places the subscript m has been deleted where the unit is clear.

Note 2: The symbol F is used for the unit, Fahrenheit degree (temperature difference). One Rankine degree is equal to one Fahrenheit degree; hence, the symbol F is also used for a degree on the absolute temperature scale. The symbol °F is used for the temperature, that is, the place on the Fahrenheit temperature scale.

Note 3: The prime (′) and double prime (″) are used with such symbols as m, q, W, and w to denote that the quantity refers to a unit of length or a unit of area, respectively.

Note 4: The bar (–) over a symbol denotes a mean value of the quantity. The arrow (→) denotes a vector quantity.

Note 5: The superscript + indicates a dimensionless quantity.

Symbol	Quantity	Unit
A	area	ft^2
a	droplet radius; width of passage	ft
b	coefficient of mass transfer	ft/hr
b	height of passage	ft
C	constant	
C	total-pressure-loss-coefficient factor for diffusers	
c	pitch of currugation	ft
C_D	drag coefficient	
C_L	lift coefficient	
C_M	defined by Eq. 2-21	
C_p	pressure coefficient	
c_p	specific heat	B/lb_m F
D	mutual diffusivity of water vapor in air	ft^2/hr

Symbol	Quantity	Unit
D_d	droplet diameter	microns
D_d	duct diameter	ft
E	accumulative collection efficiency	
E_m	total collection efficiency	
F	function; factor	
F_o	compressibility factor	
f	coefficient of friction defined by Eq. 2-3	
G	ratio defined by Eq. 6-22	
G	rate of flow per unit area	$lb/hr\ ft^2$
g	constant of acceleration due to gravity	ft/sec^2
H	ratio defined by Eq. 6-23	
H	total pressure	lb/ft^2
h	coefficient of heat transfer	$B/hr\ ft^2\ F$
h_U	over-all coefficient of heat transfer	$B/hr\ ft^2\ F$
I	$(N_{St})_{mod}/N_{St}$	
i	enthalpy	B/lb
J	defined by Eq. 2-33	
J	mechanical equivalent of heat	ft lb/B
K	coefficient of total-pressure loss	
K	inertia parameter defined by Eq. 3-7	
K_{pt}	pressure-temperature correction factor	
K_S	average inertia parameter defined by Eq. 3-22	
k	thermal conductivity	B/hr ft F
L	length; chord length	ft
M	Mach number	
M	molecular weight	lb/lb-mole

Symbol	Quantity	Unit
m	Euler number	
m	rate of evaporation	lb/hr
N_{Nu}	Nusselt number, hL/k_o	
$N_{Nu,D}$	Nusselt number, hD/k_f	
$N_{Nu,L}$	Nusselt number, hL/k_f	
N_{Pr}	Prandtl number	
N_{Re}	Reynolds number, $U_o L \rho_o / \mu_o$	
$N_{Re,D}$	Reynolds number, $U_o D \rho_f / \mu_f$	
$N_{Re,d}$	Reynolds number, $U_o D_d \rho_o / \mu_o$	
$N_{Re,L}$	Reynolds number, $U_o L \rho_f / \mu_f$	
N_{Sc}	Schmidt number	
N_{St}	Stanton number, $h/(U_o \rho c_p)$	
$(N_{St})_{mod}$	modified Stanton number, b/U_o	
n	exponent; number of vanes	
p	pressure	lb/ft^2; in.-mercury; in.-water
Q	volumetric discharge	ft^3/sec
q	rate of heat transfer	B/hr
R	gas constant	ft lb_f/lb_m F
r	radius	ft
s	profile distance	ft
s_H	heated distance	ft
T	absolute temperature	°R
t	temperature	°F
U	velocity	ft/sec; knots
u	local velocity of air relative to airfoil	ft/sec

Symbol	Quantity	Unit
v	specific volume	ft^3/lb
v	local velocity of droplet relative to airfoil	ft/sec
W	rate of impingement	lb/hr
w	rate of flow	lb/hr
X	width	ft
x	profile abscissa	ft
Y	height; depth	ft
y	profile ordinate	ft
$(\Delta y)_{max}$	airfoil thickness	ft
z	defined by Eq. 6-13 and -14	
α, β	angles	degrees
α, β	fractions	
β	local collection efficiency defined by Eq. 3-28	
β	defined by Eq. 4-3	
γ	specific weight	lb/ft^3
δ	angle	degrees
δ	boundary layer thickness in Eq. 2-9	ft
ϵ	surface wetness fraction	
η	fin effectiveness	
η_r	local recovery factor	
Θ	defined by Eq. 2-26	
Θ	half divergence angle of diffuser	
θ	defined by Eq. 6-15	F
κ	ratio of specific heats	
λ	defined by Eq. 2-24 in Section 2-12.1	

Symbol	Quantity	Unit
λ	empirical parameter in Sections 2-11.1 and -11.2	
λ	latent heat of vaporization in Chapter 6	B/lb
μ	dynamic viscosity	slug/ft sec; lb_m/ft hr
ν	kinematic viscosity	ft^2/sec; ft^2/hr
Π	defined by Eq. 2-25	
ρ	density	slug/ft^3; lb_m/ft^3
ϕ	angle	degrees
ϕ	parameter defined by Eq. 3-15	
ψ	parameter defined by Eq. 3-14	
ω	specific humidity	
ω_w	liquid water content	g/cu meter

SUBSCRIPTS

Symbol	Quantity
A,B,C,D,...	chordwise stations along double-skin passages
a	air; air in double-skin passage
b	bulk; branch
c	contraction; convection; cylinder; corrugation
d	droplet; duct
e	effective; equivalent; elbow;
ex	exit; expansion
f	film
G	double-skin gap or passage
i	incompressible; inlet; index
iso	isothermal

Symbol	Quantity
j	index
l	lower surface
lam	laminar
o	free stream; orifice
m	mean
s	surface
sk	skin
st	stagnation point
tot	total or stagnation condition
tr	transition
turb	turbulent
u	upper surface
v	vapor
w	water
x	x-direction
y	y-direction
1	outer edge of boundary layer
1,2,3,...	sections; stations

Chapter 1: INTRODUCTION

1-1 Scope and Objectives.

This manual deals with steady-state, or continuous, thermal anti-icing of wing and tail surfaces. The heating medium of any system considered here is assumed to be hot air flowing along inner surfaces of the skin, that is, through so-called double-skin heat exchangers.

Specific objectives of the manual are to provide methods and reference material for the design of continuous thermal anti-icing systems in wings and empennages insofar as the thermal design is to be considered. Other aspects of the design, such as the selection of a heat source, the performance of the power plant during icing conditions, the effect on range of flight, the economic aspects, etc, are not treated here but may be found in other places. For example, Tribus (Ref. 124, Chapter III) deals with some of these problems.

While only anti-icing is being considered, a large amount of the reference material, such as the data from calculation of water droplet trajectories, may be used for calculations on mechanical, chemical, and cyclic de-icing systems.

1-2 Meteorological Design Data

The rate of water impingement will be found to depend upon the following meteorological quantities: liquid water content, droplet sizes, and temperature. A typical set of these quantities is:[1]

liquid water content.....0.5 gram/cubic meter
droplet size (uniform).....20 microns
air temperature.....15°F

Several investigators (see, for example, Ref. 52, 67, and 83) have taken steps to reach methods of selecting the meteorological quantities as well

[1] The units are those generally employed in this field of application. To change to consistent engineering units, consult Table A-4 in the Appendix of this manual.

as horizontal and vertical extent of icing conditions. It will be supposed that the designer enters the text with knowledge of the icing conditions against which he desires to protect the airplane. The next few sections contain the approximate ranges of the meteorological quantities and some of their influences. In regarding them, it should be borne in mind that extreme combinations of the meteorological quantities have been found to be infrequent. Thus, while simultaneous low temperatures and high amounts of liquid water content would produce extremely hazardous icing, this combination of properties has a low probability because the supercooled water droplets in a cloud freeze in increasing numbers as the temperature decreases. Other more or less fortuitous relationships between meteorological quantities seem to occur. Moreover, the experienced pilot, whenever possible, avoids or reduces the effect of icing by changing his course, speed, or both.

1-2.1 Influence and Range of Liquid Water Content

The rate of water catch increases in direct proportion to the liquid water content. Its maximum value is reported to range up to 1.8 grams per cubic meter in cumulus clouds (Ref. 129). Stratus-type clouds seldom exceed 1.0 gram per cubic meter and usually have only a few tenths gram per cubic meter (Ref. 129).

1-2.2 Influence and Range of Droplet Size

The droplet size influences the rate of water catch in a very complex way. All other variables remaining fixed, the rate of water catch increases with increasing droplet size. Calculations are usually based on a mean effective diameter, which is the diameter of the droplet such that half the liquid water content lies in droplets of lesser diameter and the other half in droplets of greater diameter. Mean effective diameters range from about 5 to 50 microns diameter. Tribus (Ref. 124, page I-3) shows that at moderate altitudes and temperatures, high liquid water contents and large droplets seldom occur simultaneously.

The experimental results of Dorsch and Hacker (Ref. 36) and the statistical investigation by Levine (Ref. 82) indicate that droplets of any

given size freeze spontaneously at a markedly high rate when their temperature is lowered to a particular value peculiar to that drop size and that the average spontaneous freezing temperature of each size group decreases with decreasing droplet size. It appears that for all practical purposes of the present application it may be assumed that no liquid water exists in the atmosphere when its temperature falls to -40°F or below, although in laboratory tests supercooled water has been shown to exist at lower temperatures.

1-2.3 Mean Icing Atmosphere

From 300 icing observations studied by Hacker and Dorsch (Ref. 52), it was found by Brun, Serafini, and Moshos (Ref. 27) that the average icing temperature of the atmosphere at any altitude differs somewhat from the corresponding temperature of the NACA Standard Atmosphere (Table A-1). These temperatures are plotted in Fig. A-1; average icing temperatures are represented by the solid line and standard temperatures by the dotted line. In this manual many of the calculation aids are constructed with the idea that the temperature of the atmosphere is uniformly 15°F. This is consistent with the assumption that large droplets and high water contents may occur at any altitude and allows conservative bases for design. In any case, the relationship between pressure and altitude is that given in Table A-1.

1-2.4 Influence of Meteorological and Flight Parameters on Heat Requirements

It will be seen that the heat provided to the skin of a wing to protect it from icing is dissipated mainly in heating the water that collects on the surface, in evaporating the water, and by forced convection. J. L. Orr (Ref. 103) presents results of calculations to show the effects of variations of the major meteorological and flight parameters on the heat required per unit time per unit area to maintain the stagnation region of a circular cylinder free from ice and at 32°F. Some results of those calculations are now summarized.

The heat required is almost a linear function of the air temperature, increasing as the temperature decreases. Also, the heat required is

a linear function of the liquid water content, increasing as the liquid water content increases. As the mean effective droplet diameter increases and approaches 20 to 30 microns, the heat load increases, approaching a practically uniform amount.

The altitude has a relatively minor effect. The reason is that the reduction in convective losses due to decreased density is offset by an increase in evaporation losses due to reduced pressure.

Small cylinders are less effective in deflecting the water droplets than large cylinders. For this reason small cylinders require relatively much more heat per unit area than large cylinders. The influence of size is less noticeable among cylinders of large diameters.

Velocity has an important influence. As the speed increases from zero velocity the heat requirement reaches a peak and then diminishes, chiefly on account of the kinetic heating due to skin friction. It is highly probable that any airfoil moving with Mach number greater than unity would remain free of ice, not requiring any heat other than that provided by aerodynamic heating. Certainly, under ordinary circumstances, at Mach number 1.5 any auxiliary heating would be unnecessary; the water would remain in the liquid phase and run off the trailing edge. However, if the criterion of design is complete evaporation without runoff, the required rate of heating is very high, even when the speed is well in the supersonic region.

The qualitative remarks in the preceding paragraphs apply equally well to the stagnation region of airfoils. Beyond the region of stagnation, the relative amounts of heat lost by sensible heating of the water, by evaporation, and by convection can be considerably different from those illustrated in Orr's graphs.

Also, runback beyond the heated area can be tolerated when speeds are high enough so that the aerodynamic heating maintains the runback in the liquid phase.

1-3 Description of Hot Air Anti-Icing Systems

Figure 1-1 is a cross section of a typical double-skin heat exchanger in the leading edge of a wing. The inner skin may have any of the shapes shown in Fig. 1-2. The corrugated and dimpled types are usually made of a thin metal which can be easily pressed. The height of the gaps may vary from a large fraction of an inch in the case of the sinusoidal shapes to about 1/8-inch in the case of the rectangular or trapezoidal shapes, although much smaller gaps have been reported. Some typical dimensions of the passages are shown in Fig. 1-2(e), -(f), and -(g). The heights of passages made with spacers or by milling operations are most easily controlled in production. The passageways must be kept clear of any foreign materials during assembly, particularly if they are thin. The inner skin is usually fastened to the outer skin by means of rivets.

The entrance to the passages shown in Fig. 1-1 is rounded by means of metal strips fastened over the peaks of the corrugations. However, in other constructions the entrances have been left sharp, and in some cases the upper and lower panels have been made continuous, the air entering at the leading edge through one or more orifices per passage. The orifices are sized, often by test, to meter and balance the flows through the corrugations. The same purpose is served by the orifices at the outlets of the corrugations shown in Fig. 1-1.

The seals at the end of the corrugations and similar seals along the edges of the individual panels are important. If they are not provided, the system may become so unbalanced that insufficient heat will be provided along many passages, and icing will occur. Several mastics or caulking compounds are available to make the seals.

Other types of distribution systems are shown in Fig. 1-3. In Fig. 1-3(a) a liner is used and the air is directed in such a way that it makes a double pass. The liner is used to provide a more uniform channel through the D duct so that pressure losses are reduced (Ref. 98).

In Fig. 1-3(b), the supply duct passes behind the front spar. This duct should be insulated because it is in a region of low temperature.

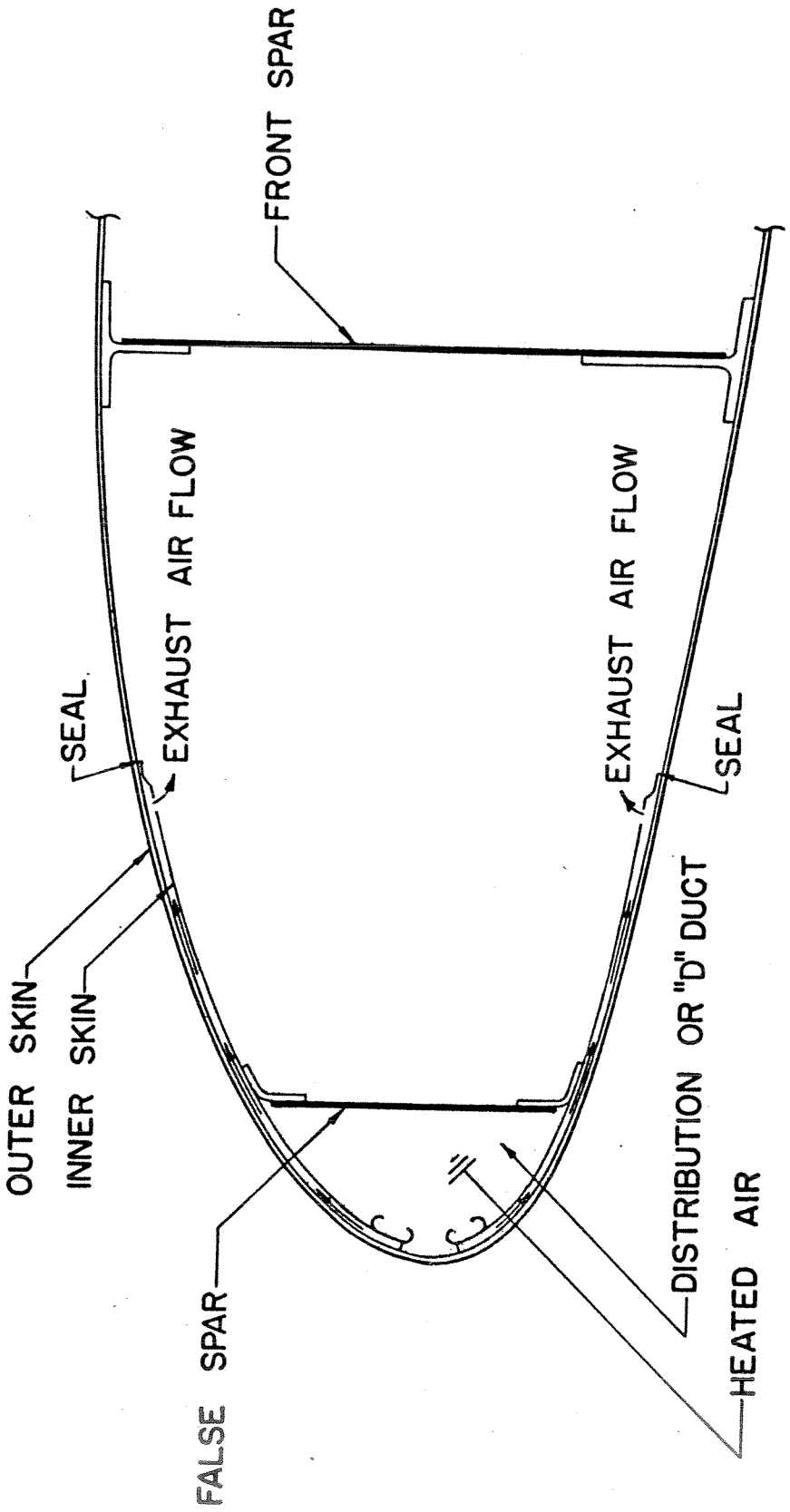

FIG. 1-1 DOUBLE-SKIN SECTION OF A WING

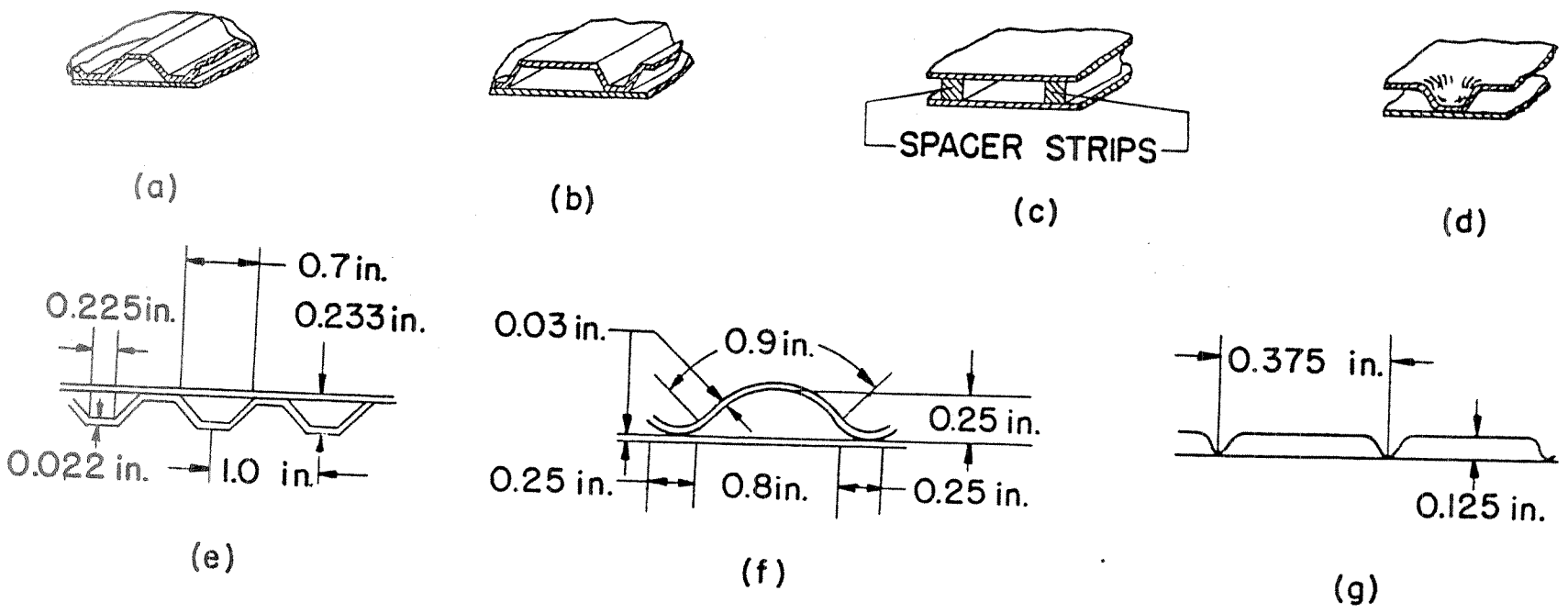

FIG. 1-2 TYPICAL CROSS SECTIONS OF DOUBLE - SKIN PASSAGES

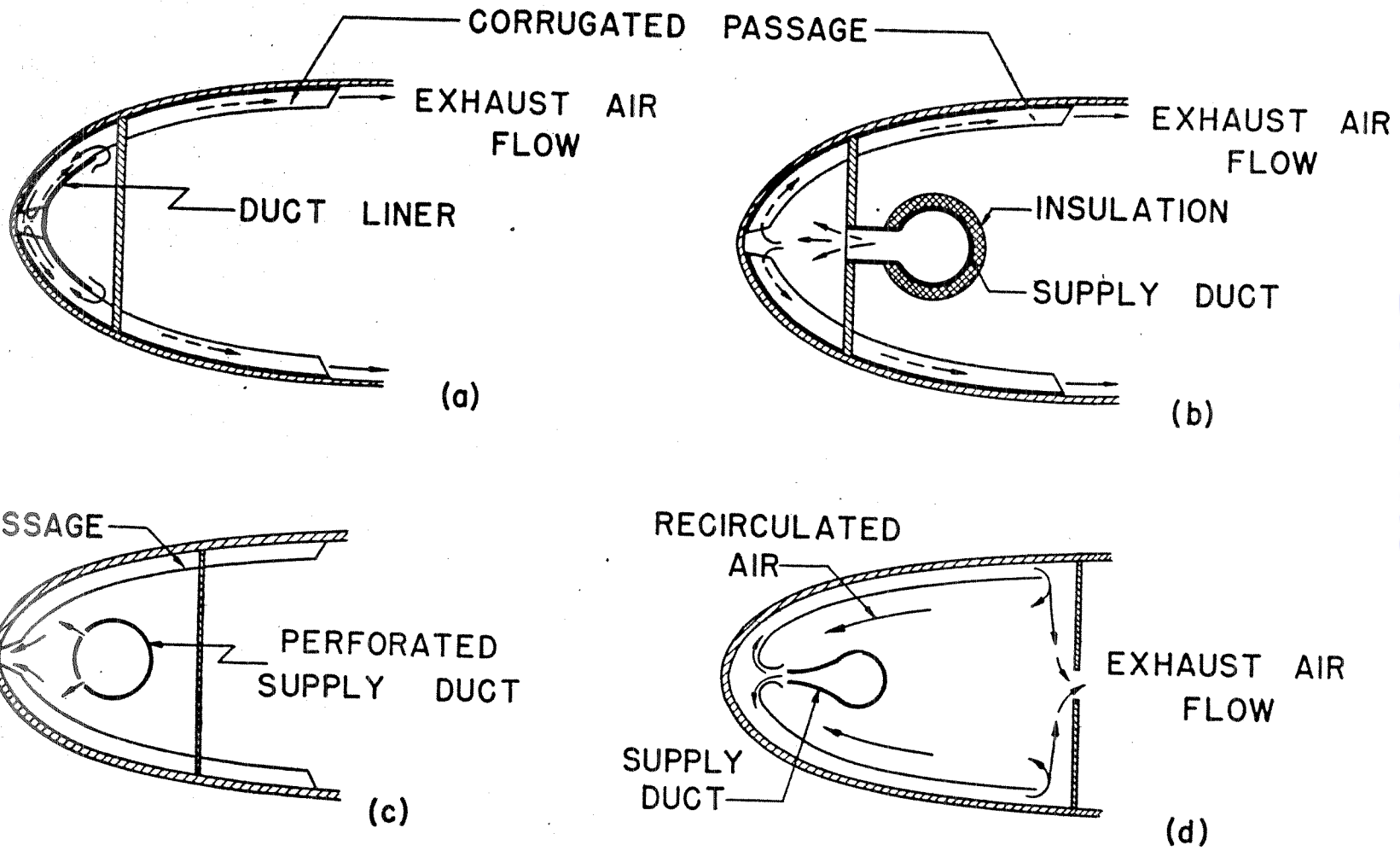

FIG. 1-3 AIR FLOW IN SOME TYPICAL LEADING EDGES OF HEATED WINGS

Insulation should be inserted between the duct and the supporting brackets in order to reduce the influence of through-metal conduction. This type of distribution is suitable where large ducts are needed as in low-pressure anti-icing systems in thick wings.

A modification of this type of distribution system is shown in Fig. 1-3(c). The supply duct, which is perforated, passes through the D duct. This arrangement has been used in high-pressure anti-icing systems where wings are thin, where little space is available forward of the front spar, and where the supply duct is small. The orifices meter and balance the flow.

Another modification for a high-pressure system is shown in Fig. 1-3(d). Here, part of the air is recirculated. In this case the supply air may be at quite a high temperature. In one design, about 70 per cent of the air flowing through the corrugations has been recirculated.

Other types of distribution systems have been employed and suggested. An anti-icing system based upon spanwise flow of the hot air instead of chordwise flow is analyzed in Ref. 28. Only the chordwise heaters, which at this time seem to be more practical from the viewpoint of manufacture, are considered in this manual.

The simple types of passages shown diagrammatically in Fig. 1-2 may be combined in a single double-skin heat exchanger, and in some cases the distribution system may be quite complex. Figure 1-4 is a sketch of a heater comprised of spacer and dimple-type passages in the leading edge of a wing with a slat. Warm air exhausting through the orifices in the slat passes down between the slat and the main part of the wing to keep the space between them free of ice. The heater on the lower surface is longer than the heater in the upper surface because the area of impingement on the lower surface is larger.

Some of the complex details of the supply duct and corrugated double-skin heaters in a vertical stabilizer are shown in Fig. 1-5.

FIG. 1-4 SPACER AND DIMPLE TYPE PASSAGES IN THE LEADING EDGE OF A WING WITH A SLAT

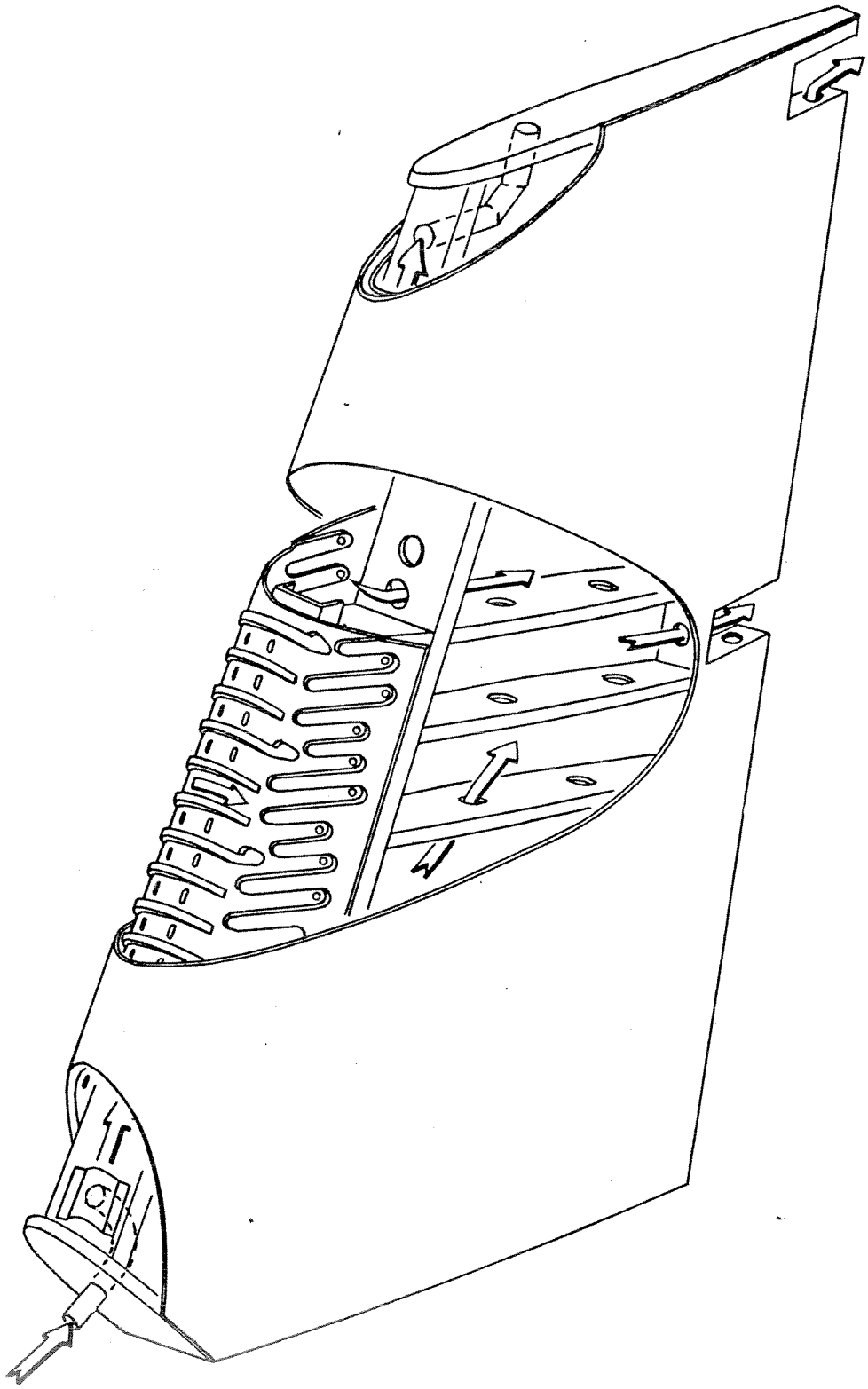

FIG. 1-5 DOUBLE-SKIN HEATER IN THE LEADING EDGE OF A VERTICAL STABLIZER

1-4 The Designer's Problem

The designer must determine the size of the passages, their arrangement, the amount of heated air, and the air temperature required to keep the exterior surfaces free of ice. Having determined a physical arrangement, he will also be called upon to analyze its performance under any given flight and icing conditions. Neel (Ref. 98) suggests that space limitations and the available heat supply often will determine the physical arrangement of the anti-icing system and that the design procedure becomes one of determining what temperature and what rate of air flow should be supplied to an arbitrarily chosen system.

The purpose of the next chapters is to provide some methods and reference materials to aid the designer in the calculations to meet these ends. Details of many individual problems are still unsolved; therefore, the designer must bring to this task his knowledge of the engineering sciences and the arts of engineering practice which he gains by experience. So far, experience has shown that the general techniques set forth in the following pages lead to rather satisfactory results.

Following Neel's suggested procedure, the designer, either by experience or by preliminary calculations to be described later, arrives at a double-skin heat exchanger and supply system. Then he analyzes the system, adjusting the inlet temperature of the air and its rate of flow until effective operation is obtained. If this condition cannot be met within the limits of available flow, permissible temperatures, and allowable expenditure of energy, the design must be altered until a satisfactory solution is attained.

The final check is obtained by flight tests in icing weather.

Chapter 2: AIR FLOW IN COMPONENTS OF ANTI-ICING SYSTEMS

2-1 Introductory Remarks

The designer may be faced with either of two general problems. Ducts will have to be sized for the proper distribution of a predetermined amount of hot air. Or the distribution of the flow through a given anti-icing system will have to be determined in order to analyze the performance of the system. The purpose of this chapter is to provide some relationships and reference material to aid in solving either of these problems.

Results from many investigations on frictional resistance in straight circular ducts have often been shown in the literature to be in satisfactory agreement. Investigations on other components such as elbows, branching ducts, and so forth, have been so diverse with regard to configurations and flow characteristics, that generalization of this information usually has presented difficulties. Fortunately, calculations based on the methods and data of this manual, which have been taken mainly from well known sources, seem to be sufficiently accurate for the present application.

Energy losses of air flowing in a duct system depend upon the configuration of the conduit, the nature of the flow, and the physical properties.

2-1.1 Configuration

The configurations and the material of the conduit play the most important role in consideration of the pressure drop. Changes of magnitude and direction of the fluid velocity and distributions of the flow and static pressure are influenced primarily by the geometry of the passages. Thus, an abrupt change of cross section may cause large energy losses. The surface roughness may change the nature of the flow and increase the frictional losses.

2-1.2 Nature of the Flow

The distribution of velocity approaching any elbow or other fitting is known to have considerable influence on the losses. This influence is

extremely complex, and the designer is usually satisfied to approximate the losses by assuming that the distribution is uniform.

As is well known, frictional losses are much greater in the case of turbulent flow than in the case of laminar flow. In a straight circular tube, the flow may be considered laminar if the Reynolds number is less than 2300; in a curved tube the critical Reynolds number may be greater. Above 10,000 and in long ducts, it may be assumed that fully developed turbulence has developed. Between these two values a transition occurs which cannot be well defined. In any case, a region of transition occurs inside the entrance.

2-1.3 Physical Properties

The major properties entering the discussion of fluid flow in internal systems are density ρ and dynamic viscosity μ. The ratio μ/ρ also occurs; it is denoted by ν and called the kinematic viscosity. Tables A-1 and -2 may be used to evaluate these quantities. The density of the air may be calculated, also, by means of the relationship of state,

$$\rho = \frac{p}{RT} \qquad (2\text{-}1)$$

Taking[1] $[p] = lb_f/ft^2$, $[T] = {}^\circ R$, and $R = 53.3$ ft $lb_f/lb_m F$, the units of ρ are lb_m/ft^3. For all practical purposes the specific weight γ has the same numerical value as ρ but its units are lb_f/ft^3. It may be recalled that if ρ is expressed in $slug/ft^3$ then $\gamma = \rho g$.

The flow is considered incompressible or compressible, depending upon whether the density changes with the pressure or not. In most cases the density may be regarded as virtually constant and in the following sections, unless otherwise specified, the flow will be considered incompressible.

---

[1] For the bracketed expressions, "[...]", read, "the units of ...".

2-1.4 Frictional and Fitting Losses

The sum of the static pressure and the dynamic pressure is called the total pressure:

$$H = p + \frac{1}{2}\rho U^2 \qquad (2\text{-}2)$$

In a system without energy losses, H would be uniform. In this manual losses of total pressure due to fluid friction, as in the case of flow through straight tubes, will be called frictional losses; all other losses, such as those due to elbows, diffusers, branches, and so forth, will be called fitting losses.

In accordance with the principle of continuity, since the effect of non-uniform velocity distribution is not considered, the dynamic pressure $\rho U^2/2$ in a duct of constant cross-sectional area is constant and the loss of total pressure is equal to the loss of static pressure.

Since, in most practical cases, the pressure losses are approximately proportional to the square of the air velocity, losses may be reduced by using ducts of large size. Frictional losses in short straight ducts of constant cross-sectional area are relatively small compared with fitting losses. Therefore, care should be taken to keep the number of fittings as small as possible.

2-2 Pressure Drop in Straight Tubes

The pressure drop due to friction of a fluid flowing in a tube is calculated by means of the Darcy-Weisbach equation,

$$\frac{\Delta p}{\gamma} = f \frac{L}{D} \frac{U^2}{2g} \qquad (2\text{-}3)$$

where U is the mean velocity. If $[U]$ = ft/sec, $[\gamma]$ = lb/ft^3, g = 32.17 ft/sec^2, then $[\Delta p]$ = lb/ft^2. The friction coefficient f is a function of the Reynolds number and surface roughness. Figure 2-1 shows the friction coefficient f for smooth tubes based on values from Ref. 96. It may be noticed that there are well established correlations for the friction

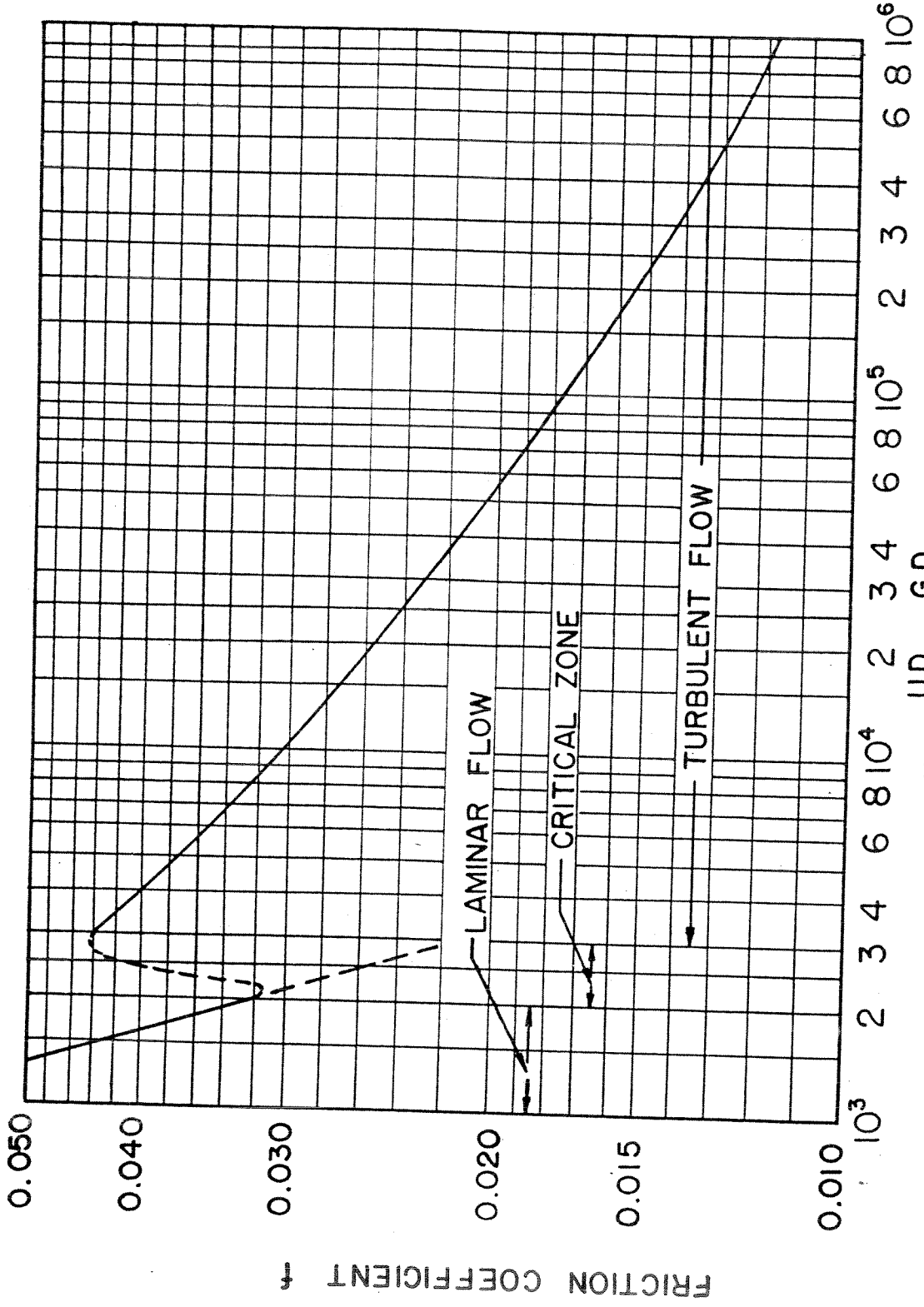

FIG. 2-1 FRICTION COEFFICIENT FOR SMOOTH TUBES

coefficient of entirely laminar or fully developed turbulent flow. Information for the transition region, which probably extends over a broader range of N_{Re} than that shown, is not well established.

In order to facilitate the calculation of pressure drop for air in straight tubes Fig. 2-2 and -3 have been constructed.[1] Figure 2-2 shows values of pressure drop in in.-water per foot length of tube as a function of the weight rate of flow and tube diameter. The diagram is based on 300°F temperature and 29.92 in.-mercury pressure.

To obtain a pressure drop for any temperature and pressure the value of $\frac{\Delta p}{L}$ taken from Fig. 2-2 must be multiplied by the correction factor K_{pt} given in Fig. 2-3. The factor K_{pt} includes the influences of pressure and temperature on the fluid properties.

2-3 Pressure Drop in Elbows

A loss of total pressure occurs when air passes around a bend. This loss is caused mainly by regions of reverse flow due to separation and by eddying motions whose kinetic energy cannot be completely recovered. A relatively small loss is caused by friction.

For a bend of uniform cross-sectional area the loss of static pressure is equal to the loss of total pressure and may be expressed as a fraction of the dynamic pressure. Thus,

$$\Delta p = \Delta H = K_e \cdot \frac{1}{2} \rho U^2 \qquad (2\text{-}4)$$

where K_e is the coefficient of total-pressure loss. Locklin (Ref. 84) shows that the value of K_e depends on (1) the Reynolds number, (2) the radius ratio and the aspect ratio, (3) the angle of deflection, and (4) the termination of the elbow.

[1] Similar figures appear in Ref. 111.

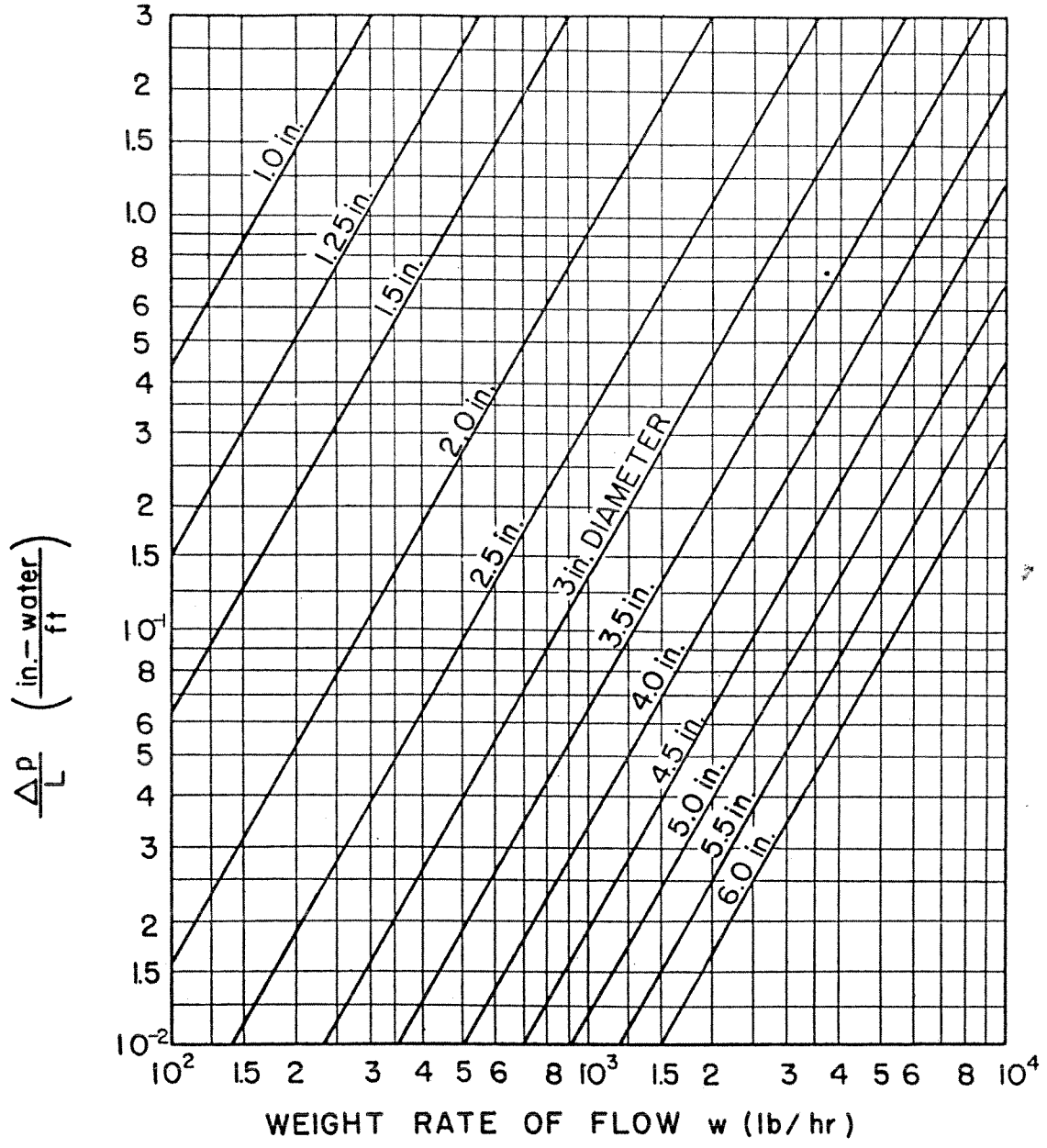

FIG. 2-2 PRESSURE DROP IN STRAIGHT TUBES FOR AIR AT 300°F AND 29.92 IN.-MERCURY

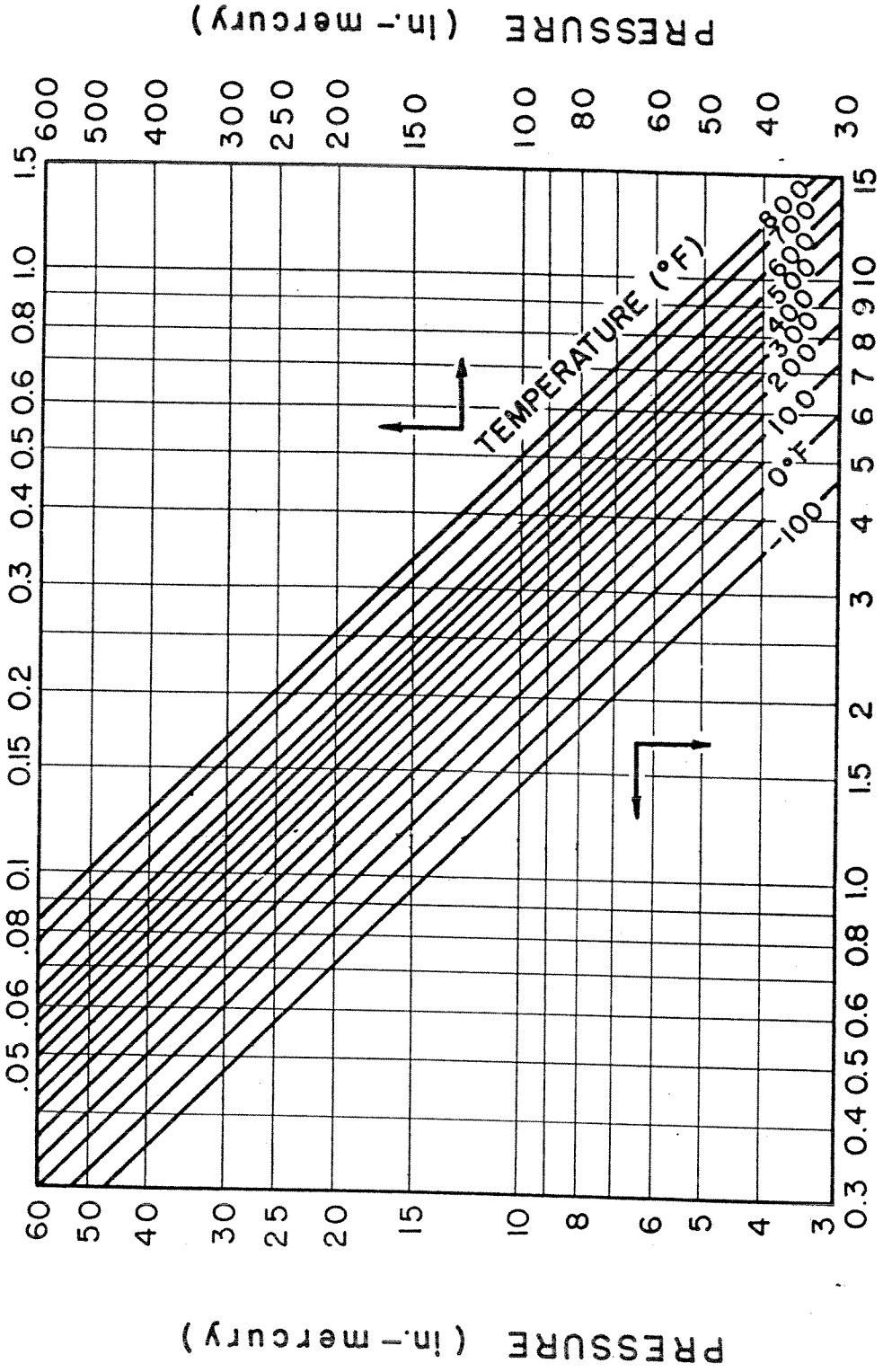

FIG. 2-3 CORRECTION FACTOR FOR USE IN CONJUNCTION WITH FIG. 2-2

2-3.1 Influence of Reynolds Number

Patterson (Ref. 104) noted that a ten-fold increase of Reynolds number may reduce the bend-loss coefficient about 40 per cent. Pigott (Ref. 106) has introduced the influence of surface roughness and Reynolds number in the following empirical equation for the loss coefficient in round and square elbows,

$$K_e = 0.106 \left(\frac{R}{Y}\right)^{-2.5} + 2000\, f^{2.5} + f\,\frac{L}{Y} \qquad (2\text{-}5)$$

The first term represents the net loss coefficient for a fictitious smooth elbow; R is the radius of the curve and Y is the depth in the plane of curvature.[1] The second term gives the increase due to combined effects of roughness and Reynolds number, the friction factor being used to characterize these two factors. The last term gives the frictional loss, L being the length of the centerline.

2-3.2 Influence of Radius and Aspect Ratios

The results of investigations by Wirt (Ref. 132) and Hoffmann (Ref. 61) on the effect of radius ratio (the radius of curvature of the centerline divided by the depth in the plane of curvature, that is, R/Y) on the loss around 90° corners revealed that for best performance of the elbow the radius ratio must be 3 or more. Whereas it is generally agreed that the inside corner must be well rounded some question remains about the outside corner. Wirt (Ref. 132) states that the loss of total pressure of an elbow may be improved about 10 per cent by using a square outside corner. McLellan and Bartlett (Ref. 93) find that although an elbow with a square outer corner is better than an elbow with a well rounded corner for ducts of low aspect ratio (the height normal to the plane of curvature divided by the depth in the plane of curvature, say, X/Y), the square outer corner is not better at high aspect ratio.

According to results obtained by Wirt the aspect ratio of 90° bends should be about 6 or more for best performance. The influences of the

[1] In the case of the round or square duct, Y is the diameter or the length of the side, respectively.

radius and aspect ratios are shown quantitatively in Fig. 2-4 to 2-8.

2-3.3 Influences of Angles of Deflection

The experiments by Kirchbach (Ref. 73), Bauchayer (Ref. 8), and others show that the losses decrease as the angle of deflection decreases. This variation of bend losses as function of deflection angle is shown in Fig. 2-9, which is reproduced from Ref. 111.

2-3.4 Influence of the Termination of the Elbow

The works of Beij (Ref. 10) and Schubert (Ref. 116) point to the fact that the influence of the elbow may persist for as many as 50 diameters downstream in round pipes, particularly following bends of large radius ratio.

For good performance the bend should be followed by a portion of straight duct having a length of at least four times the larger dimension in the cross section of the bend. With reference to Fig. 2-4, comparison of Curves 3 and 4 and of Curves 1 and 5 shows that without the straight duct at the outlet an elbow may have as much as 60 per cent higher pressure loss than the same elbow with the straight portion.

2-3.5 Calculation of Elbow Losses

Equation 2-4 gives the pressure loss of an elbow. The value of the pressure loss coefficient K_e may be obtained from Fig. 2-4 to 2-12. All coefficients shown include the pressure losses due to the friction. Figure 2-4 is a plot of K_e versus the radius ratio R/Y for square and round elbows (aspect ratio $Y/X = 1$) and for Reynolds number up to about 10^6.

For an aspect ratio other than 1.0 the pressure loss coefficient may be obtained by multiplying the value from Fig. 2-4 with the correction factor taken from Fig. 2-5. The curve marked "with pipe" is to be used with Curves 1, 2, and 3 of Fig. 2-4; the curve marked "no pipe" is to be used with Curves 4 and 5.

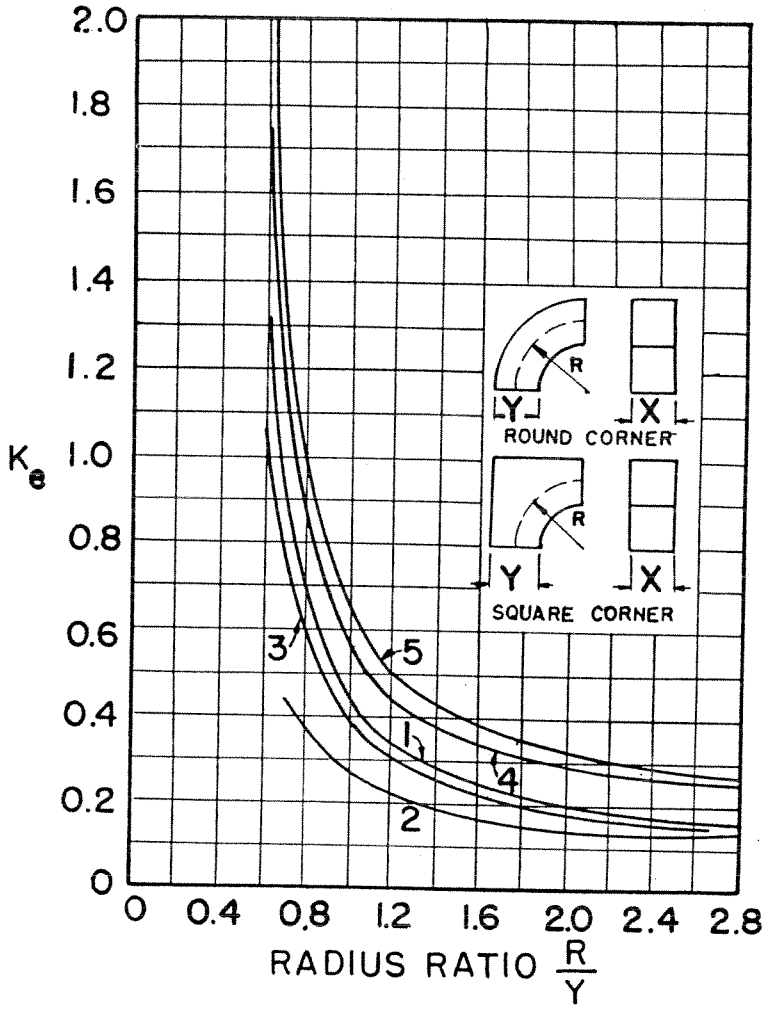

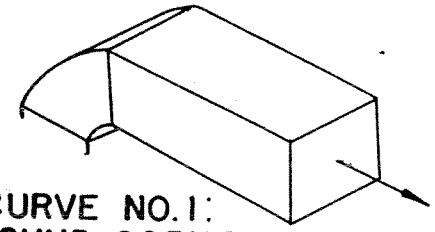

CURVE NO. 1: ROUND CORNER & SQUARE PIPE

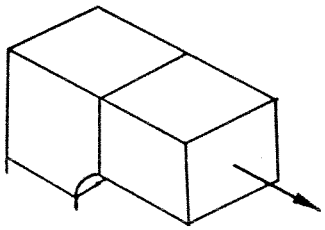

CURVE NO. 3: SQUARE CORNER & SQUARE PIPE

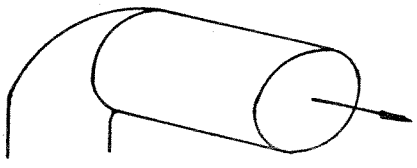

CURVE NO. 2: ROUND CORNER & ROUND PIPE

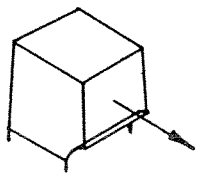

CURVE NO. 4: SQUARE CORNER FOR SQUARE PIPE

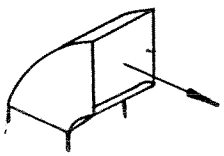

CURVE NO. 5: ROUND CORNER FOR SQUARE PIPE

FIG. 2-4 TOTAL-PRESSURE-LOSS COEFFICIENTS FOR ELBOWS

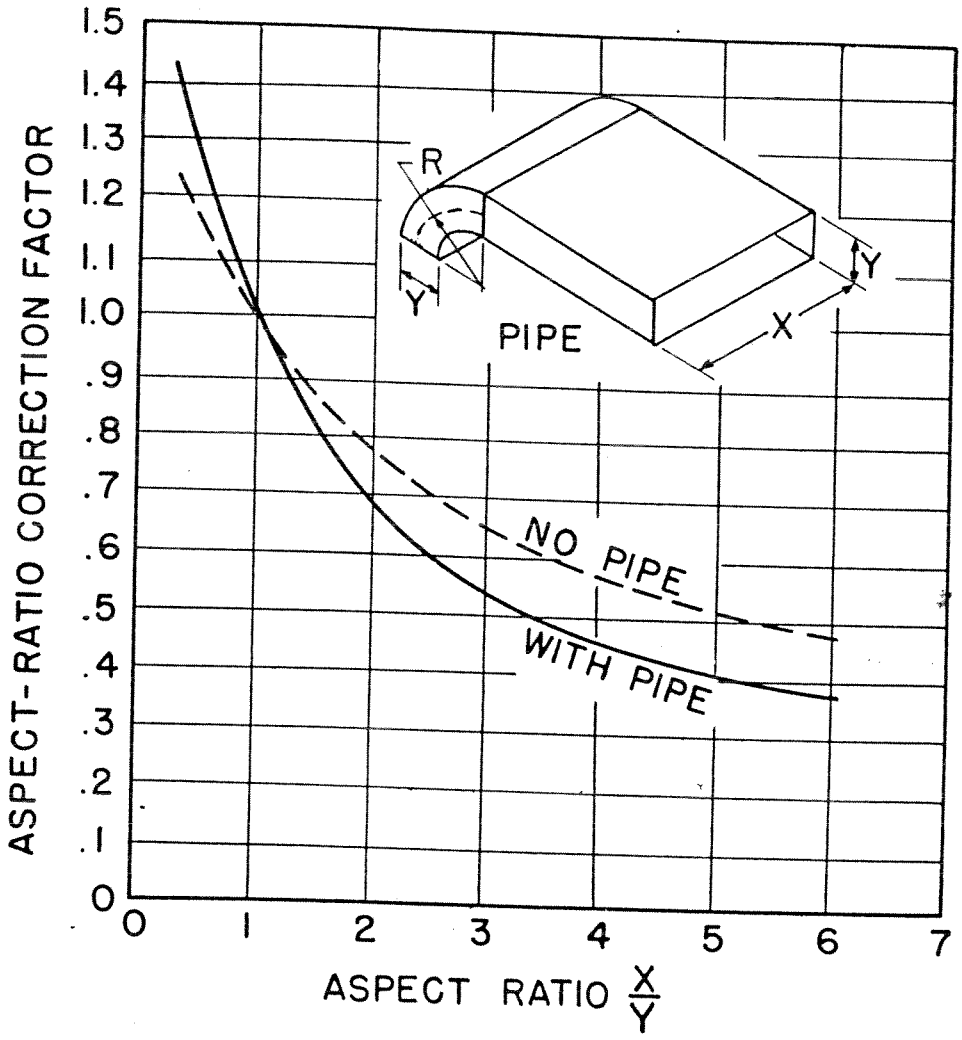

FIG. 2-5 ASPECT-RATIO CORRECTION FACTOR TO BE USED WITH VALUES FROM FIG. 2-4

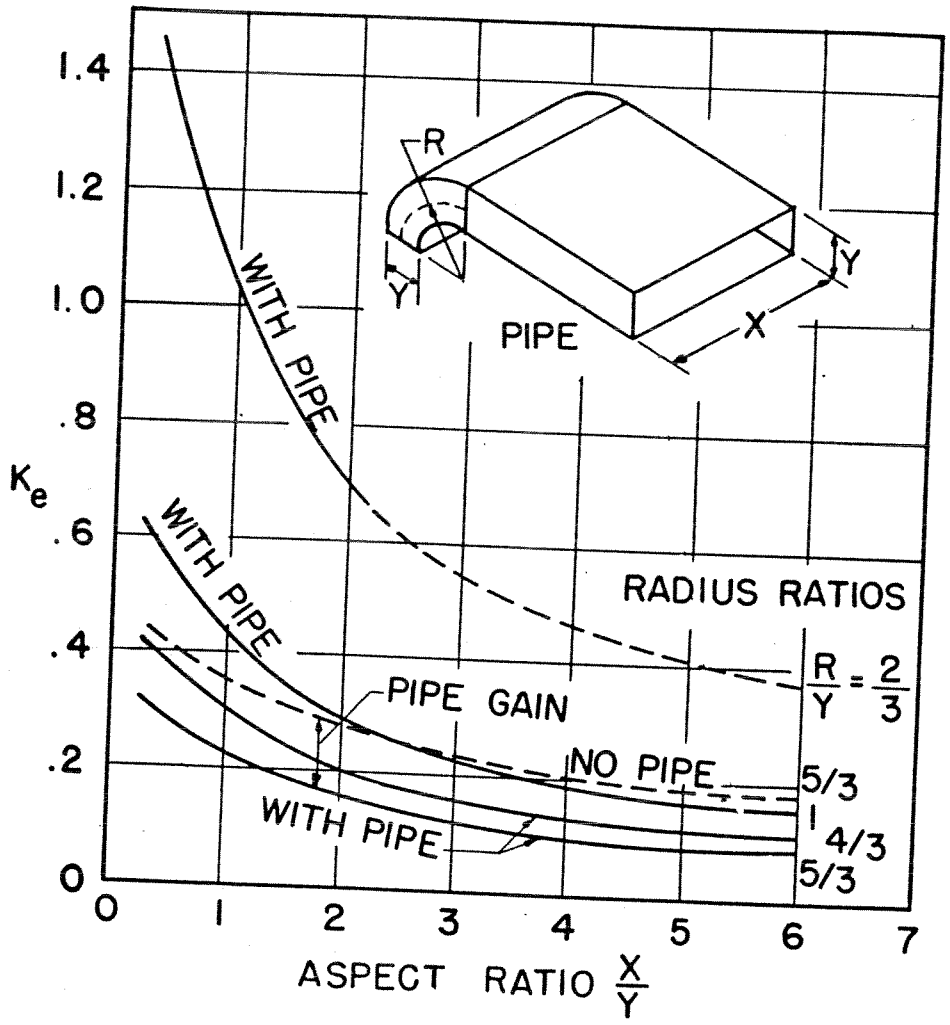

FIG. 2-6 PRESSURE-LOSS COEFFICIENTS OF RECTANGULAR ELBOWS

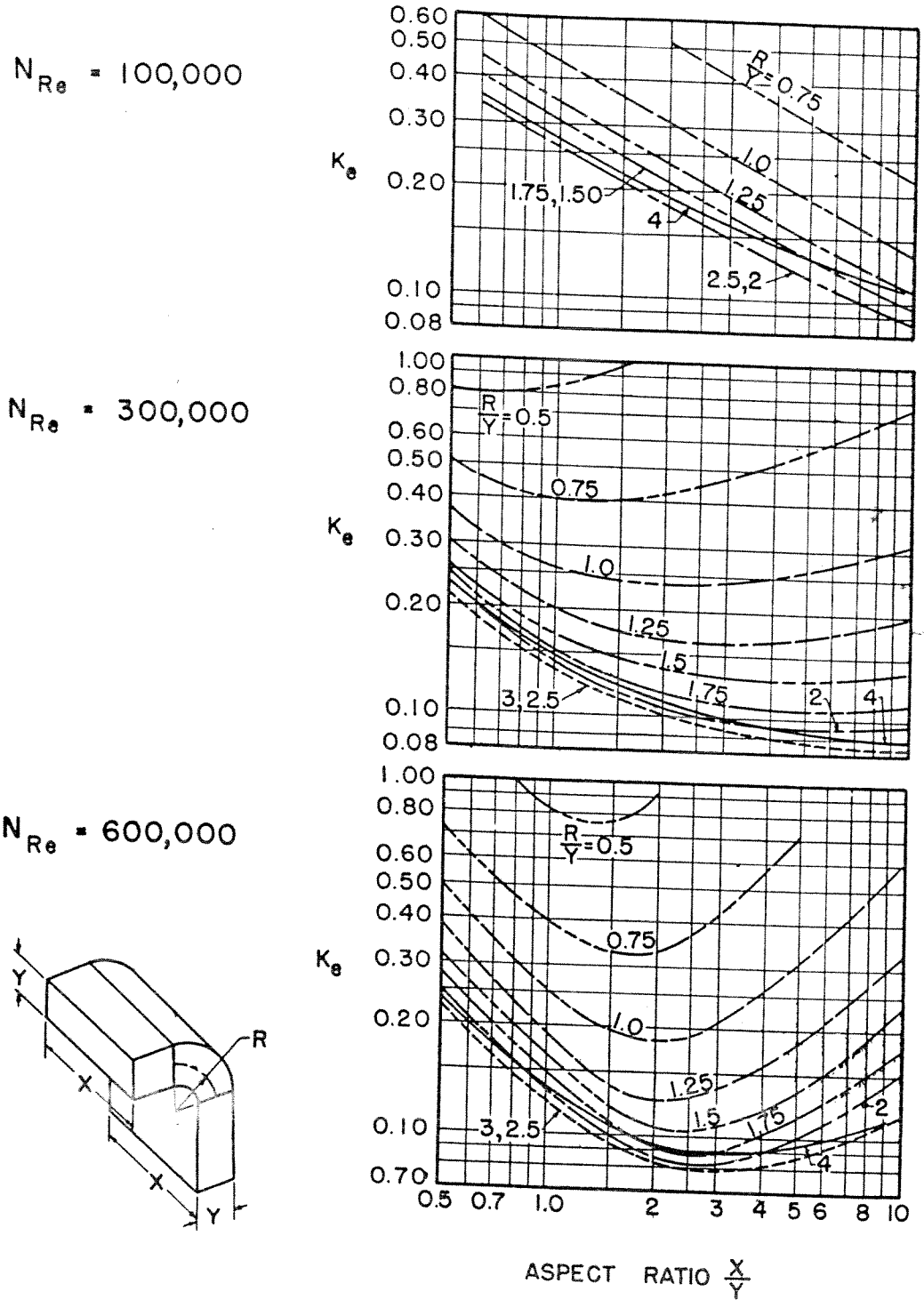

FIG. 2-7 TOTAL-PRESSURE-LOSS COEFFICIENTS FOR RECTANGULAR 90° BENDS

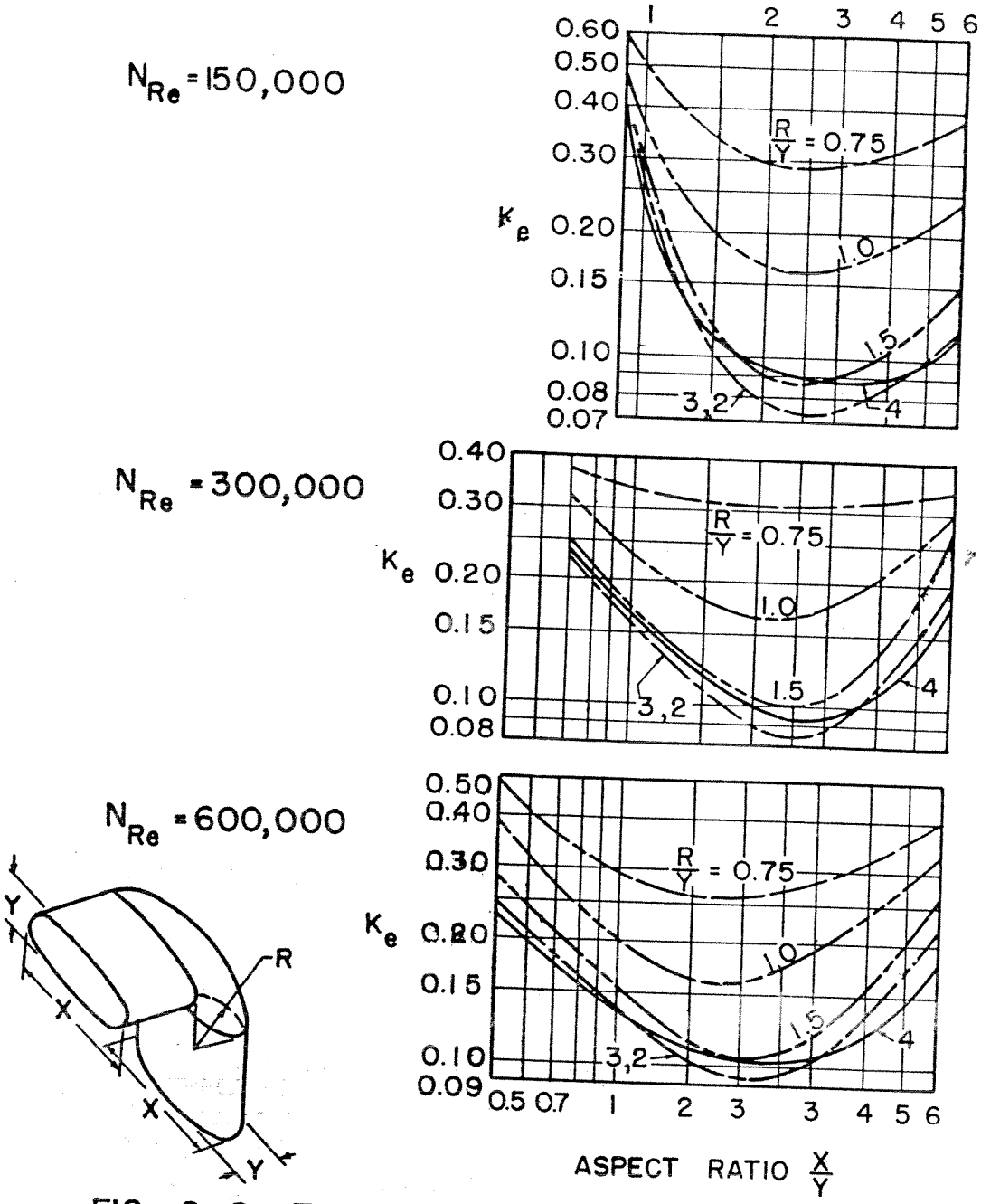

FIG. 2-8 TOTAL-PRESSURE-LOSS COEFFICIENTS FOR ELLIPTICAL 90° BENDS

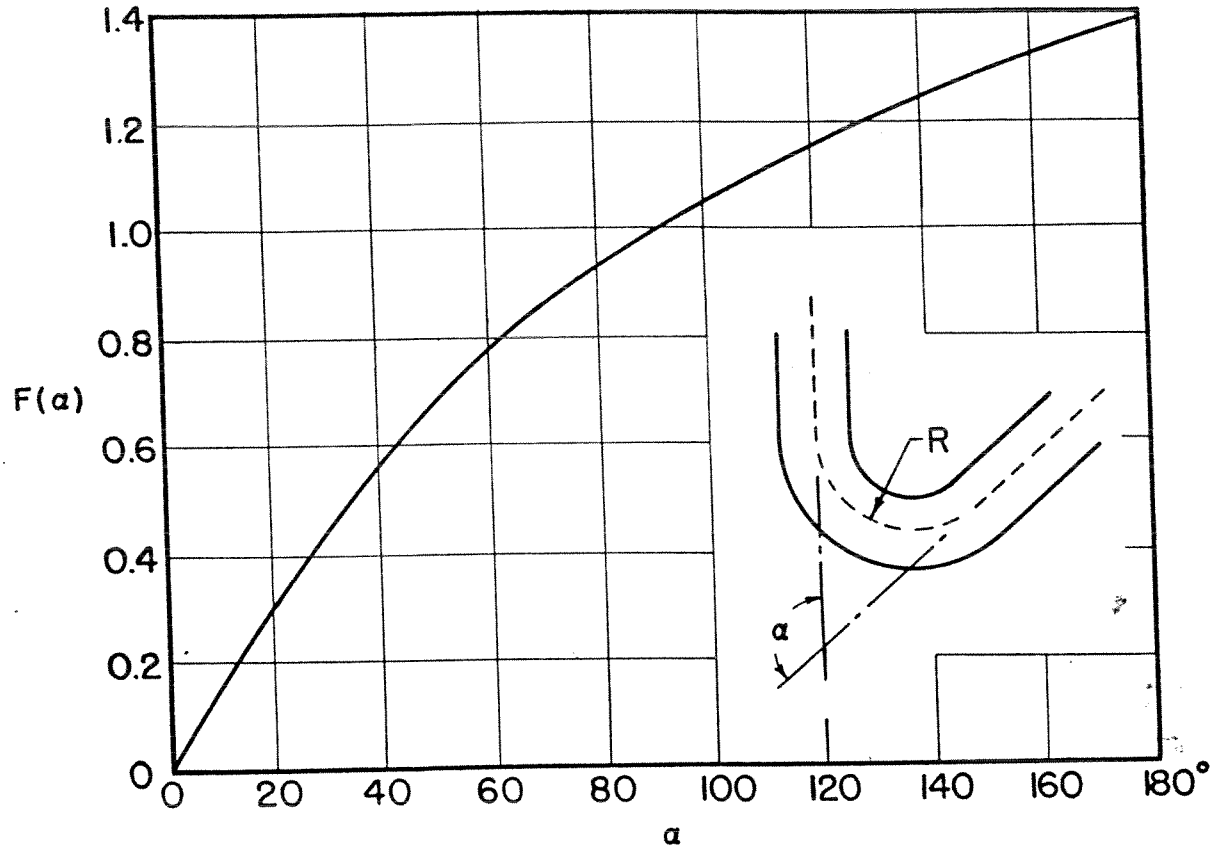

FIG. 2-9 ANGLE FACTOR OF TOTAL-PRESSURE LOSS IN ACUTE AND OBLIQUE ELBOWS

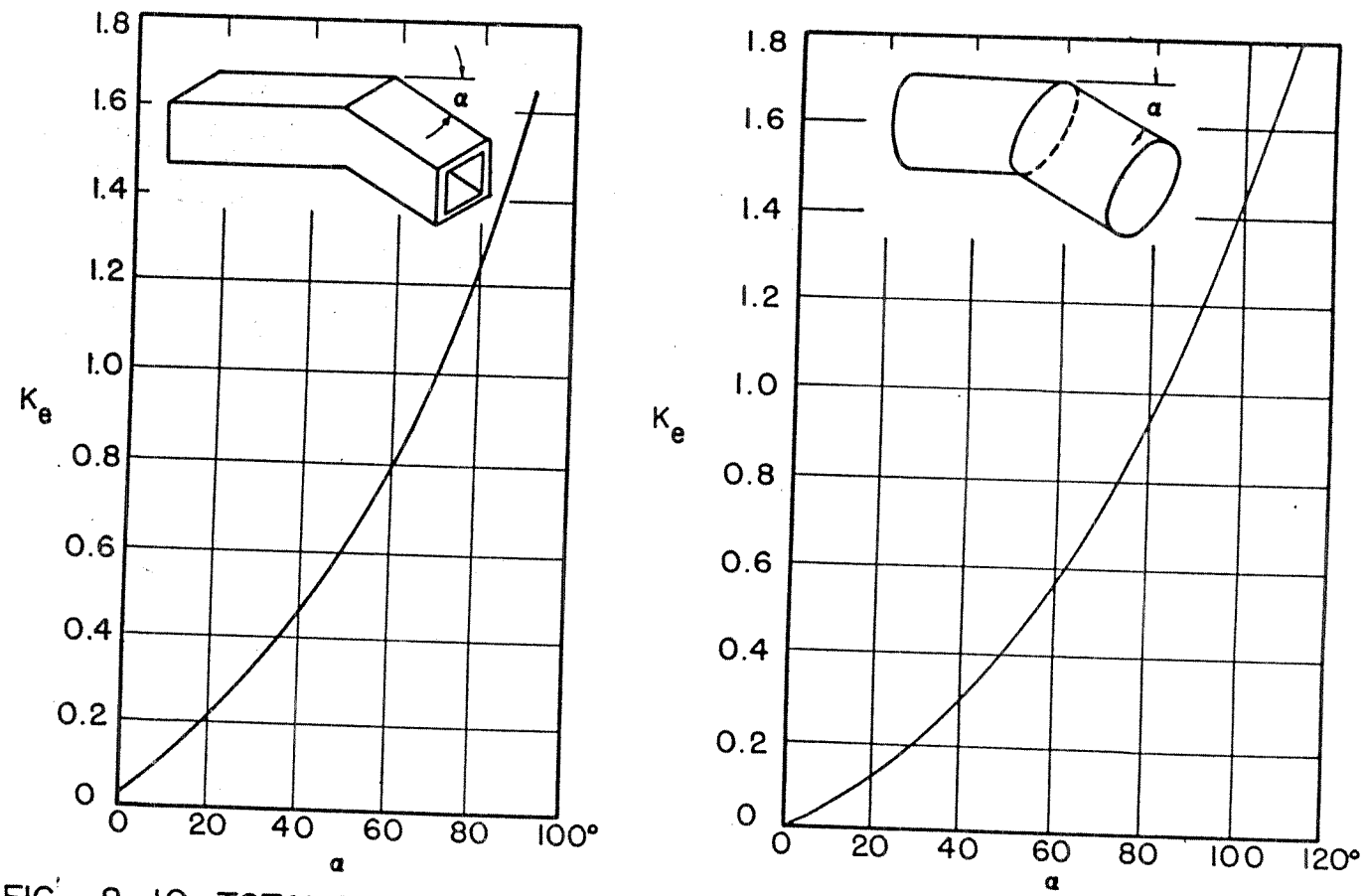

FIG. 2-10 TOTAL-PRESSURE-LOSS COEFFICIENT FOR MITERED ELBOWS IN SQUARE AND ROUND DUCTS ($10^4 < N_{Re} < 10^5$)

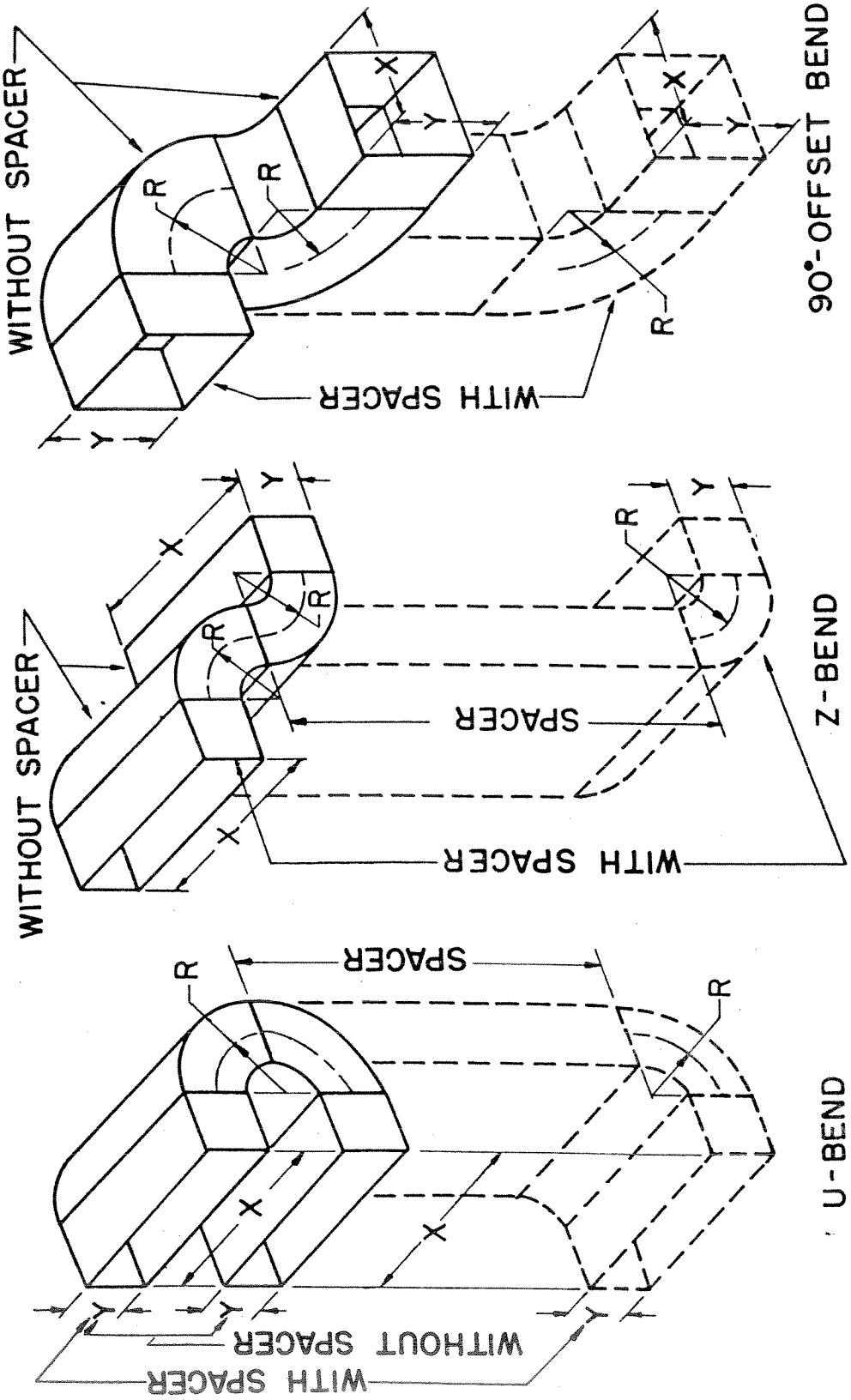

FIG. 2-11 RECTANGULAR COMPOUND BENDS

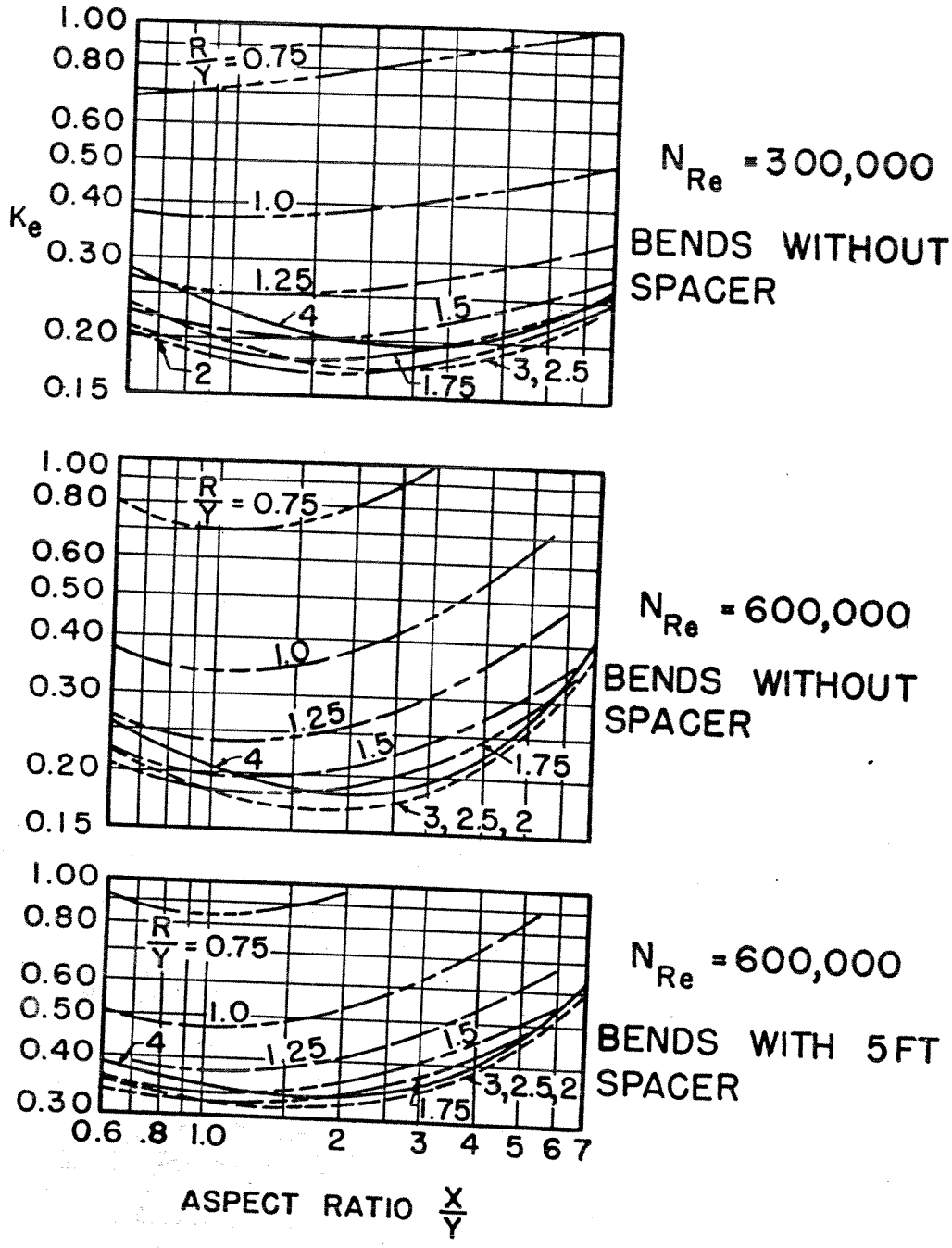

FIG. 2-12 TOTAL-PRESSURE-LOSS COEFFICIENTS FOR COMPOUND RECTANGULAR U, Z, AND 90° OFFSET BENDS

Figure 2-6 shows the coefficient of pressure drop in rectangular bends of radius ratios R/Y = 2/3, 5/3, 1, 4/3, with or without pipe.

For values of Reynolds numbers up to 600,000 the pressure-loss coefficient may be obtained from Fig. 2-7 for rectangular cross section and from Fig. 2-8 for elliptical cross section.

For circular bends other than 90°, the pressure loss coefficient must be multiplied by a correction factor obtained from Fig. 2-9.

The pressure-loss coefficient for mitered elbows of circular and rectangular profile is shown in Fig. 2-10.

The pressure-loss coefficients of the compound bends illustrated in Fig. 2-11 are presented in Fig. 2-12.

Additional information on pressure loss of bends may be found in Ref. 2, 84, 93, and 131.

2-4 Improvement of Bend Efficiency

In practice it is not always possible to design a corner with radius and aspect ratios to give small pressure loss. When this happens, improvements may be made by partitioning with a sufficient number of guide surfaces, or vanes, so that each compartment has a high aspect ratio, or a good radius ratio, depending upon what is needed. However, the increase of frictional losses limits the improvement of the turn by this method. According to Wirt (Ref. 132) the loss of a 90° turn improved in this way may be as low as 20 or 30 per cent of the dynamic pressure.

2-4.1 Circular Sheet-Metal Vanes

Figure 2-13 is a diagram illustrating the application of circular arc vanes to a bend (Ref. 59). The spacing and radii of the vanes are uniform. With reference to the nomenclature in Fig. 2-13 the number of vanes required is

$$n = \frac{2}{C_L} \frac{|\bar{U}_2 - \bar{U}_1|}{|\bar{U}_1|} \frac{Y_1}{L} - 1 \qquad (2\text{-}6)$$

FIG. 2-13 BEND WITH THIN CIRCULAR ARC VANES

where $L = 2r \sin(\beta/2)$ and C_L is the lift coefficient of the vanes. It was suggested in Ref. 59 that for thin vanes installed in a 90° bend, a lift coefficient of 0.8 will give approximately the minimum losses and a satisfactory velocity distribution. A small amount of experimental evidence indicates that the value 0.8 will apply to bends other than 90°. Kroeber (Ref. 77) found that for a 90° bend the angle of attack α should be 48°, or 3° more than the half angle of the 90° bend. Henry suggests that in a bend of angles other than 90° the amount by which the angle of attack should exceed half the amount of the bend may be taken as the proportional part of the 3°. For example, for a 45° bend, an angle of attack of 24° would be obtained.

For a 90° bend with inlet and outlet area the same in size and shape, Eq. 2-6 may be simplified to

$$n = \frac{2}{C_L} \frac{Y}{\bar{r}} - 1 \qquad (2\text{-}7)$$

where $\bar{r}$ denotes the arithmetic mean radius of the inside and outside walls of the bend. If $C_L = 0.8$,

$$n = 2.5 \frac{Y}{\bar{r}} - 1 \qquad (2\text{-}8)$$

2-4.2 Thin Vanes of Non-Circular Profile

Figure 2-14 and Table 2-1, taken from Ref. 59, show the contours of thin vanes of non-circular profiles, which may be used in bends of uniform cross section. Their theoretical development is due to Kroeber (Ref. 77). The performance of these vanes is shown in Fig. 2-15. The required number of vanes can be found directly from the chord length and the gap-to-chord ratio of Fig. 2-15. Vanes with large chord lengths should be used in preference to those with small chord lengths.

2-4.3 Thick Vanes

Although it is expected that thick vanes would not be employed for the present application, some performance data are presented for comparison with sheet-metal-vane performance. The performances of thick vanes

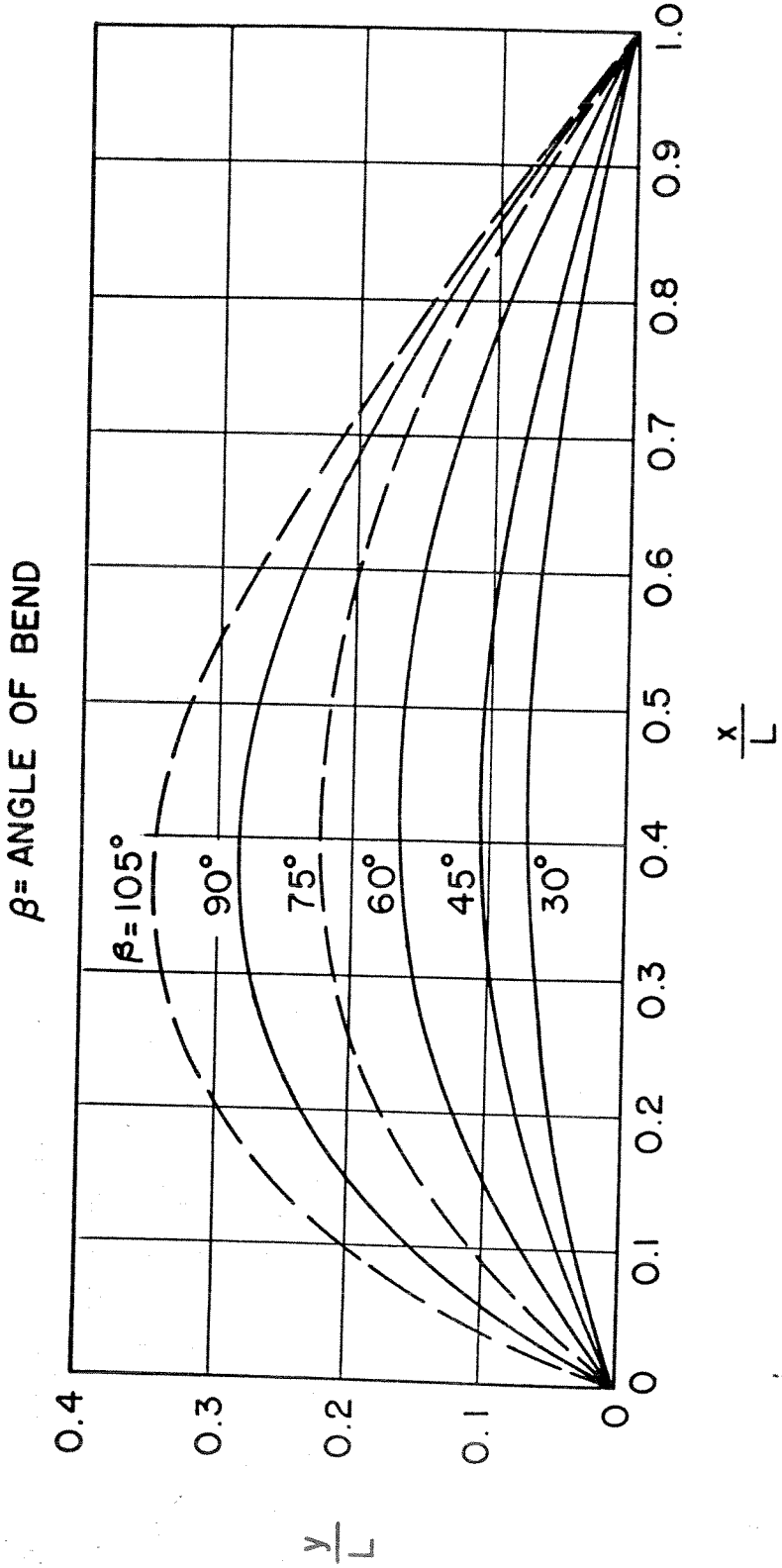

FIG. 2-14 DESIGN DATA FOR KROEBER THIN VANE PROFILES

TABLE 2-1 ORDINATES FOR KROEBER THIN-VANE PROFILES

x/L	y/L			
	90° bend	60° bend	45° bend	30° bend
0.00	0.000	0.000	0.000	0.000
0.05	0.087	0.041	———	———
0.10	0.154	0.074	0.044	0.031
0.15	0.200	0.100	———	———
0.20	0.236	0.124	0.075	0.051
0.25	0.262	0.140	———	———
0.30	0.277	0.153	0.094	0.067
0.35	0.284	0.161	———	———
0.40	0.284	0.166	0.105	0.071
0.45	0.283	0.168	———	———
0.50	0.273	0.164	0.103	0.071
0.55	0.260	0.157	———	———
0.60	0.242	0.151	0.094	0.067
0.65	0.219	0.142	———	———
0.70	0.192	0.129	0.078	0.055
0.75	0.167	0.111	———	———
0.80	0.137	0.096	0.058	0.043
0.85	0.104	0.072	———	———
0.90	0.071	0.048	0.030	0.024
0.95	0.037	0.026	———	———
1.00	0.000	0.000	0.000	0.000

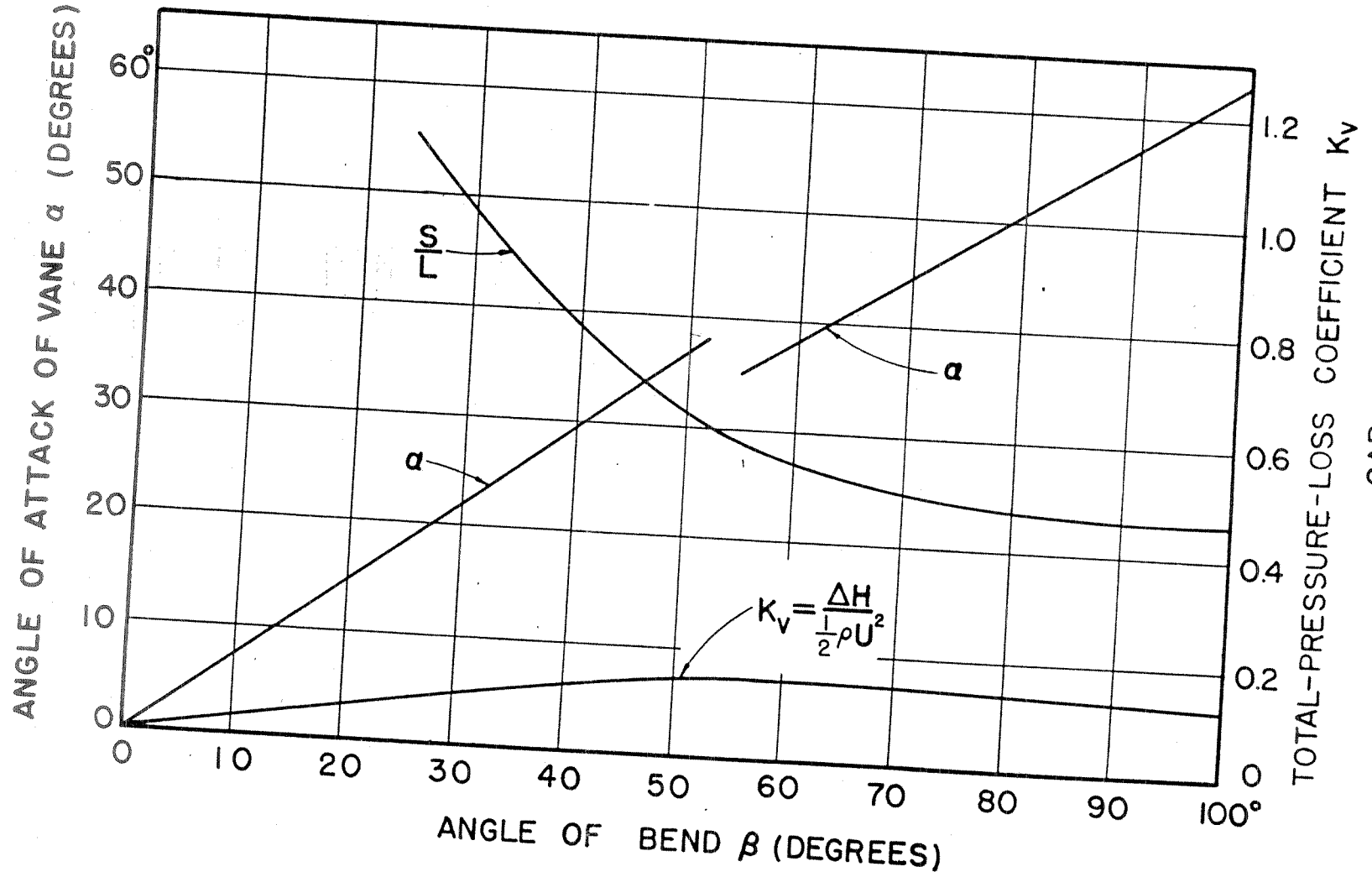

FIG. 2-15 THIN-VANE CHARACTERISTICS

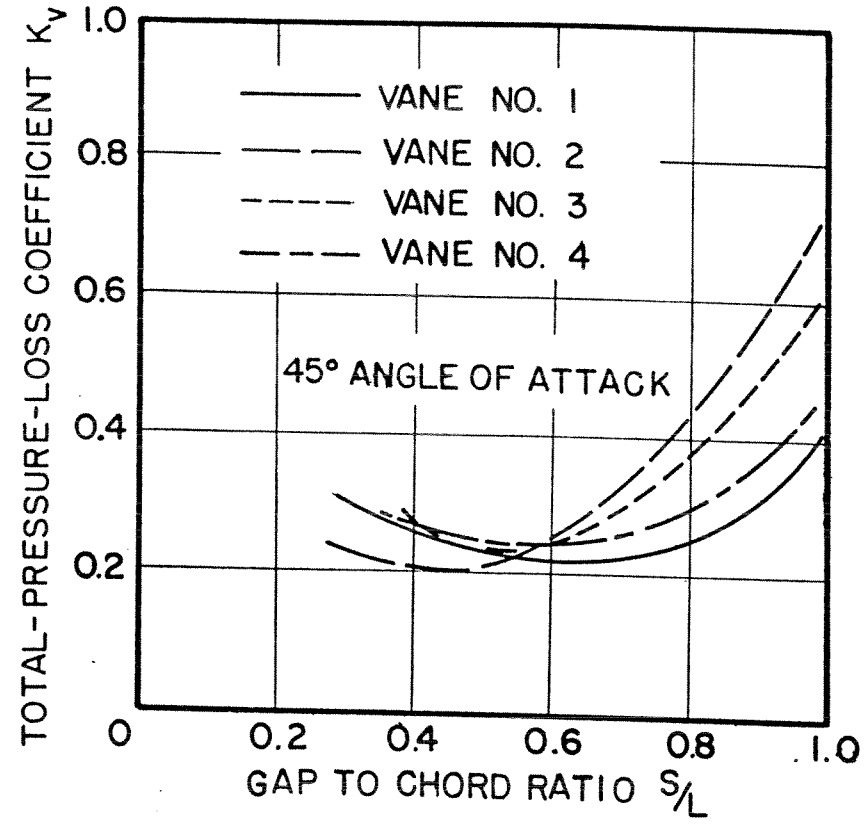

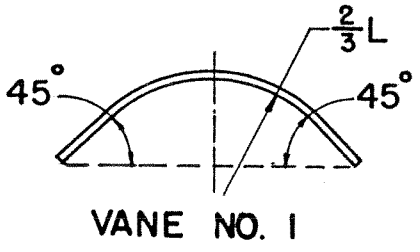

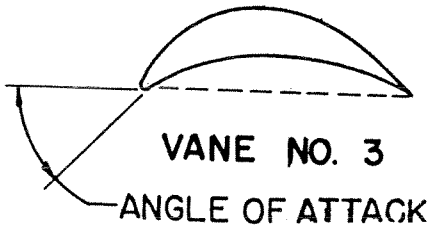

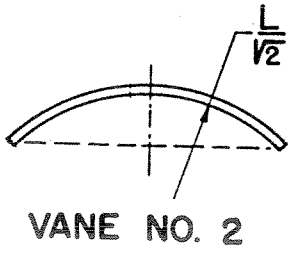

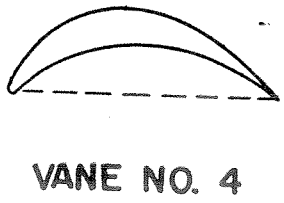

FIG. 2-16 VANE PROFILES FOR 90° BEND

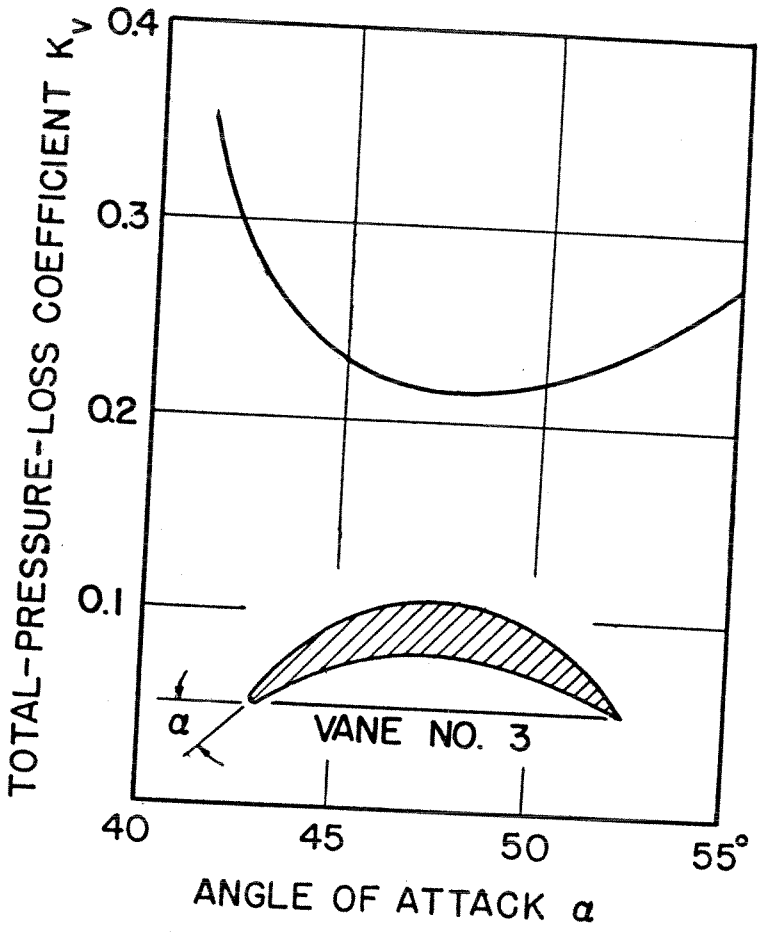

FIG. 2-17 VARIATION OF THE PRESSURE-LOSS COEFFICIENT WITH ANGLE OF ATTACK OF A THICK VANE IN 90-DEGREE BEND

and circular arc sheet-metal vanes are shown in Fig. 2-16. The profile of Vane No. 1 is a circular arc with radius 2L/3 joined tangentially to two straight lines inclined at 45° to the chord. The profile of Vane No. 2 is the arc of a quarter-circle (radius $L/\sqrt{2}$). Vane No. 3 has a thick profile resembling the shape used in a wind tunnel. The maximum thickness is near the center of the chord. The profile of Vane No. 4 is a modification of a foreshortened RAF 30 section arranged along a circular arc, the maximum thickness being located about one-third the chord length from the leading edge. The profiles of Vanes No. 3 and 4 are given in Ref. 75. Experiments show that the most uniform velocity distribution is obtained with Vanes No. 2 and 3.

With regard to the coefficient K_v, the graph of Fig. 2-16 shows that the minimum value is obtained for definite gap-to-chord ratio. Further, it appears that the difference between values of K_v for the thin and thick vanes is not appreciable.

The graph of Fig. 2-16 is plotted for the angle of attack $\alpha = 45°$. In Fig. 2-17 the influence of the angle of attack is shown; the optimum angle is about 48°. The same value was found for thin circular-arc vanes. Clearly, small variations from the optimum angle have small influence on the pressure losses of the thick vanes. For these vanes values of C_L from 0.9 to 1.0 may be used in Eq. 2-7 to determine the number of vanes.

2-5 Internal Inlets

An internal inlet taps air from a chamber in which the air is essentially stagnant. Figure 2-18 shows pressure losses for a few such inlets. It may be seen that flared types have low pressure-loss coefficients. The lowest pressure-loss coefficient was obtained using a lemniscate for the inlet profile.

2-6 External Air Intake Scoops

An external inlet takes air aboard from the flow outside. It is a normal requirement of such a duct intake that it recover practically the entire total pressure corresponding to the flight speed of the airplane. The

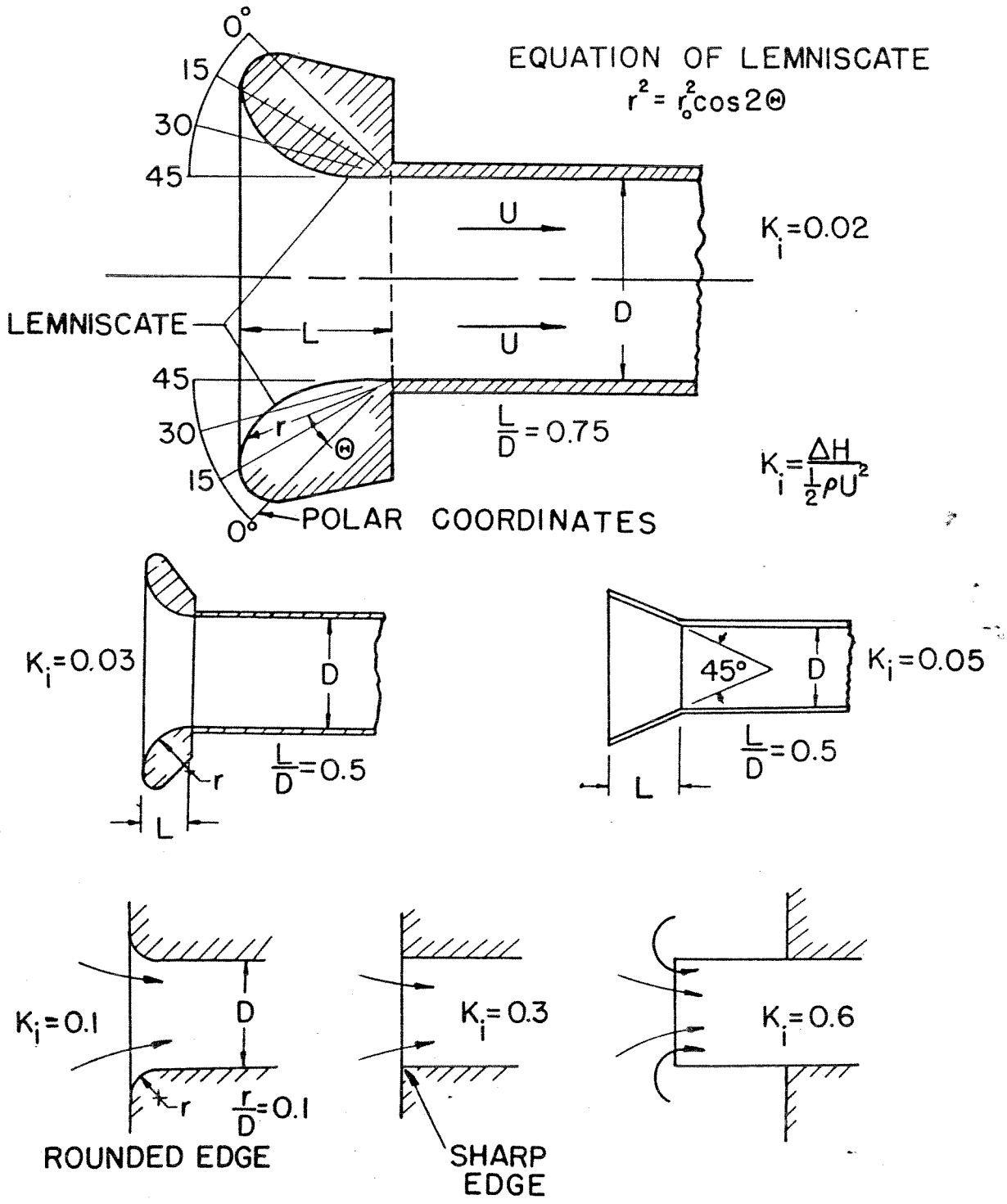

FIG. 2-18 TOTAL-PRESSURE-LOSS COEFFICIENTS FOR INTERNAL INLETS

influence of the boundary layer, velocity ratio, and angle of attack on total-pressure distribution at the scoop entrance may be seen on Fig. 2-19.

The shape of the scoop inlets was nearly rectangular with well rounded corners. The profile coordinates of the scoops may be found in Ref. 6. Scoops a, b, and c and Scoops d, e, and f were mounted at distances from the nose equal to 9.5 per cent and 37 per cent fuselage length, respectively.

Scoops d, e, and f were similar except for the method used to separate the boundary-layer air from the inlet air. The boundary layer approaching Scoop d was bypassed under a screen and taken into the scoop with the rest of the air. Scoop e was entirely outside the layer, and provisions were made to divert the boundary layer around the scoop. In order to prevent any spillage of boundary layer into Scoop f, a metal sheet of length equal to the height of the inlet was extended forward of the scoop.

Employing a few empirical principles as a guide, the designer can devise a scoop whose performance is satisfactory for the present application. The performance should finally be checked by tests. Dearborn and Silverstein (Ref. 34) suggest some of the following rules for the design of efficient scoops.

2-6.1 Scoop Location

It may happen that the scoop is in a region where the boundary layer is thick. Since the mean dynamic pressure of the boundary layer is smaller than the dynamic pressure of the air at the outer edge of the boundary layer, the performance can be improved by placing the scoop above the boundary layer. Assuming that the mounting surface of the scoop can be considered as a flat plate, the boundary-layer thickness on a flat plate may be used as a guide for determining the distance between the mounting surface and the lower edge of the scoop inlet. Thus, if the flow is turbulent, the height would be

$$\delta = 0.37 \cdot \left(\frac{\nu s^4}{U_1}\right)^{1/5} \qquad (2\text{-}9)$$

where s is the profile distance from the forward stagnation point to the

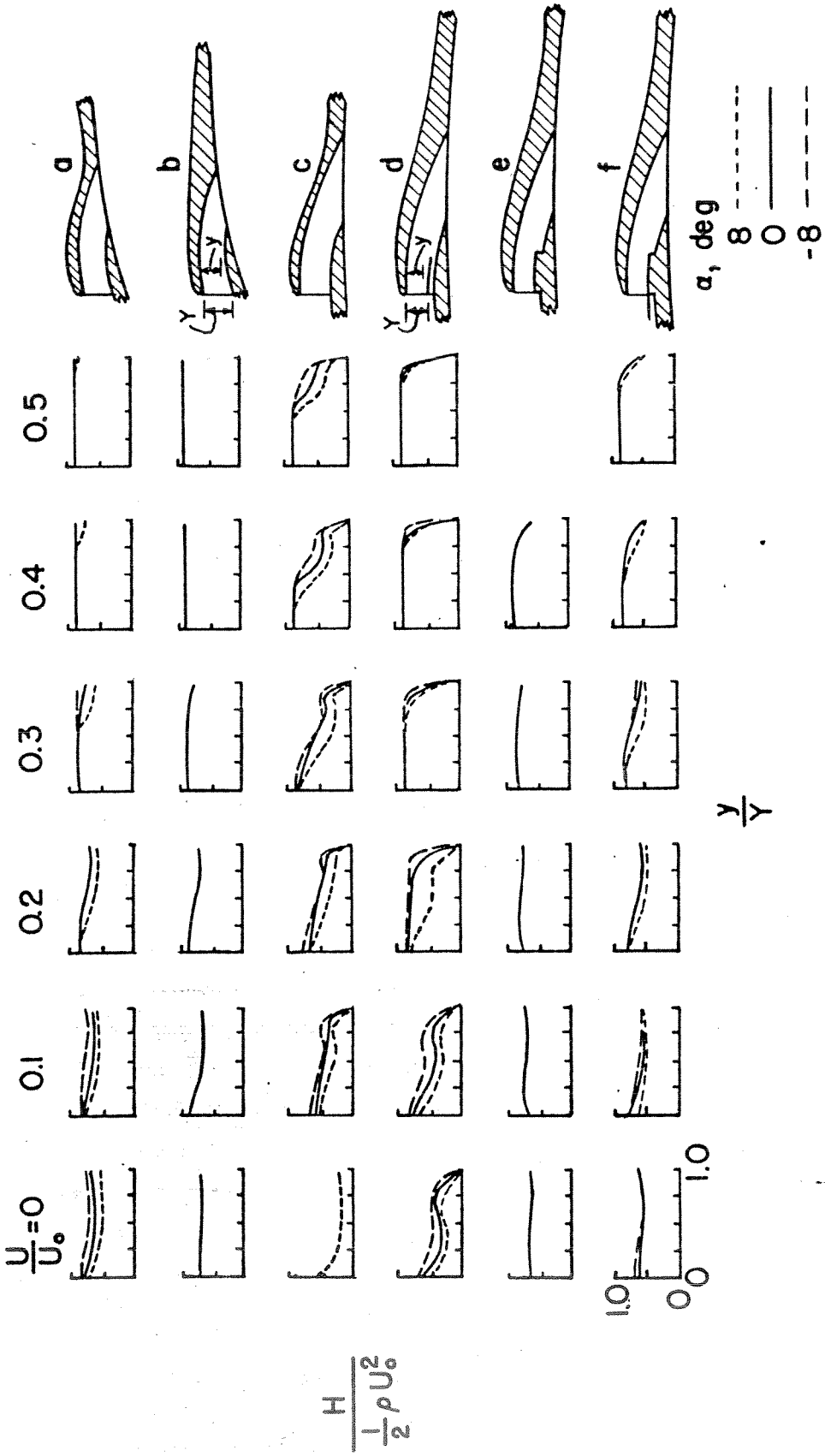

FIG. 2-19 DISTRIBUTION OF TOTAL PRESSURE IN SCOOP ENTRANCES

scoop inlet, and U_1 is the velocity which would occur at the outer edge of the boundary layer if the scoop were not there.

2-6.2 Scoop Area

The scoop entrance area should be designed for air inlet velocity of 0.5 of 0.6 of the free stream velocity. It may be assumed that the total pressure at the scoop entrance is free stream static plus 0.9 free stream dynamic pressure. Employing these factors in conjunction with a given rate of flow through the intake, the designer can calculate the area of the entrance and the static pressure at the entrance.

2-6.3 Scoop Shape

The shape of the lips should be similar to an airfoil shape. A sharp-edge scoop should not be used.

The afterbody behind the maximum scoop section must be well shaped and sufficiently long to avoid flow separation. Four times the scoop height should generally suffice.

For air intakes other than scoops Ref. 33 and 78 may be consulted.

2-7 Sudden Contraction and Expansion

When a sudden enlargement of the flow passage occurs (no diffuser), the kinetic energy of the fluid in the small conduit is not fully recovered; the losses are called expansion losses.

When a stream flows from a large conduit through a sharp-edge entrance into a small conduit, large losses may occur on account of separation and subsequent incomplete recovery. These losses are called contraction losses. If the entrance is round, the separation may not occur; the losses would be mainly frictional and could be neglected with respect to other losses in the system.

In both cases the drop of the total pressure is obtained by multiplying the dynamic pressure in the smaller duct by the corresponding loss coefficient. Total-pressure-loss coefficients K_c and K_{ex} for contraction and

expansion, are shown in the graphs of Fig. 2-20 and -21, respectively. The values of K_{ex} are theoretical (Ref. 46). The values of K_c are experimental (Ref. 37); results of several investigators (Ref. 58 and 88) fall below the values presented in Fig. 2-20 as much as 25 per cent in some instances.

2-8 Diffusers

The purpose of a diffuser is to transform kinetic energy into pressure when the air flows from a duct of small cross-sectional area to a region of large cross section. Theoretically, we could immediately predict the increase in pressure using Bernoulli's equation. However, the transition introduces losses due to wall separation, eddying motions, and friction. The losses of a long diffuser of gentle taper are mainly due to friction. In a short diffuser the walls may be so divergent that the conditions of a sudden expansion (Section 2-7) are approached. In practice an intermediate configuration is needed.

The pressure drop of a diffuser depends upon the angle of expansion, the inlet and discharge lengths, and the area ratio. The characteristics of some diffusers are summarized in the following sections.

Assuming an incompressible flow and uniform velocity distribution over the cross section, the pressure drop of a diffuser may be obtained from the following equation:

$$\frac{\Delta H}{\frac{1}{2}\rho U_1^2} = C\left(1 - \frac{A_1}{A_2}\right)^2 \qquad (2\text{-}10)$$

Thus, the total-pressure loss is expressed as a fraction of a dynamic pressure based on the difference between the inlet and outlet velocities. The total-pressure-loss-coefficient factor C used in Eq. 2-10 is shown in the graphs of Fig. 2-22 and -23, which were obtained from Ref. 46.

2-8.1 Influence of the Angle of Expansion

It may be observed from Fig. 2-22 that the angle of expansion for least loss falls in the range 6° to 8° for a conical diffuser, 6° for a

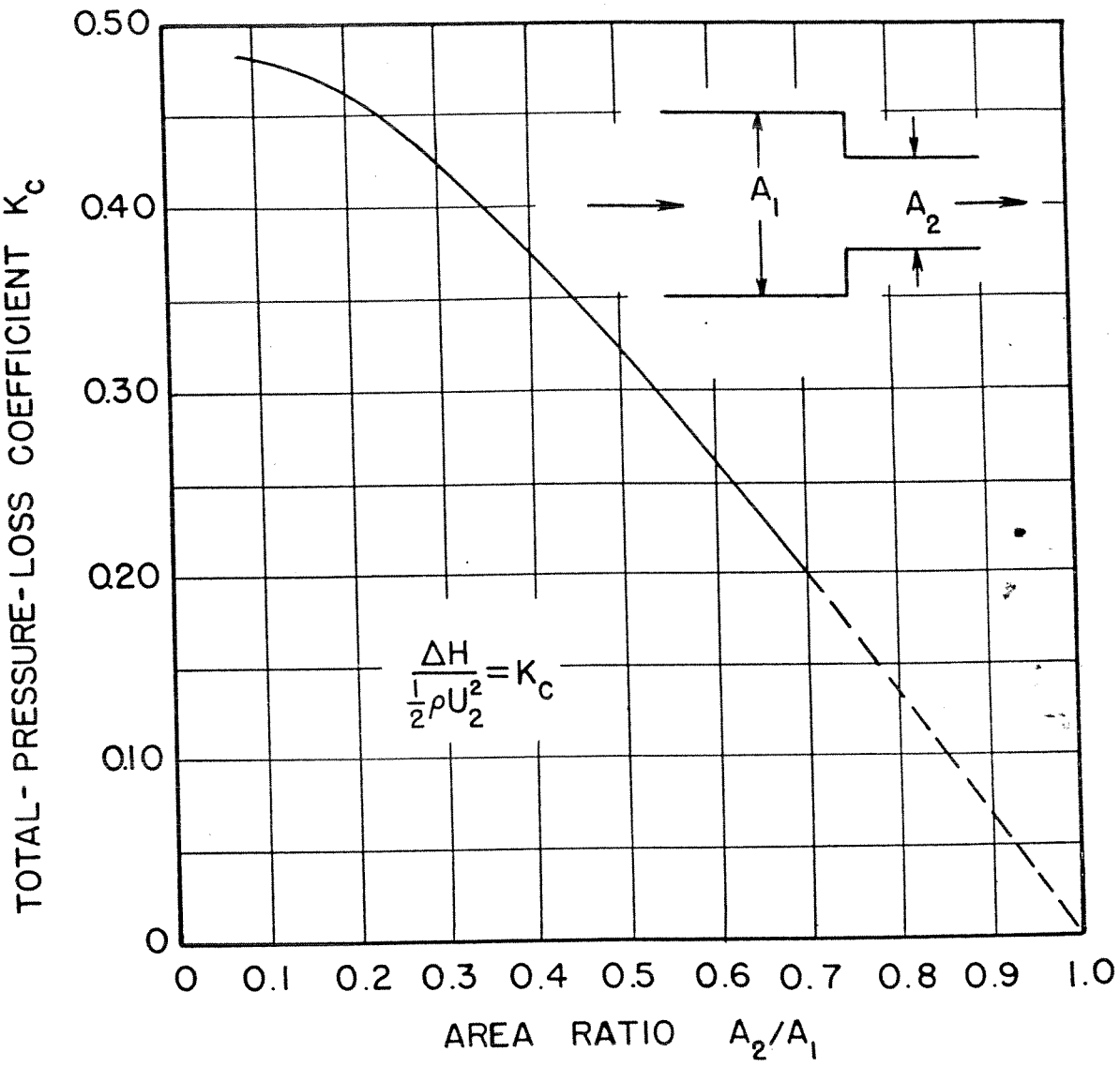

FIG. 2-20 TOTAL-PRESSURE-LOSS COEFFICIENT FOR SUDDEN SHARP-EDGE CONTRACTION

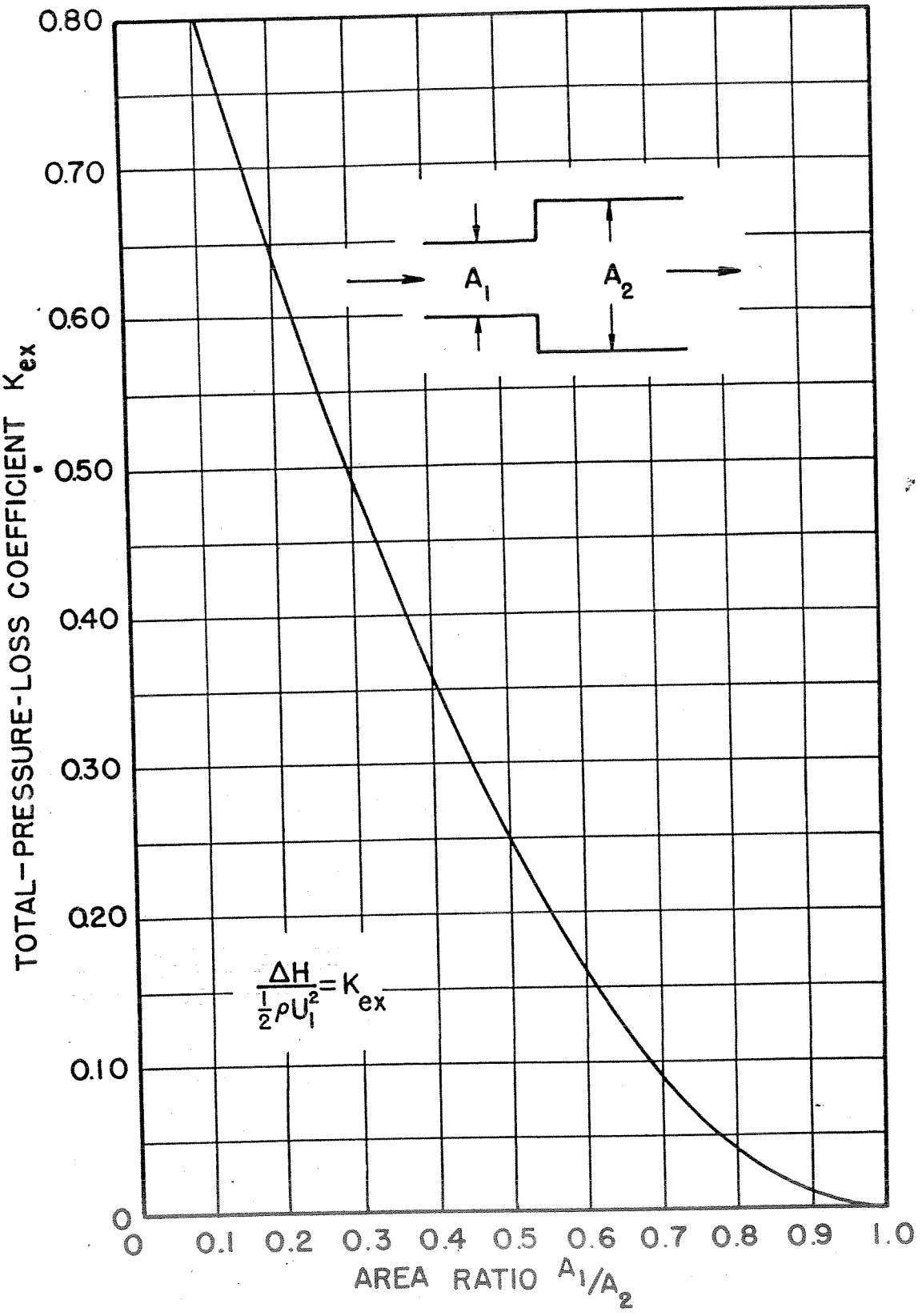

FIG. 2-21 TOTAL-PRESSURE-LOSS COEFFICIENT FOR SUDDEN SHARP-EDGE EXPANSION

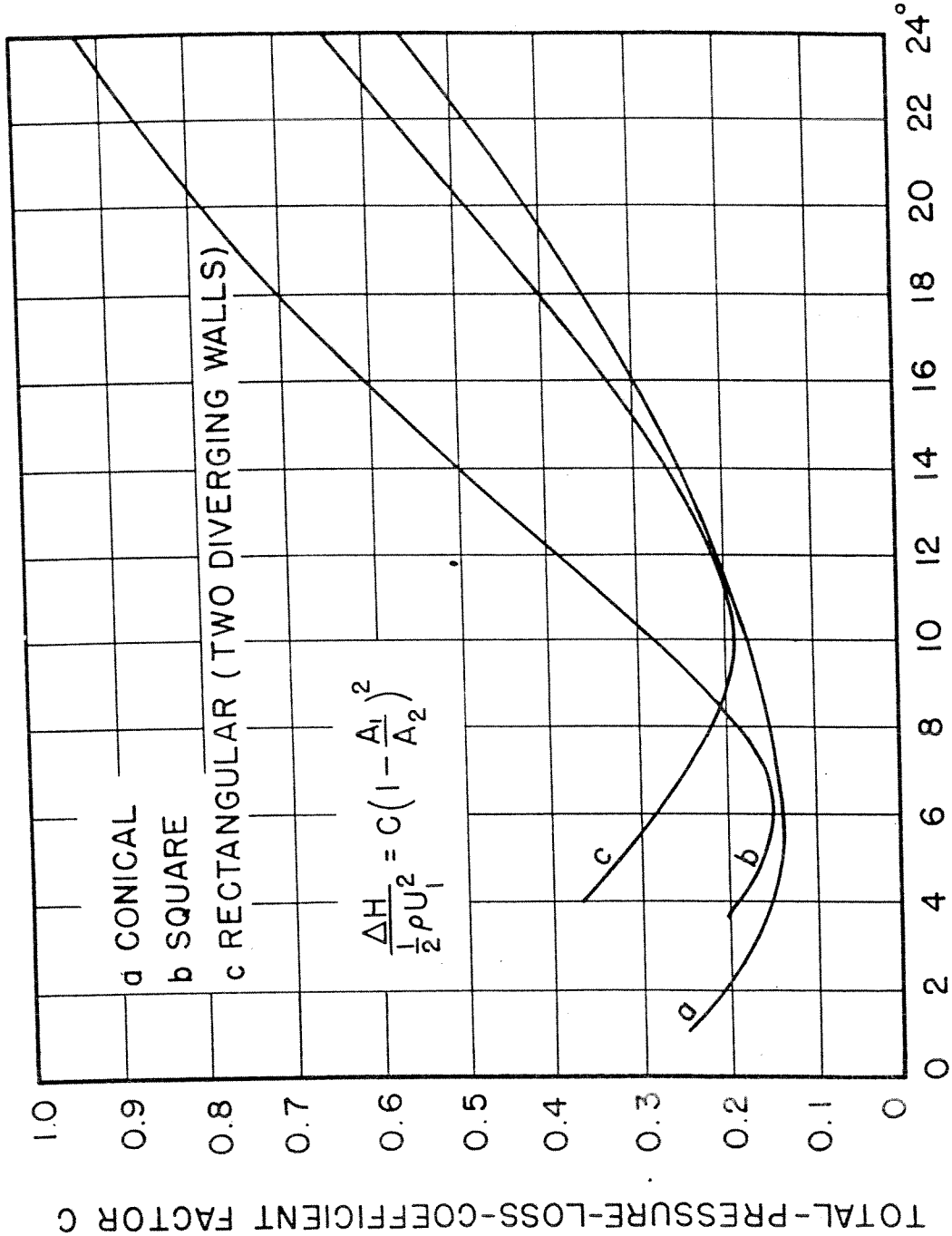

FIG. 2-22 TOTAL-PRESSURE-LOSS-COEFFICIENT FACTOR C FOR STRAIGHT-WALL DIFFUSERS

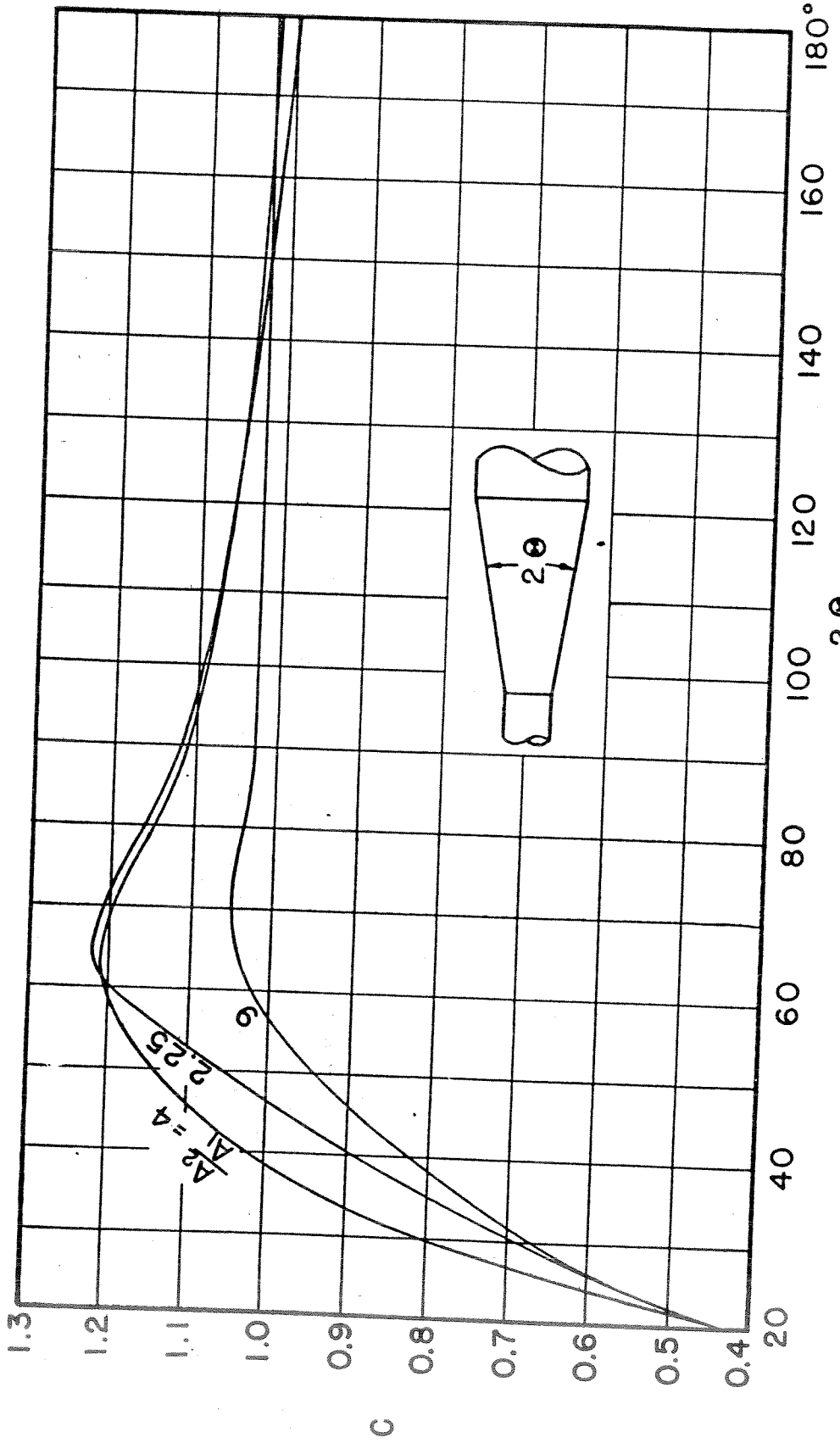

FIG. 2-23 TOTAL-PRESSURE-LOSS-COEFFICIENT FACTOR FOR CIRCULAR DIFFUSERS

diffuser with a square section throughout, and 11° for a rectangular diffuser with one pair of walls diverging and one pair parallel. For angles greater than 11°, the pressure loss of a rectangular diffuser (two walls diverging) is considerably less than that of a square diffuser (four walls diverging).

In the range of the angle of expansion from 0° to 24°, the factor C is virtually independent of the ratio of the outlet area to the inlet area (A_2/A_1). Figure 2-23 shows how the area ratio affects conical diffusers of area ratio 4 and 9. The factor C reaches a maximum value in the range from 60° to 70° and then gradually falls to the value of 1.0 corresponding to an abrupt expansion loss to an infinitely large area (cf. Fig. 2-21). Obviously, small angles of expansion are desirable from the viewpoint of good design.

2-8.2 Influences of Inlets and Exits

The length of straight duct preceding the diffuser influences the velocity distribution at the inlet. The diffuser efficiency[1] decreases as the inlet length increases because the boundary-layer thickness at the entrance becomes larger. A thick boundary layer (due to a long inlet duct) will decrease the efficiency of the diffuser by about 7 per cent in the range of 2θ between 5 and 30 degrees. Hence, the diffuser should be placed into the system as far upstream as possible. This also has the advantage of decreasing the duct losses.

The discharge length following the diffuser improves the efficiency. According to Ref. 105, if a short length of duct precedes the diffuser the discharge length should be about four times the maximum width or diameter of the diffuser. If a long duct is ahead of the diffuser, the discharge length should be about six times the maximum width.

---

[1] The diffuser efficiency is the ratio of the static pressure increase to the change of dynamic pressure.

2-8.3 Design for Large Area Ratio

In practice the length of the diffuser is often determined by the amount of space available. Therefore, when a large change of area must occur in a short distance some compromise must be reached and the data presented above can be only a guide to the loss in the configuration finally selected. One such compromise is to diffuse the air partially and to follow the diffuser with an abrupt expansion (Ref. 14).

Another method is to use a curved wall diffuser. The profile of a curved diffuser is shown in Fig. 2-24. Reference 59 gives the following equation for the coordinates of this profile:

$$y\left[1 + \frac{x}{L}\sqrt{\frac{A_1}{A_2} - 1}\right] = \frac{D_1}{2} \qquad (2\text{-}11)$$

The total-pressure-loss-coefficient factor C of this diffuser also is given in Fig. 2-24. Experiments performed by Gibson (Ref. 46) lead to the conclusion that the diffuser can be improved most effectively by curving the walls in the range of $2\Theta_2$ from 15 to 30°.

2-8.4 Design of Non-Circular Diffusers

A few data for non-circular diffusers are discussed in Section 2-8.1. Where those data are not applicable, Ref. 59 suggests the use of a so-called "equivalent conical diffuser" which is a diffuser of circular cross section having the length and the inlet and outlet areas equal to those of the non-circular diffuser. Berry (Ref. 14) suggests a similar method of treatment.

2-9 Orifices

The distribution of air flow in double-skin passages is often controlled by providing suitable outlet orifices at the end of the passages. Reference 37 gives the following expression to obtain the diameter of an orifice at the end of a tube for a required static-pressure loss and a known weight rate of air flow:

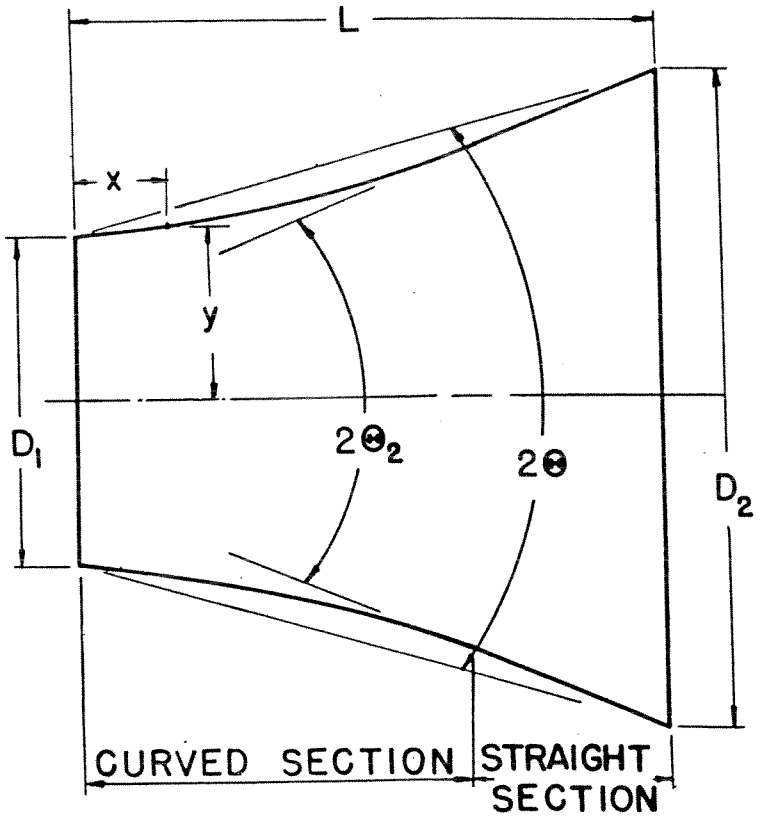

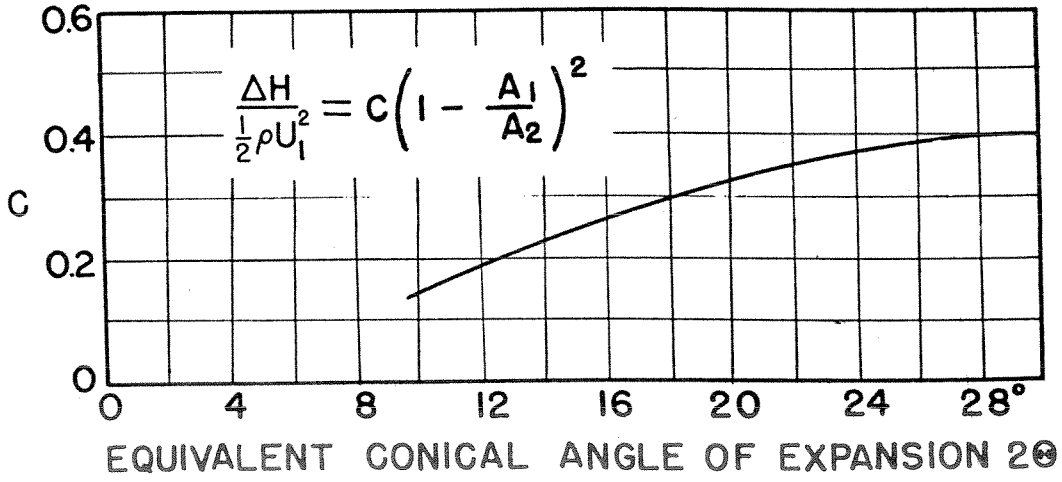

FIG. 2-24 TOTAL-PRESSURE-LOSS-COEFFICIENT FACTOR C FOR CURVED WALL CONICAL DIFFUSER

$$\frac{K_o\left(\frac{A_2}{A_1}\right)}{\sqrt{1-\left(\frac{A_2}{A_1}\right)^2}} = \frac{w}{65{,}790\, A_1 \sqrt{\gamma(p_2 - p_1)}} \qquad (2\text{-}12)$$

where K_o is the coefficient of discharge shown in Table 2-2; A_1 and A_2 are the areas of the double-skin cross section and of the orifice, respectively; $[w]$ = lb/hr, $[\gamma]$ = lb/ft^3; $[p]$ = in.-water; and $[A_1]$ = ft^2. For convenience of calculation, the left-hand member of Eq. 2-12 is presented as a function of A_2/A_1 in Table 2-2.

TABLE 2-2 COEFFICIENTS OF DISCHARGE THROUGH ORIFICES

	A_2/A_1								
	0.1	0.2	0.3	0.4	0.5	0.6	0.7	0.8	0.9
K_o	0.604	0.612	0.625	0.643	0.666	0.695	0.730	0.770	0.840
$\sqrt{\frac{1}{1-\left(\frac{A_2}{A_1}\right)^2}}$	1.005	1.02	1.047	1.09	1.15	1.25	1.40	1.66	2.29
$\frac{K_o\left(\frac{A_2}{A_1}\right)}{\sqrt{1-\left(\frac{A_2}{A_1}\right)^2}}$	0.061	0.125	0.196	0.280	0.383	0.521	0.715	1.023	1.73

2-10 Exit Openings

The pressure loss of an outlet to the atmosphere depends upon the configuration of the system, the position of the outlet relative to other plane components, and the velocity of the free stream outside of the exit. The main consideration in design of an air outlet should be given to the prevention of flow separation outside of the outlet. Becker (Ref. 9) suggests that the desired conditions for any outlet location are obtained by making the streamlines of both internal and external flow parallel. Under this

circumstance it may be assumed that the static pressure at the outlet is equal to the free stream pressure near the outlet.

Results of experiments on several exits are presented in Ref. 109. The tests were performed with main stream velocities of 40 and 80 miles per hour, and the correlations of the pressure losses were virtually independent of those velocities. Rogallo's graphs present $p_B/(\frac{1}{2}\rho U_o^2)$ as a function of the dimensionless discharge ratio $Q/(A\,U_o)$. The ordinates in the graphs of Fig. 2-25, -26, and -27 are related to Rogallo's ordinates by the equation,

$$\frac{\Delta H}{\frac{1}{2}\rho U_o^2} \equiv \frac{H_B - H_o}{\frac{1}{2}\rho U_o^2} = \frac{p_B}{\frac{1}{2}\rho U_o^2} + \left(\frac{Q}{A\,U_o}\right)^2 - 1 \qquad (2\text{-}13)$$

All static pressures are referred to $p_o = 0$ as datum. Thus, the total pressure of the free stream is $H_o = \frac{1}{2}\rho U_o^2$. Subscript B refers to the position B in Fig. 2-27 and to the plenums in Fig. 2-25 and -26.

The reader may consult Ref. 109 for other types of outlets.

2-11 Branching Ducts

Henry (Ref. 59) presents the sketch of the branched duct shown in Fig. 2-28 and remarks that it illustrates the application of principles of good design. It shows the division of the main stream, the diversion of one stream, and the subdivision of the diverted stream. The dividers have a blunt-nose airfoil shape as, for example, the shape of the NACA 0021 airfoil. To attain best performance of a divider, according to the author, the direction of the flow should be normal to the entrances of branching ducts. Further, he recommends that the cross-sectional areas of the branches be proportioned as nearly as possible to the rates of flow.

Vazsonyi (Ref. 128), combining analytical and experimental results, has correlated in a general way the pressure drop for the case of a duct branching into two ducts as shown in Fig. 2-29 and for the case of two ducts uniting into one duct as indicated in Fig. 2-30.

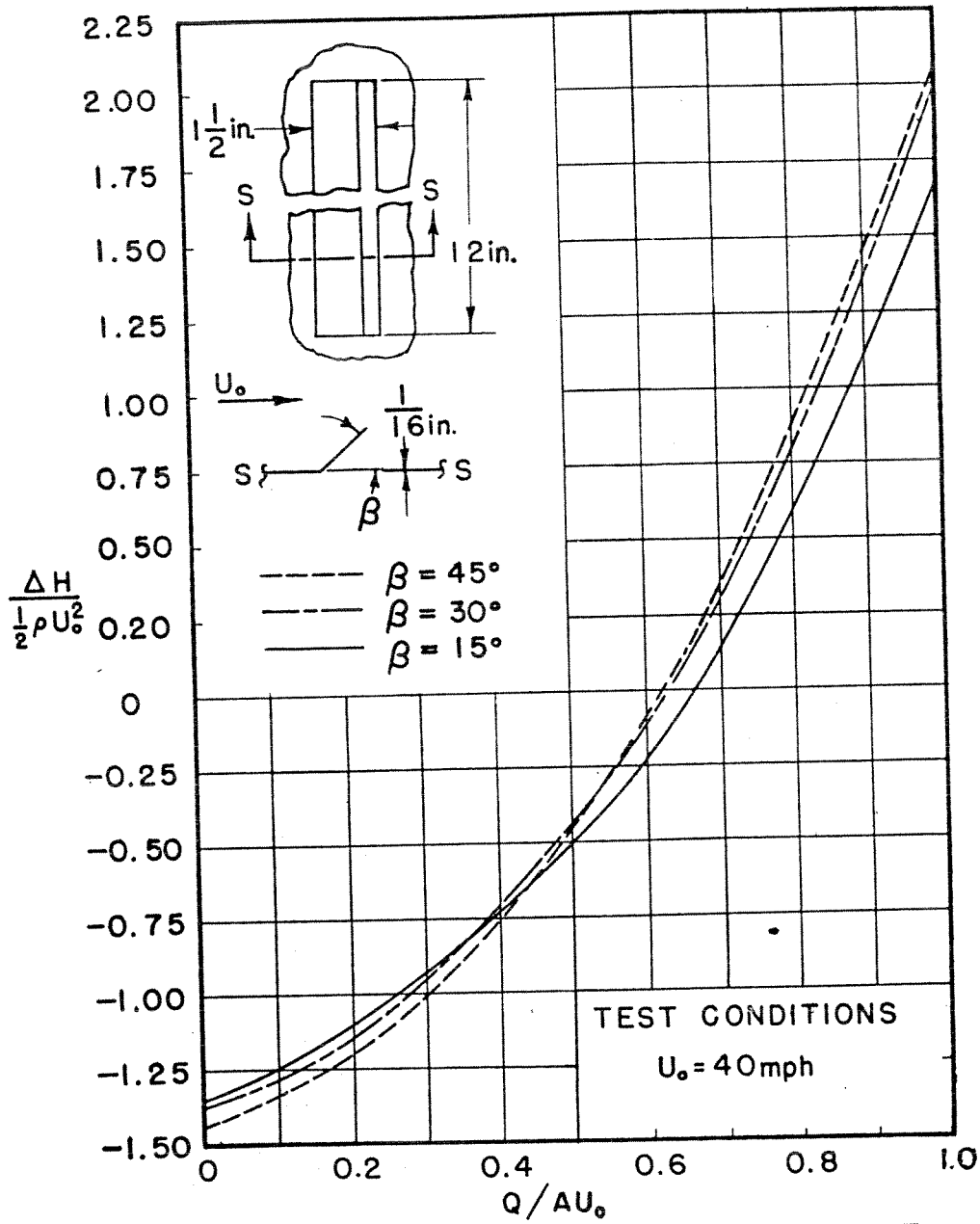

FIG. 2-25 TOTAL-PRESSURE-LOSS COEFFICIENT FOR EXTERNAL FLAP OUTLET IN A FLAT PLATE

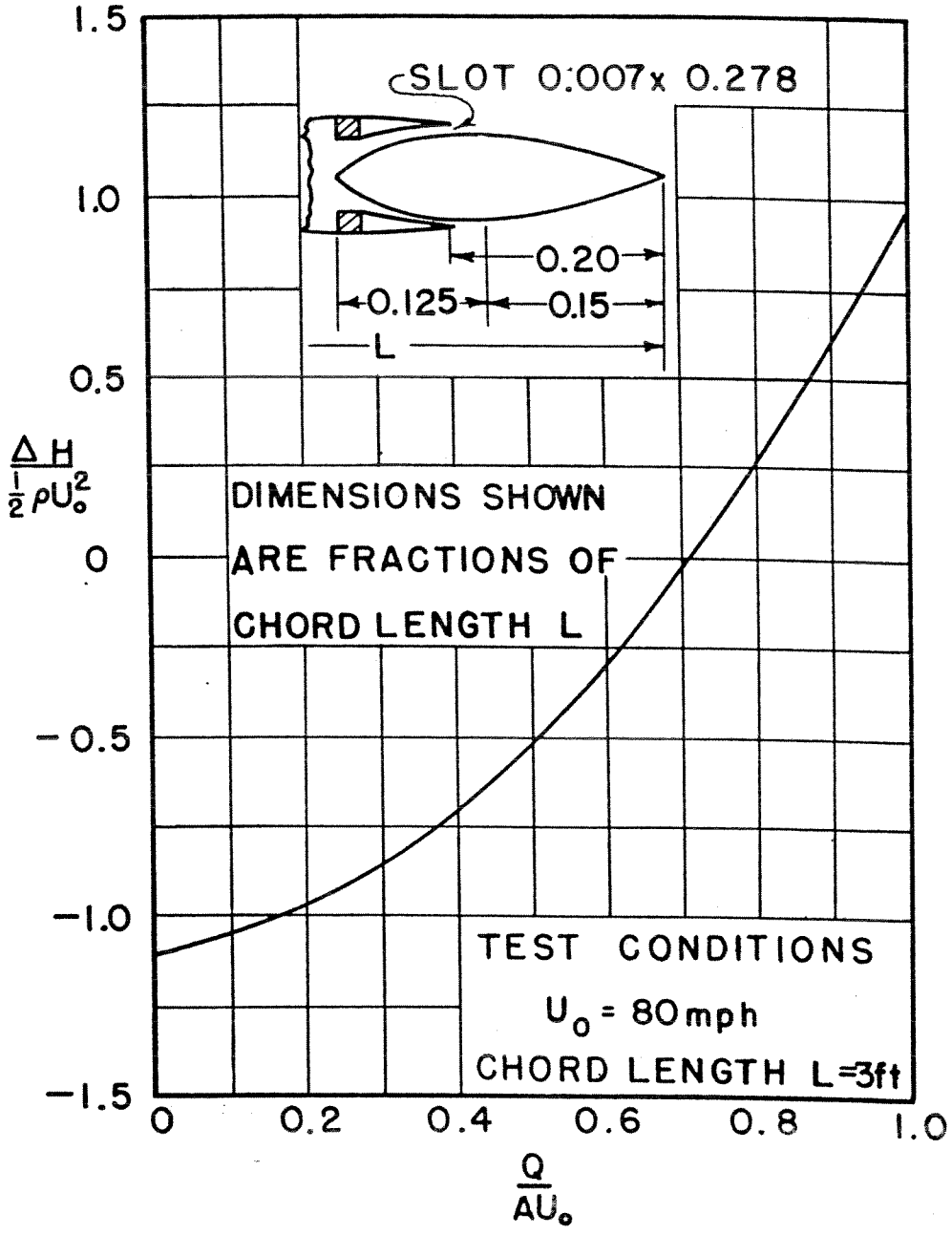

FIG. 2-26 TOTAL-PRESSURE-LOSS COEFFICIENTS FOR FAIRED OUTLET IN AN NACA 0018 WING

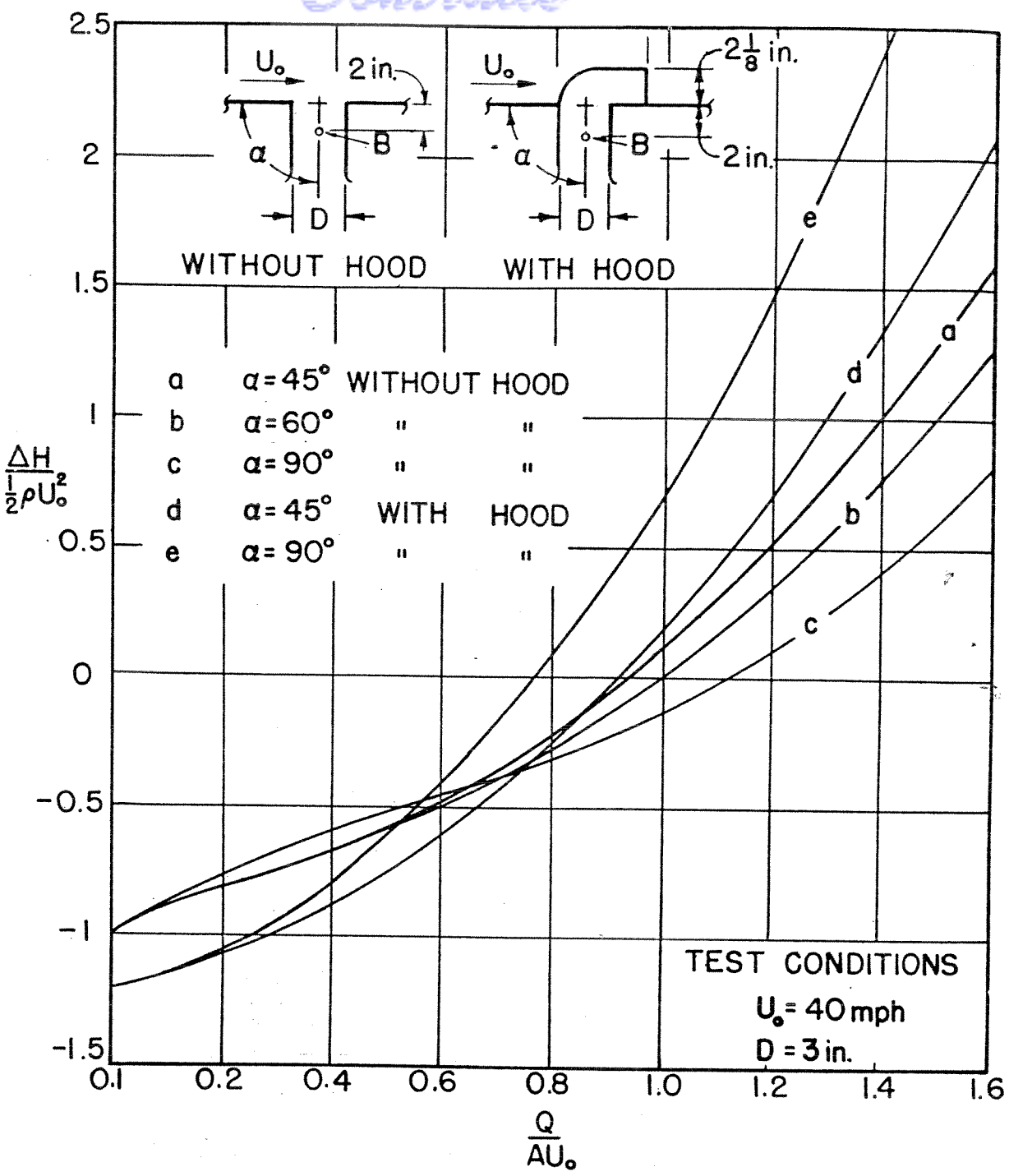

FIG. 2-27 TOTAL-PRESSURE-LOSS COEFFICIENTS FOR A FLUSH CIRCULAR DUCT OUTLET IN A FLAT PLATE WITH AND WITHOUT A HOOD

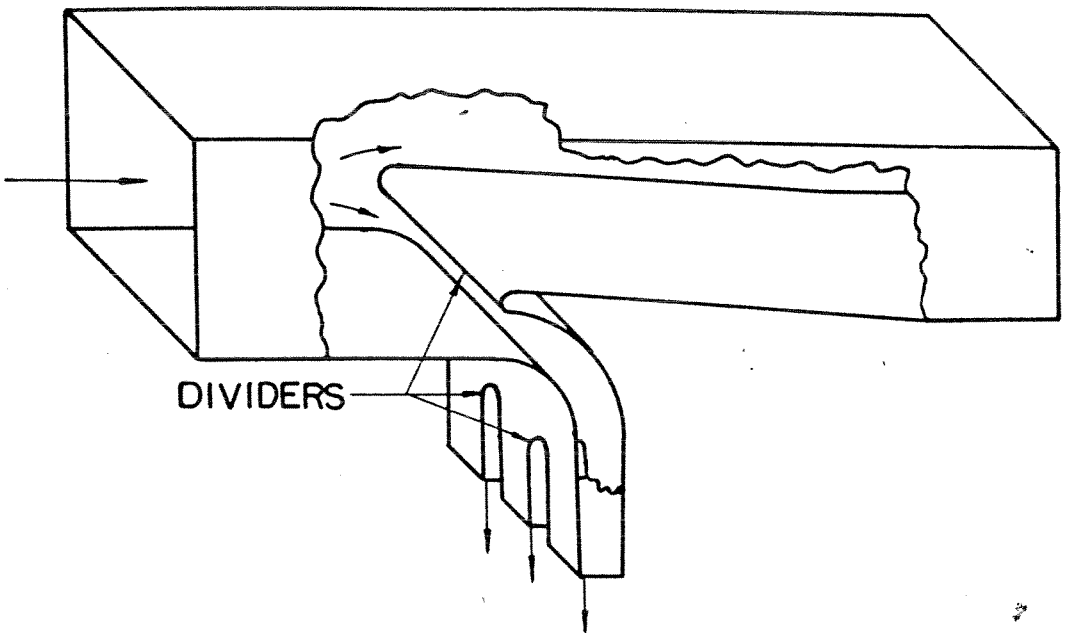

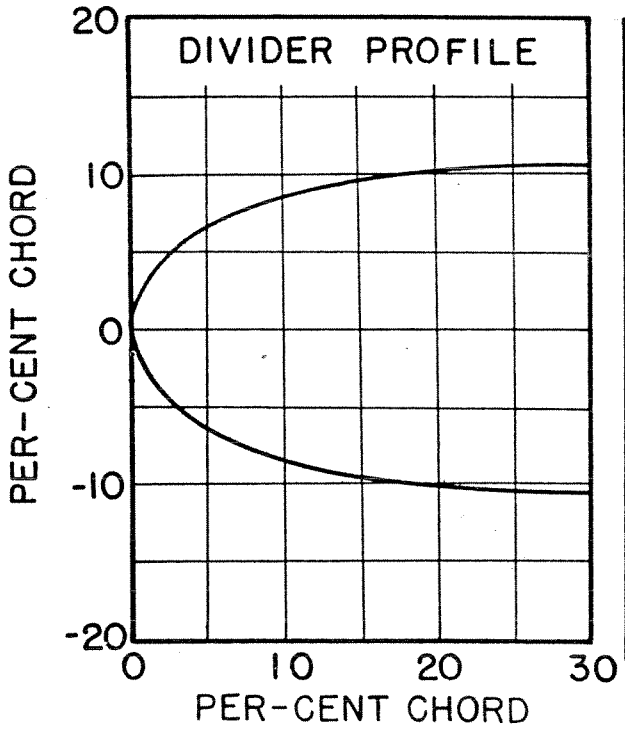

DIVIDER-PROFILE ORDINATE		
STATION PERCENT CHORD	UPPER SURFACE	LOWER SURFACE
0	0	0
1.25	3.31	-3.31
2.50	4.58	-4.58
5.00	6.22	-6.22
7.50	7.35	-7.35
10.00	8.20	-8.20
15.00	9.35	-9.35
20.00	10.04	-10.04
25.00	10.40	-10.40
30.00	10.50	-10.50

FIG. 2-28 DESIGN OF A BRANCHED DUCT (DIVIDER PROFILE NACA 0021 NOSE SECTION)

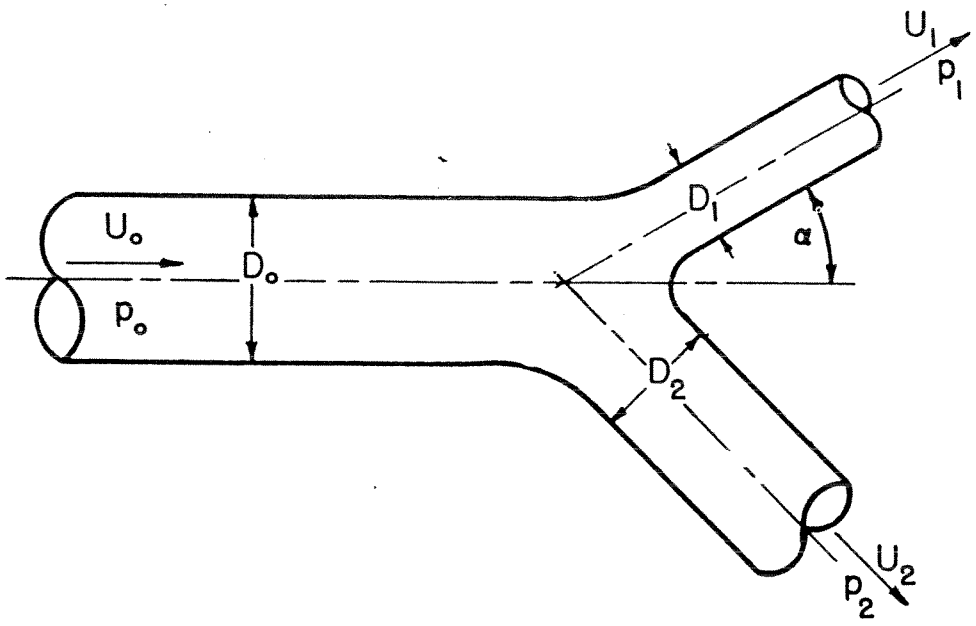

FIG. 2-29 STRAIGHT DUCT BRANCHING INTO TWO DUCTS

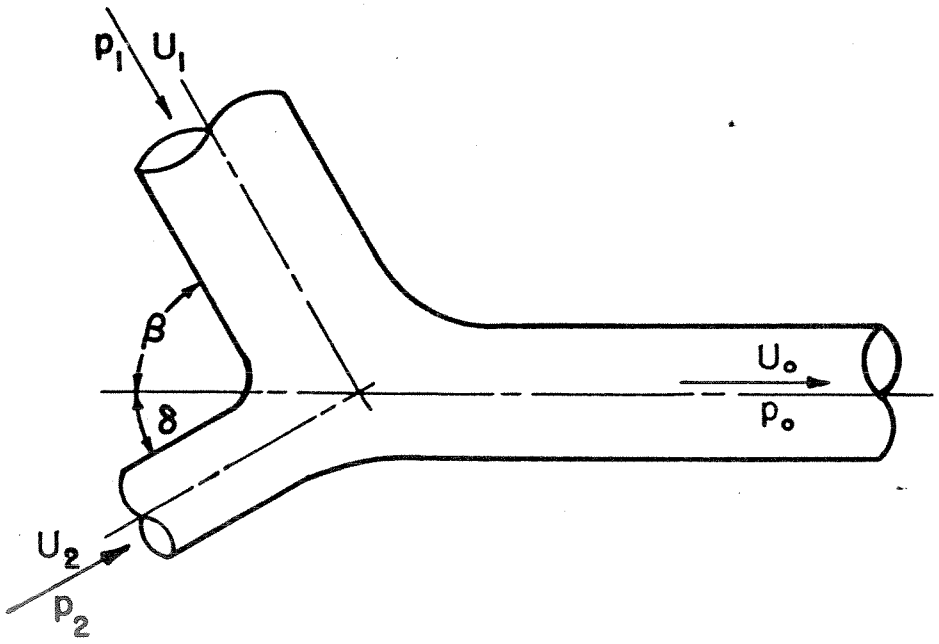

FIG. 2-30 TWO STRAIGHT DUCTS DISCHARGING INTO ONE DUCT

2-11.1 Duct branching into Two Ducts

The total-pressure-loss coefficient may be expressed by

$$\frac{H_o - H_1}{\frac{1}{2}\rho U_o^2} = \lambda_1 + (2\lambda_2 - \lambda_1)\left(\frac{U_1}{U_o}\right)^2 - 2\lambda_2(\cos\alpha_1')\frac{U_1}{U_o} \qquad (2\text{-}14)$$

where the velocities are defined in Fig. 2-29 and α_1', a modified angle of deflection, is a function of the geometric angle of deflection α_1. The quantities λ_1, λ_2, and α_1' are shown in Fig. 2-31 and -32 as functions of the angle α.

To facilitate the calculations, the right-hand member of Eq. 2-14 may be regarded as a function of α and U_1/U_o. The pressure-loss may then be obtained from

$$H_o - H_1 = K_b \cdot \frac{1}{2}\rho U_o^2 \qquad (2\text{-}15)$$

where K_b is given in Fig. 2-34.

Branch No. 2 may be treated in the same way.

2-11.2 Two Ducts uniting into One Duct

In this case, the relationship between pressure loss, fluid velocities, and duct geometry can be represented by the following equation:

$$H_1 - H_o = \frac{1}{2}\rho\left[\lambda_3 U_1^2 + U_o^2 - \frac{2}{A_o}(A_1 U_1^2 \cos\beta' + A_2 U_2^2 \cos\delta')\right] \qquad (2\text{-}16)$$

The meaning of the symbols is shown in Fig. 2-30, the primed quantities representing modified angles of deflection; β', δ', and λ_3 can be obtained from Fig. 2-32 and -33 for known values of β and δ. If $[\rho]$ = slug/ft^3 and $[U]$ = ft/sec, then $[p]$ = lb/ft^2.

For specific experimental information about pressure losses in various 90° and 45° joints and for some discussion of Vazsonyi's work, the reader may consult Ref. 76.

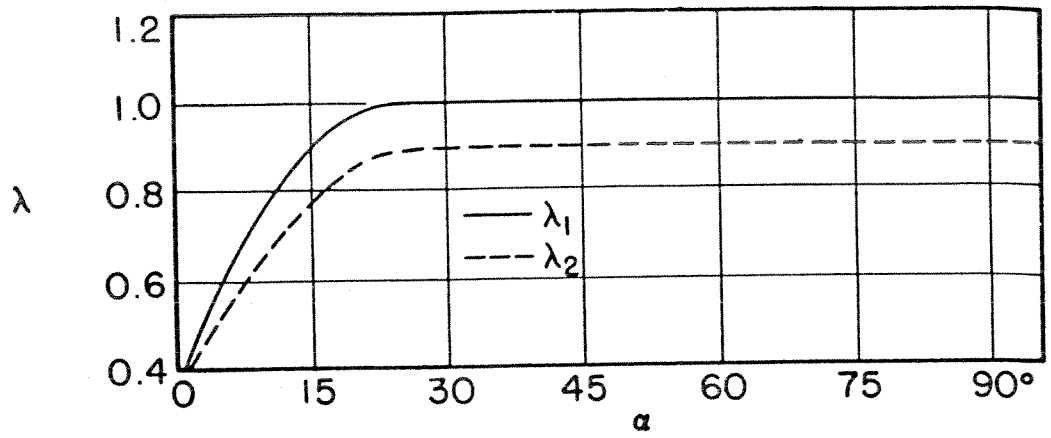

FIG. 2-31 λ_1 AND λ_2 AS FUNCTION OF DEFLECTION ANGLE α

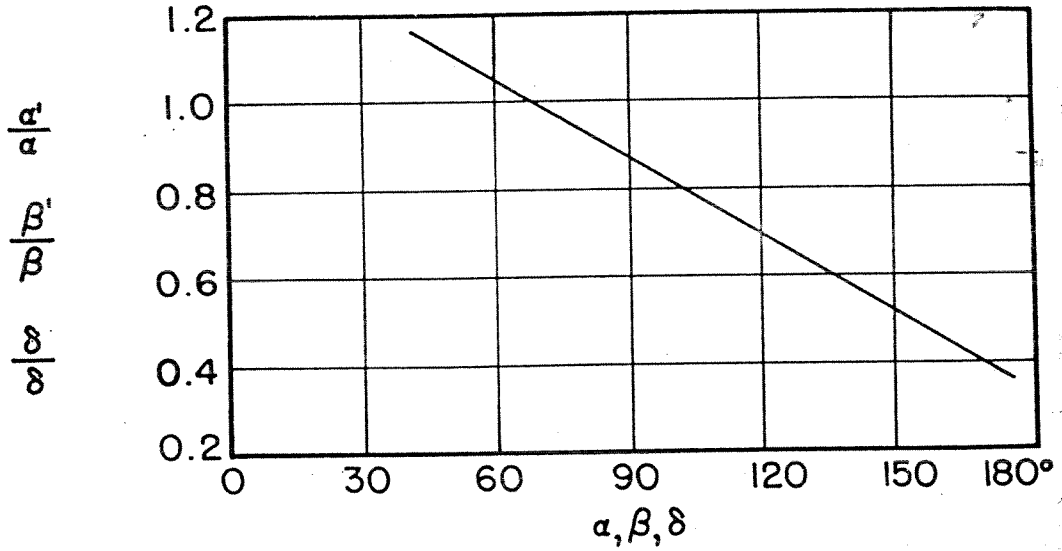

FIG. 2-32. EFFECTIVE ANGLE OF DEFLECTION AS FUNCTION OF DEFLECTION ANGLE

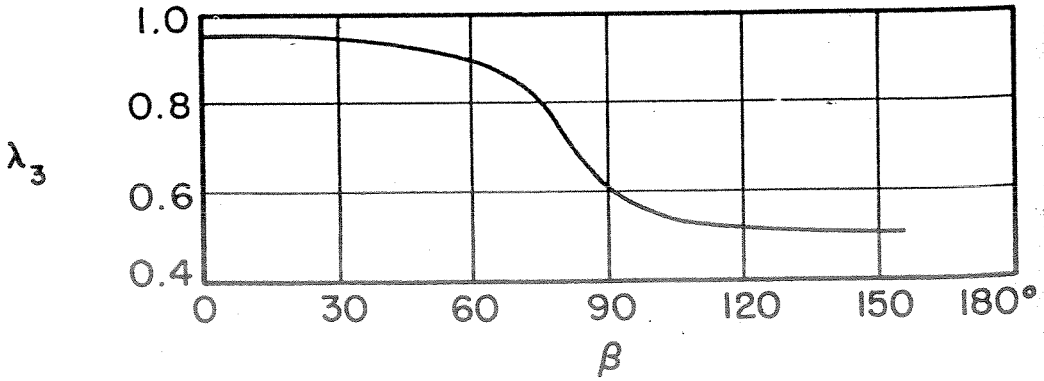

FIG. 2-33 λ_3 AS FUNCTION OF DEFLECTION ANGLE β

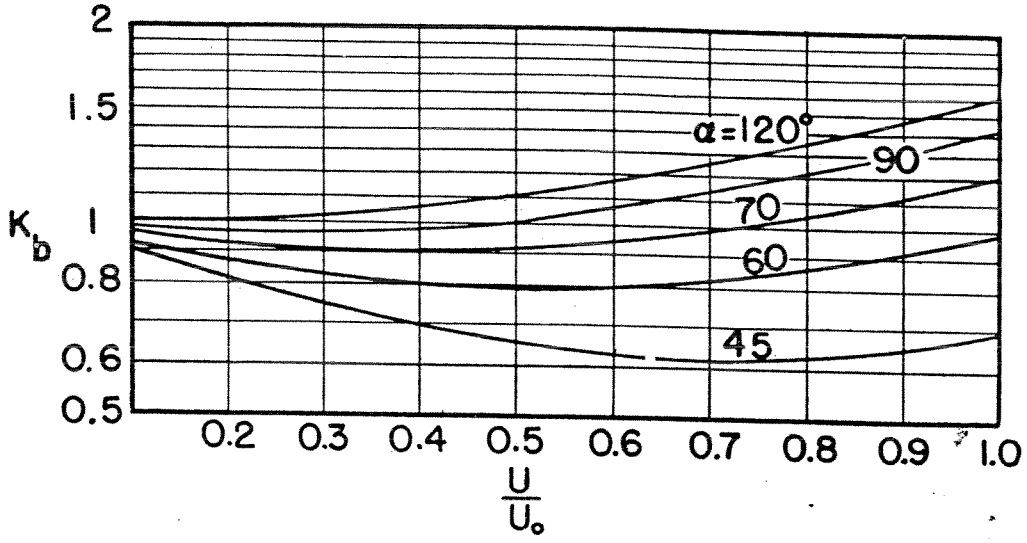

FIG. 2-34 TOTAL-PRESSURE-LOSS COEFFICIENT FOR DIVIDING FLOW IN BRANCHED DUCTS

2-12 Pressure Drop for Compressible Flow

In thin airfoils used for high-speed flight, the air conduits are made small and in high-pressure systems velocities of the air in the ducts may rise to values which require that the air flow in the ducts be considered compressible instead of incompressible.

2-12.1 Parametric Representation

To facilitate the evaluation of pressure losses for compressible flow, a parametric representation is introduced in the manner given by McGann (Ref. 92). It is assumed that the system is one-dimensional and adiabatic. A total absolute temperature at the cross section 1 is defined.

$$T_{tot} = T_1 + \frac{U_1^2}{2Jgc_p} \tag{2-17}$$

where $[T] = {}^\circ R$, $[U] =$ ft/sec, $J = 778$ ft lb/B, $c_p = 0.24$ B/lb F, and $g = 32.17$ ft/sec^2. Because the flow is adiabatic, the total temperature is constant. Introducing a Mach number,

$$M = U/a = U(\kappa gRT)^{-0.5} \tag{2-18}$$

with $\kappa = c_p/c_v$ and $R = 53.3$ ft/F, it may be shown that

$$\frac{T_{tot}}{T} = 1 + \frac{\kappa - 1}{2} M^2 \equiv B \tag{2-19}$$

Also, after some calculations,

$$\frac{B}{\kappa M^2} + \frac{\kappa + 1}{2\kappa} \cdot \ln \frac{M^2}{B} = \frac{B_1}{\kappa M_1^2} + \frac{\kappa + 1}{2\kappa} \ln \frac{M_1^2}{B_1} - f \frac{L}{D} \tag{2-20}$$

Defining

$$C_M \equiv \frac{B}{\kappa M^2} + \frac{\kappa + 1}{2\kappa} \ln \frac{M^2}{B} \tag{2-21}$$

we obtain from Eq. 2-20

$$C_M = C_{M,1} - \frac{fL}{D} \tag{2-22}$$

where $C_{M,1}$ represents an upstream condition and C_M a downstream condition. It may be observed that C_M and $C_{M,1}$ depend upon the respective values of the Mach number.

The equation for the rate of flow of air can be represented by

$$w = 0.9192\ A\ H\ T_{tot}^{-0.5} \cdot \lambda \qquad (2\text{-}23)$$

where A is the cross-sectional area of the duct, ft^2; H is the total pressure, lb/ft^2; and

$$\lambda = \frac{M}{B^3} \qquad (2\text{-}24)$$

is a dimensionless parameter computed using $\kappa = 1.4$. To calculate the rate of flow the following parameters are introduced:

$$\pi_i = \frac{H_i}{p_o} = \frac{H_i}{2116} \qquad (2\text{-}25)$$

$$\theta_i = \frac{T_{tot,i}}{T_o} = \frac{T_{tot,i}}{518.4} \qquad (2\text{-}26)$$

Subscript i refers to any cross section. Equation 2-23 then becomes

$$\frac{w \cdot \theta_i^{0.5}}{\pi_i} = 85.45\ A_i\ \lambda_i \qquad (2\text{-}27)$$

where $[w] = lb/sec$.

2-12.2 Calculation of the Pressure and Temperature Distributions in a Given Duct with Known Initial Conditions

Consider two cross sections 1 and 2 of a duct with known geometry and sizes. Station 1 is an upstream cross section where the static pressure, static temperature, and Mach number are known.[1] Station 2 is

[1] For known static temperature and velocity the Mach number can be found using the graph of Fig. A-2.

an arbitrary cross section downstream. We would like to determine the static pressure, static temperature, and the Mach number at Station 2. A stepwise procedure for performing the calculations is presented below. In Steps 1 through 5 it is assumed that the discharges through both cross sections are equal; that is, the duct is uniform and no branching occurs.

Step 1. Obtain from Fig. 2-35 and -36 the values of λ_1, $C_{M,1}$, $(H/p)_1$, and $(T_{tot}/T)_1$. Then calculate H_1. Observe that $T_{tot,1} = T_{tot,2}$.

Step 2. Estimate the sum of the pressure-loss coefficients including the friction losses. This sum will be of the form,

$$\sum K + \sum \frac{fL}{D_e} \equiv K_{1,2}. \tag{2-28}$$

Step 3. Calculate $C_{M,2}$ in the manner suggested by Eq. 2-22, namely,

$$C_{M,2} = C_{M,1} - K_{1,2}$$

Step 4. Using the value of $C_{M,2}$ from Step 3, find M_2 and λ_2 from Fig. 2-35.

Step 5. With this value of λ_2 calculate H_2 by means of the following equation, which is a general relationship:

$$H_2 = \frac{\lambda_1}{\lambda_2} \cdot H_1 \tag{2-29}$$

Step 6. If the cross-sectional areas of Stations 1 and 2 differ, the following adjustment must be made: The values of $C_{M,2}$ and M_2, found in Steps 3 and 4 should now be regarded as fictitious; however, they are still useful and, in fact, the total pressure H_2 is not changed from the value given by Eq. 2-29. The true value λ_2' is obtained by the relationship,

$$\lambda_2' = \lambda_2 \cdot \frac{A_1}{A_2} \tag{2-30}$$

where A denotes the cross-sectional area. Returning to Fig. 2-35 with

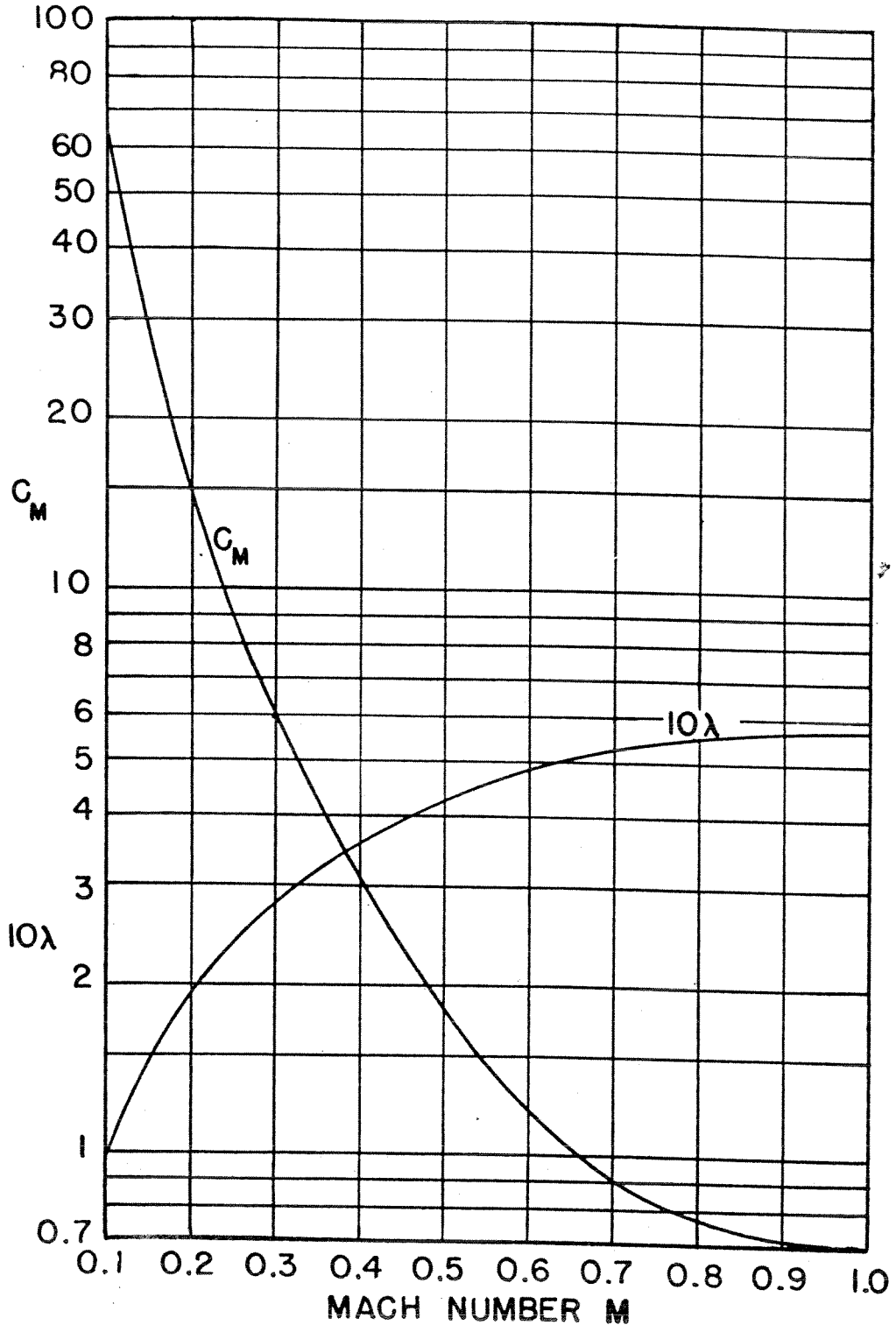

FIG. 2-35 PARAMETER C_M AND λ AS FUNCTION OF MACH NUMBER

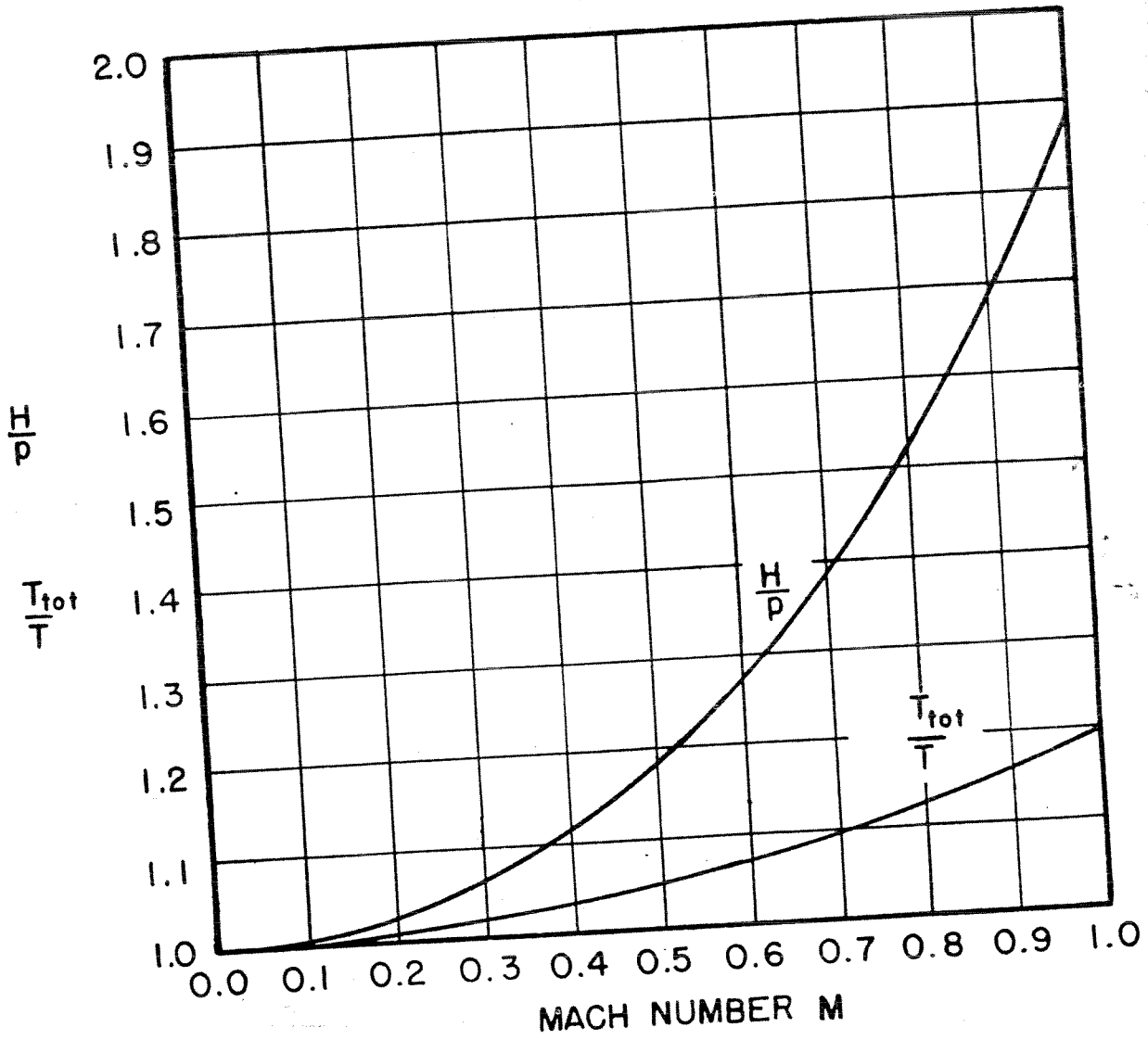

FIG. 2-36 PRESSURE AND TEMPERATURE RATIOS AS FUNCTION OF MACH NUMBER

λ'_2, we obtain the true value[1] of the Mach number. Also, $C'_{M,2}$ can be found for use in calculations on the distribution between Stations 2 and 3.

Step 7. With M'_2, enter Fig. 2-36 and obtain the ratios $(H/p)_2$ and $(T_{tot}/T)_2$.

Step 8. Calculate the static pressure and static temperature from the results of Steps 1, 5, and 7.

Step 9. The discharge w may be conveniently calculated by means of Eq. 2-23 as a check on the calculations. Having found all conditions at Station 2, the same procedure may be repeated to arrive at the conditions of Section 3, and so forth.

It may be observed that the assumption of the upstream value of the Mach number determines all other downstream conditions. In particular, the ratio H_1/H_2 is determined. By several assumptions for values of M_1, a graphical representation of total-pressure ratios and rates of flow may be obtained. In this way the system may be analyzed in all details. For example, the discharge of the duct system, operating in conjunction with a compressor of known performance and discharging to a known static pressure, can be determined.

Figures 2-35 and -36 have been obtained from the tables of Ref. 92, which may be consulted if greater accuracy is desired. The author remarks that experimental results and predictions based on the method presented are in good agreement, the maximum deviation being about 3 per cent.

Using other types of graphs, Thomson (Ref. 123) also presented a solution of this problem. The methods of both Ref. 92 and Ref. 123 seem equally satisfactory from the viewpoint of computations.

[1] If the true Mach number lies below 0.3, it may be assumed for most practical purposes that the velocity of the system is decreased to a point where the flow may be considered as incompressible.

2-13 Pressure Drop in a Duct with Heat Transfer

Where heat is being transferred on walls of a duct system, the air properties may change considerably. The temperature changes affect the density, thus causing variations of dynamic head in addition to the usual variations caused by non-uniform cross sections. Further, the frictional and fitting losses, which depend upon the dynamic pressure and viscosity, also are altered from the values that would occur if there were no heat transfer.

An approximative method to calculate the pressure distribution in a duct with heat transfer is presented by Boelter, Morrin, Martinelli, and Poppendiek (Ref. 17) and Martinelli, Weinberg, Morrin, and Boelter (Ref. 90). In two cases, the authors find differences of 7 and 27 per cent between experimental and predicted pressure drops. These differences are allowable for most practical calculations. A summary of the method used by the authors is presented in the next sections. The reader is also referred to Hall's (Ref. 53) chapter on diabatic flow.

2-13.1 Distribution of Total Pressure in a Duct with Heat Transfer and with Frictional and Fitting Losses

The differential of the total pressure for one-dimensional flow[1] is

$$dH \equiv dp + \rho U \cdot dU \tag{2-31}$$

If there were no losses, this quantity would be zero, Bernoulli's equation would be obtained, and the total pressure would be constant along the duct. However, when losses occur, an additional term must be added to the right member, and the change of total pressure between any two cross sections, Stations 1 and 2, is found by integrating dH with the result that

$$\int_1^2 dp + \int_1^2 \rho U \, dU = - F_{1,2} \tag{2-32}$$

[1] Velocities, temperatures, and all other properties of the fluid are assumed to be uniform at each cross section.

The quantity $F_{1,2}$ represents the sum of all frictional and fitting losses between Stations 1 and 2; it is positive and its units are lb/ft^2. Performing the integration of the first term, replacing the density ρ in $slug/ft^3$ in terms of the specific volume ($\rho \cdot gv = 1$), and eliminating the velocity from Eq. 2-32 and the equation of continuity, the following expression for the drop of static pressure is obtained:

$$p_1 - p_2 = \frac{1}{g}\left(\frac{w}{3600}\right)^2 \int_1^2 \frac{1}{v} \cdot \left(\frac{v}{A}\right) d\left(\frac{v}{A}\right) + F_{1,2} \qquad (2\text{-}33)$$

The evaluation of each term in the right member is considered in the next two sections.

2-13.2 Evaluation of the Losses $F_{1,2}$

The sum of the total-pressure losses $F_{1,2}$ will be found by applying a correction to the value of the losses in the duct for the case that the flow is isothermal and incompressible.

Letting $(F_{1,2})_{iso}$ be the sum of the losses for the case of isothermal, incompressible flow and using certain simplifying assumptions, Martinelli, et al (Ref. 90) have shown that

$$\frac{F_{1,2}}{(F_{1,2})_{iso}} = \left(\frac{w}{w_{iso}}\right)^n \left(\frac{T_1 + T_2}{2T_{iso}}\right)^{0.13} \frac{v_1 + v_2}{2v_{iso}} \qquad (2\text{-}34)$$

The isothermal losses are of the form,

$$(F_{1,2})_{iso} = \sum_1^2 f \rho \frac{U^2}{2} \frac{L}{D_e} + \sum_1^2 K \rho \frac{U^2}{2} \qquad (2\text{-}35)$$

or

$$(F_{1,2})_{iso} = \frac{v_{iso}}{2g}\left(\frac{w}{3600}\right)^2 \left\{\sum_1^2 f \frac{L}{D_e A^2} + \sum_1^2 \frac{K}{A^2}\right\} \qquad (2\text{-}36)$$

The temperature T_{iso} is arbitrary. If both T_1 and T_2 are known, then the choice T_{iso} equal to their arithmetic mean will simplify the calculation. Usually, T_2 is unknown but can be estimated from the

heat balance. In a few trials, or by graphical solution, values of w and T_2 can be found to satisfy the pressure-drop and the heat-transfer equations.

The specific volumes in Eq. 2-34 can be calculated using corresponding temperatures and pressures by means of the relationship of state

$$p \cdot v = RT \tag{2-37}$$

Usually, the relative changes of absolute pressure are small, and in a first approximation, the pressure may be assumed uniform at the value p_1 in order to calculate v_1, v_2, and v_{iso}. After the first approximation of p_2 has been found the calculation may be repeated if greater accuracy is desired.

The exponent n lies between 1.75 and 2.00. If the losses are predominantly frictional, the exponent lies close to 1.75 and if caused mainly by fittings it lies near 2.00. The value may be established from a bilogarithmic plot of $(F_{1,2})_{iso}$ versus w_{iso}. The points can be found by calculation or, if possible, by experimentation. Since w_{iso} is arbitrary, it will be convenient for types of calculation in which w is known to place $w_{iso} = w$; then the relationship between $F_{1,2}$ and $(F_{1,2})_{iso}$ is independent of n.

2-13.3 Evaluation of $J_{1,2} = \int_1^2 \frac{1}{v} \left(\frac{v}{A}\right) d\left(\frac{v}{A}\right)$ in Equation 2-33

In many cases the first term in the right number of Eq. 2-33 is small compared with the second and may be neglected. In other cases it may be evaluated by making certain simplifying assumptions.

For example, in the most common case, namely, isothermal flow with non-uniform cross-sectional area, the integral becomes

$$J_{1,2} = \frac{v}{2}\left(\frac{1}{A_2^2} - \frac{1}{A_1^2}\right) \tag{2-38}$$

If the temperature difference $T_2 - T_1$ is small, a mean specific volume v_m may be used in the approximation,

$$J_{1,2} \approx \frac{1}{2v_m} \cdot \left[\left(\frac{v_2}{A_2}\right)^2 - \left(\frac{v_1}{A_1}\right)^2\right] \tag{2-39}$$

If the cross-sectional area is uniform,

$$J_{1,2} = \frac{1}{A^2}(v_2 - v_1) \tag{2-40}$$

If the cross-sectional area is nearly uniform a mean value A_m may be used in the approximation,

$$J_{1,2} \approx \frac{1}{A_m}\left(\frac{v_2}{A_2} - \frac{v_1}{A_1}\right) \tag{2-41}$$

2-13.4 Pressure Drop across a Heat Exchanger in a Uniform Duct

Kays (Ref. 70) and Kays and London (Ref. 71) have presented numerous data for heat exchanger cores. The cross-sectional area of the duct A_d leading to the cores is equal to the area of the duct leading away; that is, the frontal area is uniform. Summing the contraction, frictional, and expansion losses, assuming that the change of pressure is small relatively to the absolute pressure, and simplifying, the change of static pressure across such a configuration is

$$p_1 - p_2 = \frac{G^2}{2g\gamma_1}\left[\left(K_c + \frac{T_2}{T_1}K_{ex}\right) + \left(1 + \frac{A_c^2}{A_d^2}\right)\left(\frac{T_2}{T_1} - 1\right) + f\frac{L}{D_e}\frac{T_m}{T_1}\right] \tag{2-42}$$

where G is the weight rate of flow per unit area in the core in lb/sec ft^2; D_e is the equivalent diameter of a passageway of the core in ft; A_c is the free-flow cross-sectional area of the core in ft^2; and

$$T_m = T_s - \frac{T_2 - T_1}{h_U/G\,c_p} \tag{2-43}$$

In Eq. 2-43 T_s is a mean surface temperature and h_U is the over-all coefficient of heat transfer.[1]

---

[1] The quantity in the denominator is a sort of Stanton number. Usually it is called the number of transfer units, and in many places is found improperly denoted by the symbol NTU.

Values of K_c, K_{ex}, and f are presented for particular heat exchanger cores in Ref. 70 as functions of A_c/A_d and a Reynolds number. However, Eq. 2-42 is quite general and could be used in other similar cases if the values of the coefficients are known. In particular, it is believed that this equation may be found useful for double-skin heat exchangers $(A_c^2/A_d^2 \ll 1)$ if values of K_{ex} and K_c could be well established.

2-14 Pipes in Series and Parallel

Two or more pipes of different diameters or roughnesses connected so that the discharge from one flows into another are said to be in series. Two or more pipes having inlets and outlets in common headers or plenums are said to be in parallel. Double-skin passages in a single bay may be considered as parallel passages. But two groups of double-skin passages at different spanwise positions may not be in parallel because a drop of pressure occurs in the supply duct or the distribution duct.

In pipes connected in series the same fluid flows through all the pipes and the pressure losses are cumulative; in parallel arrangements the losses over any member from one junction to another are equal, and the discharges are cumulative.

In dealing with combinations of systems of pipes in series and parallel or inter-connected systems, it is often convenient to reduce complex members of the system to equivalent elements. Some methods to perform such simplifications are treated in the next two sections.

2-15 Equivalent Length

Losses due to fittings are sometimes conveniently expressed in terms of an equivalent length L_e of a pipe that has equal pressure energy loss for the same weight rate of flow as in the fittings. Expressing the fitting losses as a percentage of the kinetic energy, and equating them to the frictional losses of a pipe of length L_e,

$$f \cdot \frac{U^2}{2g} \gamma \cdot \frac{L_e}{D} = K \frac{U^2}{2g} \gamma \qquad (2\text{-}44)$$

ere K is the sum of all pressure-loss coefficients (except those of iction). Solving for L_e,

$$L_e = \frac{KD}{f} \qquad (2\text{-}45)$$

16 Pipes in Series

A complex system of pipes and fittings in series may be replaced by a -called "equivalent pipe", which would have the same pressure drop and scharge as the given system. In some cases it is advantageous to use . 2-45 and -46. Consider, for instance, Pipes 1 and 2 (diameters D_1, , and lengths L_1, L_2) connected in series. The sum of the fitting losses r each pipe may be expressed in the form of an equivalent length $L_{e,1}$ d $L_{e,2}$ by means of Eq. 2-45. In this way the system is reduced to a ries of two pipes of adjusted lengths $L_1' \equiv L_1 + L_{e,1}$ and $L_2' \equiv L_2 + L_{e,2}$ thout fitting losses.

Further simplification may be obtained by expressing, for example, the -- justed length L_2' of Pipe 2 in terms of a fictitious length of Pipe 1. ls fictitious length having the same discharge and pressure drop as pe 2 is

$$L_{2,1}' = L_2' \cdot \frac{f_2}{f_1}\left(\frac{D_1}{D_2}\right)^5 \qquad (2\text{-}46)$$

a fictitious pipe of total length $L_1' + L_{2,1}'$ and of diameter D_1 is uivalent to the system comprised of Pipes 1 and 2, including their fitting sses. Subsequent calculations can be made using the equivalent pipe. eries of more than two components can be treated in the same way.

7 Parallel Pipes

The following steps lead to the solution of the distribution of flow pressure losses for a given total rate of flow w through a system of allel pipes, Pipe 1, Pipe 2, etc.

p 1. For a first approximation assume a discharge $w_1^{(1)}$ through Pipe 1.

Step 2. Solve for the loss of total pressure ΔH using the assumed discharge $w_1^{(1)}$.

Step 3. Using ΔH find $w_2^{(1)}$, $w_3^{(1)}$, ... If the assumption of $w_1^{(1)}$ is correct, the sum of $w_1^{(1)}$ and other calculated values, namely, $w_2^{(1)}$, $w_3^{(1)}$, ..., must be equal to w. If this condition is satisfied, the calculation may be concluded with Step 3. However, if the sum, $w^{(1)} = w_1^{(1)} + w_2^{(1)} + \ldots$, is not equal to w, the calculation must be continued as indicated in Steps 4 and 5.

Step 4. Assume that the given flow w is divided among the pipes in the same proportion as $w_1^{(1)}$, $w_2^{(1)}$, ...; thus, the second approximations are obtained:

$$w_1^{(2)} = \frac{w_1^{(1)}}{w^{(1)}} \cdot w, \qquad w_2^{(2)} = \frac{w_2^{(1)}}{w^{(1)}} \cdot w, \qquad \ldots \qquad (2\text{-}47)$$

Step 5. Check the values of $w_1^{(2)}$, $w_2^{(2)}$, ..., to see whether they satisfy the condition,

$$\Delta H = \Delta H_1 = \Delta H_2 = \ldots. \qquad (2\text{-}48)$$

If the results of the first and second approximations are nearly equal, this check is unnecessary.

2-18 Pressure Losses in Double-Skin Passages

Passing through the double-skin heaters, the hot air encounters the resistance due to friction in the passages and abrupt changes at the inlets and exits. The resistance is also influenced by the curvature of the passageways. The complexity of the shapes of double-skin heaters and their odd orientation with respect to the flow have made prediction of their pressure losses difficult. The main reason seems to be that the available literature on entrance effects deals with flow conditions which are not accurately representative of those encountered in an anti-icing system.

Neel (Ref. 98) using the data shown in Ref. 16, presents the following equation for the sum of the coefficients of total-pressure drop in the double-skin gaps:

$$K_G = K_i + \frac{f_G L}{D_e} \qquad (2\text{-}49)$$

Employing $K_i = 0.75$, as suggested in Ref. 16, Neel calculated the friction factor f_G shown in Fig. 2-37. The values of f_G are not in agreement with the values of f in Fig. 2-1. The reason may be that the value of K_i has been taken to be a constant independent of the geometry and the Reynolds number of the flow in the gaps.

When K_G is evaluated by means of Eq. 2-49, it is used in the following equation to obtain the loss of static pressure between a point in the plenum and a point at the end of the passage:

$$\Delta p = K_G \cdot \frac{1}{2} \rho U^2 \qquad (2\text{-}50)$$

where U is the mean velocity in the passages. If an orifice is at the exit, its contribution to the pressure loss should be added. It may be found convenient to obtain the pressure drop in terms of the weight rate of flow in pounds per hour per foot span:

$$\Delta p = K_G \cdot \frac{1}{2g\gamma} \left(\frac{w'}{3600}\right)^2 \cdot \frac{1}{(A')^2} \qquad (2\text{-}51)$$

where $[\Delta p] = \text{lb/ft}^2$; γ is the mean specific weight of air in lb/ft^3; A' is the cross-sectional area of the passages in square feet per foot span; $[w'] = \text{lb/hr ft}$; and $g = 32.17 \text{ ft/sec}^2$.

According to Neel (Ref. 98), Eq. 2-49 and -50 may be used equally as well whether heat transfer is occurring or not. Further, the author is of the opinion that even though the estimate of f_G is based only on a particular type of corrugated double-skin, the values may be generally applied.

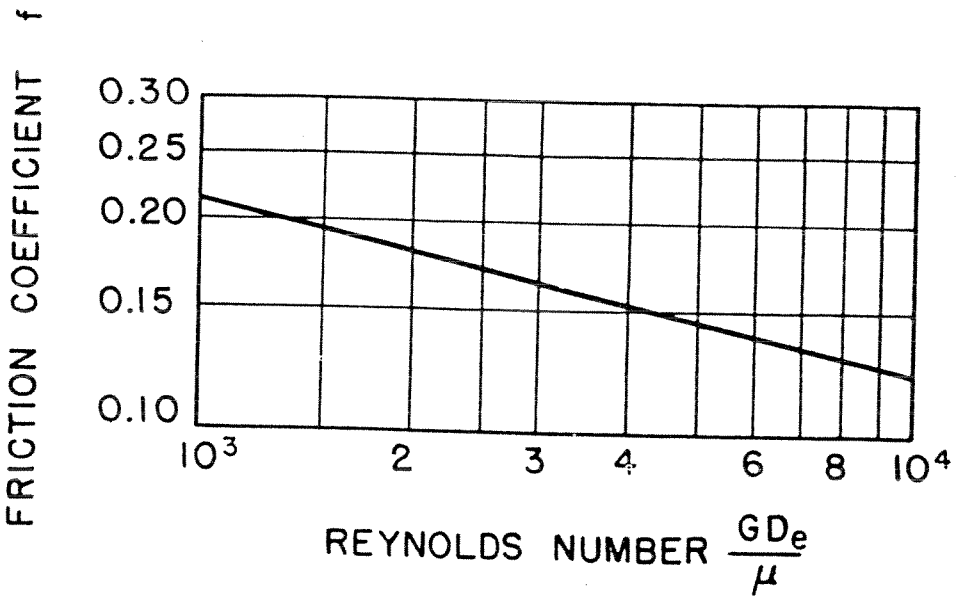

FIG. 2-37 FRICTION COEFFICIENT TO BE USED IN CONJUNCTION WITH EQUATION 2-49

Chapter 3: WATER IMPINGEMENT ON AIRFOILS

3-1 Droplet Trajectories

The interception of cloud droplets by an airfoil depends upon the physical configuration of the airfoil, the flight conditions, and the inertia of the cloud droplets. In order to obtain the rate and extent of the droplet impingement on the airfoil, the droplet trajectories with respect to the airfoil must be determined. Some trajectories intersect the surface; others miss the surface. Only the trajectories lying between those which are tangent to the upper and lower surfaces are effective during the collection process.

3-1.1 Fundamental Differential Equations

To set up the differential equations that describe the droplet motion in a two-dimensional flow field, the following simplifying assumptions are used:

(1) The droplets are always spherical and do not change size.
(2) No gravitational force acts on the droplets.

The first assumption is valid for the order of accuracy usually required in the design of anti-icing equipment. The second assumption is reasonable because the inertia force of the droplets is much greater than the gravitational force.

The drag force of a spherical drop of radius a moving in air

$$F_D = C_D \pi a^2 \cdot \frac{1}{2} \rho_o \left|\bar{u} - \bar{v}\right|^2 = \frac{C_D N'_{Re,d}}{4} \pi a \mu \left|\bar{u} - \bar{v}\right| \qquad (3\text{-}1)$$

The quantity C_D is the drag coefficient which depends upon the Reynolds number.

$$N'_{Re,d} = \frac{2a \rho_o}{\mu} \left|\bar{u} - \bar{v}\right| \qquad (3\text{-}2)$$

where $\bar{u}$ and $\bar{v}$ are the vector velocities of the air and droplet,

respectively. These velocities are measured in a coordinate system fixed in the airfoil. The air velocity $\bar{u}$ is taken to be that of the potential field of an ideal, incompressible fluid. One method to calculate $\bar{u}$ is summarized in Ref. 23. In a rectangular coordinate system the equations of motion of a water droplet without the influence of gravity are

$$\frac{4}{3}\pi a^3 \rho_w \frac{dv_x}{d\tau} = \frac{C_D N'_{Re,d}}{4} \pi a(u_x - v_x) \tag{3-3}$$

$$\frac{4}{3}\pi a^3 \rho_w \frac{dv_y}{d\tau} = \frac{C_D N'_{Re,d}}{4} \pi a(u_y - v_y) \tag{3-4}$$

where subscripts x and y refer to the components in the x and y directions, respectively. Dividing all velocities by the mainstream velocity U_o and employing the dimensionless time ratio $\tau(U_o/L) \equiv \tau^+$, Eq. 3-3 and -4 assume the dimensionless form

$$\frac{dv_x^+}{d\tau^+} = \frac{C_D \cdot N'_{Re,d}}{24} \cdot \frac{1}{K}(u_x^+ - v_x^+) \tag{3-5}$$

$$\frac{dv_y^+}{d\tau^+} = \frac{C_D \cdot N'_{Re,d}}{24} \cdot \frac{1}{K}(u_y^+ - v_y^+) \tag{3-6}$$

where

$$u_x^+ = \frac{u_x}{U_o}, \quad v_x^+ = \frac{v_x}{U_o},$$

and

$$K \equiv \frac{2}{9} \frac{a^2 \rho_w U_o}{L\mu} \tag{3-7}$$

The space coordinates of Eq. 3-5 and -6 are $x^+ \equiv x/L$ and $y^+ \equiv y/L$. The dimensionless quantity K is called the inertia parameter.

The Reynolds number $N'_{Re,d}$ can be obtained conveniently in terms of the free stream Reynolds number,

$$N_{Re,d} = \frac{2a \rho_o U_o}{\mu} \tag{3-8}$$

by means of the relationship,

$$\left(\frac{N'_{Re,d}}{N_{Re,d}}\right)^2 = (u_x - v_x)^2 + (u_y - v_y)^2 \qquad (3\text{-}9)$$

The drag coefficient C_D in Eq. 3-5 and -6 is customarily obtained from Table 3-1 taken from Ref. 81 and based upon previous experimental data for large spheres in steady-state conditions. However, Morton (Ref. 97) points out that these values may be inaccurate for small spheres.

A solution of Eq. 3-5 and -6 gives the trajectory of a droplet. Several solutions are required to obtain the rate, area, and distribution of the water impingement. It is seen from these equations and the definition of K that, for a given shape, size, and angle of attack of the airfoil, the trajectories depend on the radius of droplets, the free stream velocity, the air viscosity, and the air density as first-order variables.

3-1.2 Water Impingement Parameters

The following relations are convenient for evaluation of the dimensionless parameters K and $N_{Re,d}$:

$$K = 1.963 \cdot 10^{-12} \frac{D_d^2 U_o}{\mu L} \qquad (3\text{-}10)$$

$$N_{Re,d} = 5.545 \cdot 10^{-6} \frac{D_d \rho_o U_o}{\mu} \qquad (3\text{-}11)$$

$$D_d = 7.141 \cdot 10^5 \sqrt{\frac{K \mu L}{U_o}} \qquad (3\text{-}12)$$

$$\rho_o = 0.0412 \frac{p_o}{T_o} \qquad (3\text{-}13)$$

where $[D_d]$ = microns; $[U_o]$ = knots; $[\mu]$ = slug/ft sec; $[L]$ = ft; $[\rho_o]$ = slug/ft^3; $[p_o]$ = in.-mercury; and $[T_o]$ = °R. Based upon these relations, Fig. 3-1 and -2 were prepared for the rapid determination of the parameters K^{-1} and $N_{Re,d}$, respectively, for 15°F icing atmosphere. The value of K^{-1} is independent of the pressure and is dependent on temperature mainly

TABLE 3-I

VALUES OF $C_D \cdot N_{Re,d}/24$ AND λ / λ_S AS FUNCTIONS OF $N_{Re,d}$

$N_{Re,d}$	$C_D N_{Re,d}/24$	λ/λ_S	$N_{Re,d}$	$C_D N_{Re,d}/24$	λ/λ_S
0.00	1.00	1.00	200	6.52	0.2668
0.05	1.009	0.9956	250	7.38	0.2424
0.1	1.018	0.9911	300	8.26	0.2234
0.2	1.037	0.9832	350	9.00	0.2080
0.4	1.073	0.9652	400	9.82	0.1953
0.6	1.103	0.9493	500	11.46	0.1752
0.8	1.142	0.9342	600	12.97	0.1597
1.0	1.176	0.9200	800	15.81	0.1375
1.2	1.201	0.9068	1000	18.62	0.1215
1.4	1.225	0.8950	1200	21.3	0.1097
1.6	1.248	0.8842	1400	24.0	0.1003
1.8	1.267	0.8744	1600	26.9	0.0927
2.0	1.285	0.8653	1800	29.8	0.0863
2.5	1.332	0.8452	2000	32.7	0.0809
3.0	1.374	0.8273	2500	40.4	0.0703
3.5	1.412	0.8120	3000	47.8	0.0624
4.0	1.447	0.7978	3500	55.6	0.0562
5.0	1.513	0.7734	4000	63.7	0.0513
6.0	1.572	0.7527	5000	80.0	0.0439
8.0	1.678	0.7185	6000	96.8	0.0385
10	1.782	0.6905	8000	130.6	0.0311
12	1.901	0.660	10000	166.3	0.0262
14	2.009	0.6440	12000	204	
16	2.109	0.6242	14000	243	
18	2.198	0.6065	16000	285	
20	2.291	0.5904	18000	325	
25	2.489	0.5562	20000	365	
30	2.673	0.5281	25000	470	
35	2.851	0.5045	30000	574	
40	3.013	0.4840	35000	674	
50	3.327	0.4505	40000	778	
60	3.60	0.4237	50000	980	
80	4.11	0.3829	60000	1175	
100	4.59	0.3524	80000	1552	
120	5.01	0.3285	$1.0 \cdot 10^5$	1905	
140	5.40	0.3090	$1.2 \cdot 10^5$	2234	
160	5.76	0.2928	$1.4 \cdot 10^5$	2549	
180	6.16	0.2789	$1.6 \cdot 10^5$	2851	

FIG. 3-1 CHART OF RECIPROCAL INERTIA PARAMETER K^{-1}

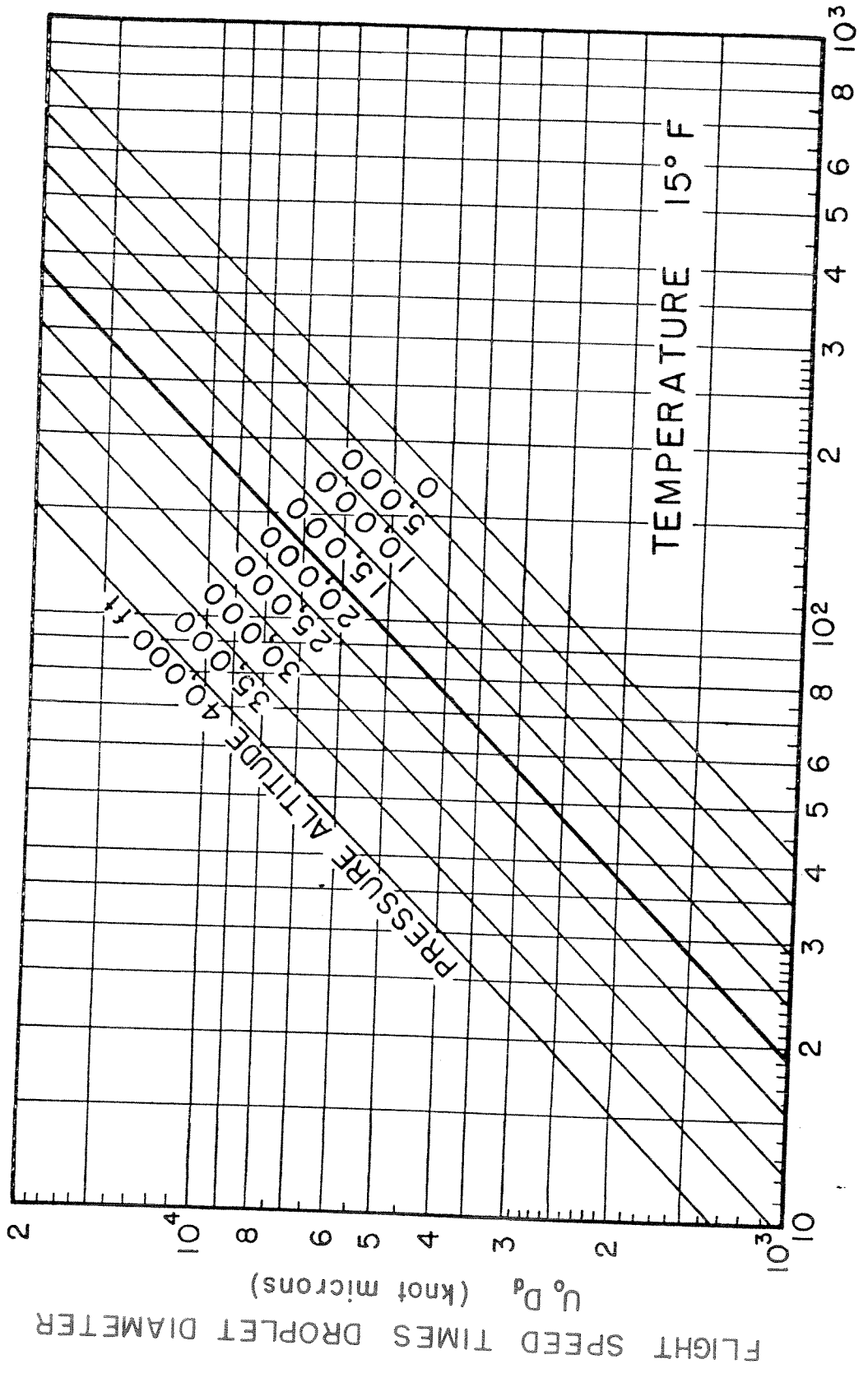

FIG. 3-2 CHART FOR EVALUATION OF DROPLET REYNOLDS NUMBER

through the temperature dependency of the viscosity; therefore, the values of K^{-1} in Fig. 3-1 may be employed for most practical purposes. The Reynolds number depends upon the pressure and the temperature. The pressure used to calculate the air density was taken from tables of the NACA Standard Atmosphere, part of which is reproduced as Table A-1 in the appendix; the viscosity, dependent only upon the temperature, was evaluated for 15°F air.

Two other useful dimensionless parameters are, in consistent engineering units,

$$\psi \equiv 9 \cdot \frac{\rho_o}{\rho_w} \cdot \frac{L}{a} \tag{3-14}$$

and

$$\phi \equiv 18 \cdot \frac{U_o \rho_o L}{\mu_o} \cdot \frac{\rho_o}{\rho_w} \tag{3-15}$$

Charts for their evaluation are presented in Fig. 3-3 and -4; both charts are for 15°F icing atmosphere and practical units are used on the coordinates.

Any two of the parameters K^{-1}, $N_{Re,d}$, ψ, and ϕ, will completely determine the rate of water catch and the region of impingement on a given airfoil, provided that flight and icing conditions are known. Further, the four parameters are simply related, in a way such that if any two are known the other two can be derived. Thus:

$$N_{Re,d} = K \cdot \psi \tag{3-16}$$

$$N_{Re,d} \cdot \psi = \phi \tag{3-17}$$

These equations are represented graphically by the criss-cross chart of Fig. 3-5. This chart may be found useful for performance studies:

(1) Generally, a wing will have variable chord length. To study the water catch at several sections of a wing flying at speed U_o through

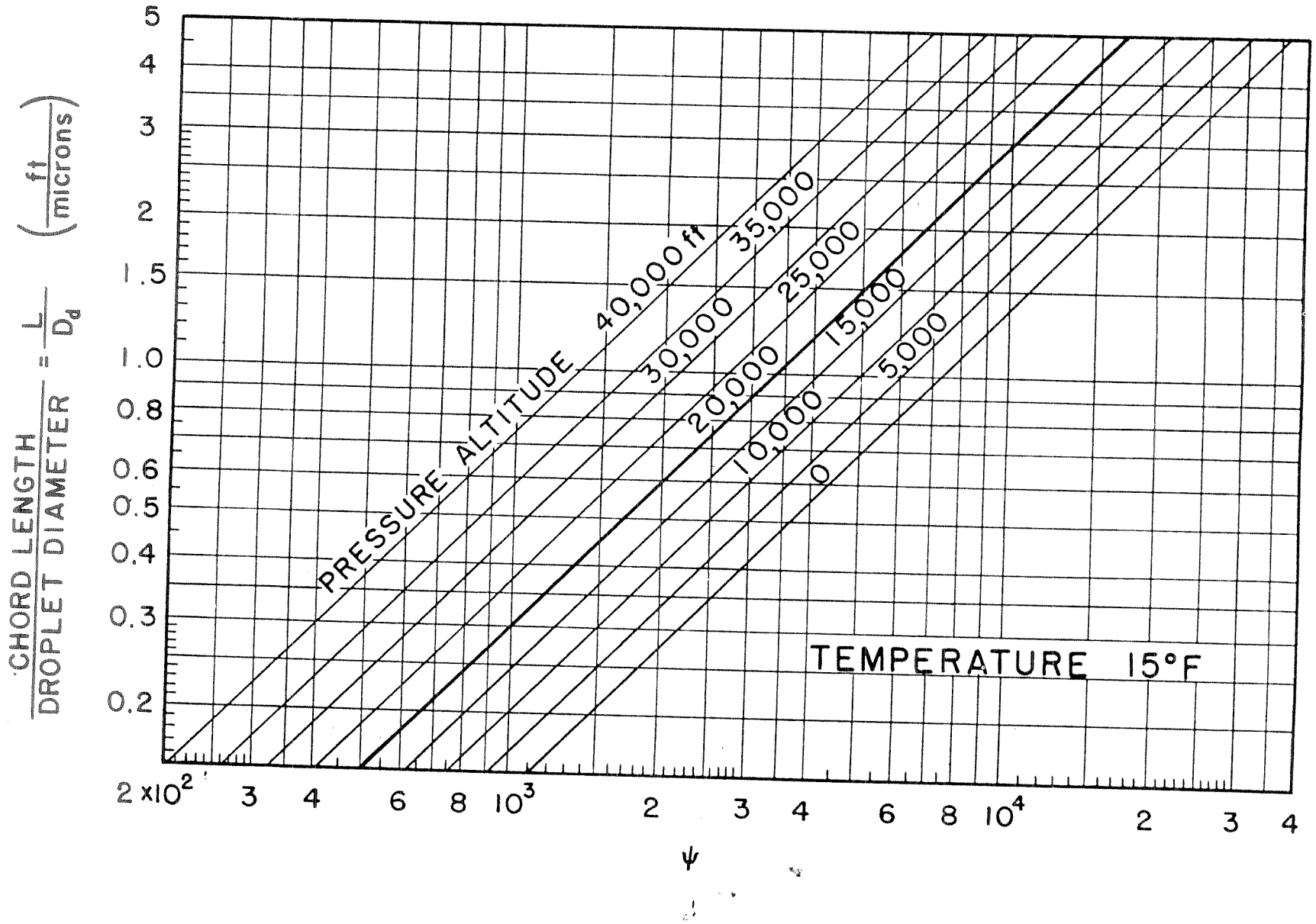

FIG. 3-3 CHART FOR EVALUATION OF SCALE FACTOR ψ

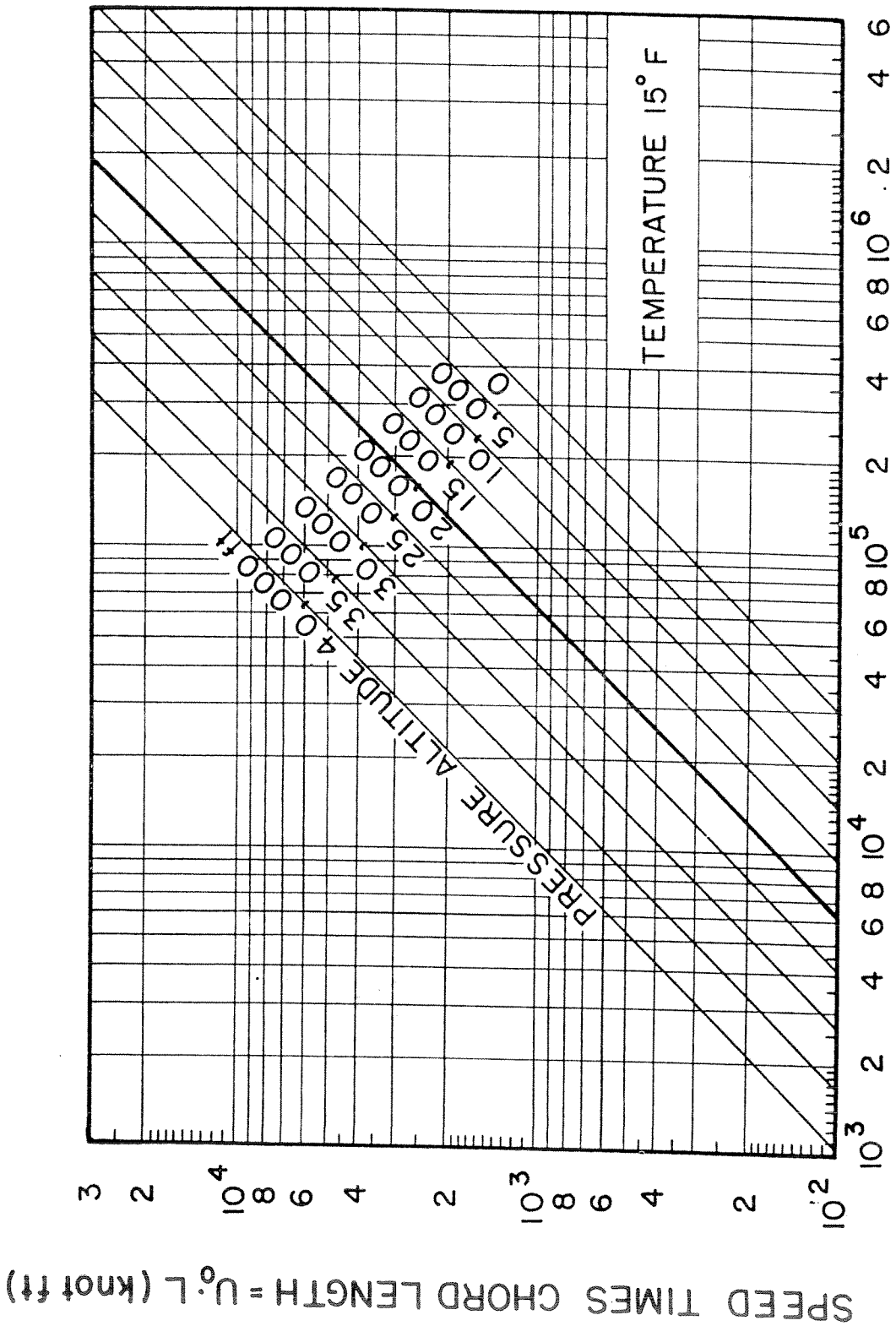

FIG. 3-4 CHART FOR EVALUATION OF PARAMETER ϕ

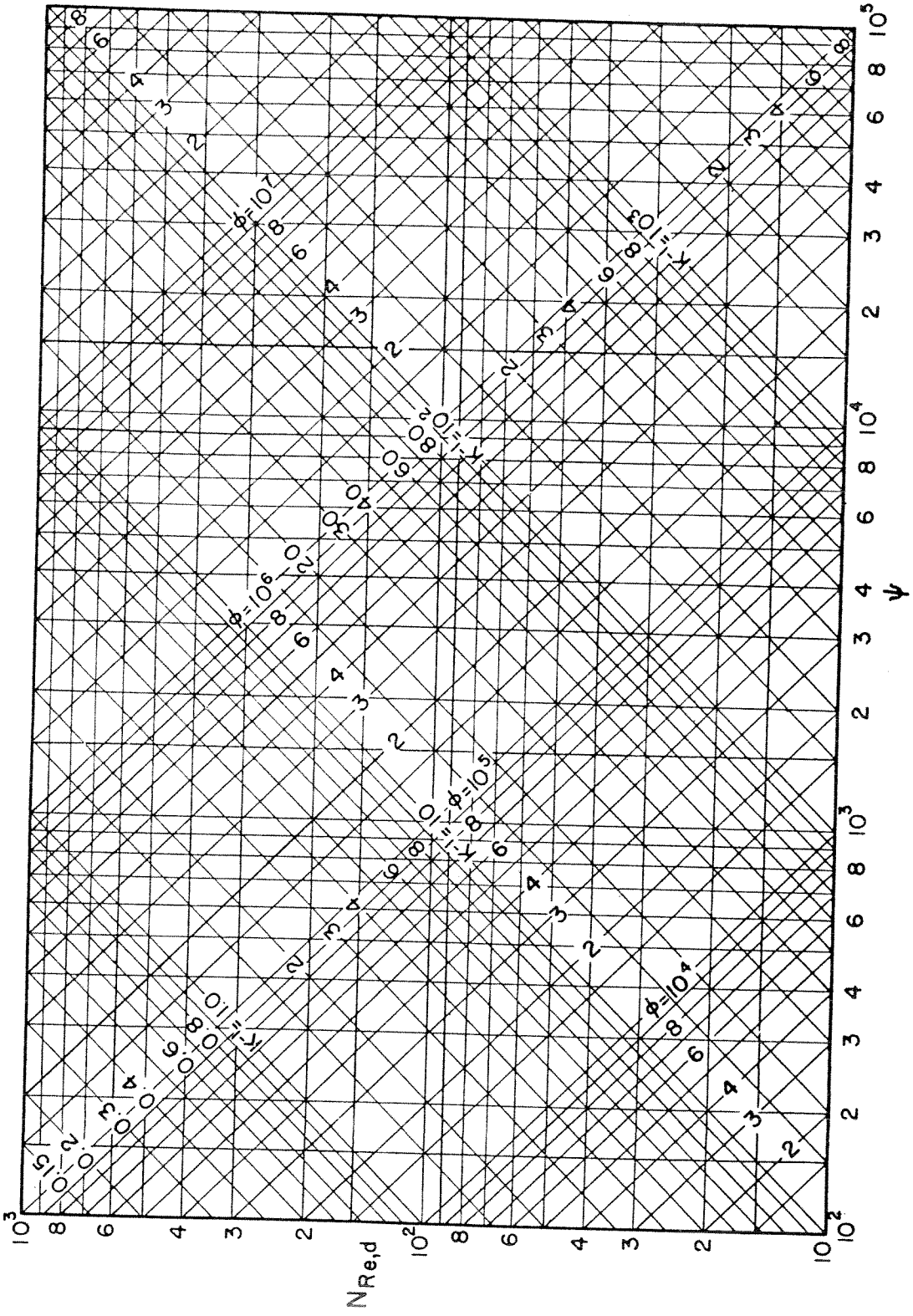

FIG. 3-5 CRISS-CROSS CHART OF WATER IMPINGEMENT PARAMETERS

droplets of size D_d at a fixed altitude, follow, or make calculations for several points on, a horizontal line ($N_{Re,d}$ = constant), which is independent of the chord length.

(2) A certain cross section of a wing is to be studied for various flight speeds at a fixed altitude. Follow a vertical line (ψ = constant), which is independent of the speed. Results will be applicable for a fixed drop size; also, the same results can be applied of the ratio L/D_d is fixed and the altitude has not changed. To study another chord length, use another vertical line.

(3) Similarly, to study the influence of variable drop size on a given airfoil section, follow a line of constant ϕ, which will be fixed for a given speed and altitude.

(4) Finally, when the influence of altitude is to be studied, all other quantities being fixed, a line of constant K^{-1} may be followed for most practical purposes.

The criss-cross chart is easily constructed on a sheet of bilogarithmic paper, and any region of particular interest can be constructed on a large scale so that the designer can achieve as much accuracy as he would like.

3-1.3 Solutions of the Trajectory Problem

After the parameters K and $N_{Re,d}$ are determined, the solution of Eq. 3-5 and -6 can be effected by any of the following methods:

(1) Numerical integration; e.g., Ref. 11, 12, 68, and 79.

(2) Mechanical analog; e.g., Ref. 23 and 24.

(3) Differential analyzer.

(a) Bush type: e.g., Ref. 13, 50, 51, and 81.

(b) Reeves type; e.g., Ref. 126.

(4) Digital computer; e.g., Ref. 28.

(5) Graphical method; e.g., Ref. 21.

(6) Experimental methods; e.g., Ref. 22 and 97.

Of these methods, No. 2 and 3a seem to give the most dependable results so far. Method 3b shows promise of giving results most rapidly, because the velocity flow field is built into the calculation system and need not be calculated independently.

3-2 Summary of Available Solutions for Airfoils

Trajectory data for the circular cylinder are presented in Ref. 81. The method of employing an "equivalent cylinder" to predict the impingement on airfoils, as suggested in Ref. 127, has been found to be a fair approximation only for certain thick Joukowski airfoils, and to be unsatisfactory for low-drag airfoils. Therefore, the trajectory data for cylinders are omitted and only data for airfoils are presented. Some solutions for airfoils are listed below:

Airfoil Shape	Reference	Remarks
Airfoil	47	Stokes' law regime
Joukowski symmetrical 15 per cent	50, 51	0°, 2°, 4° angle of attack
Joukowski cambered, 15 per cent thick	50	0° angle of attack
NACA 65_2-015	51	0° angle of attack
NACA 662-X, 16 per cent	79	2.5° angle of attack
Arbitrary airfoil	11	Graphical, based on data of Joukowski airfoils
Joukowski symmetrical 12 per cent	11	0° angle of attack
NACA 65_1-212	23	4° angle of attack
NACA 65_1-208	23	4° angle of attack
NACA 65A004	24	4°, 8° angle of attack
NACA 0006-64 (6 per cent)	102	0°, 4° angle of attack
NACA 1S (50) 002-(50)002	—*	Double wedge, 0°, 5°, 10° angle of attack

*The calculations were performed by Research, Incorporated, of Minneapolis, Minnesota. The data were received in a communication from Aeronautical Icing Research Laboratories, Ypsilanti, Michigan.

Airfoil Shape	Reference	Remarks
NACA 65A005	--*	0°, 5°, 10° angle of attack
NACA 65A006 NACA 65A00475 NACA 65A0035	28	0°, 400 miles per hour; 4°, 700 miles per hour
Swept wings	35	
Supersonic wedge	125	
Supersonic wedge and diamond airfoils	118	

The trajectory data for several of these airfoils are presented in the next sections.

3-3 Total Rate of Water Impingement

The amount of water impinging on an airfoil per unit time per unit span is equal to the effective volume that the airfoil sweeps through in unit time multiplied by the mass of liquid water contained in unit volume of the atmosphere. In consistent units,

$$W' = U_o \left| y_{o,u} - y_{o,l} \right| \omega_w \qquad (3\text{-}18)$$

Using practical flight units,

$$W' = 0.379\, U_o\, \omega_w \left| y_{o,u} - y_{o,l} \right| \qquad (3\text{-}19)$$

where W' = rate of water catch per unit span, lb/hr ft - span

$y_{o,u}$; $y_{o,l}$ = y - coordinates for upper and lower tangent trajectories at $x = -\infty$, ft

U_o = air speed, knots

ω_w = liquid water content, g/cu m

*The calculations were performed by Research, Incorporated, of Minneapolis, Minnesota. The data were received in a communication from Aeronautical Icing Research Laboratories, Ypsilanti, Michigan.

3-3.1 Total Collection Efficiency

Results of the trajectory data may be correlated to a "total collection efficiency" defined as the ratio of the amount of water intercepted by the airfoil to the amount of water contained in the volume of cloud swept out by the airfoil when at zero geometric angle of attack. Thus,

$$E_m = \frac{|y_{o,u} - y_{c,l}|}{(\Delta y)_{max}} \qquad (3\text{-}20)$$

where $(\Delta y)_{max}$ is the airfoil thickness. It follows from this definition that E_m may be greater than unity for values of the angle of attack α other than zero. Equation 3-19 may now be written,

$$W' = 0.379\, U_o\, \omega_w\, E_m\, (\Delta y)_{max} \qquad (3\text{-}21)$$

A typical graph of E_m versus ψ with $N_{Re,d}$ as parameter is shown in Fig. 3-6. It is for the water impingement on the NACA 0064-64 (6 per cent) airfoil. The calculations were performed by Lenherr and Thomson (Ref. 102).

Brun, Gallagher, and Vogt (Ref. 23 and 24) present curves of $|y_{o,u} - y_{o,l}| / L$ versus K^{-1} with $N_{Re,d}$ as parameter for the NACA 65_1-208, 65_1-212, and 65A004 airfoils. Their data apply in the following range of variables:

Variable	Range
Droplet diameter D_d	5 to 100 microns
Speed U_o	150 mph to flight critical Mach number
Altitude	1,000 to 35,000 ft
Chord length L	2 to 20 ft
Angle of attack[1]	4°

[1] In Ref. 25 the authors give data for the NACA 65A004 airfoil at 8° angle of attack. That material came too late to be included in the present manual.

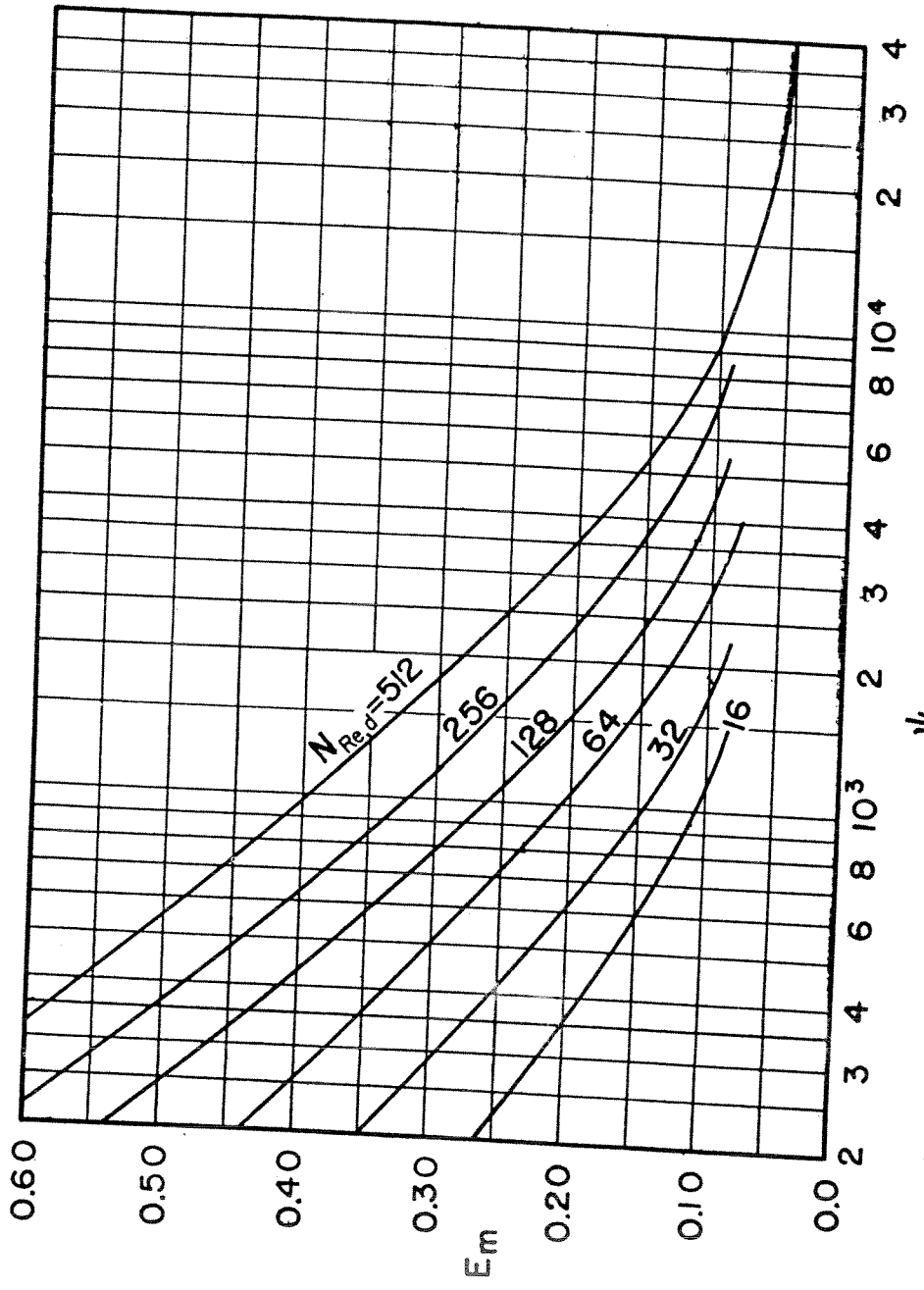

FIG. 3-6 TOTAL COLLECTION EFFICIENCY ON NACA 0006-64 AIRFOIL AT 0° ANGLE OF ATTACK

Dividing the ordinates of their curves for the NACA 65_1-208 airfoil by $(\Delta y)_{max}/L = 0.08$, we have translated the curves to the positions shown in Fig. 3-7 where the total collection efficiency E_m is plotted against K^{-1} with $N_{Re,d}$ as parameter. The line for $N_{Re,d} = 150$ was added after cross plotting the original curves. Similar figures could be constructed for the other two airfoils by translating the authors' curves. A generalization of this work will be found in Section 3-3.2.

Results of calculations by Research, Incorporated, on the NACA 1S(50)002-(50)002 double wedge and on the NACA 65A005 airfoil are presented in Fig. 3-8 and -9, respectively. The collection efficiency E_m is given as a function of K^{-1} with $N_{Re,d}$ as parameter. The coordinates of the double wedge surface are presented in Table 3-2. The data used to construct Fig. 3-8 and -9 are presented in Table 3-3.

Table 3-2 DIMENSIONLESS COORDINATES OF THE NACA 1S(50)002-(50)002 DOUBLE WEDGE

$\frac{x}{L}$	$\frac{y}{L}$	$\frac{x}{L}$	$\frac{y}{L}$
0.0	0.000	0.5	0.020
0.1	0.004	0.6	0.016
0.2	0.008	0.7	0.012
0.3	0.012	0.8	0.008
0.4	0.016	0.9	0.004
0.5	0.020	1.0	0.000

Armour Research Foundation of Illinois Institute of Technology (Ref. 28) carried out calculations to determine the total collection efficiency of three thin airfoils for specific icing and flight conditions. The calculations were performed on the basis that the potential flow around each airfoil could be well represented by the potential flow around an ellipse that would approximate a major part of the airfoil. The results are shown in Table 3-4. The values of K and $N_{Re,d}$ corresponding to the assumed conditions are shown in the last two columns.

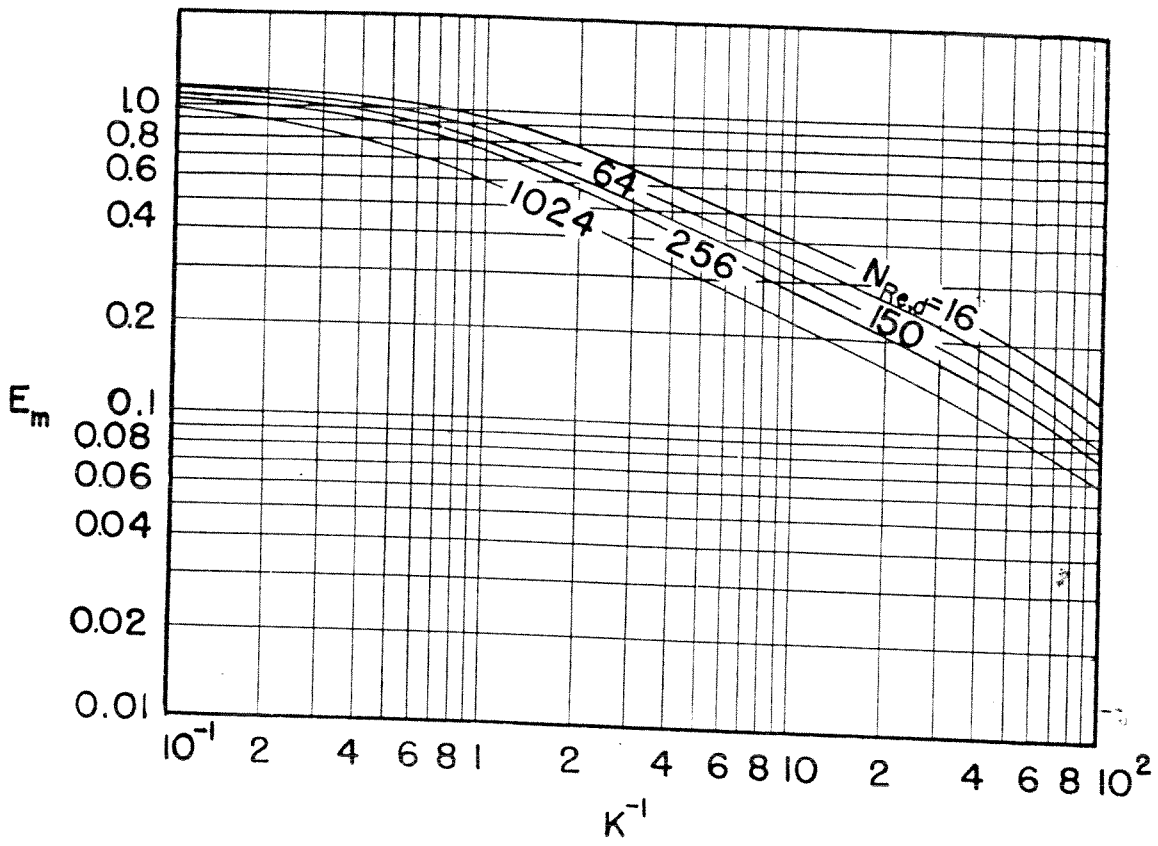

FIG. 3-7 TOTAL COLLECTION EFFICIENCY OF NACA 65_1-208 AIRFOIL AT 4° ANGLE OF ATTACK

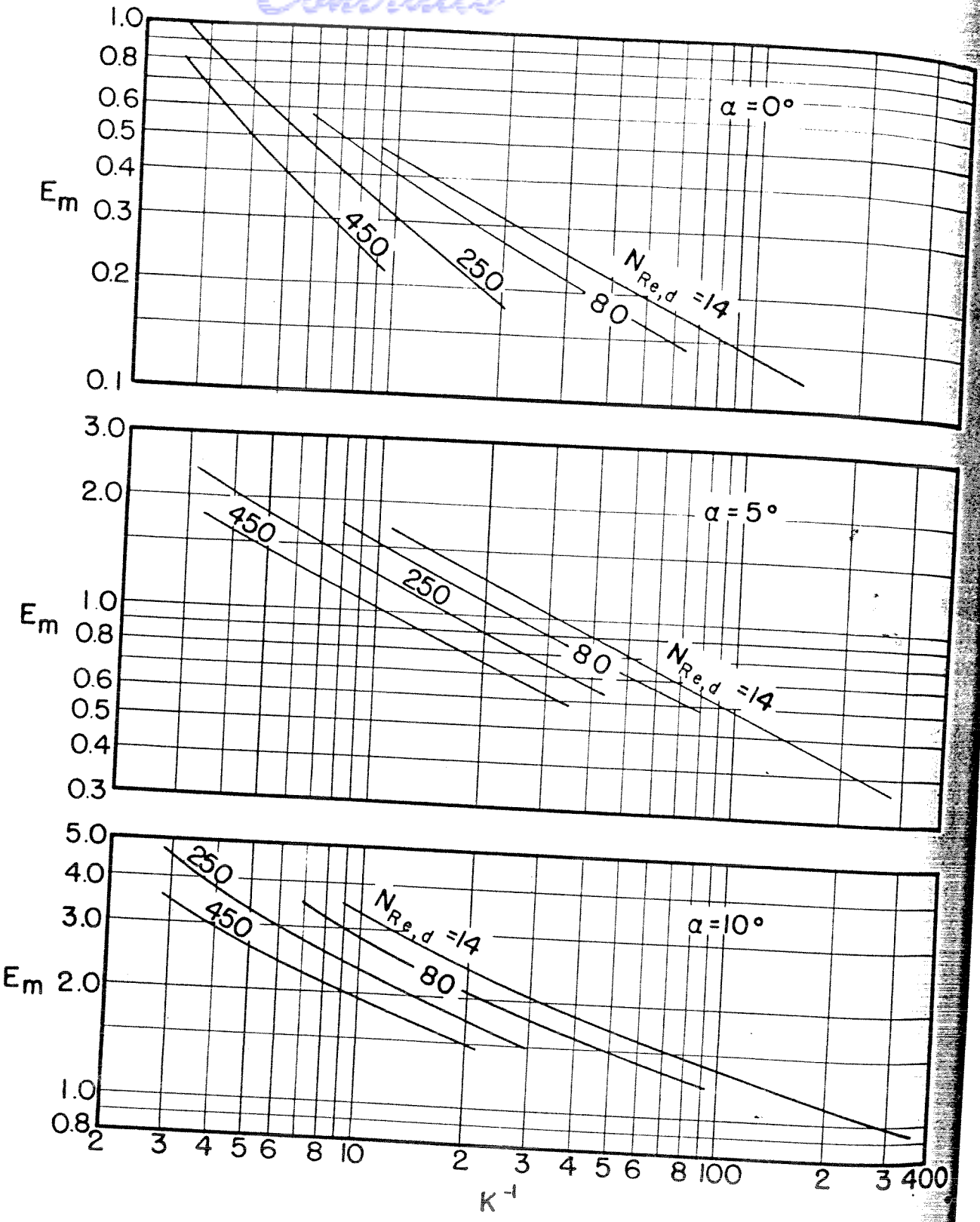

FIG. 3-8 TOTAL COLLECTION EFFICIENCY ON NACA 1S(50)002-(50)002 DOUBLE WEDGE

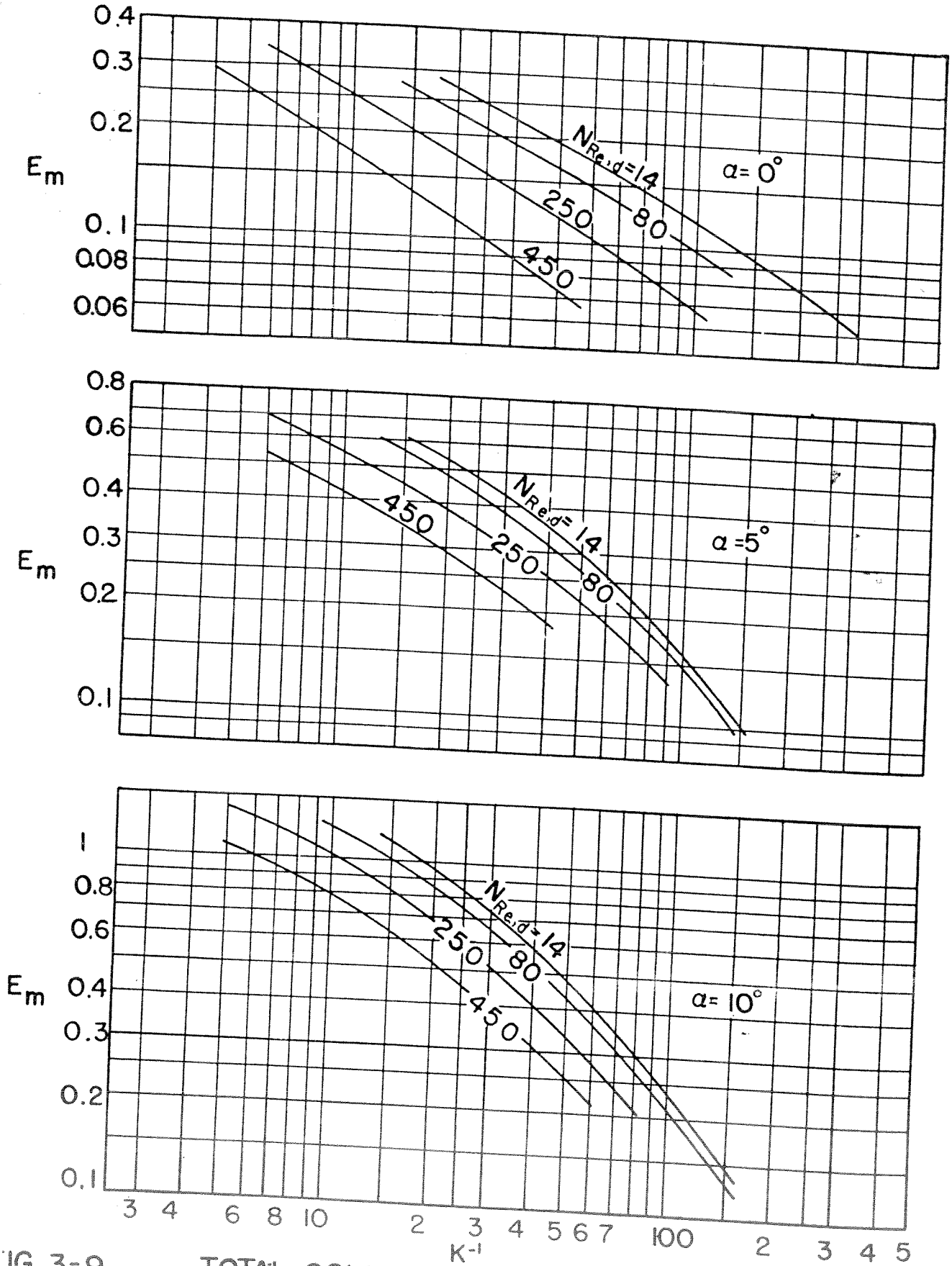

IG. 3-9 TOTAL COLLECTION EFFICIENCY ON NACA 65A005 AIRFOIL AT VARIOUS ANGLES OF ATTACK

Table 3-3 WATER DROPLET TRAJECTORY DATA OBTAINED WITH ANALOG COMPUTER FOR NACA 1S(50)002-(50)002 DOUBLE WEDGE AND NACA 65A005 AIRFOIL

NACA 1S(50)002-(50)002					NACA 65A005				
α	$N_{Re,d}$	K	$\frac{y_{o,u}-y_{o,l}}{L}$	$\frac{s_l}{L}$	α	$N_{Re,d}$	K	$\frac{y_{o,u}-y_{o,l}}{L}$	$\frac{s_l}{L}$
0°	0	0.333	0.0220	0.500	0°	0	0.100	0.019	0.068
	0	0.167	0.0128	0.500		0	0.025	0.0103	0.024
	0	0.100	0.0092	0.500		0	0.010	0.0075	0.0089
	0	0.033	0.0056	0.500					
	250	0.333	0.0175	0.500		250	0.167	0.0165	0.0525
	250	0.167	0.0096	0.500		250	0.021	0.0051	0.0092
	250	0.100	0.0058	0.500		250	0.0083	0.0040	0.0052
	450	0.333	0.0140	0.500		450	0.167	0.0115	0.0405
	450	0.167	0.0067	0.500		450	0.0416	0.0050	0.0100
						450	0.0208	0.0040	0.0065
5°	0	0.100	0.038	0.0275	5°	0	0.167	0.047	0.310
	0	0.050	0.027	0.020		0	0.0416	0.025	0.102
	0	0.010	0.0125	0.008		0	0.0167	0.014	0.042
	0	0.0026	0.0065	0.0032					
	80	0.100	0.0315	0.0225					
	80	0.025	0.0170	0.0115					
	250	0.333	0.049	0.035		250	0.167	0.0375	0.240
	250	0.100	0.0255	0.018		250	0.100	0.0285	0.155
	250	0.050	0.020	—		250	0.025	0.0132	0.047
	450	0.333	0.037	0.029		450	0.167	0.0240	0.155
	450	0.100	0.0205	—		450	0.100	0.0230	0.124
	450	0.050	0.0155	0.0085		450	0.025	0.0070	0.033
10°	0	0.167	0.103	—	10°	0	0.100	0.060	0.215
	0	0.100	0.072	—		0	0.050	0.050	0.165
	0	0.050	0.049	0.260		0	0.025	0.029	0.006
	0	0.010	0.029	—		0	0.010	0.015	0.0023
	0	0.0026	0.020	0.008					
	80	0.00833	0.048	—					
	80	0.025	0.030	—					
	250	0.333	0.092	0.420					
	250	0.167	0.042	—					
	450	0.667	0.105	0.450		450	0.100	0.040	0.115
	450	0.333	0.067	—		450	0.025	0.016	0.037
	450	0.167	0.049	0.245					
	450	0.014	0.020	—					

Table 3-4 TOTAL COLLECTION EFFICIENCY ON THREE THIN AIRFOILS IN SPECIFIC ICING CONDITIONS* (Ref. 28)

NACA Airfoil Section	Airfoil Chord Length (ft)	Major Axis of Equivalent Ellipse (ft)	Velocity U_o (mph)	Angle of Attack (deg)	Efficiency of Catch	Impingement Limit* (ft)	Inertial Parameter K	Droplet Reynolds Number $N_{Re,d}$
65A006	20	18	400	0	0.063	0.130	0.022	99
65A00475	11.5	10.35	400	0	0.11	0.134	0.038	99
65A0035	3	2.7	400	0	0.29	0.220	0.147	99
65A006	20	18	700	4	0.16	1.1	0.0386	172
65A00475	11.5	10.35	700	4	----	0.9	0.067	172
65A0035	3	2.7	700	4	0.95	1.0	0.257	172

*All results are for icing conditions of 20,000 ft pressure altitude, 15 micron droplets, and 15°F air temperature. For 4° angles of attack, the limit of impingement only on the lower surface is given.

3-3.2 Generalization of the Total Collection Efficiency

In a graph of E_m versus K^{-1} with $N_{Re,d}$ as parameter, it is quite often necessary to interpolate in $N_{Re,d}$. Further, it is difficult to represent more than one airfoil at one angle of attack with such a graph and many pages of graphs must be employed for each airfoil. If Stokes' law of drag on a sphere could be used, the quantity $C_D N'_{Re,d}/24$ in Eq. 3-5 and -6 would be identically unity, a correlation would be independent of $N_{Re,d}$, and interpolation would be unnecessary. This idea has led to the use of a kind of average inertia parameter to bring lines representing water impingement data closer together.

According to the procedure of Sherman, Klein, and Tribus (Ref. 120) the collection efficiency curves of the above airfoils for various droplet Reynolds numbers may be brought closer together by using the average inertia parameter

$$K_S \equiv \frac{\lambda}{\lambda_S} \cdot K \qquad (3\text{-}22)$$

where

$$\frac{\lambda}{\lambda_S} = \frac{1}{N_{Re,d}} \int_o^{N_{Re,d}} \frac{24}{C_D \eta} \cdot d\eta \qquad (3\text{-}23)$$

The symbol η is a dummy variable, representing the Reynolds number in Table 3-1. Physically, λ_S/λ is an average value of $C_D N_{Re,d}/24$ for a drop projected into still air, since λ_S is the distance the drop would travel if projected into still air with velocity U_o when the drag force obeys Stokes' law, while λ is the distance the drop would travel if projected into still air with velocity U_o when the drag coefficient follows the experimental values given in Table 3-1.

Figure 3-11 is a graph of E_m versus K_S curve for the NACA 65_1-208 airfoil. The curves are replotted from the graph of Fig. 3-7. The single dash-dot curve is drawn through the arithmetic averages. It correlates values for Reynolds numbers from 16 to 1024 within about 10 per cent. Similar curves are shown in Fig. 3-10 and -12 for the NACA 65A004

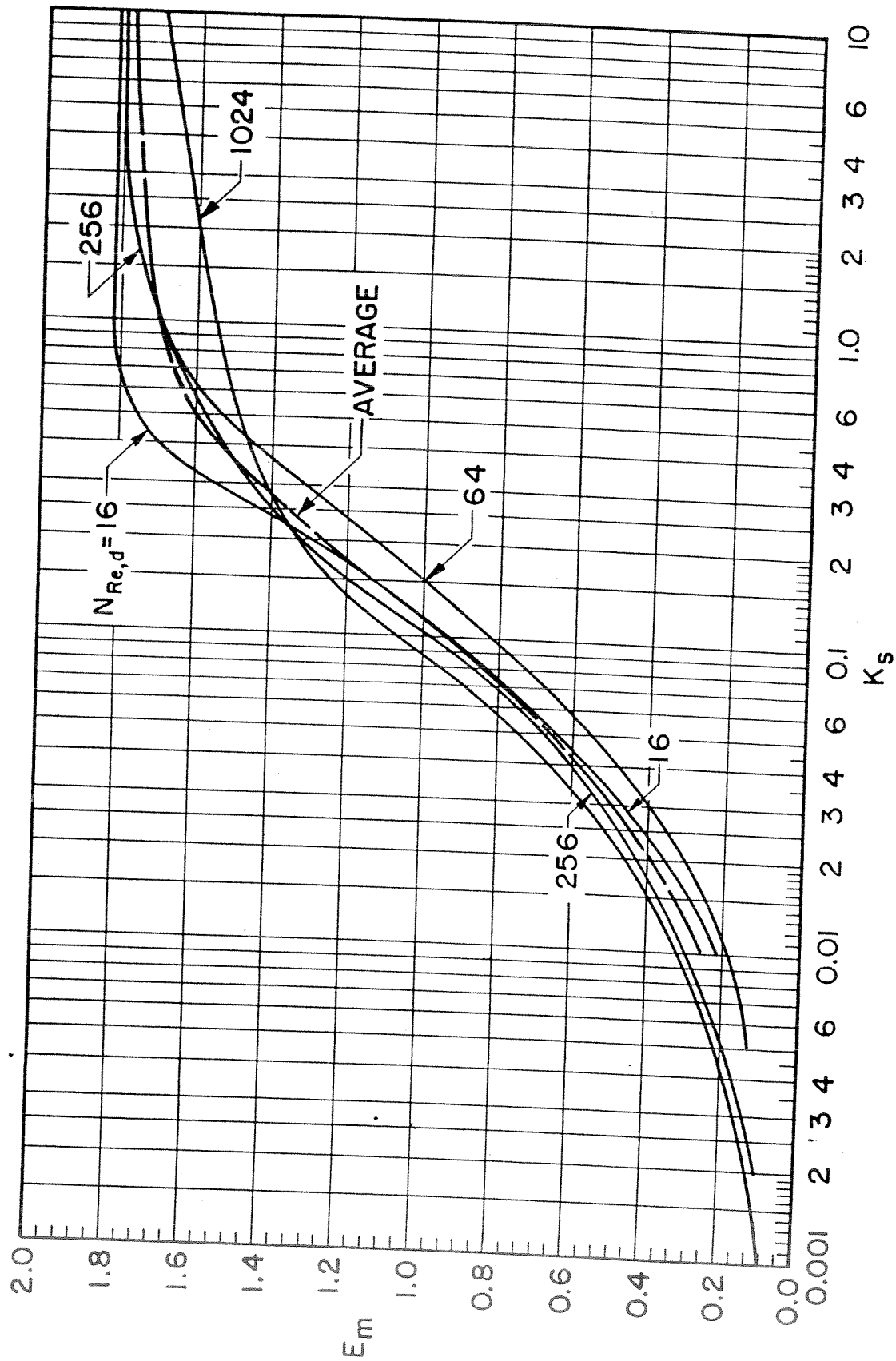

FIG. 3-10 TOTAL COLLECTION EFFICIENCY OF NACA 65A004 AIRFOIL AT 4° ANGLE OF ATTACK VERSUS K_S

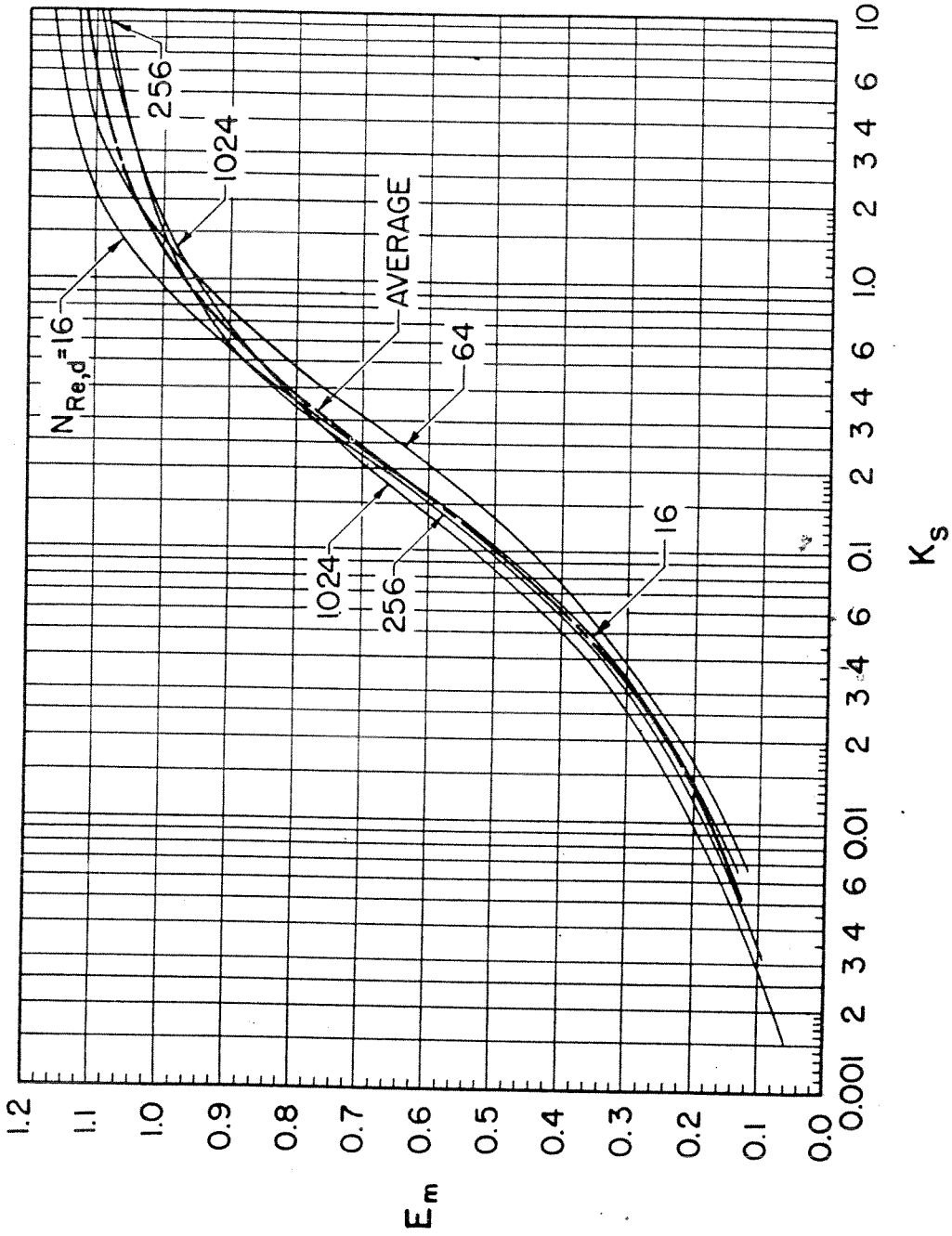

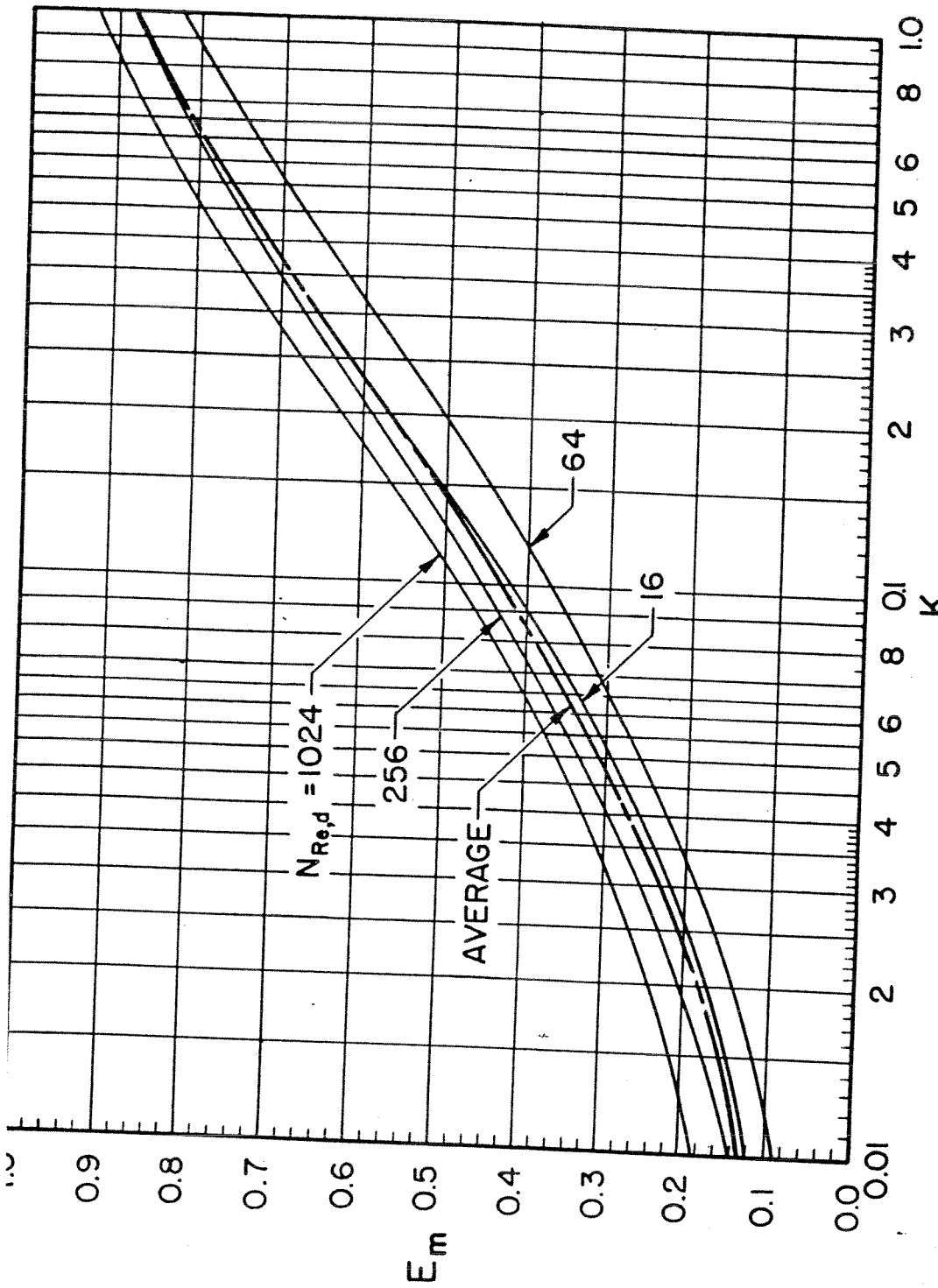

FIG.3-12 TOTAL COLLECTION EFFICIENCY OF NACA 65_1-212 AIRFOIL AT 4° ANGLE OF ATTACK VERSUS K_s

and 65_1-212 airfoils, respectively. Lenherr and Thompson (Ref. 102) have presented the aforementioned collection efficiency of the NACA 0006-64 airfoil in the same way with similar success.

Guibert, et al (Ref. 50 and 51), plotted E_m against $\mathcal{V}$ with $N_{Re,d}$ as parameter. Their data are applicable in the following range of variables:

Variable	Range
Droplet diameter D_d	20 to 100 microns
Speed U_o	100 to 400 mph
Altitude	Sea level to 20,000 ft
Chord length L	0.25 to 30 ft

Sherman, Klein, and Tribus (Ref. 120), employing their transformation, generalized this work. Average single curves for the 15 per cent thick Joukowski airfoil at various angles of attack and camber are plotted together in Fig. 3-13.

Tribus (Ref. 124) refers to a study by Drell and Valentine, who have plotted the collection efficiency curves of various airfoils in yet another fashion: $E_m \mathcal{V}$ versus $\mathcal{V}$ with $N_{Re,d}$ as parameter. For values of $\mathcal{V}$ less than 100 they brought the available data close together. For values of $\mathcal{V}$ larger than 100, however, the parameter $N_{Re,d}$ plays a significant role.

A graph of $E_m \mathcal{V}$ versus $\mathcal{V}$ has an advantage in dealing with a tapered wing of uniform per cent thickness, because each coordinate is independent of the velocity and (from Eq. 3-14, -18, and -20),

$$W' = \left[\frac{\rho_w}{9} \cdot \frac{\omega_w \cdot a}{\rho_o} \cdot \frac{(\Delta y)_{max}}{L} \cdot U_o\right] E_m \mathcal{V} \qquad (3\text{-}24)$$

where the quantity in brackets is a constant for this type of wing in given flight and icing conditions. Of course, it is supposed that the taper is small enough so that two-dimensional flow satisfactorily approximates the actual flow.

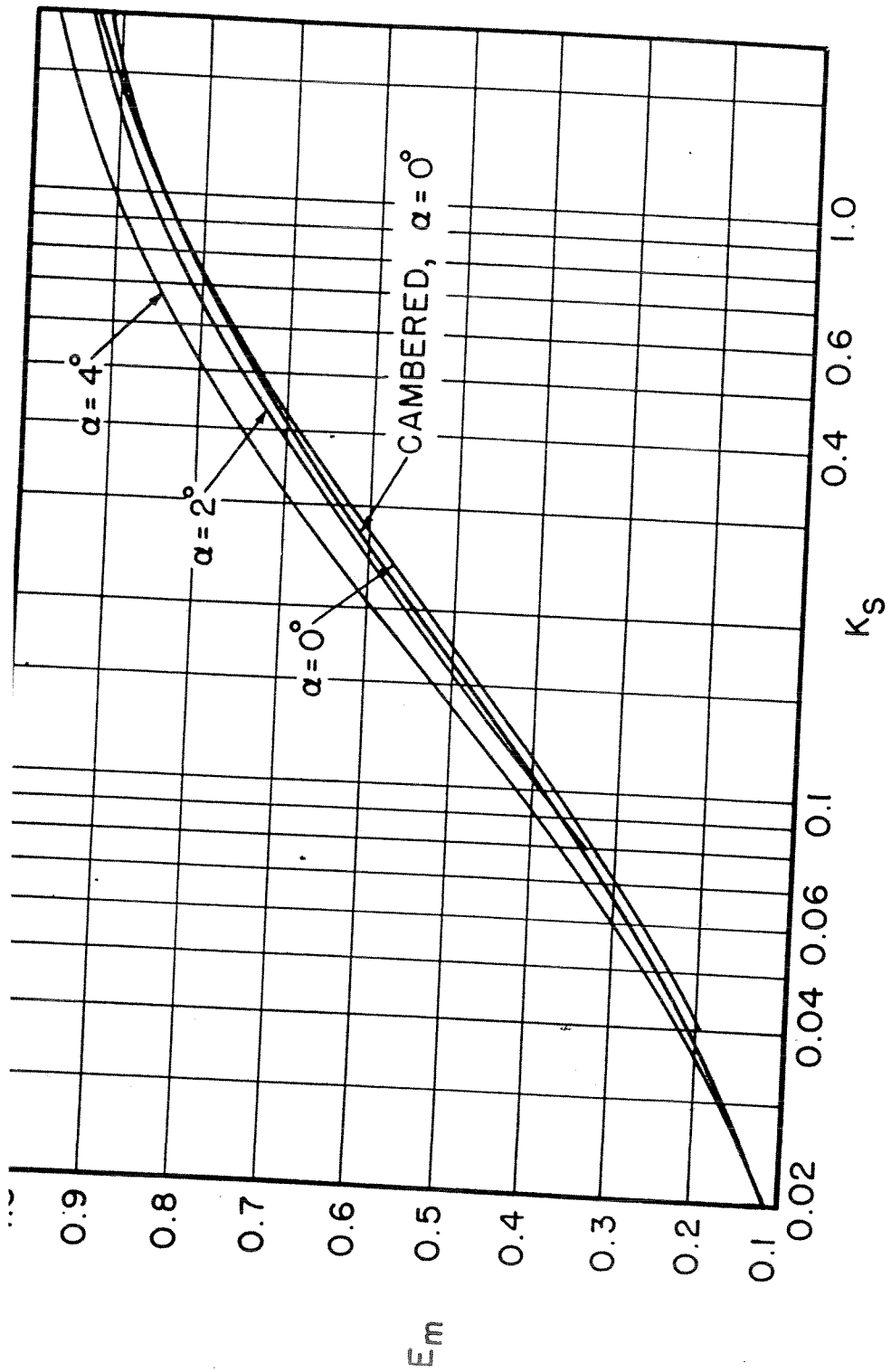

FIG. 3-13 TOTAL COLLECTION EFFICIENCY OF 15 PER-CENT JOUKOWSKI AIRFOILS AT VARIOUS ANGLES OF ATTACK

3-3.3 Dimensional Charts of Water Impingement Data

For practical calculations it is more convenient to employ dimensional charts, particularly when lengthy analyses are necessary. These charts can be constructed from the dimensionless graphs presented in the previous sections. Typical charts are shown in Fig. 3-14 to -19 for the NACA 65A004, 65_1-208, and 65_1-212 airfoils at 10,000 and 20,000 ft pressure-altitude. In constructing these charts, the air temperature was assumed to be 15°F and the mean effective droplet size 20 microns diameter. Other similar charts based on the most probable icing temperature of Fig. A-1 are presented in Ref. 23 and 26 for the same airfoils. Similar kinds of charts for other airfoils can be constructed as individual needs arise.

3-4 Area of Impingement

Knowledge of the area of impingement per unit span is needed to determine how far back the double-skin heater should extend. Also, it will be required in some calculations of Chapters 5 and 6.

The trajectories tangent to the airfoil surface separate all trajectories into those that are deflected away from the surface before reaching it and those that intersect the surface. The points of tangency determine the area of impingement. This area depends upon the largest droplet size; for simplicity, the discussion is limited here to droplets of uniform size.

The length s_u and s_l will denote the profile distances of impingement from the geometric leading edge of the airfoil on the upper and lower surfaces, respectively. The ratios of these distances to the chord length are dependent on any two of the impingement parameters K^{-1}, $N_{Re,d}$, ψ, and ϕ.

The results of Guibert et al (Ref. 50 and 51) cover Joukowski airfoils at various angles of attack and camber and the NACA 65_2-015 at 4° angle of attack. They were originally presented in the form s_u/L (or s_l/L) versus ψ with $N_{Re,d}$ as parameter. Sherman, Klein, and Tribus (Ref. 120), using the idea of the average inertia parameter K_S (see Section 3-3.2), correlated the results so that in a graph of s_u/L (or s_l/L) versus K_S,

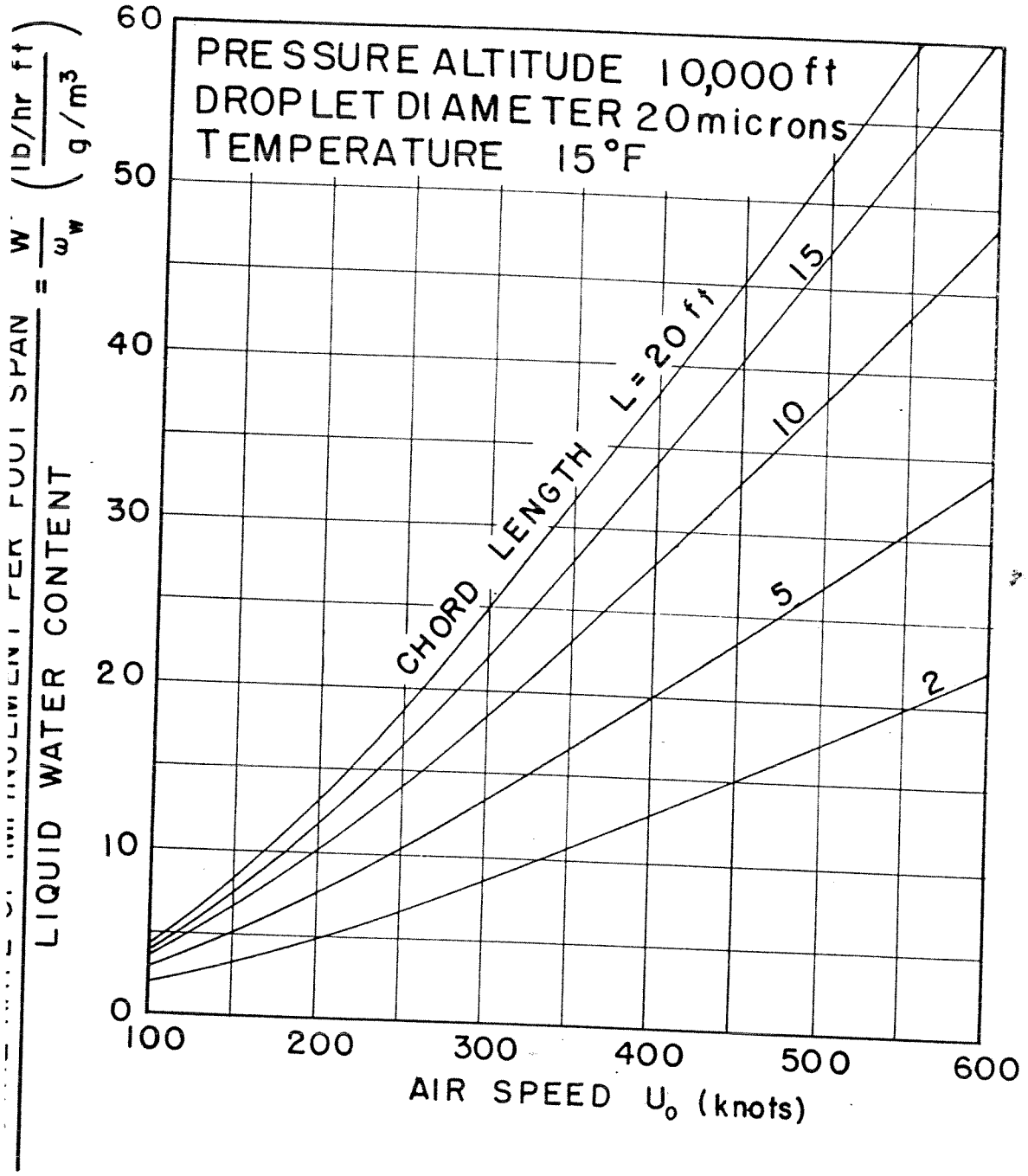

IG. 3-14 RATE OF WATER IMPINGEMENT ON NACA 65A004 AIRFOIL AT 4° ANGLE OF ATTACK (10,000 ft)

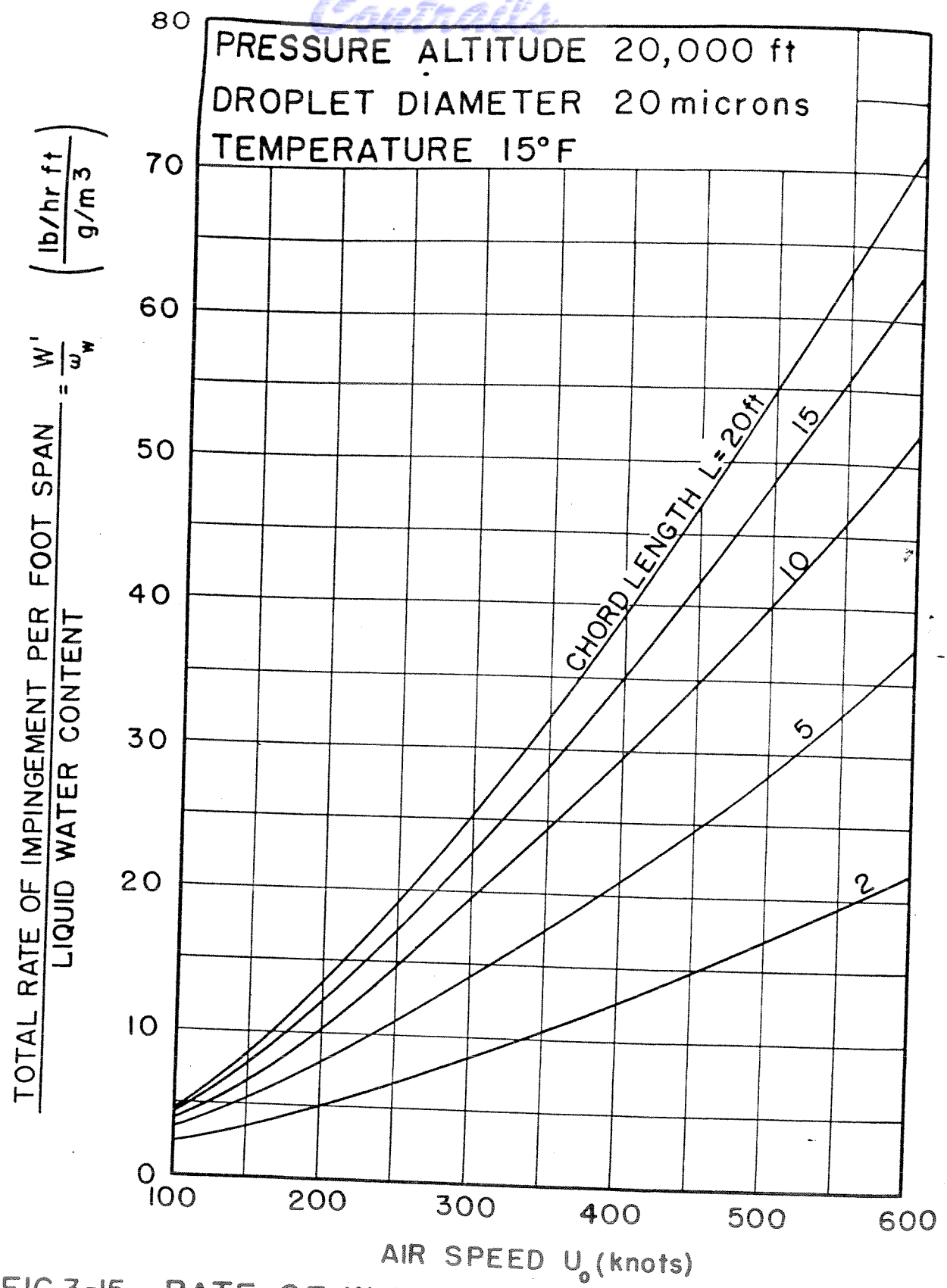

FIG.3-15 RATE OF WATER IMPINGEMENT ON NACA 65A004 AIRFOIL AT 4° ANGLE OF ATTACK (20,000 ft)

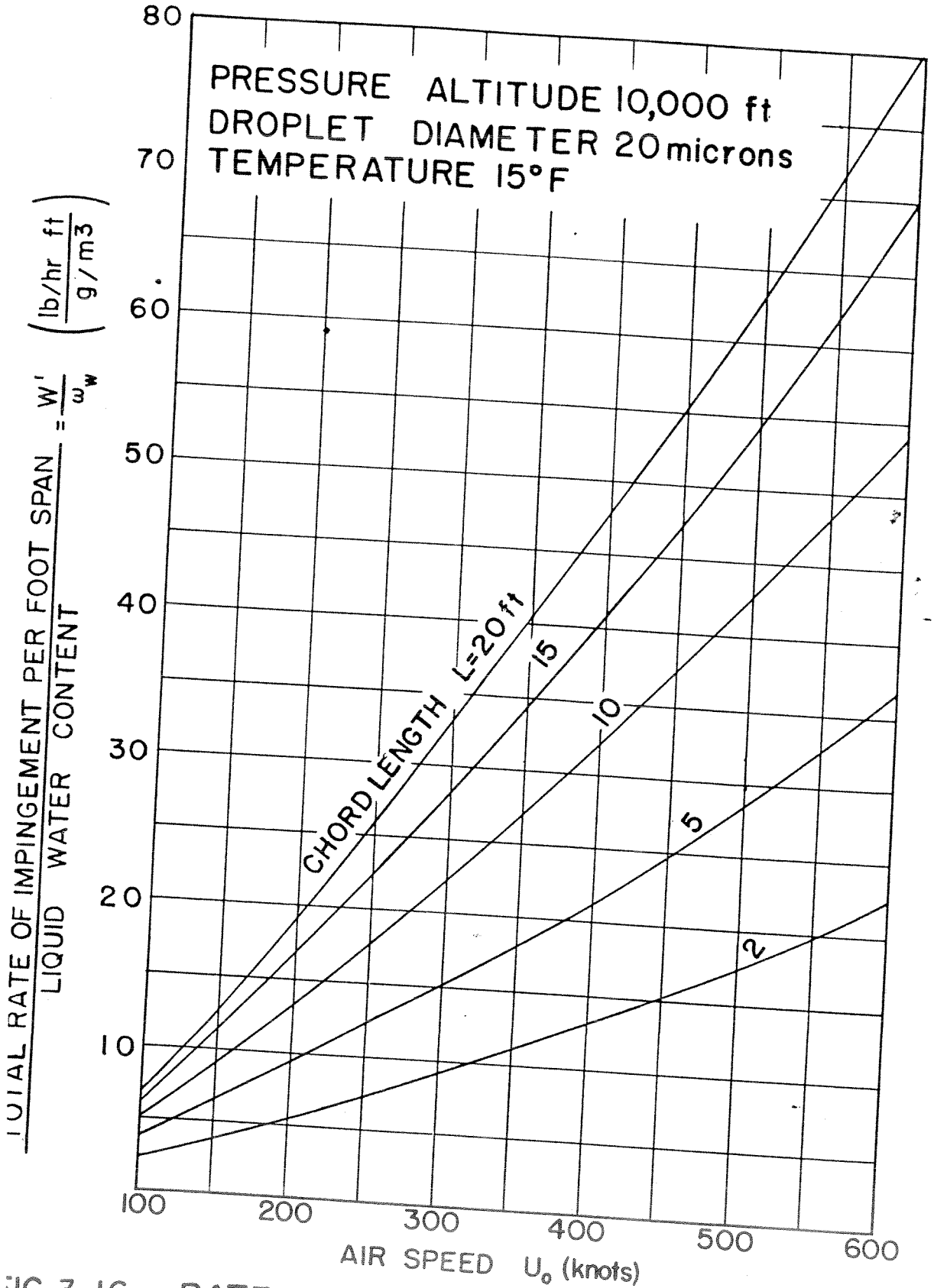

FIG. 3-16 RATE OF WATER IMPINGEMENT ON NACA 65-208 AIRFOIL AT 4° ANGLE OF ATTACK (10,000 ft)

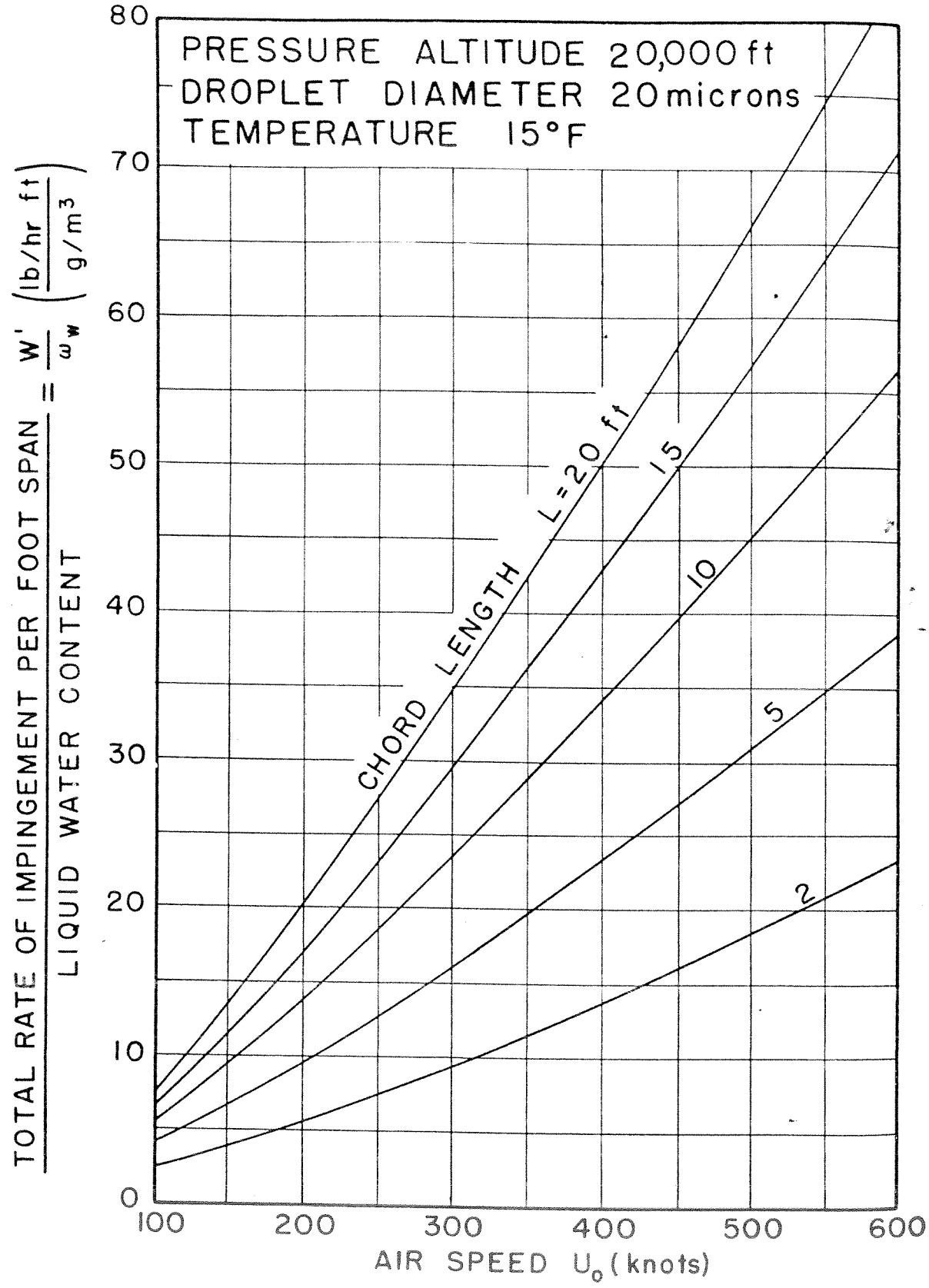

FIG. 3-17 RATE OF WATER IMPINGEMENT ON NACA 65_1-208 AIRFOIL AT 4° ANGLE OF ATTACK (20,000 ft)

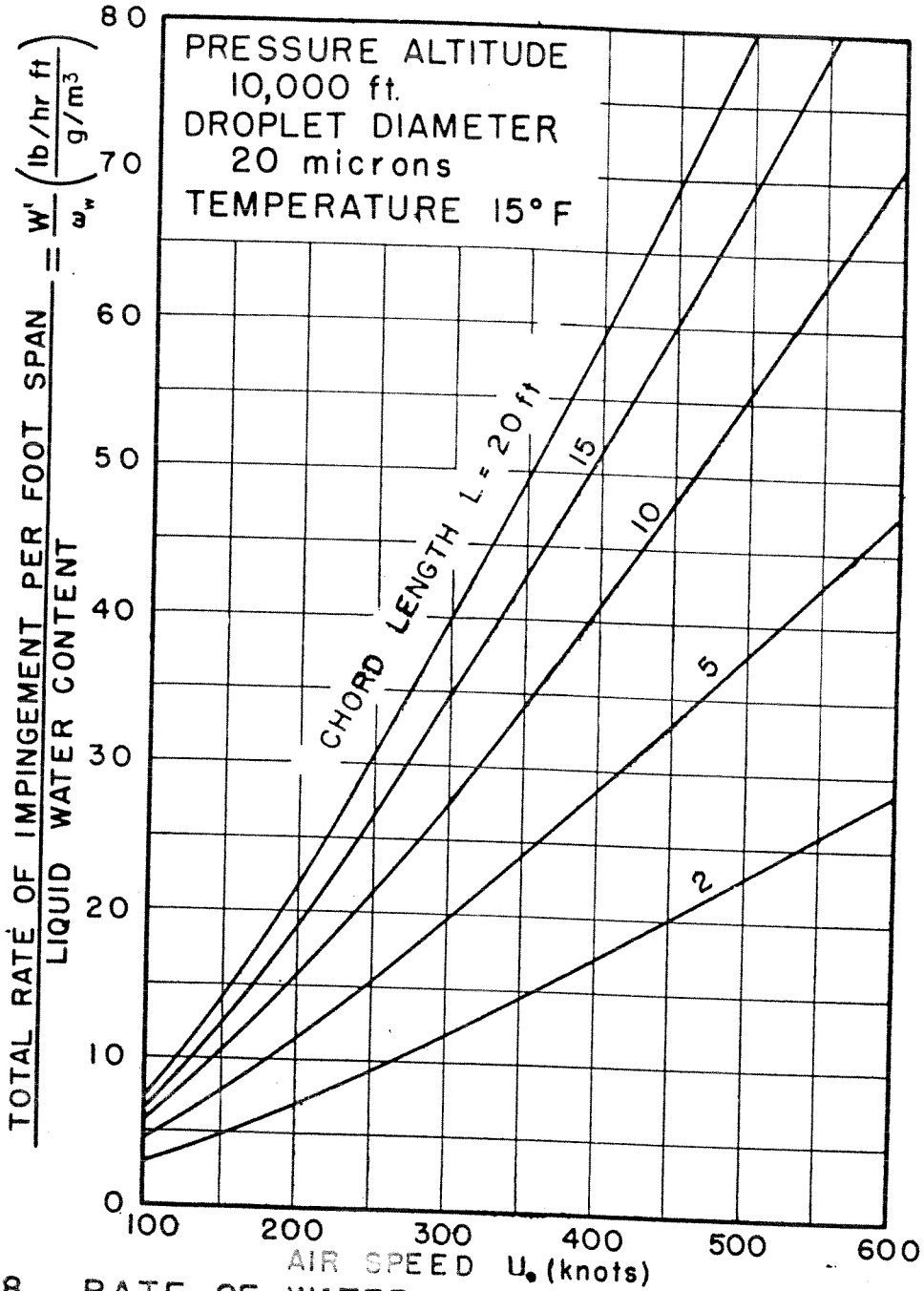

FIG. 3-18 RATE OF WATER IMPINGEMENT ON NACA 65$_1$-212 AIRFOIL AT 4° ANGLE OF ATTACK (10,000 ft)

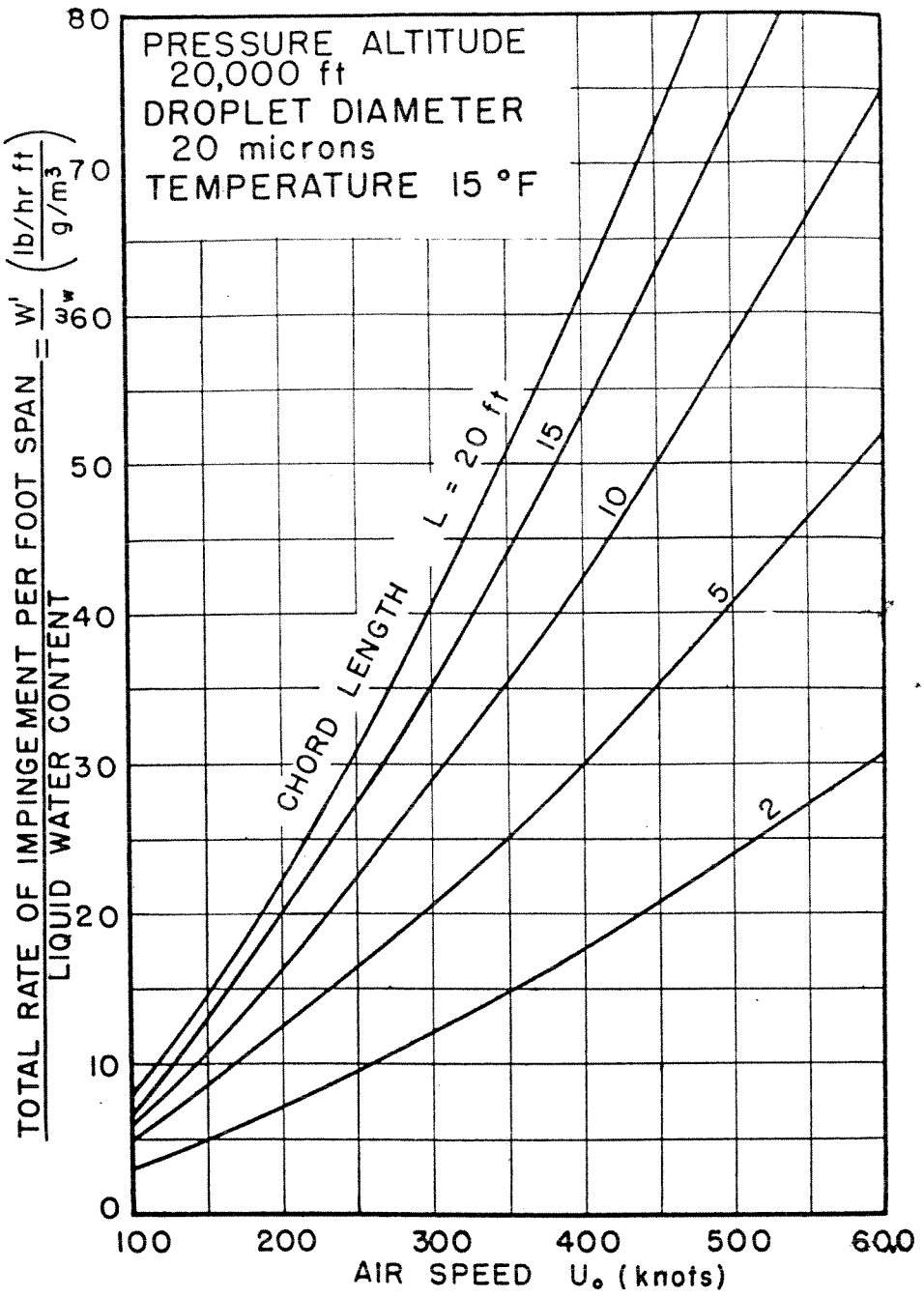

FIG. 3-19 RATE OF WATER IMPINGEMENT ON NACA 65-212 AIRFOIL AT 4° ANGLE OF ATTACK (20,000 ft)

they were virtually independent of the droplet Reynolds number. The deviations from a curve drawn through the averages for a particular airfoil at a given angle of attack could be neglected for most practical purposes. The values of s_u/L and s_l/L for the 15 per cent symmetrical and cambered Joukowski airfoils at various angles of attack are shown in Fig. 3-20.

The area of impingement per unit span for the NACA 0006-64 (6 per cent) airfoil at zero angle of attack is presented in terms of $s_u/L = s_l/L$ versus ψ with $N_{Re,d}$ as parameter in Fig. 3-21.

Brun et al (Ref. 23 and 24) presented s_u/L and s_l/L as functions of K^{-1} with $N_{Re,d}$ as parameter for the NACA 65A004, 65_1-208, and 65_1-212 airfoils at 4° angle of attack. Attempts were made during the present project to recorrelate those values in terms of K_S as suggested in Ref. 120. Deviations from the averages of the impingement areas corresponding to the droplet Reynolds numbers from 16 to 1024 were found to be fairly small in the case of the NACA 65_1-212 but excessive in the case of the NACA 65_1-208 airfoil. For this reason generalized charts for these airfoils are not recommended, and instead the graphs from Ref. 23 and 24 are reproduced as Fig. 3-22 to -25 in this manual. Apparently, the method of Ref. 120 is not dependable for thin airfoils.

Results calculated by Research, Incorporated, on the NACA 1S(50)002-50)002 and on the NACA 65A005 airfoil are presented in Fig. 3-26 and -27, respectively. At zero angle of attack, the area of impingement on the double wedge is 0.5; at 5 and 10° angles of attack, $s_u/L = 0$. The limit of impingement on the upper surface of the NACA 65A005 airfoil at 5 and 10° angles of attack is such that $0 < s_u/L < 0.001$.

3.5 Distribution of Impingement on Airfoils

The droplets strike the surface of an airfoil in greater numbers on unit area of the leading edge than on the downstream regions. While knowledge of the total rate of impingement is useful for purposes of preliminary design, the distribution of the droplet impingement is needed for detailed analysis of a given system. The distribution may be considered in two ways which are discussed in the next two sections.

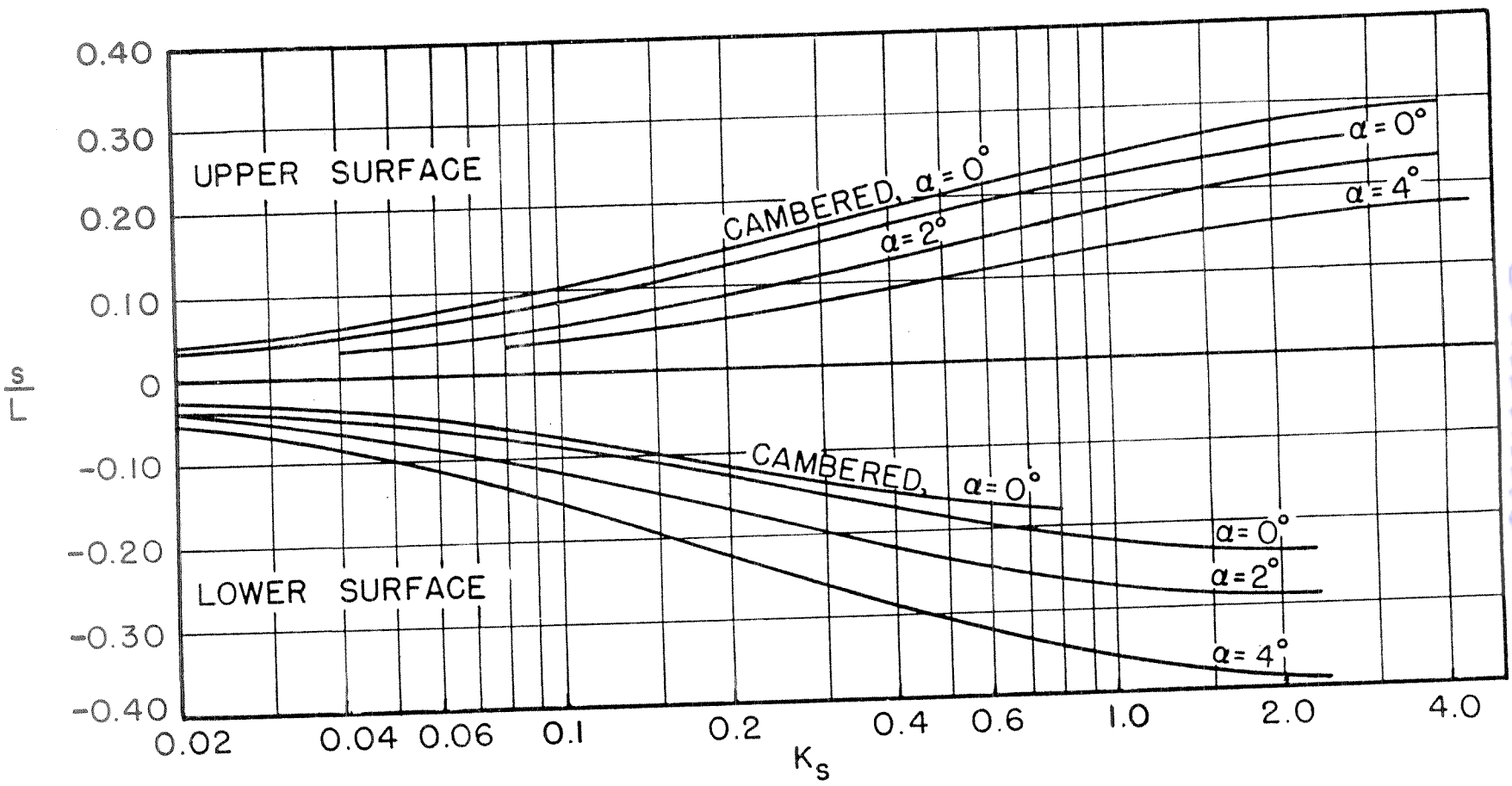

FIG. 3-20 IMPINGEMENT AREA ON JOUKOWSKI 15 PER-CENT AIRFOILS AT VARIOUS ANGLES OF ATTACK

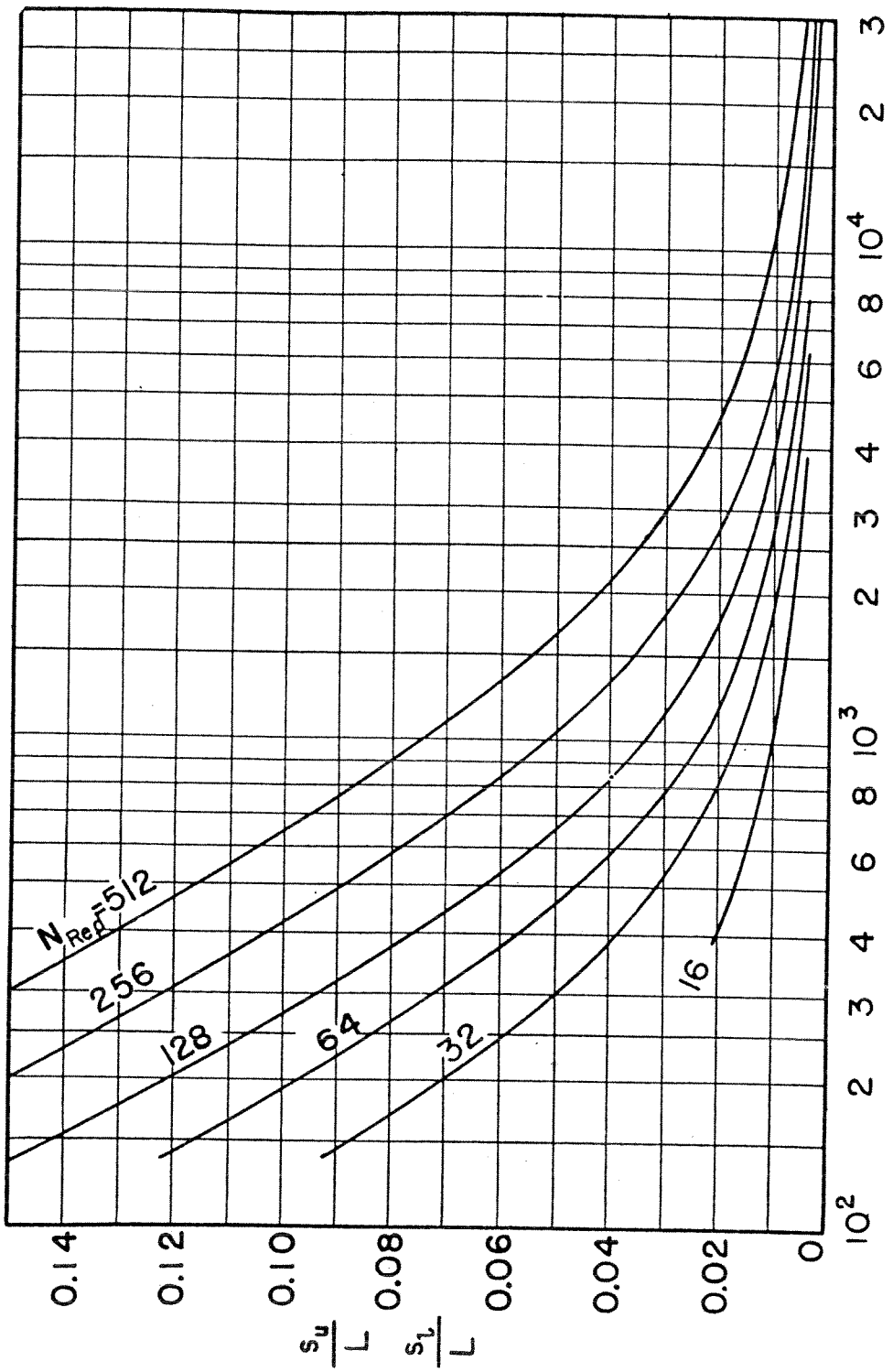

FIG. 3-21 IMPINGEMENT AREA ON NACA 0006-64 AIRFOIL AT 0° ANGLE OF ATTACK

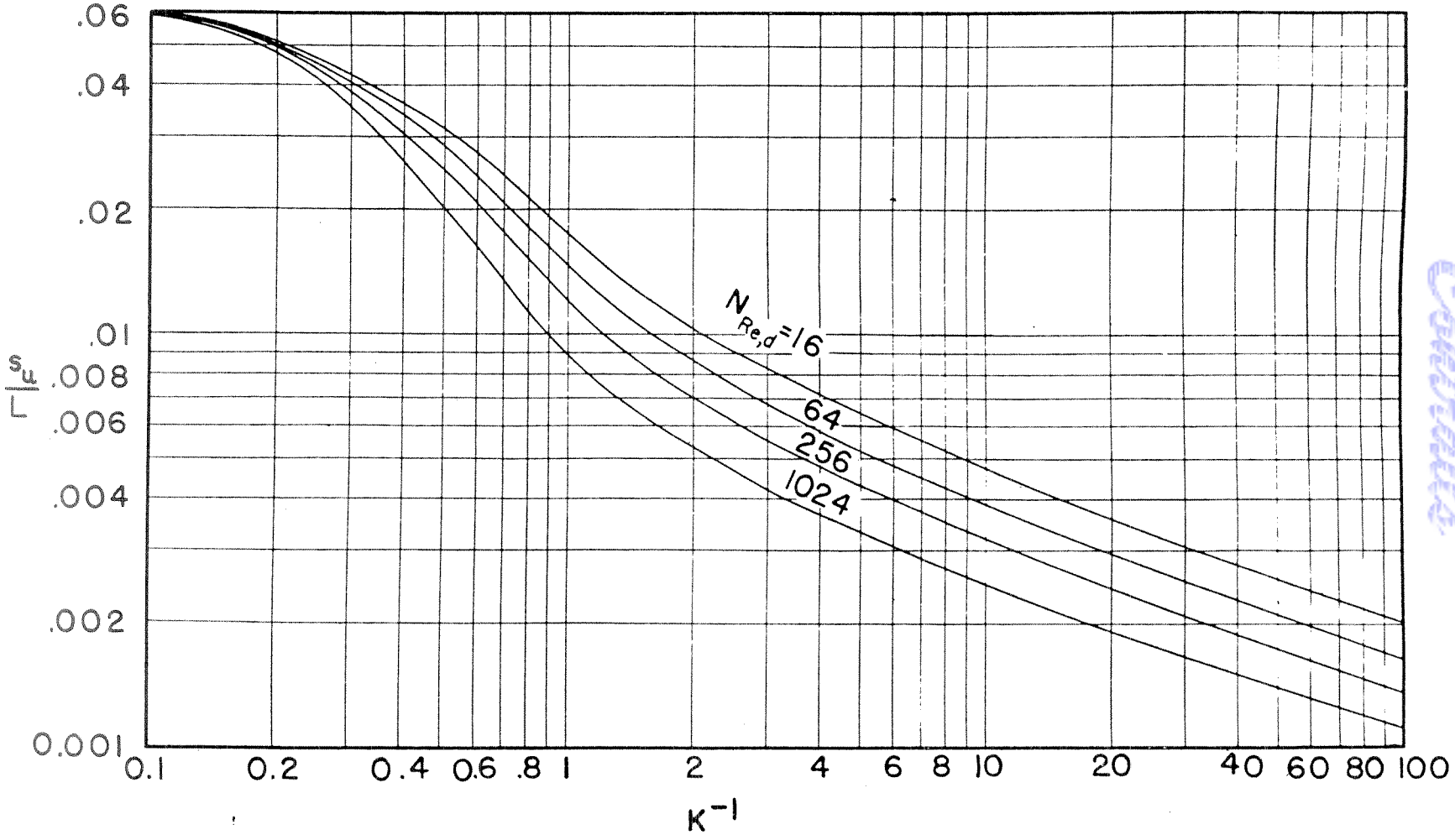

FIG. 3-22 IMPINGEMENT AREA ON UPPER SURFACE OF NACA 65A004 AIRFOIL AT 4° ANGLE OF ATTACK

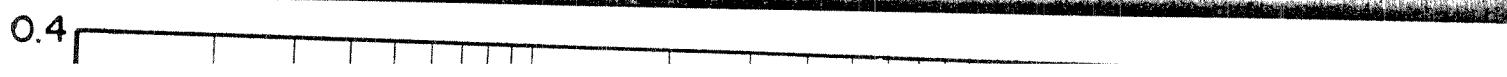

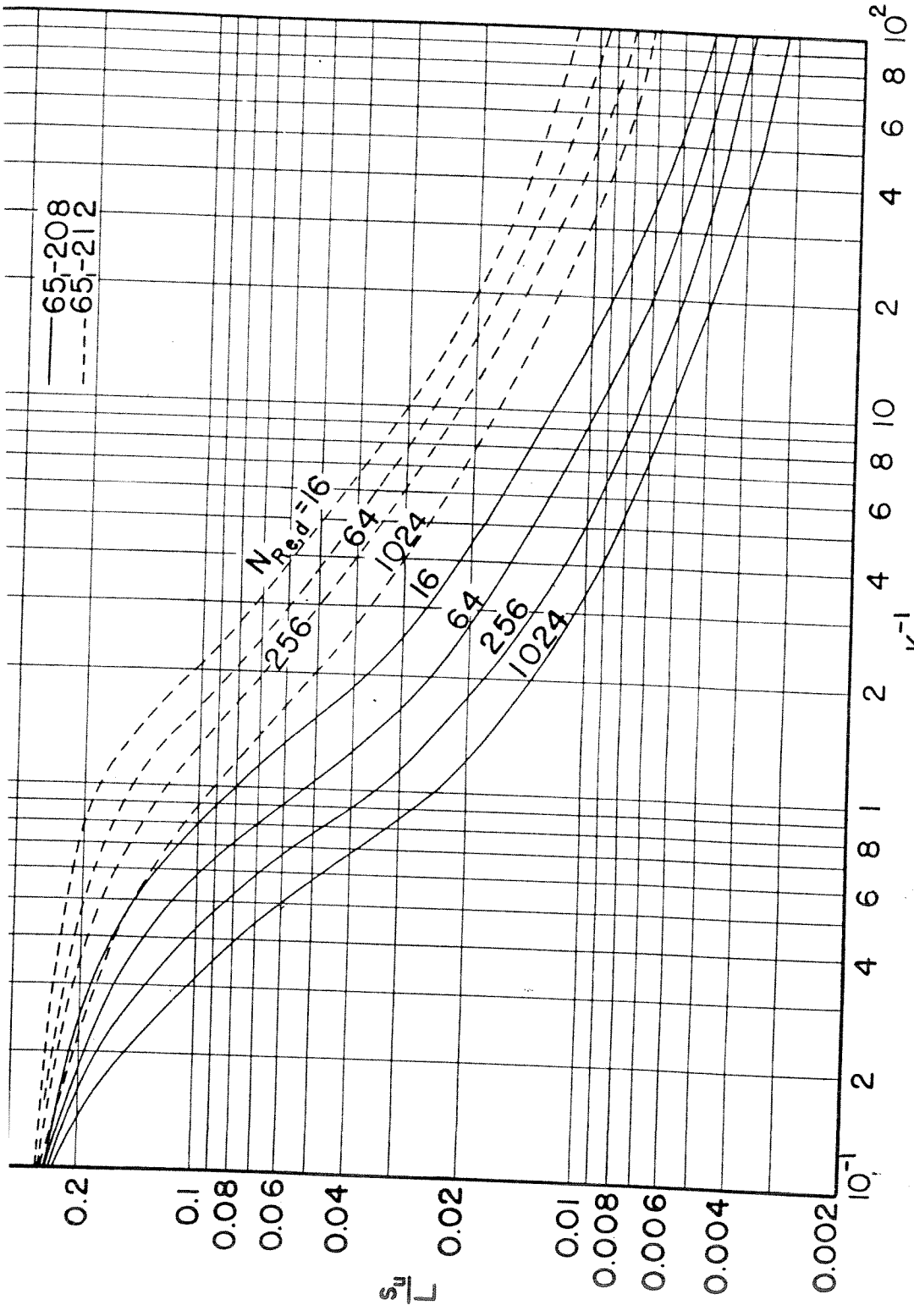

FIG. 3-23 IMPINGEMENT AREA ON UPPER SURFACES OF NACA 65_1-208 AND 65_1-212 AIRFOILS AT 4° ANGLE OF ATTACK

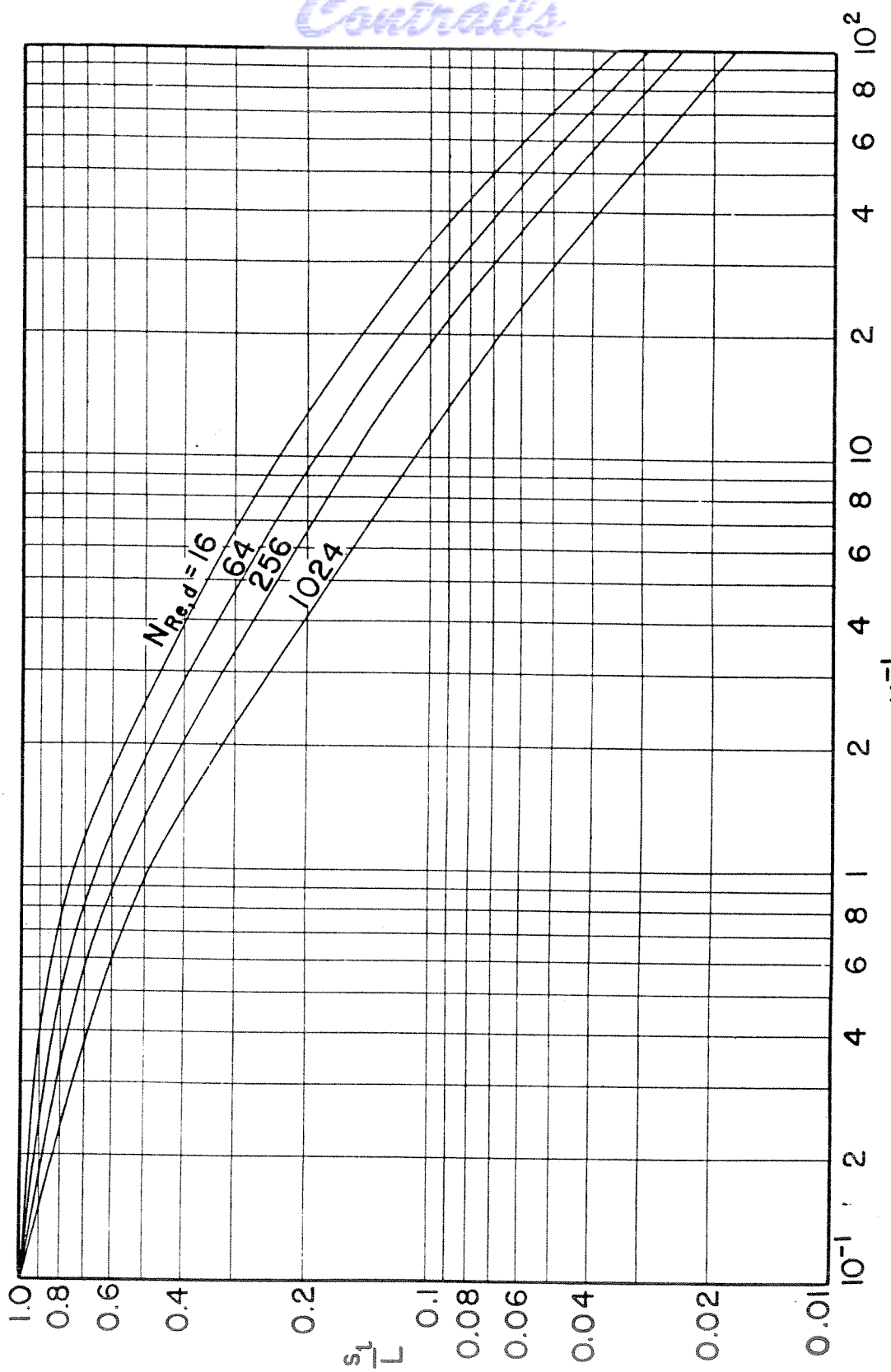

FIG. 3-24 IMPINGEMENT AREA ON LOWER SURFACE OF NACA 65A004 AIRFOIL AT 4° ANGLE OF ATTACK

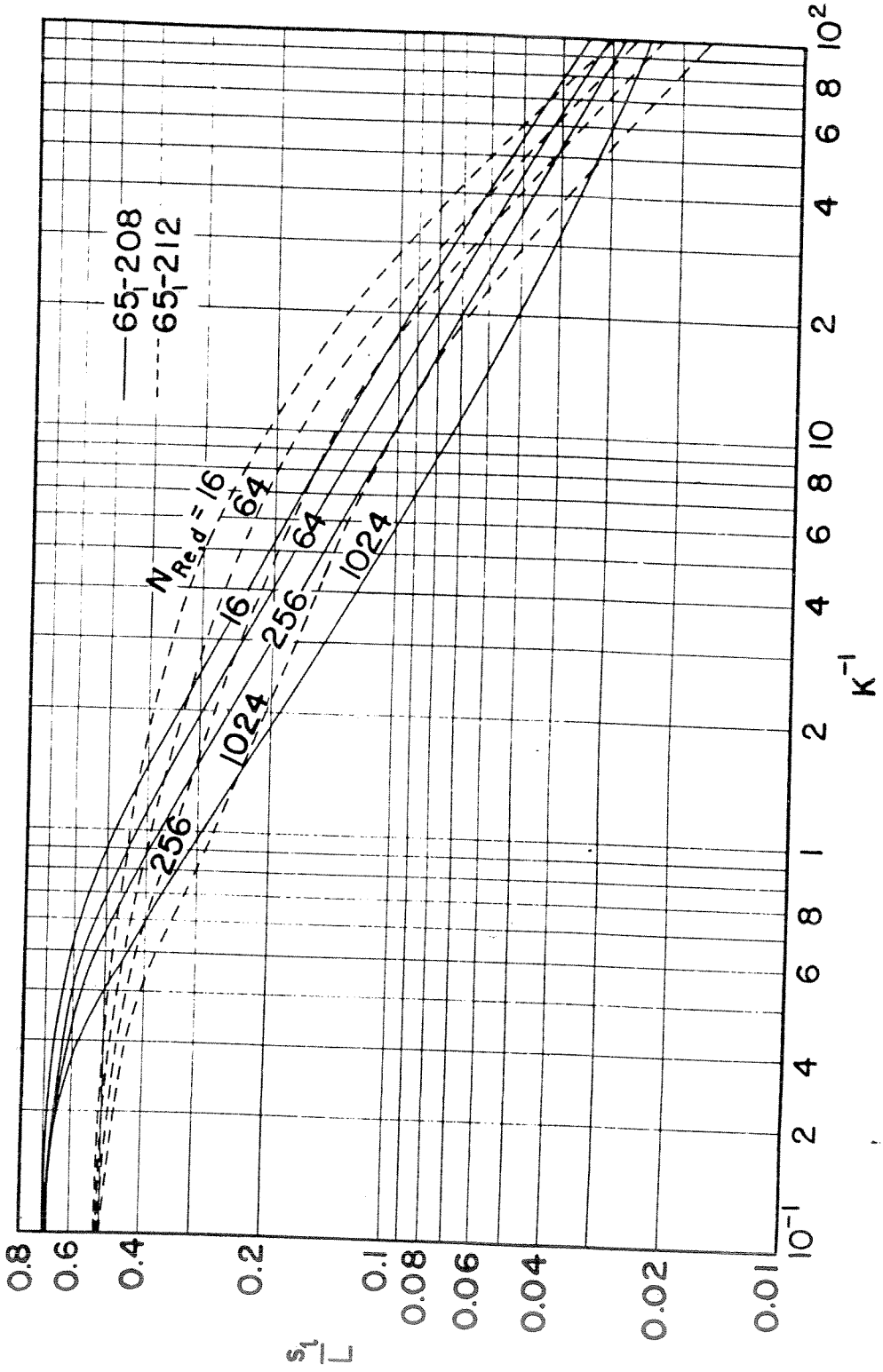

FIG. 3-25 IMPINGEMENT AREA ON LOWER SURFACES OF NACA 65_1-208 AND 65_1-212 AIRFOILS AT 4° ANGLE OF ATTACK

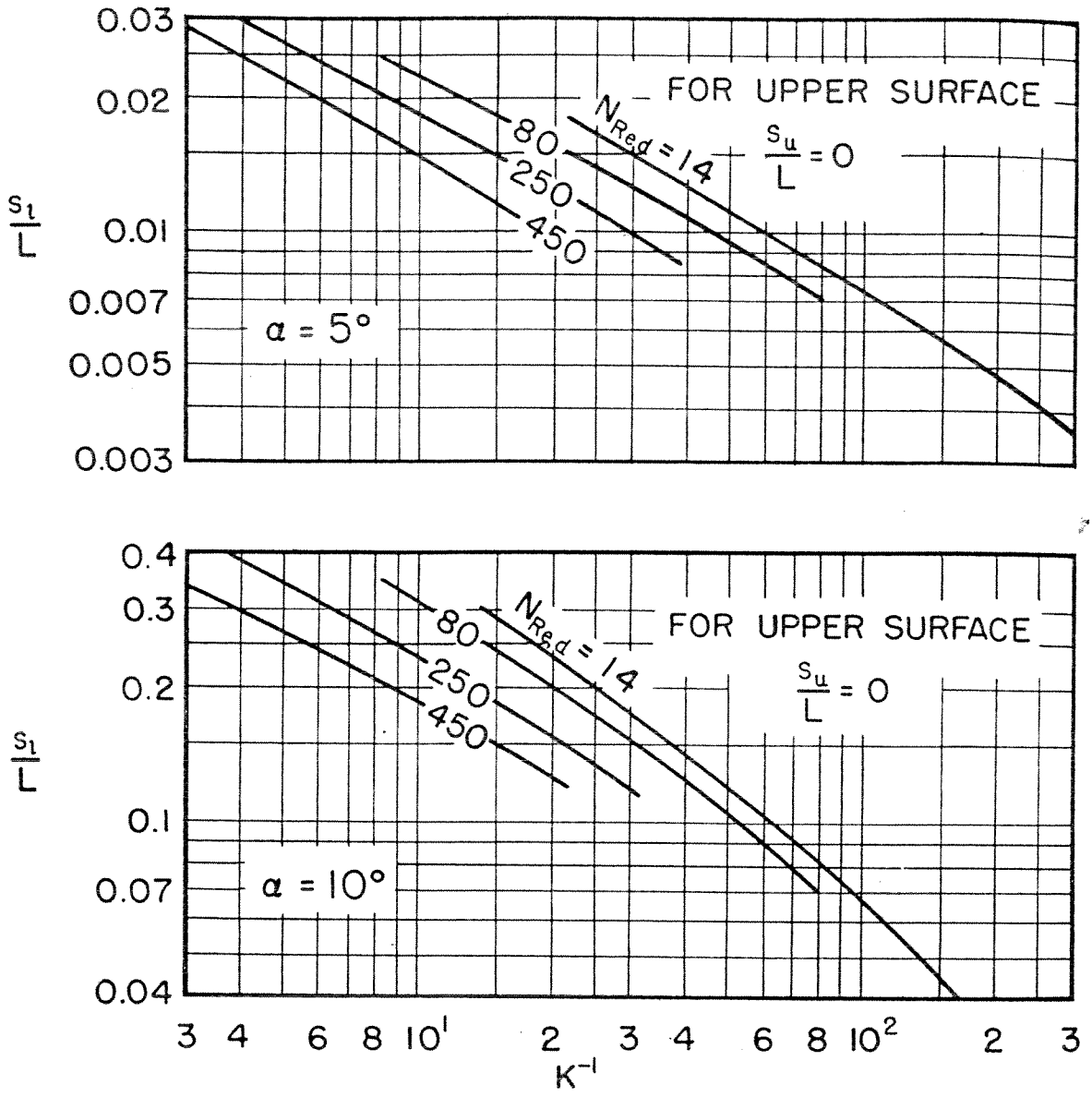

FIG. 3-26 IMPINGEMENT AREA ON NACA IS(50)002-(50)002 DOUBLE WEDGE AT 5° AND 10° ANGLE OF ATTACK

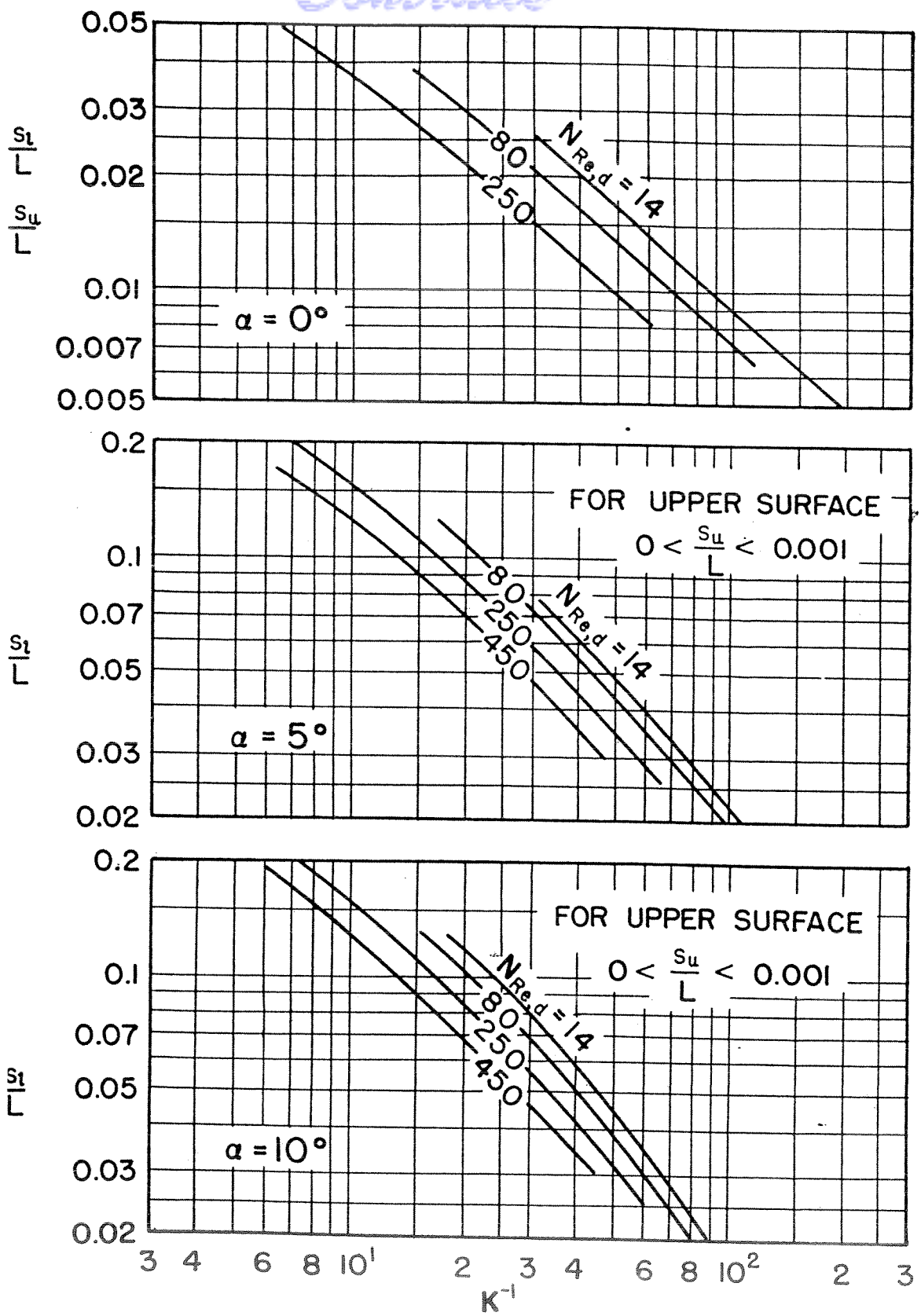

FIG 3-27 IMPINGEMENT AREA ON NACA 65A005 AIRFOIL AT VARIOUS ANGLES OF ATTACK

3-5.1 Accumulated Collection Efficiency

The rate of impingement per unit span may be considered a function of s/L, say $W'(s/L)$. This function is defined so that $W'(s_l/L) = 0$; that is, it represents the rate of impingement on the portion of the surface bounded by the tangent point at s_l/L on the lower surface and the impingement point at s/L where the intermediate trajectory strikes the surface. For example, $W'(s_u/L) = W'$, which is the quantity plotted in Fig. 3-14 through -19.

An accumulated collection efficiency E, which depends upon s/L, is defined,

$$W'(s/L) = U_o \cdot (\Delta y)_{max} \cdot E \cdot \omega_w \tag{3-25}$$

It follows from the definitions of E and E_m that

$$W'(s/L) = \frac{E}{E_m} \cdot W' \tag{3-26}$$

The ratio E/E_m depends upon any two of the impingement parameters K^{-1}, $N_{Re,d}$, ψ, and ϕ. Obviously, the rate of water catch between points s_A/L and s_B/L is equal to

$$W'(s_B/L) - W'(s_A/L) = \left(\frac{E_B}{E_m} - \frac{E_A}{E_m}\right) W' \tag{3-27}$$

Guibert et al (Ref. 50 and 51) calculated the distribution data for the Joukowski symmetrical 15 per cent airfoil at 0°, 2°, and 4° angles of attack, for the Joukowski cambered 15 per cent airfoil at 0° angle of attack, and for the NACA 65_2-015 airfoil at 4° angle of attack. They presented their results by plotting E/E_m against s/L with $N_{Re,d}$ and K^{-1} as parameters. These charts are reproduced as Fig. 3-28 to -45.

Inspection of these distribution curves reveals that for a given value of K^{-1}, the effect of $N_{Re,d}$ is small; but that for a given value of $N_{Re,d}$, the effect of varying K^{-1} is quite large. This means that droplet size is relatively more important than velocity in determining the distribution of the water impingement.

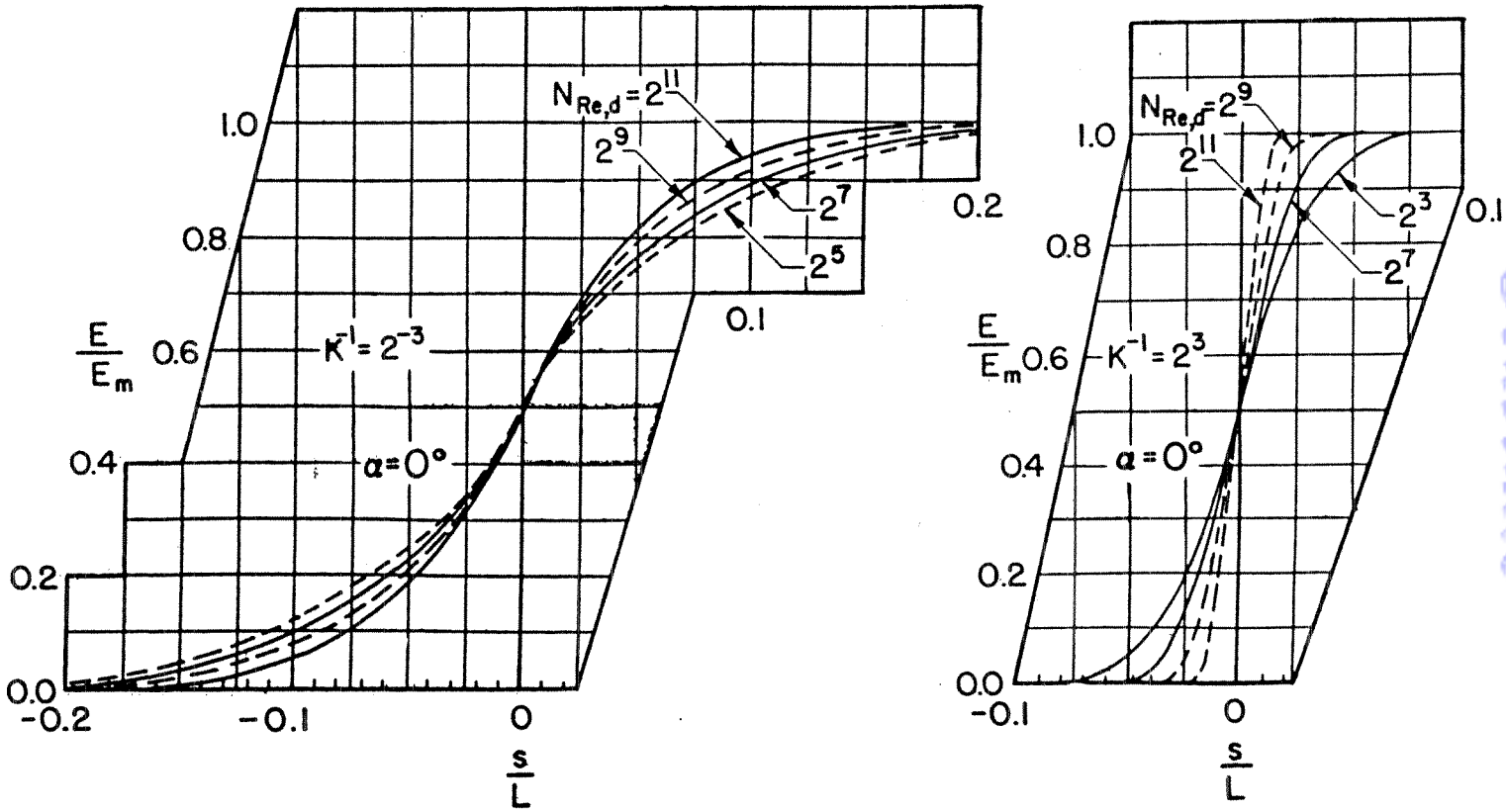

FIG.3-28 ACCUMULATED COLLECTION EFFICIENCY FOR JOUKOWSKI SYMMETRICAL 15 PER-CENT AIRFOIL AT 0° ANGLE OF ATTACK

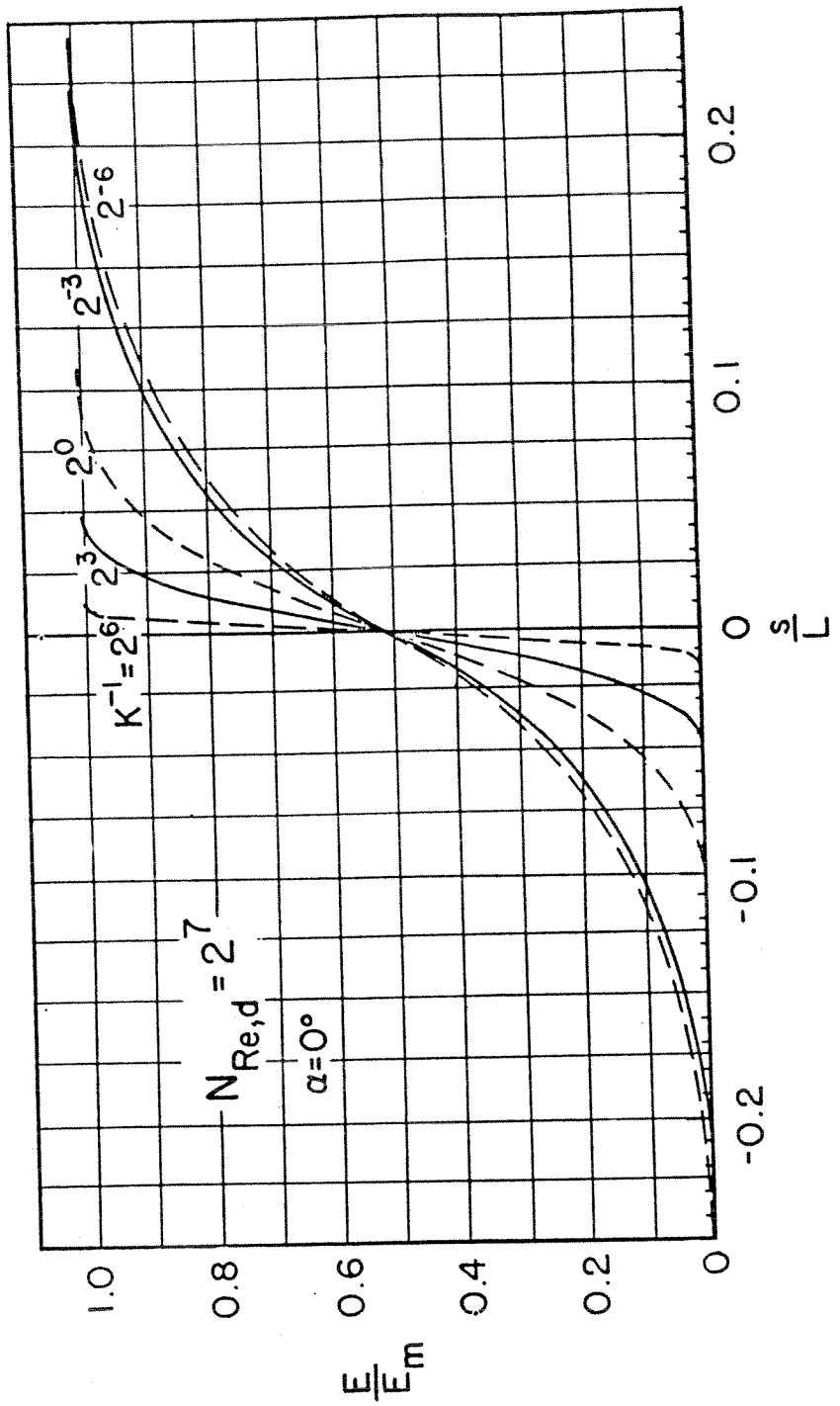

FIG. 3-29 ACCUMULATED COLLECTION EFFICIENCY FOR JOUKOWSKI SYMMETRICAL 15 PER-CENT AIRFOIL AT 0° ANGLE OF ATTACK

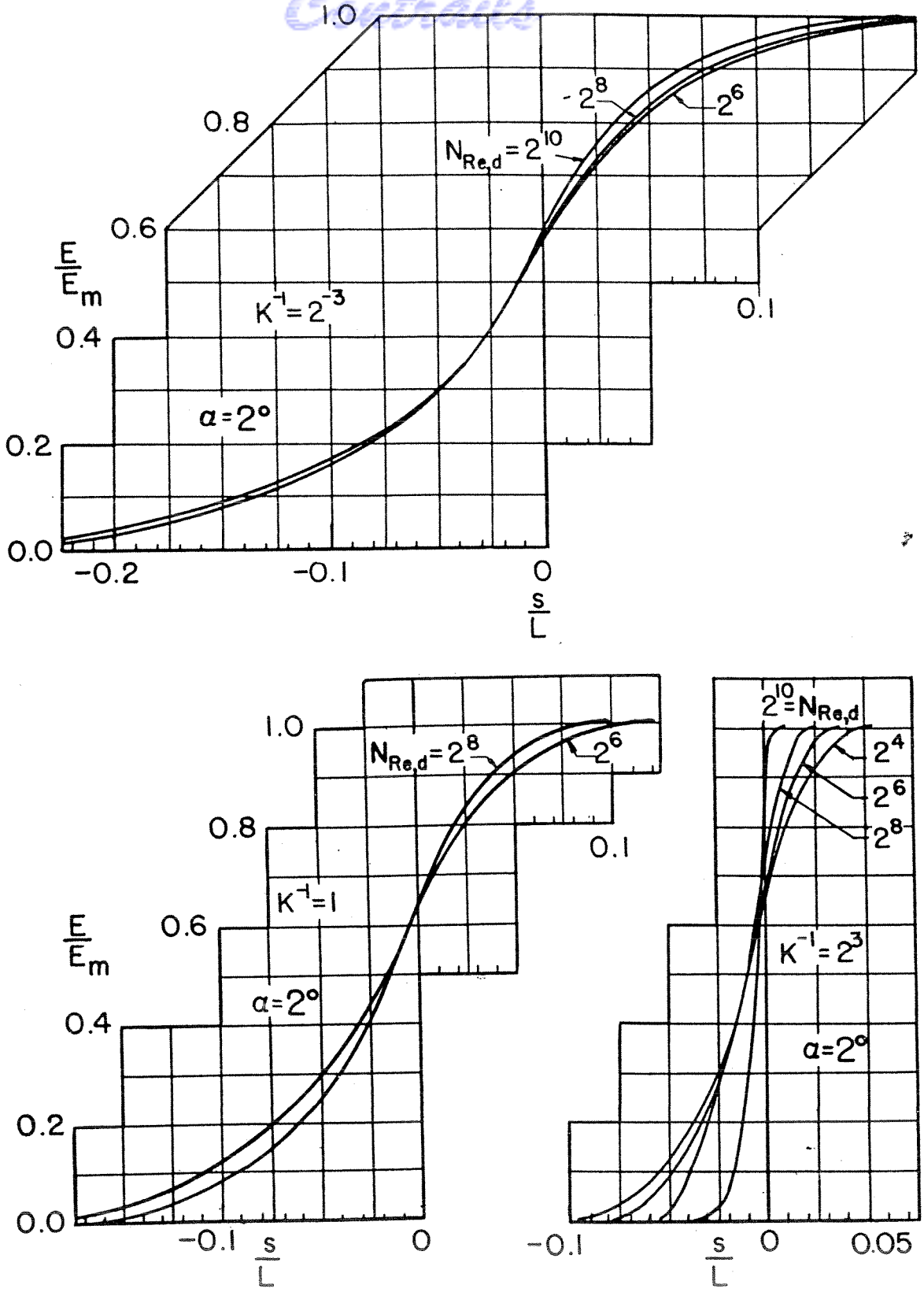

FIG. 3-30 ACCUMULATED COLLECTION EFFICIENCY FOR JOUKOWSKI SYMMETRICAL 15 PER-CENT AIRFOIL AT 2° ANGLE OF ATTACK

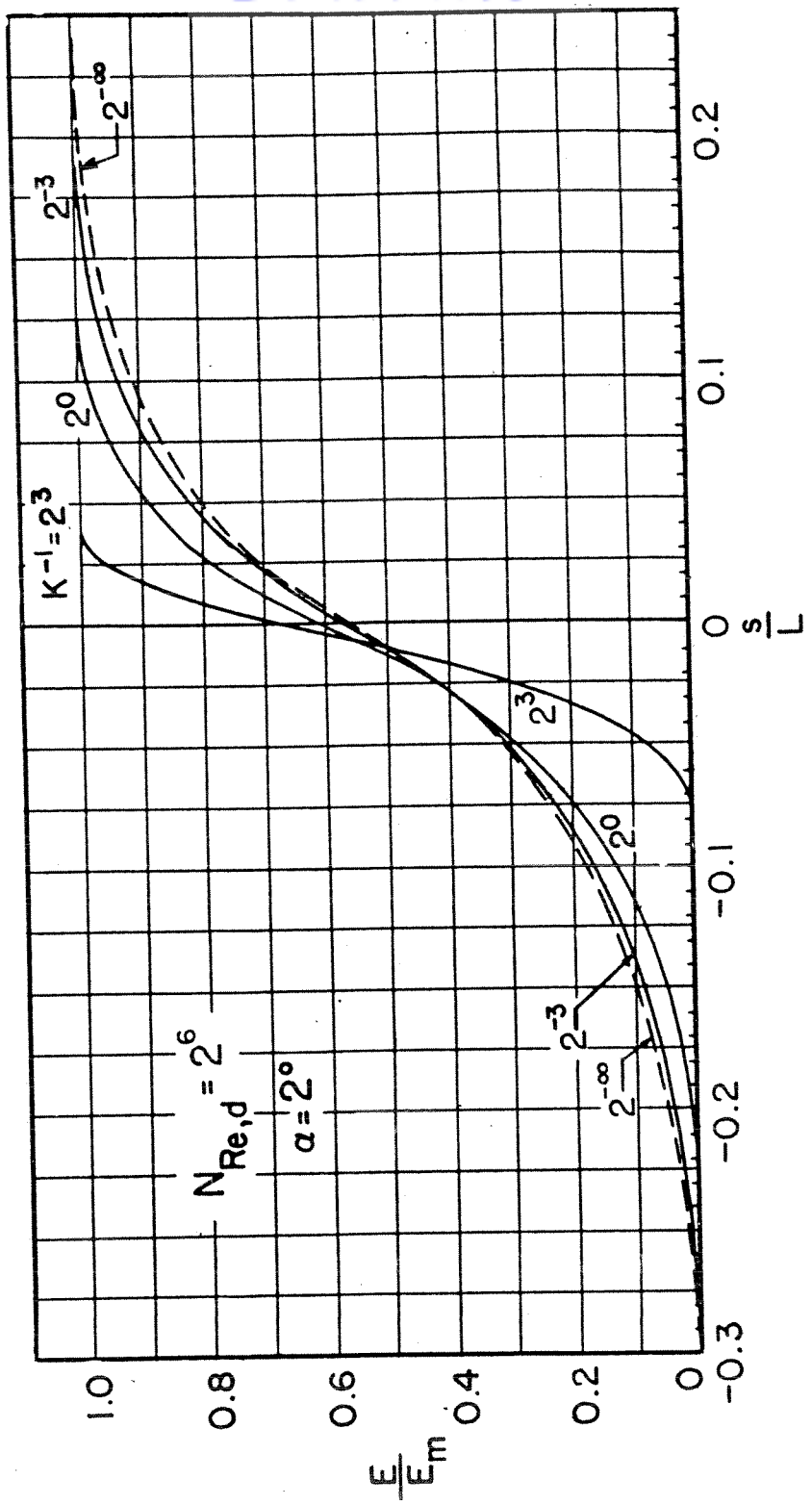

FIG. 3-31 ACCUMULATED COLLECTION EFFICIENCY FOR JOUKOWSKI SYMMETRICAL 15 PER-CENT AIRFOIL AT 2° ANGLE OF ATTACK

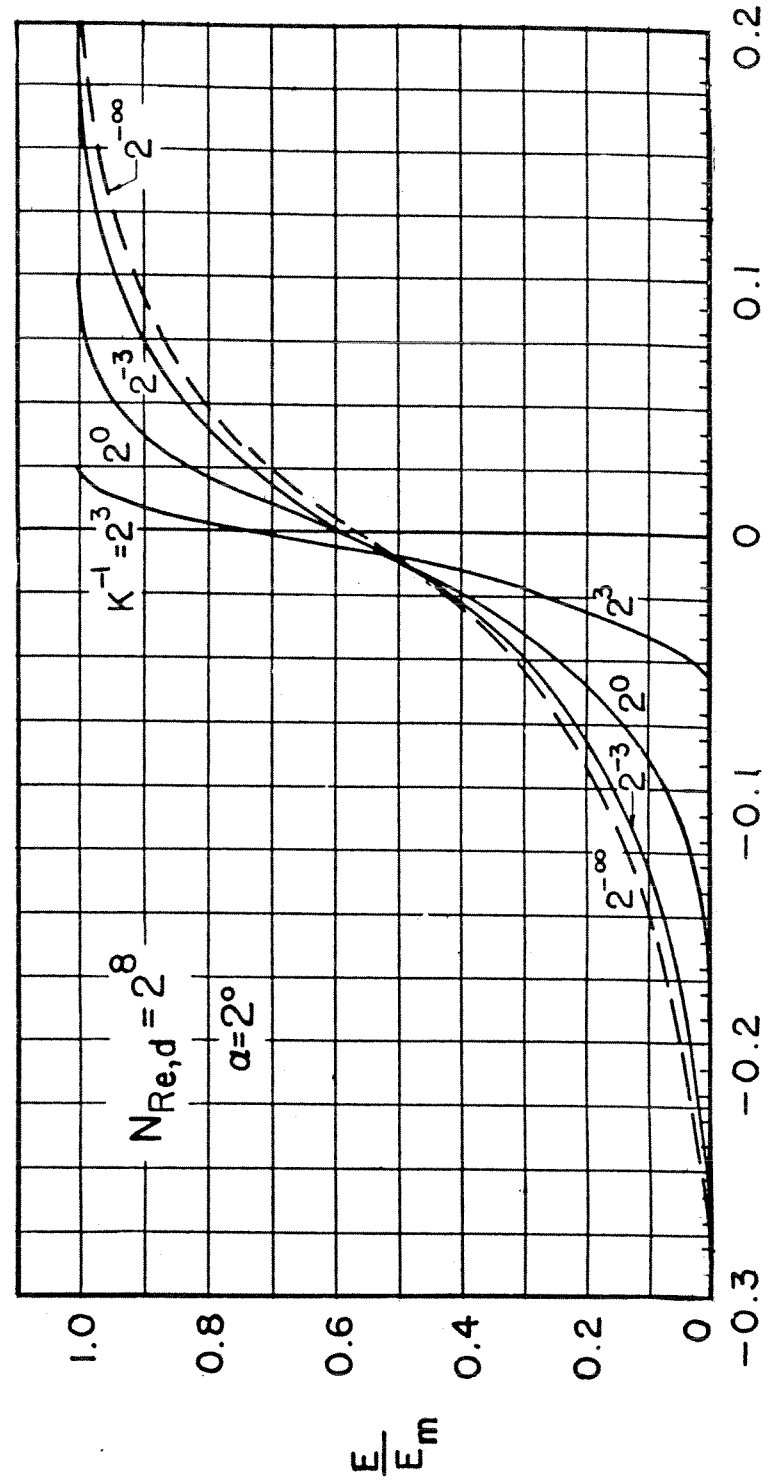

FIG. 3-32 ACCUMULATED COLLECTION EFFICIENCY FOR JOUKOWSKI SYMMETRICAL 15 PER-CENT AIRFOIL AT 2° ANGLE OF ATTACK

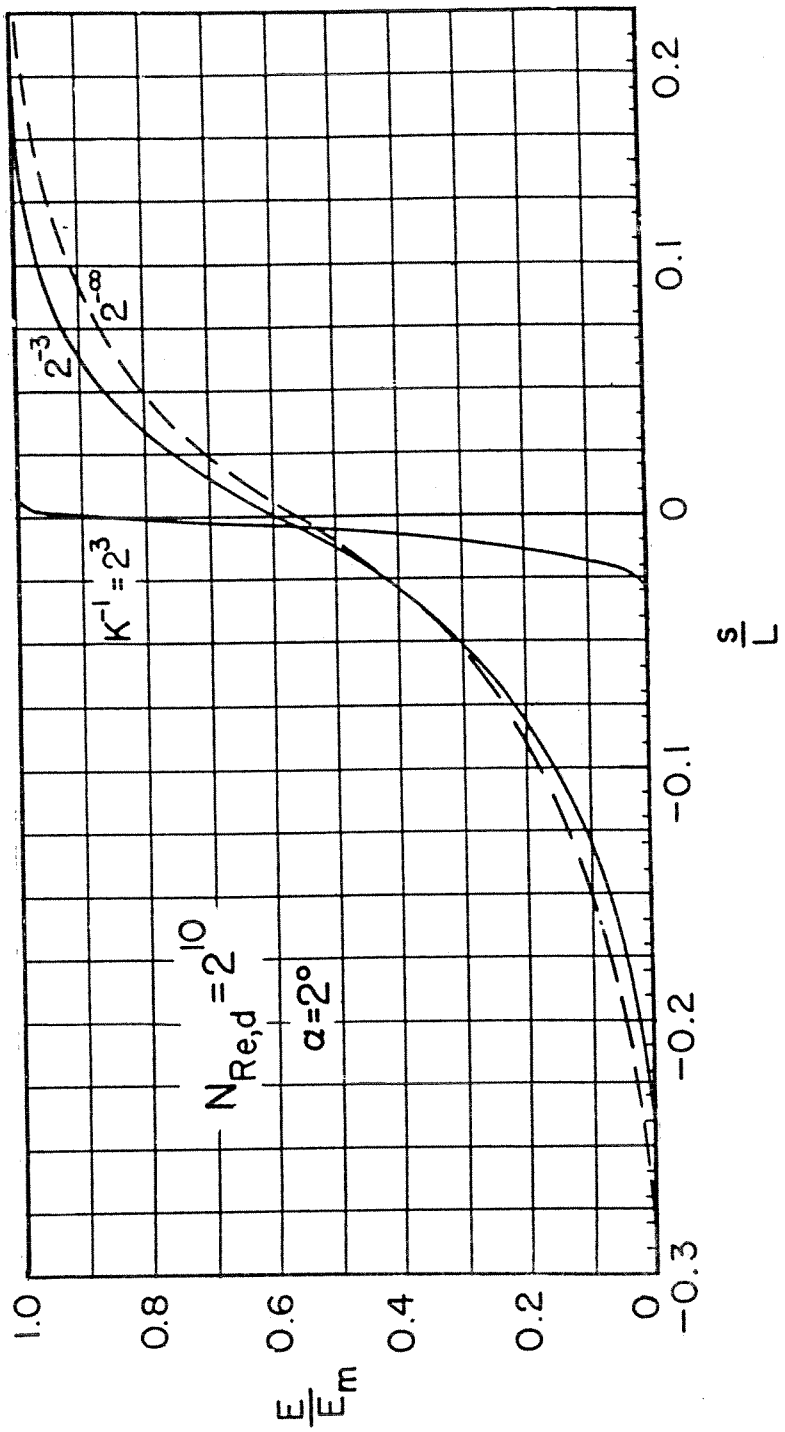

FIG. 3-33 ACCUMULATED COLLECTION EFFICIENCY FOR JOUKOWSKI SYMMETRICAL 15 PER-CENT AIRFOIL AT 2° ANGLE OF ATTACK

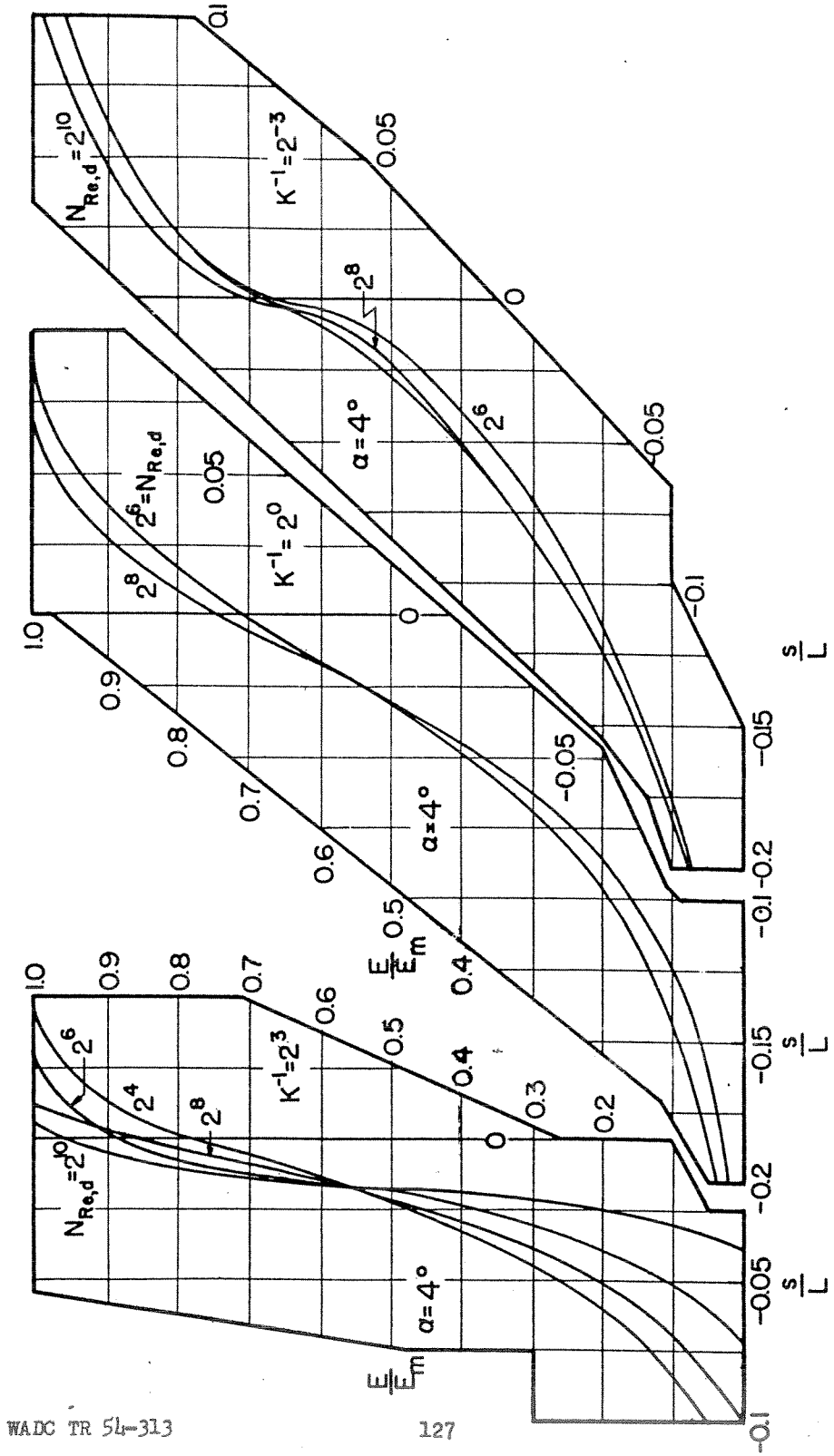

FIG. 3-34 ACCUMULATED COLLECTION EFFICIENCY FOR JOUKOWSKI SYMMETRICAL 15 PER-CENT AIRFOIL AT 4° ANGLE OF ATTACK

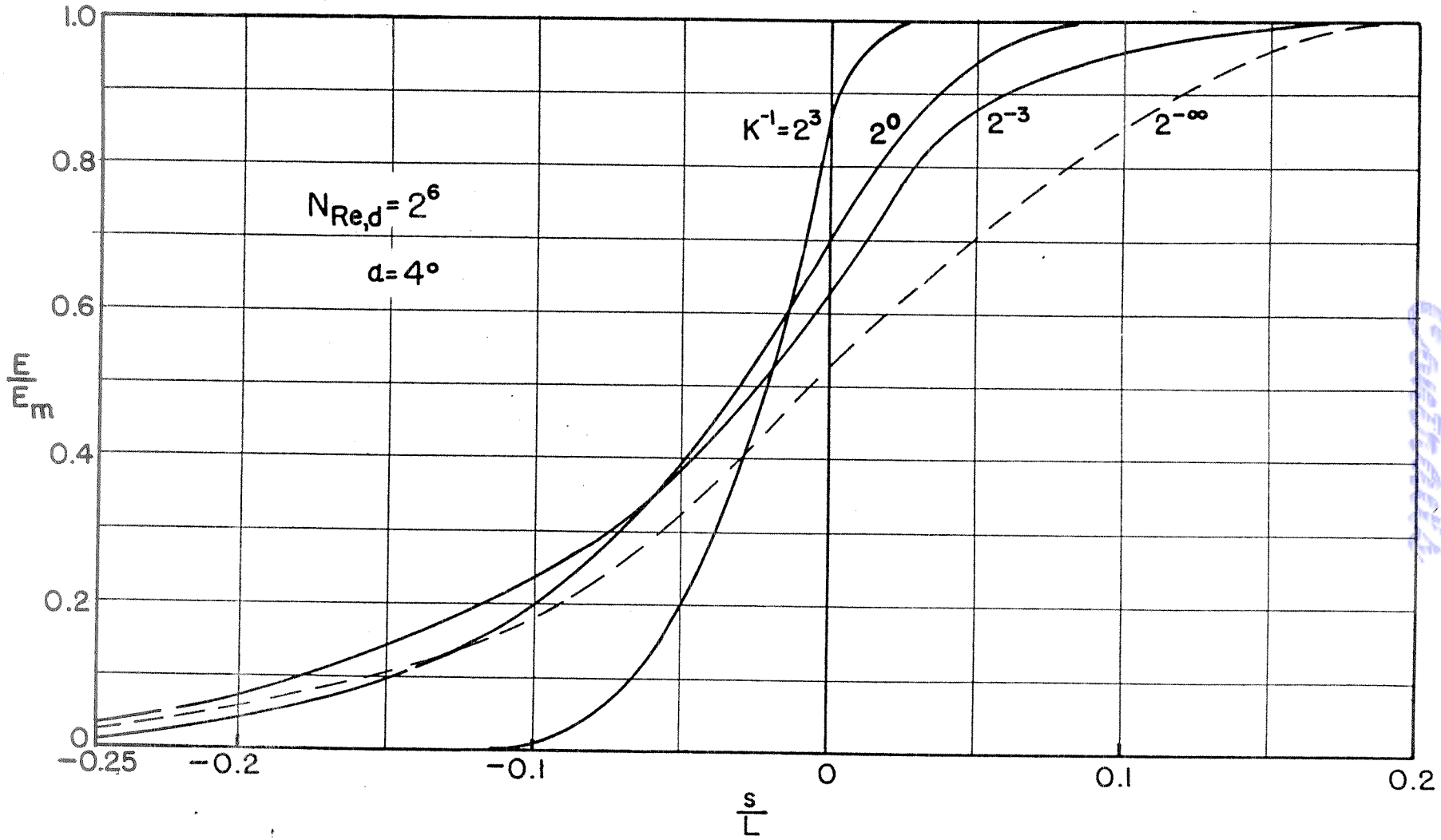

FIG. 3-35 ACCUMULATED COLLECTION EFFICIENCY FOR JOUKOWSKI SYMMETRICAL 15 PER-CENT AIRFOIL AT 4° ANGLE OF ATTACK

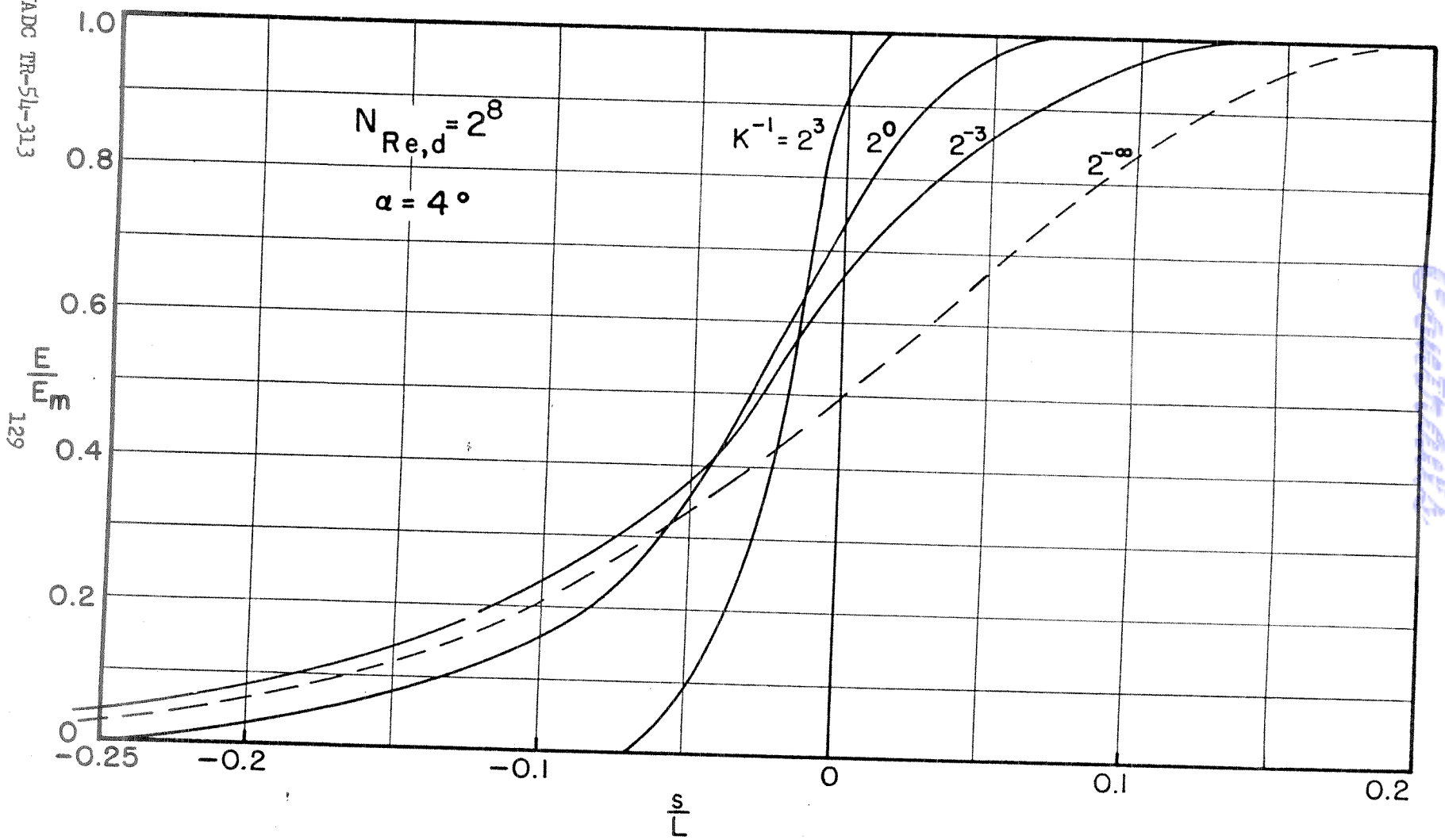

FIG. 3-36 ACCUMULATED COLLECTION EFFICIENCY FOR JOUKOWSKI SYMMETRICAL 15 PER-CENT AIRFOIL AT 4° ANGLE OF ATTACK

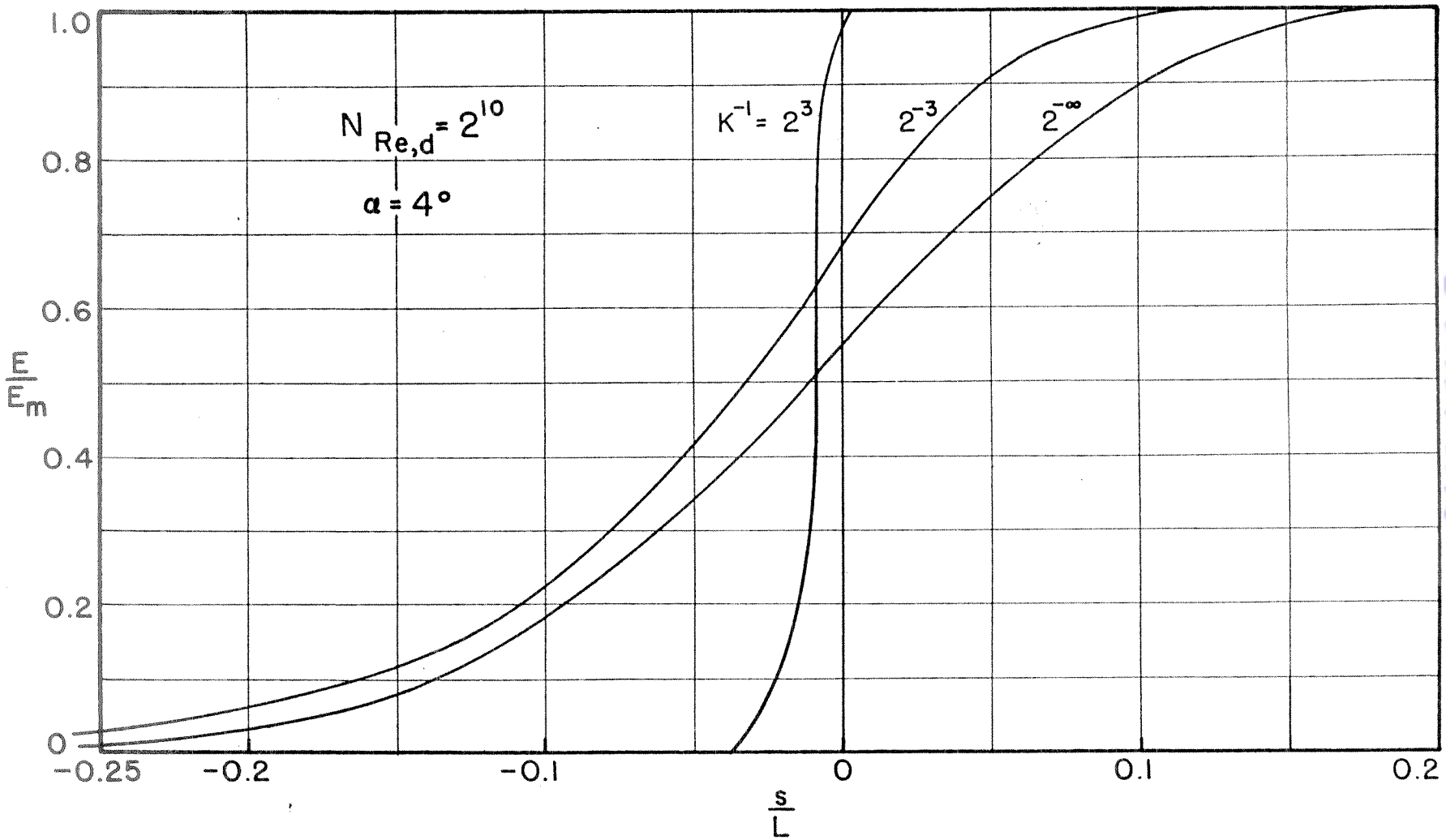

FIG. 3-37 ACCUMULATED COLLECTION EFFICIENCY FOR JOUKOWSKI SYMMETRICAL 15 PER-CENT AIRFOIL AT 4° ANGLE OF ATTACK

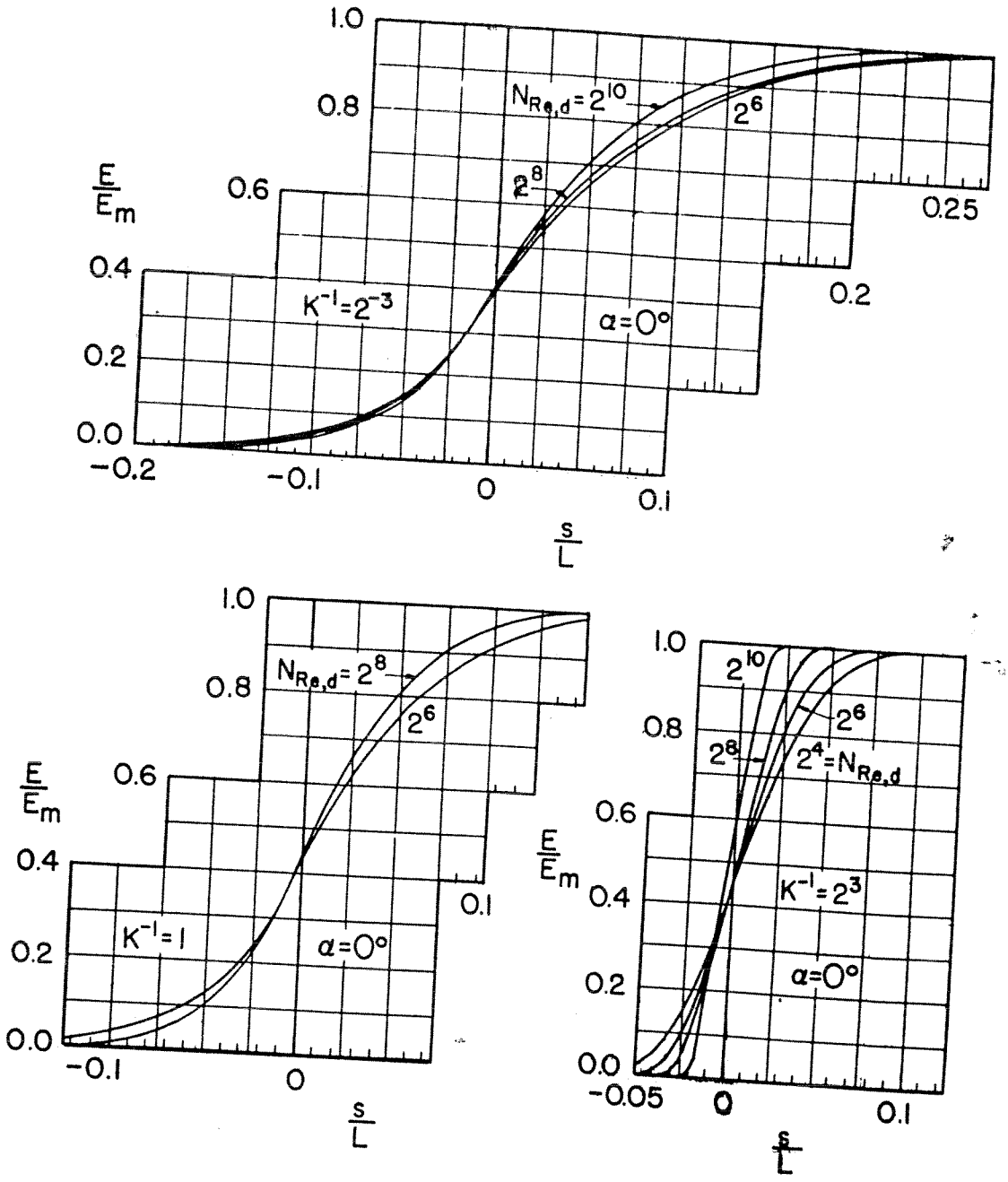

FIG. 3-38 ACCUMULATED COLLECTION EFFICIENCY FOR JOUKOWSKI CAMBERED 15 PERCENT AIRFOIL AT 0° ANGLE OF ATTACK

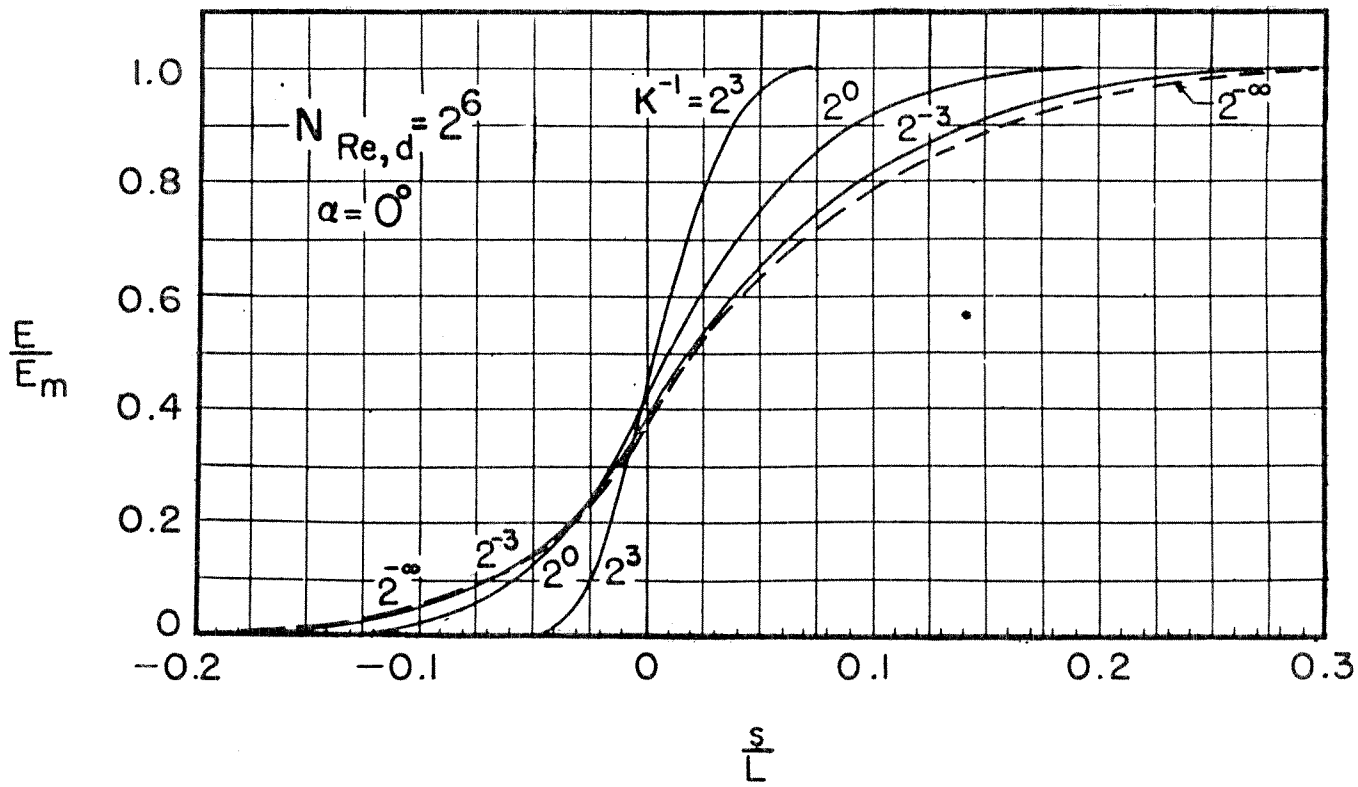

FIG. 3-39 ACCUMULATED COLLECTION EFFICIENCY FOR JOUKOWSKI CAMBERED 15 PER-CENT AIRFOIL AT 0° ANGLE OF ATTACK

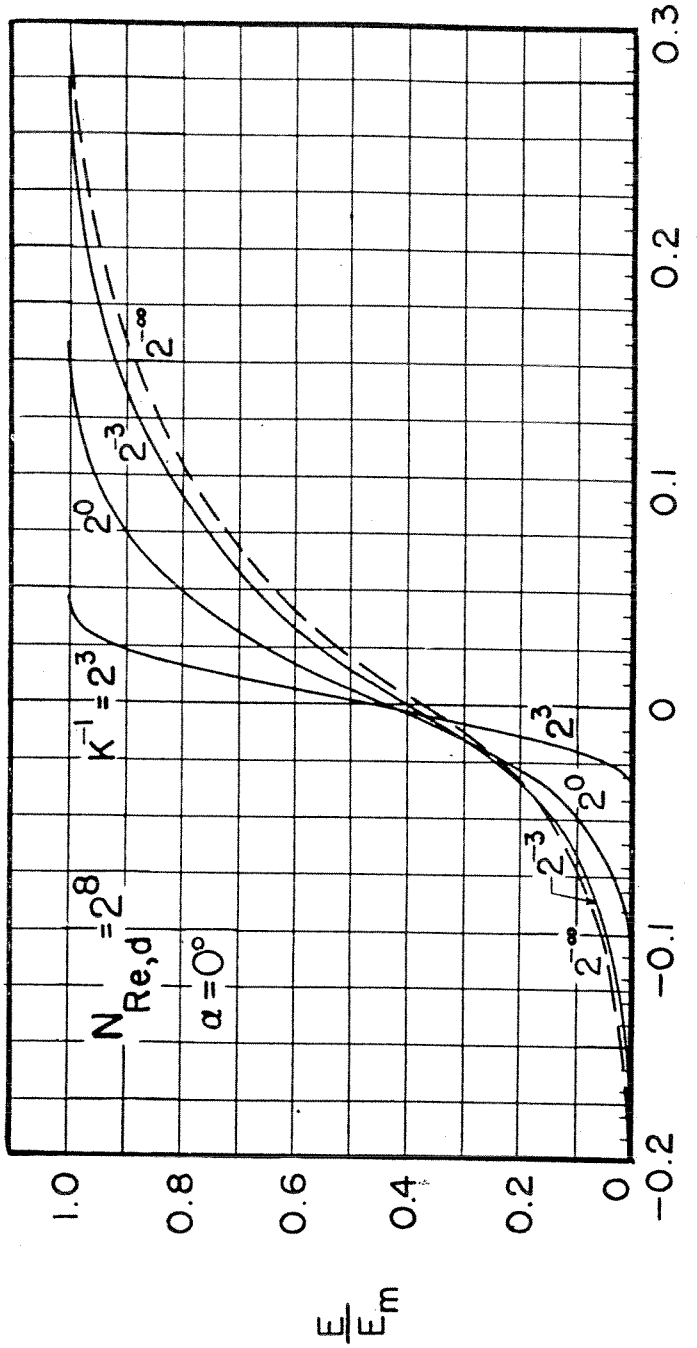

FIG. 3-40 ACCUMULATED COLLECTION EFFICIENCY FOR JOUKOWSKI CAMBERED 15 PER-CENT AIRFOIL AT 0° ANGLE OF ATTACK

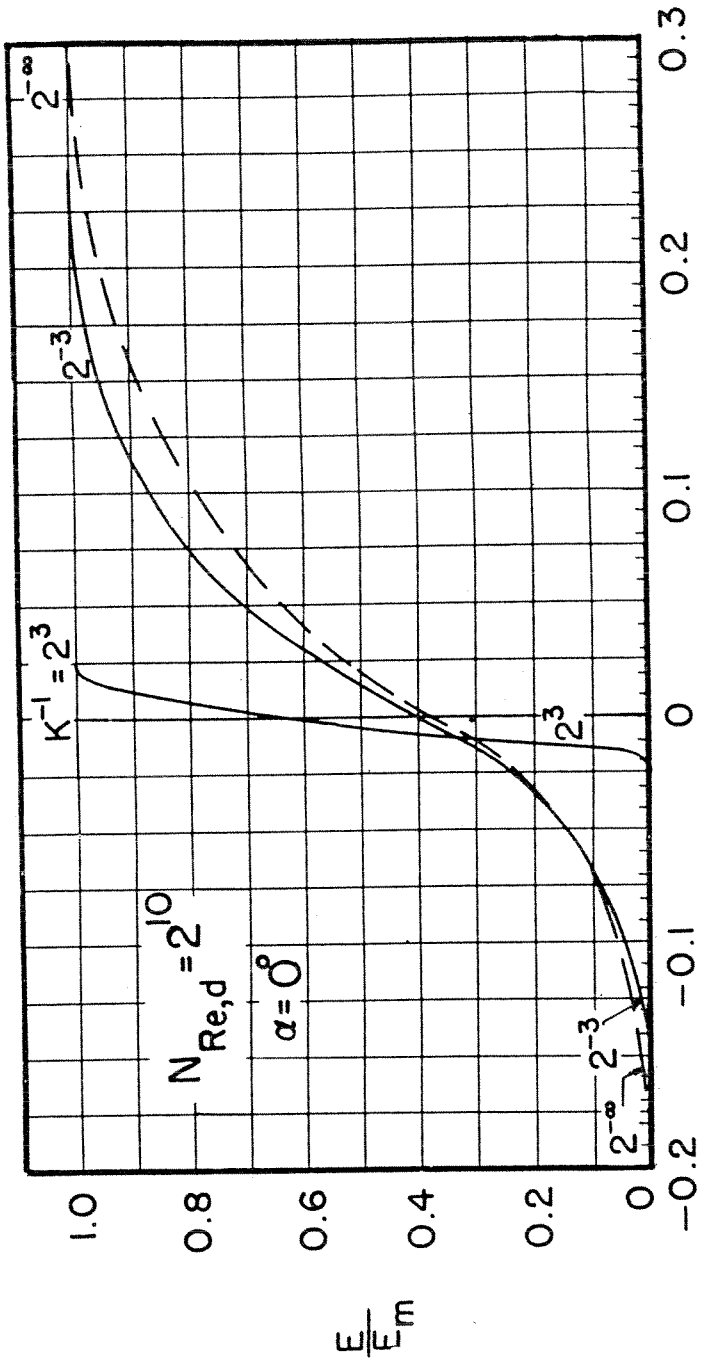

FIG. 3-41 ACCUMULATED COLLECTION EFFICIENCY FOR JOUKOWSKI CAMBERED 15 PER-CENT AIRFOIL AT 0° ANGLE OF ATTACK

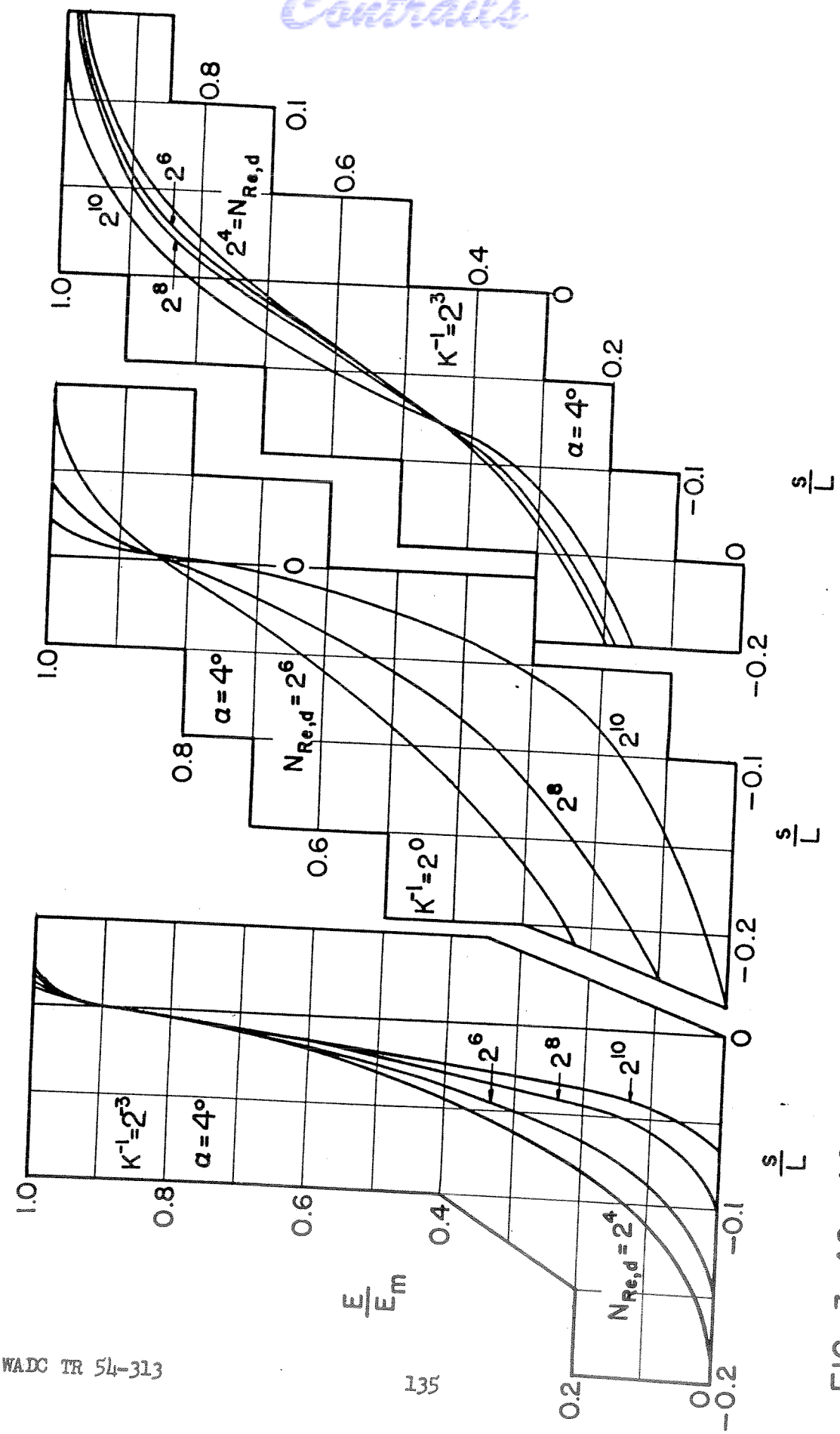

FIG. 3-42 ACCUMULATED COLLECTION EFFICIENCY FOR NACA 65_2-015 AIRFOIL AT 4° ANGLE OF ATTACK

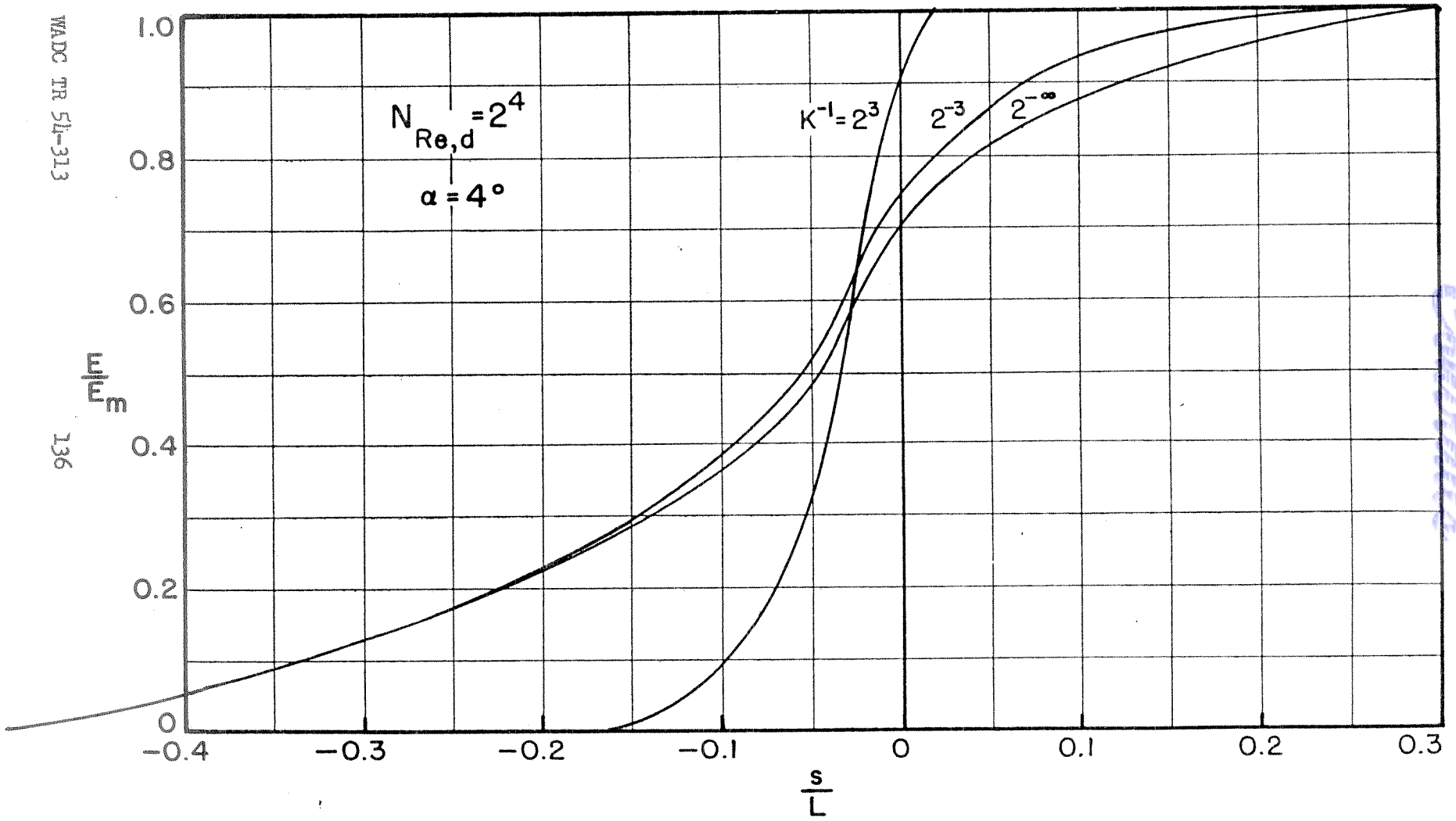

FIG. 3-43 ACCUMULATED COLLECTION EFFICIENCY FOR NACA 65_2-015 AIRFOIL AT 4° ANGLE OF ATTACK

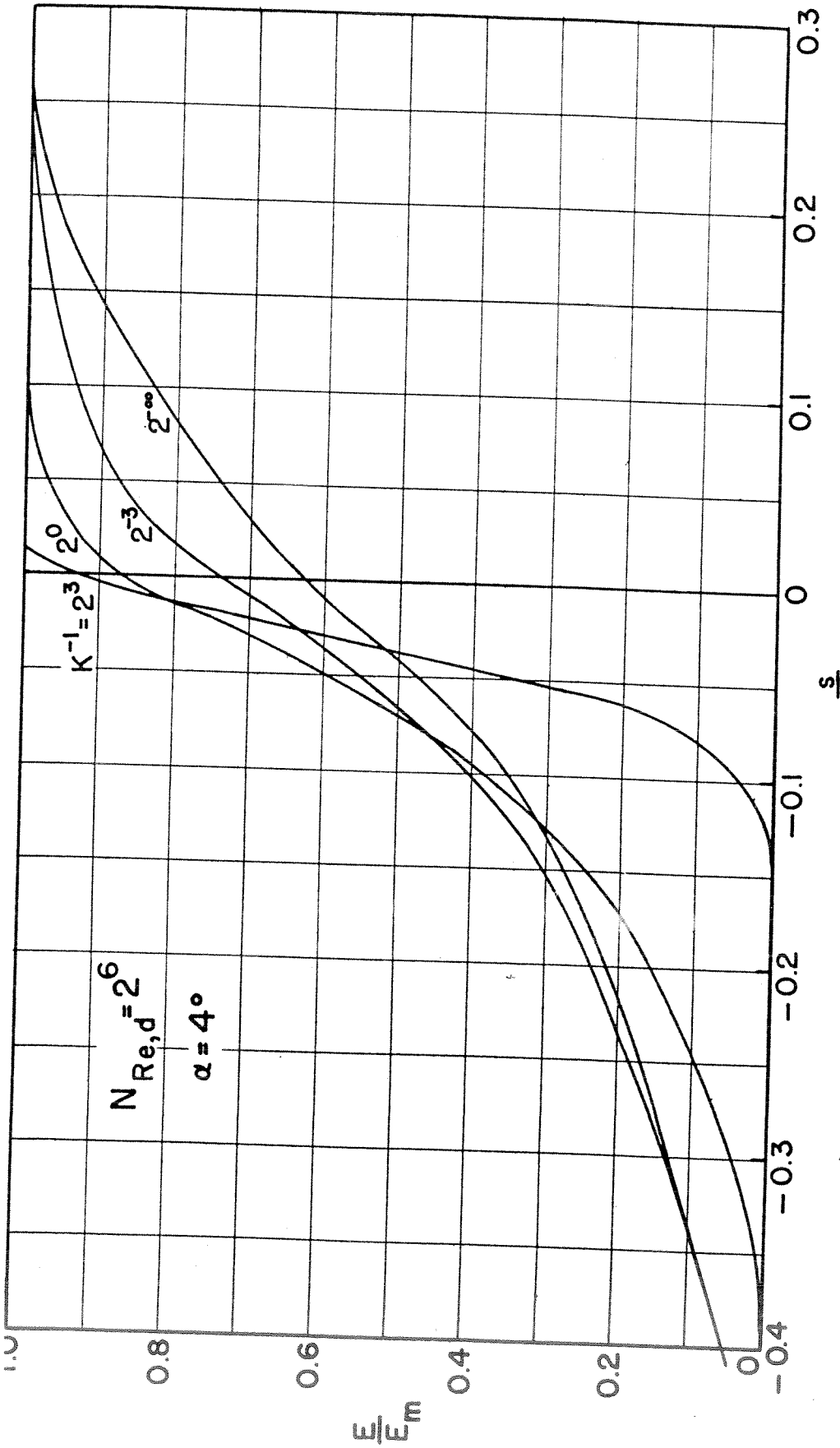

FIG. 3-44 ACCUMULATED COLLECTION EFFICIENCY FOR NACA 65_2-015 AIRFOIL AT 4° ANGLE OF ATTACK

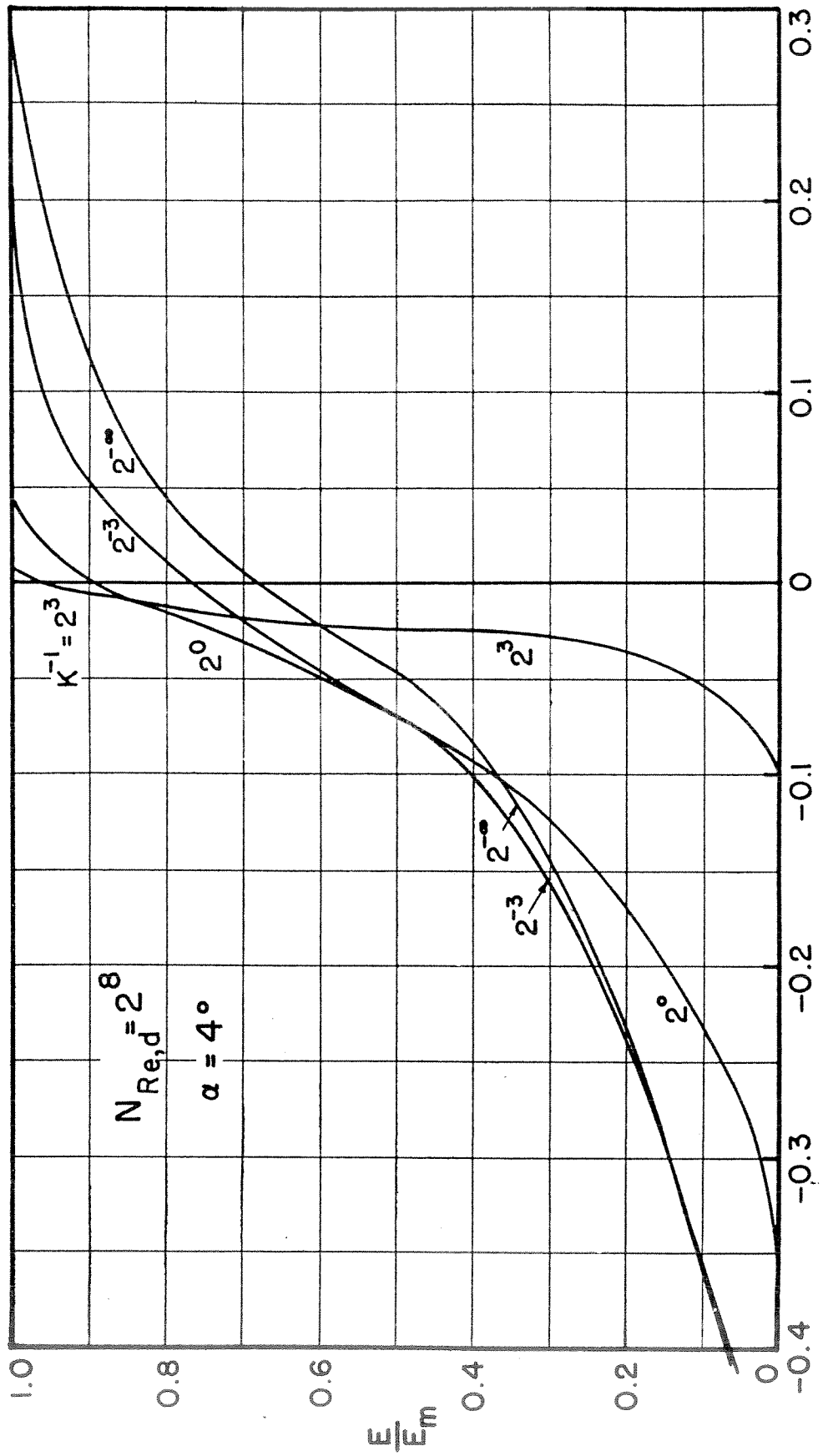

FIG. 3-45 ACCUMMULATED COLLECTION EFFICIENCY FOR NACA 65_2-015 AIRFOIL AT 4° ANGLE OF ATTACK

3-5.2 Local Collection Efficiency

The local rate of droplet impingement per unit area of airfoil surface can be determined from the expression (in practical units),

$$W'' = 0.379\ U_o\ \omega_w \cdot \frac{dy_o}{ds} = 0.379\ U_o\ \omega_w\ \beta \qquad (3\text{-}28)$$

The dimensionless local collection efficiency β is defined by Eq. 3-28, in which $[U_o]$ = knots and $[\omega_w]$ = g/cu m. Figures 3-46 through -54 reproduced from Ref. 23 and 24 show β plotted against K^{-1} as parameter for the NACA 65A005, 65_1-208, and 65_1-212 airfoils at 4° angle of attack. These graphs are based on the slopes of y_o/L versus s/L curves obtained from the trajectory data.

It may be noticed that the maximum rates of impingement occur between the air stagnation line and the geometric leading-edge line. On account of the airfoil geometry and the manner in which the droplets approach the airfoils in this neighborhood, the graphs of y_o/L versus s/L are not well defined in the range $-0.01 < s/L < 0.0$. The possible error in the maximum value of β is estimated to lie between $\pm$ 10 to $\pm$ 25 per cent, depending on the value of K^{-1} and the airfoil. This possible error is not considered serious because only a small portion of the total water catch would require redistribution if the maximum value of β is changed by as much as the maximum possible error. The total area under the curve should not be changed when a change in the maximum value of β is made, because the total amount of water impinging, determined by $y_{o,u} - y_{o,l}$ and by $\int_{s_l/L}^{s_u/L} \beta\ d(s/L)$ is independent of the manner in which the water is distributed near the leading edge.

Distribution curves for the NACA 0006-64 and 65A005 airfoils and for the double wedge 1S(50)002-(50)002 were not calculated.

3-6 Influence of Angle of Attack and Airfoil Maximum Thickness

There is available to date only a limited number of data on airfoils of different series, angle of attack, camber, and thickness. Reliable interpolation techniques, therefore, are of practical importance. The work of

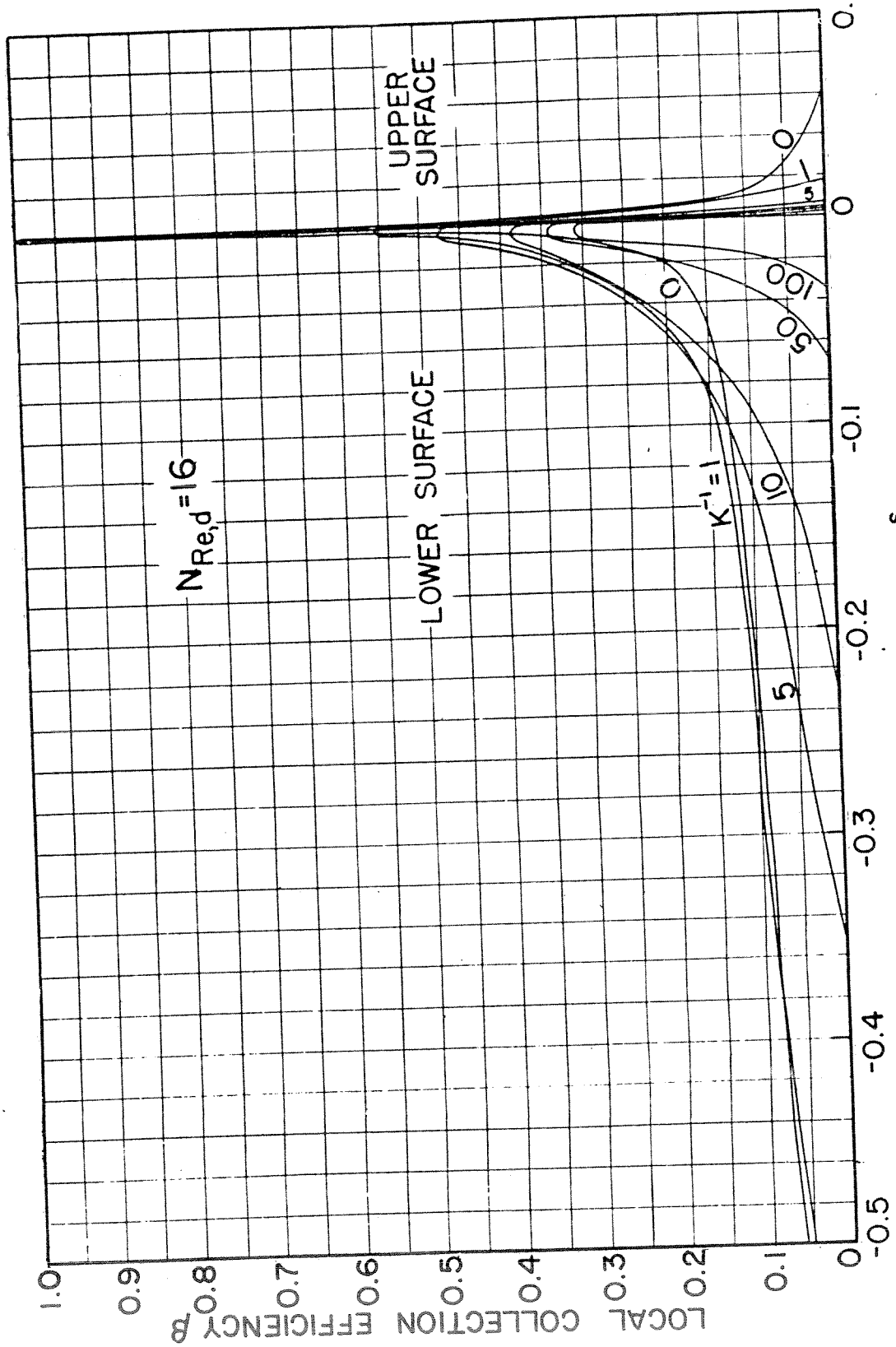

FIG. 3-46 LOCAL COLLECTION EFFICIENCY ON NACA 65A004 AIRFOIL AT 4° ANGLE OF ATTACK ($N_{Re,d}$=16)

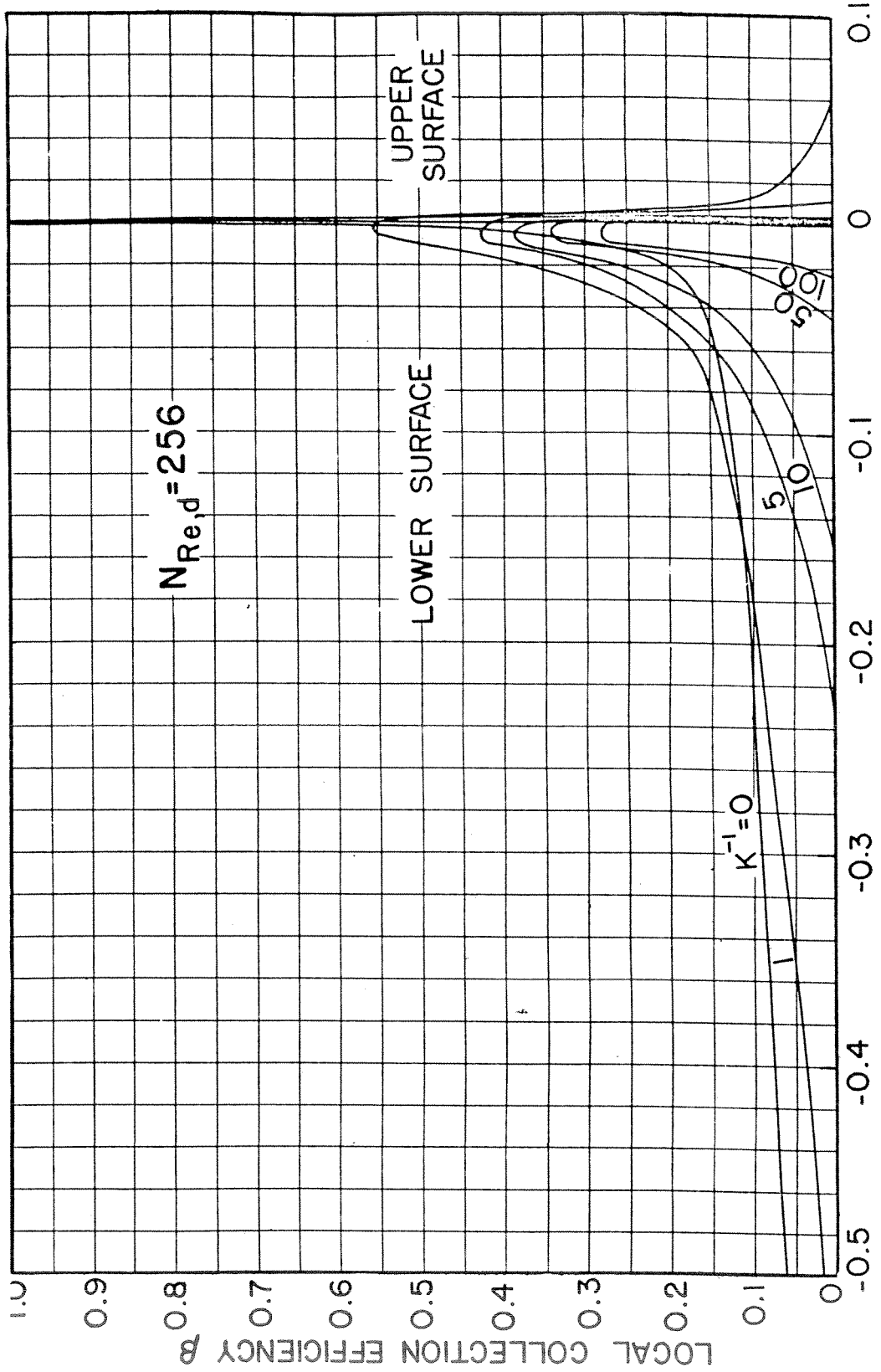

FIG. 3-47 LOCAL COLLECTION EFFICIENCY ON NACA 65A004 AIRFOIL AT 4° ANGLE OF ATTACK ($N_{Re,d}$=256)

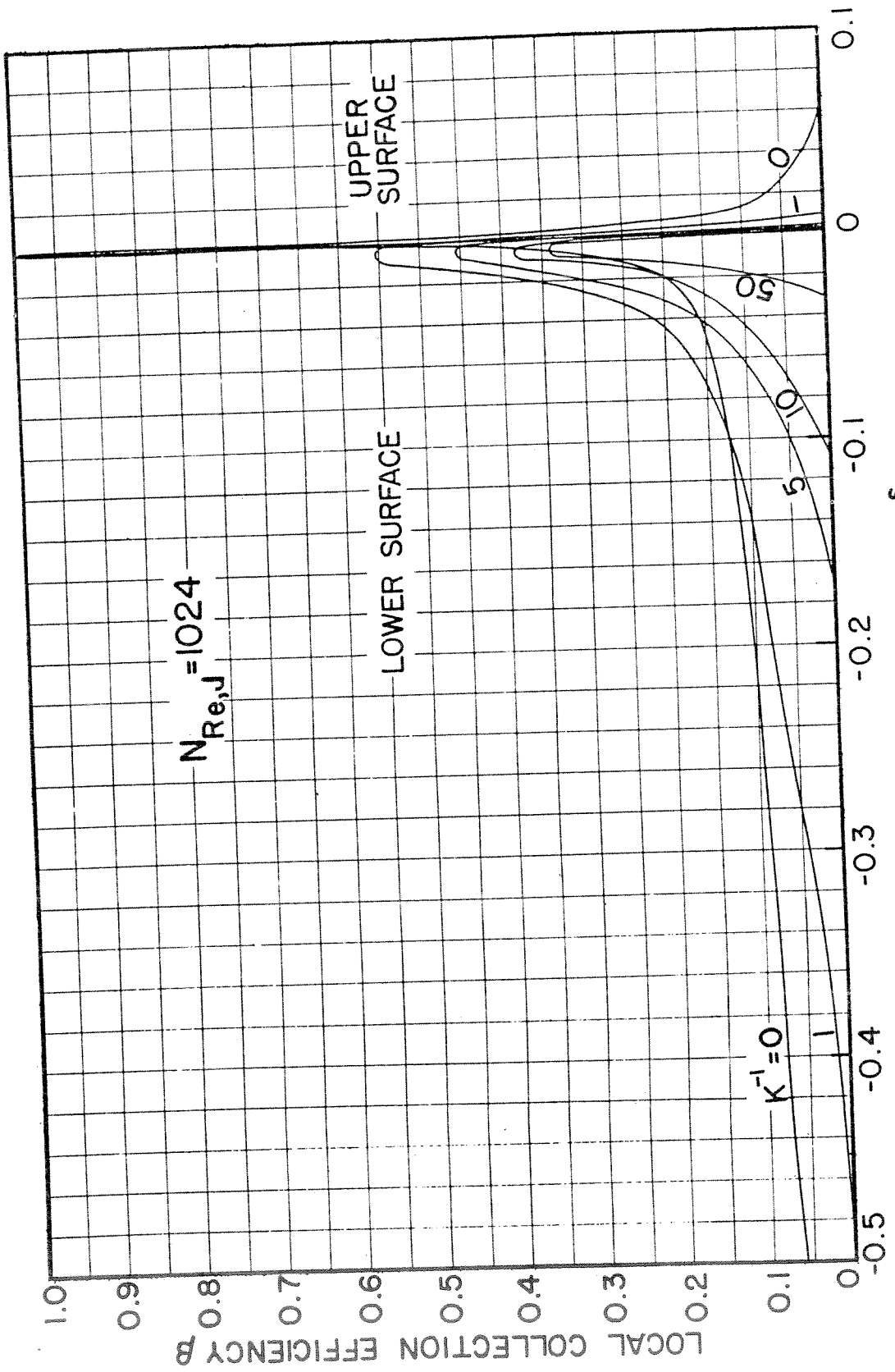

FIG. 3-48 LOCAL COLLECTION EFFICIENCY ON NACA 65A004 AIRFOIL AT 4° ANGLE OF ATTACK ($N_{Re,d}$ = 1024)

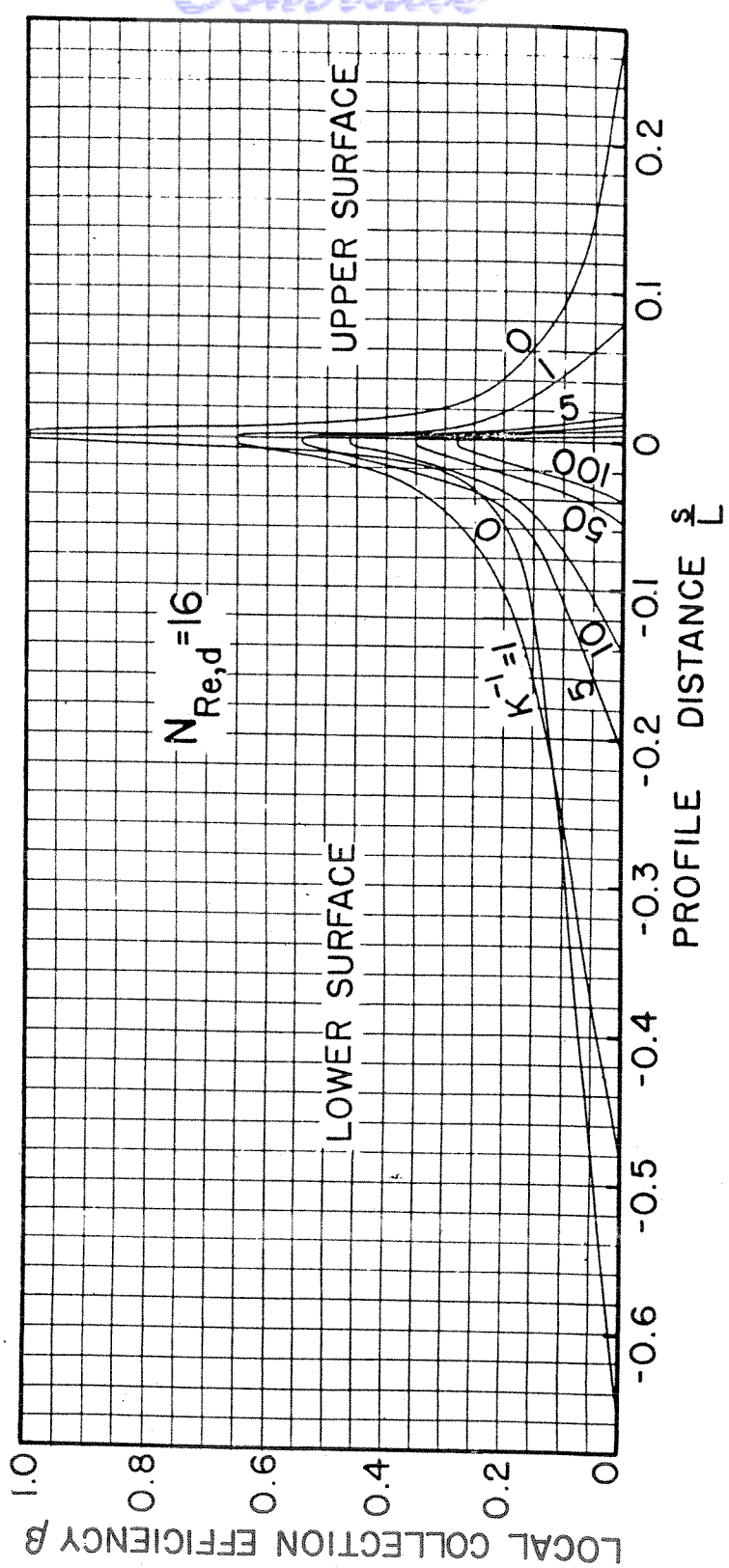

FIG. 3-49 LOCAL COLLECTION EFFICIENCY ON NACA 65_1-208 AIRFOIL AT 4° ANGLE OF ATTACK ($N_{Re,d}$=16)

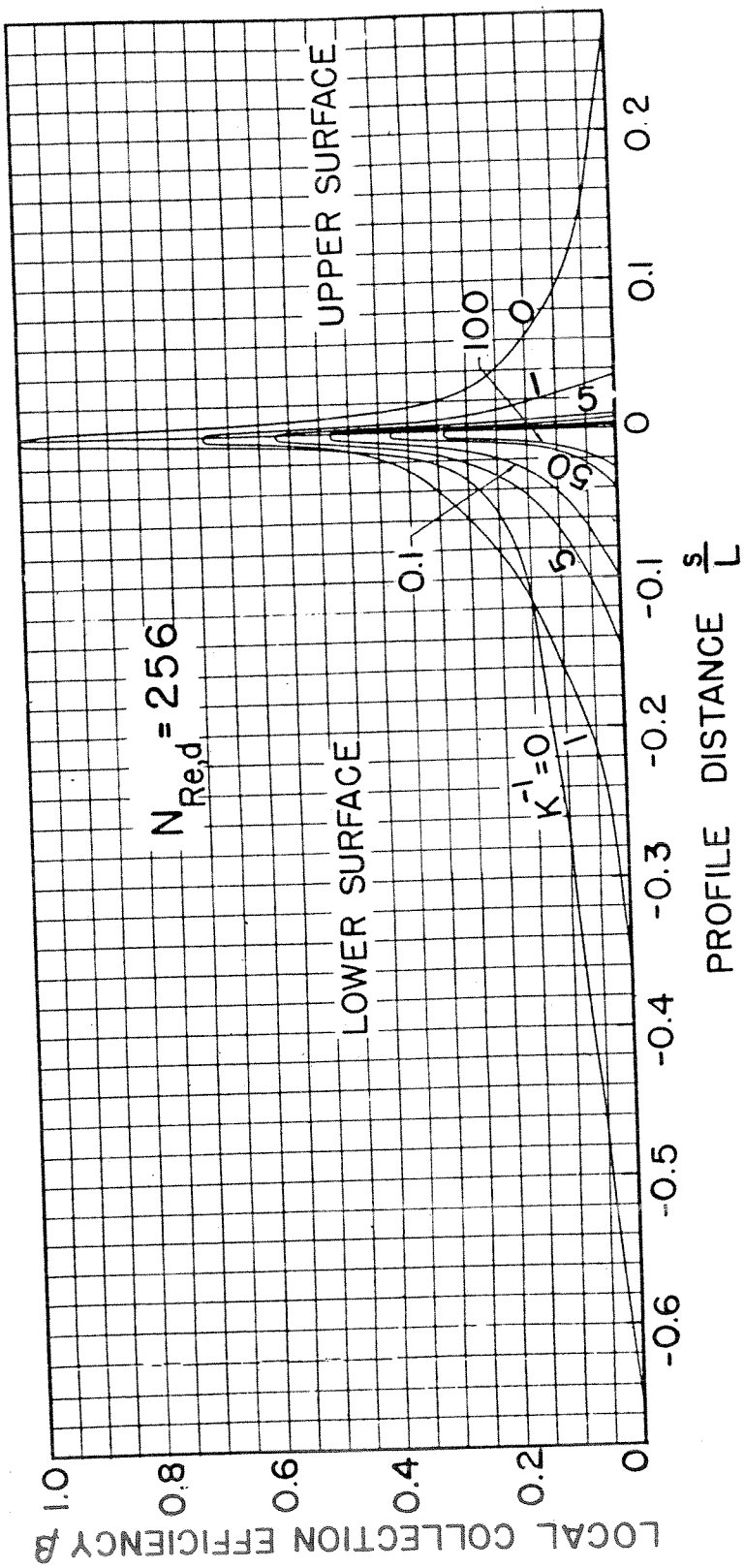

FIG. 3-50 LOCAL COLLECTION EFFICIENCY ON NACA 65,-208 AIRFOIL AT 4° ANGLE OF ATTACK ($N_{Re,d}$ = 256)

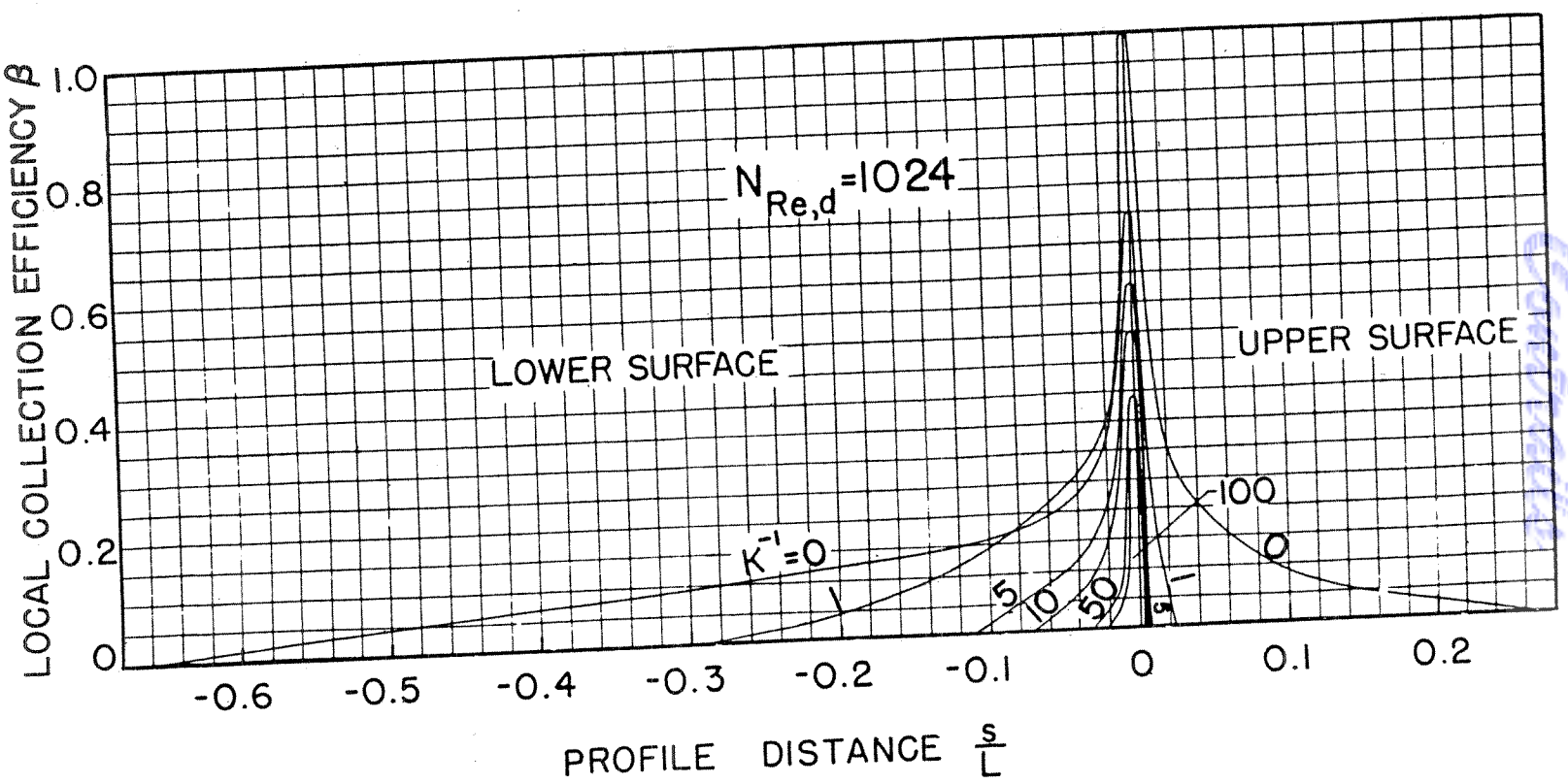

FIG. 3-51 LOCAL COLLECTION EFFICIENCY ON NACA 65_1-208 AIRFOIL AT 4° ANGLE OF ATTACK ($N_{Re,d}$=1024)

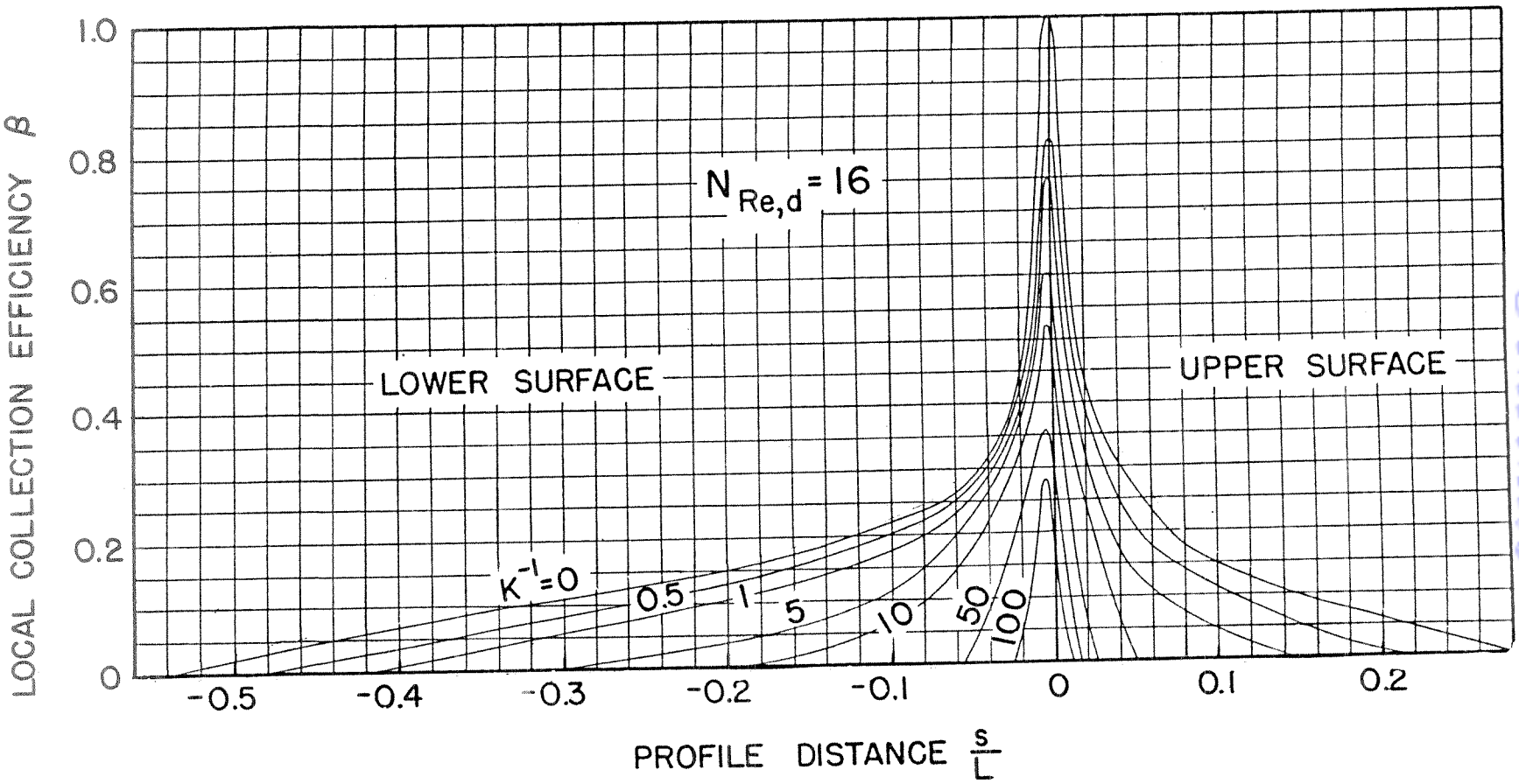

FIG. 3-52 LOCAL COLLECTION EFFICIENCY ON NACA 65_1-212 AIRFOIL AT 4° ANGLE OF ATTACK ($N_{Re,d} = 16$)

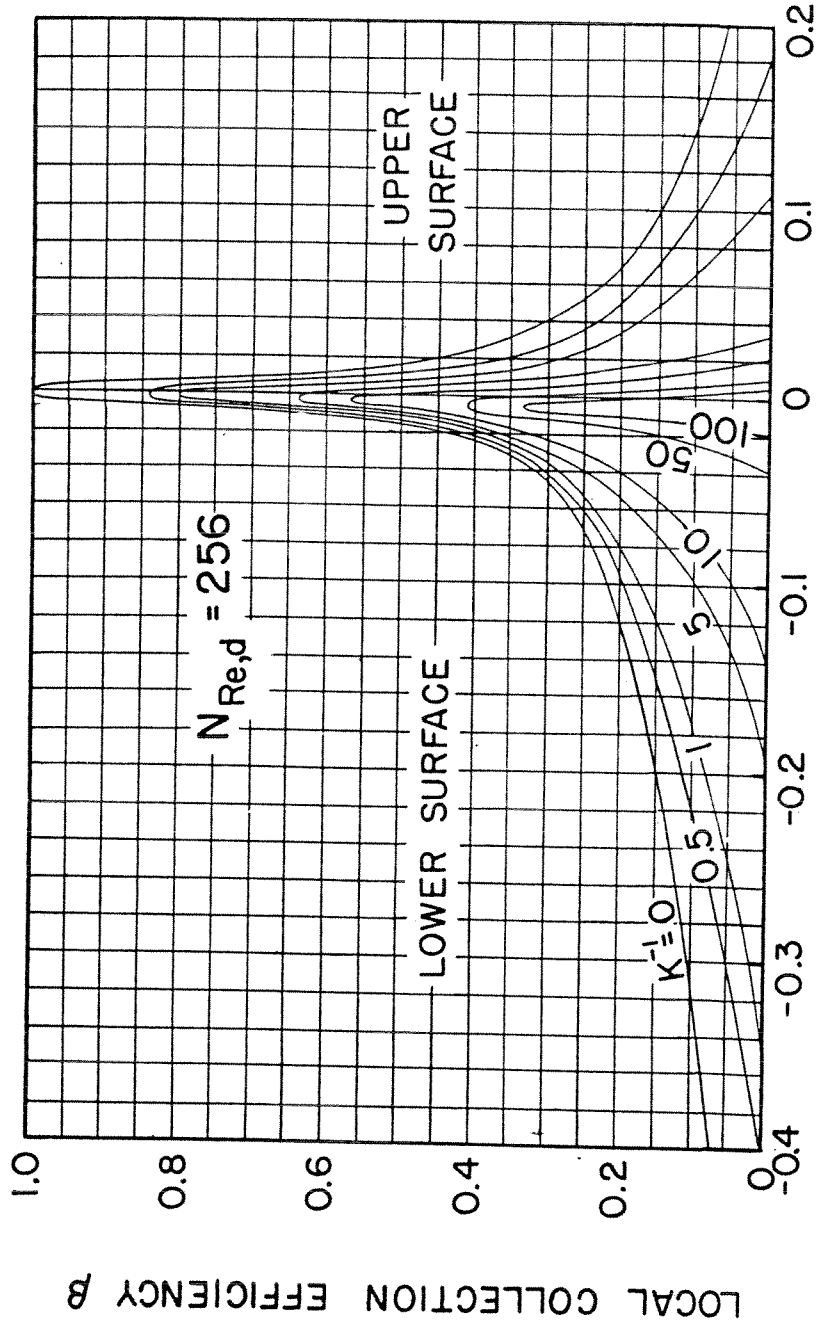

FIG. 3-53 LOCAL COLLECTION EFFICIENCY ON NACA 65$_1$-212 AIRFOIL AT 4° ANGLE OF ATTACK ($N_{Re,d}$ = 256)

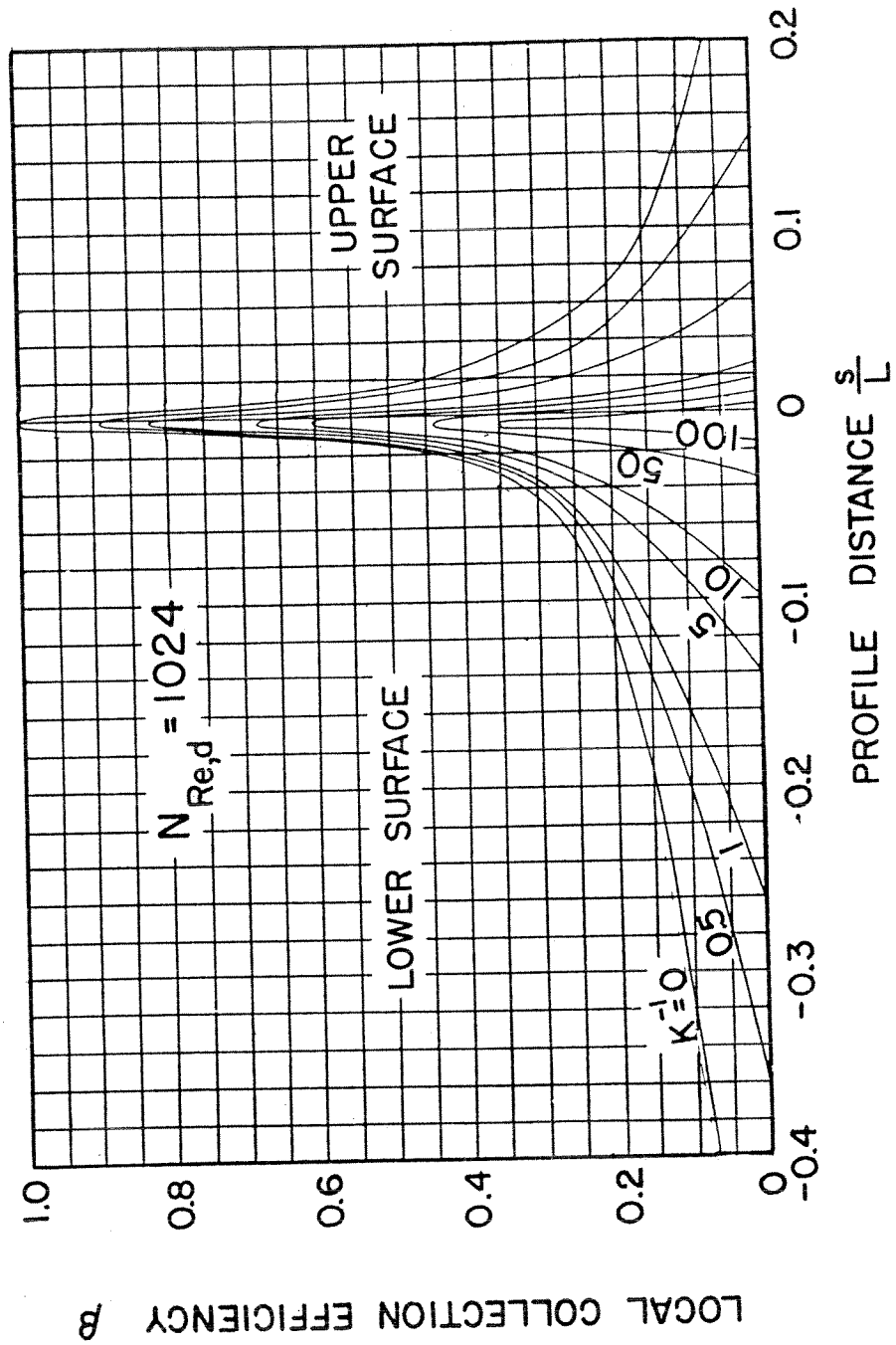

FIG. 3-54 LOCAL COLLECTION EFFICIENCY ON NACA 65,-212 AIRFOIL AT 4° ANGLE OF ATTACK ($N_{Re,d}$=1024)

Sherman et al (Ref. 120) indicates that by introducing K_S the effect of the Reynolds number in the charts is minimized. For many practical purposes a single curve is all that is necessary to correlate computor data of collection efficiency or impingement area for a particular airfoil at a specific angle of attack. A superposition of curves for a particular airfoil at several angles of attack or for airfoils of different maximum thickness (in terms of per cent chord) at identical angle of attack may permit the interpolation or extrapolation of existing results.

3-6.1 Influence of Angle of Attack on Rate of Water Impingement

Impingement data for a few airfoils at more than one angle of attack are available. Figure 3-55 is a graph of the ratio $E_m/E_{m,0}$ versus angle of attack α, the quantity $E_{m,0}$ being the total collection efficiency at zero angle of attack. The curves, which represent the 2 per cent double wedge, the symmetrical 5 per cent airfoil, and the Joukowski symmetrical 15 per cent airfoil, were obtained by cross plotting the graphs of Fig. 3-8, -9, and -13, respectively. They are drawn for particular values of K and $N_{Re,d}$ or of K_S; but curves for other values of the parameters can be constructed whenever exact calculations must be carried out. Clearly, the influence of increasing the angle of attack is to increase the rate of impingement, and this influence is greatest for the thinnest airfoils.

3-6.2 Influence of Angle of Attack on Impingement Area

Increasing the angle of attack increases the extent of impingement on the lower surface of the airfoil and decreases it on the upper surface. The influence of increasing camber is opposite to that of increasing the angle of attack. Compare, for example, the curves of Fig. 3-20 at equal values of K_S and the graphs of Fig. 3-26 and of Fig. 3-27 at corresponding values of the parameters K^{-1} and $N_{Re,d}$.

3-6.3 Influence of Airfoil Thickness on Total Collection Efficiency

Individual curves showing average values of E_m plotted against K_S for several airfoils at 4° angle of attack are presented in the graph

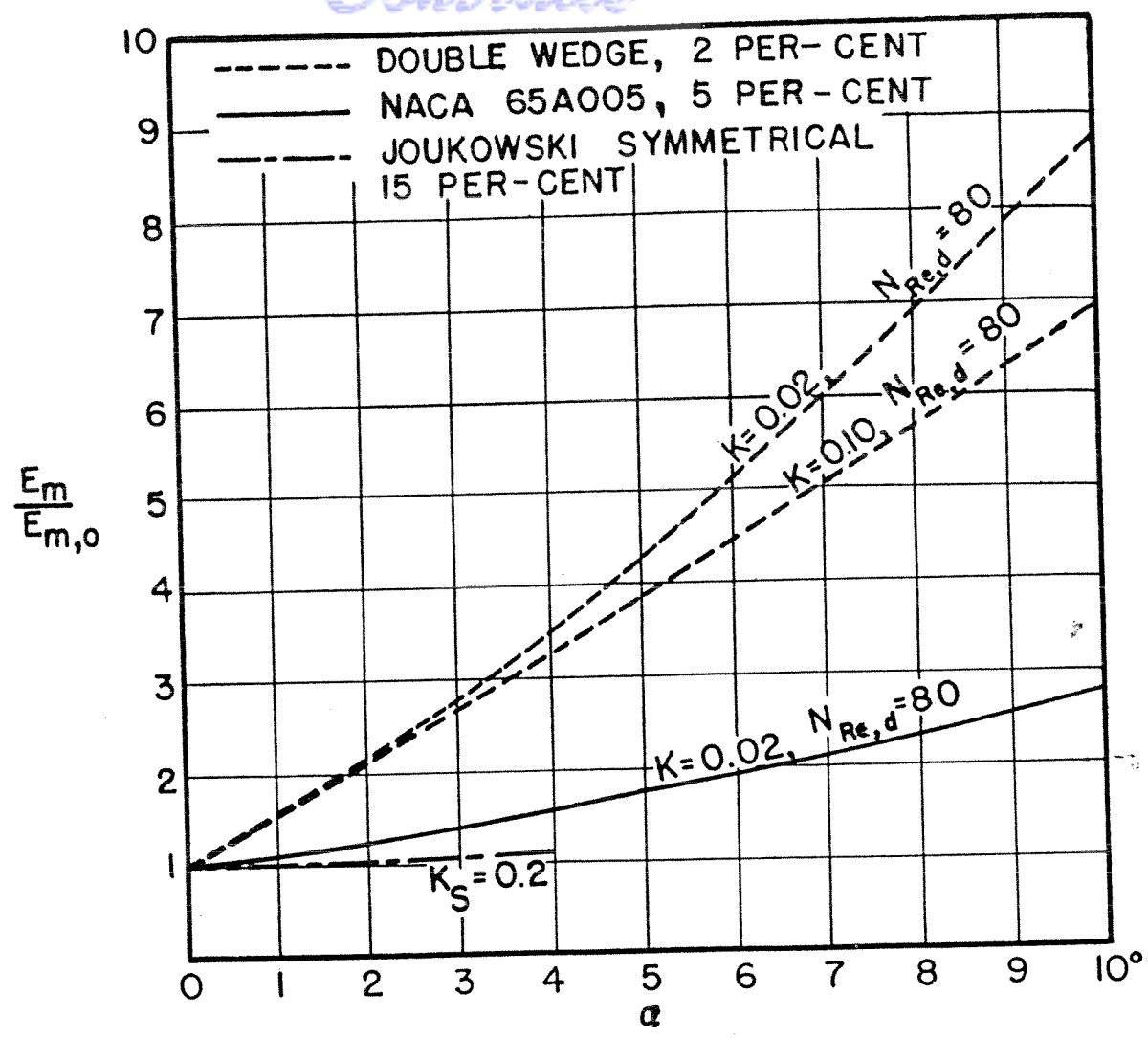

FIG. 3-55 INFLUENCE OF ANGLE OF ATTACK ON TOTAL COLLECTION EFFICIENCY

of Fig. 3-56. Airfoils having thicknesses from 4 to 15 per cent are represented. The thinner airfoils display the highest efficiencies, because they are less effective in deflecting the droplets. This chart may be useful when exact data for a similar airfoil are unavailable.

The influence of airfoil thickness on the total collection efficiency is possibly best illustrated by a cross plot of Fig. 3-56 as shown in Fig. 3-57. Here E_m is plotted against the thickness ratio in per cent. In this graph $N_{Re,d} = 170$ and $K^{-1} = 26$. These values were selected so that the fourth entry in Table 3-4, calculated for the 6 per cent airfoil, could be included for comparison. The curve, which was faired through the points to show the trend, was drawn beneath the points of the cambered airfoils. It appears that the results for the NACA 0006-64 airfoil may be somewhat low.

While the total collection efficiency is greater on the thinner airfoils, it should be observed that the rate of water impingement on the thin airfoils is less than it is on thick airfoils of equal length under identical flight and icing conditions.

3-6.4 Influence of Airfoil Thickness on Impingement Area

Impingement areas on airfoils at 4° angle of attack are shown in Fig. 3-58. These curves which represent arithmetic averages for several Reynolds numbers are presented to show the trend. For accurate results, particularly with regard to the thinner airfoils, individual curves should be used (see Section 3-4).

Brun et al (Ref. 24) have made further comparisons of the impingement conditions on the NACA 65A004, 65_1-208, and 65_1-212 airfoils at 4° angle of attack. They considered one each of the three airfoils of equal length flying at the same speed and altitude. Then they investigated the extent of impingement and the rate of water impingement for $K^{-1} = 1$, 10, and 100. They came to the following conclusions:

The rearward limit of impingement on the upper surface decreases as the thickness ratio decreases. On the lower surface, as the thickness

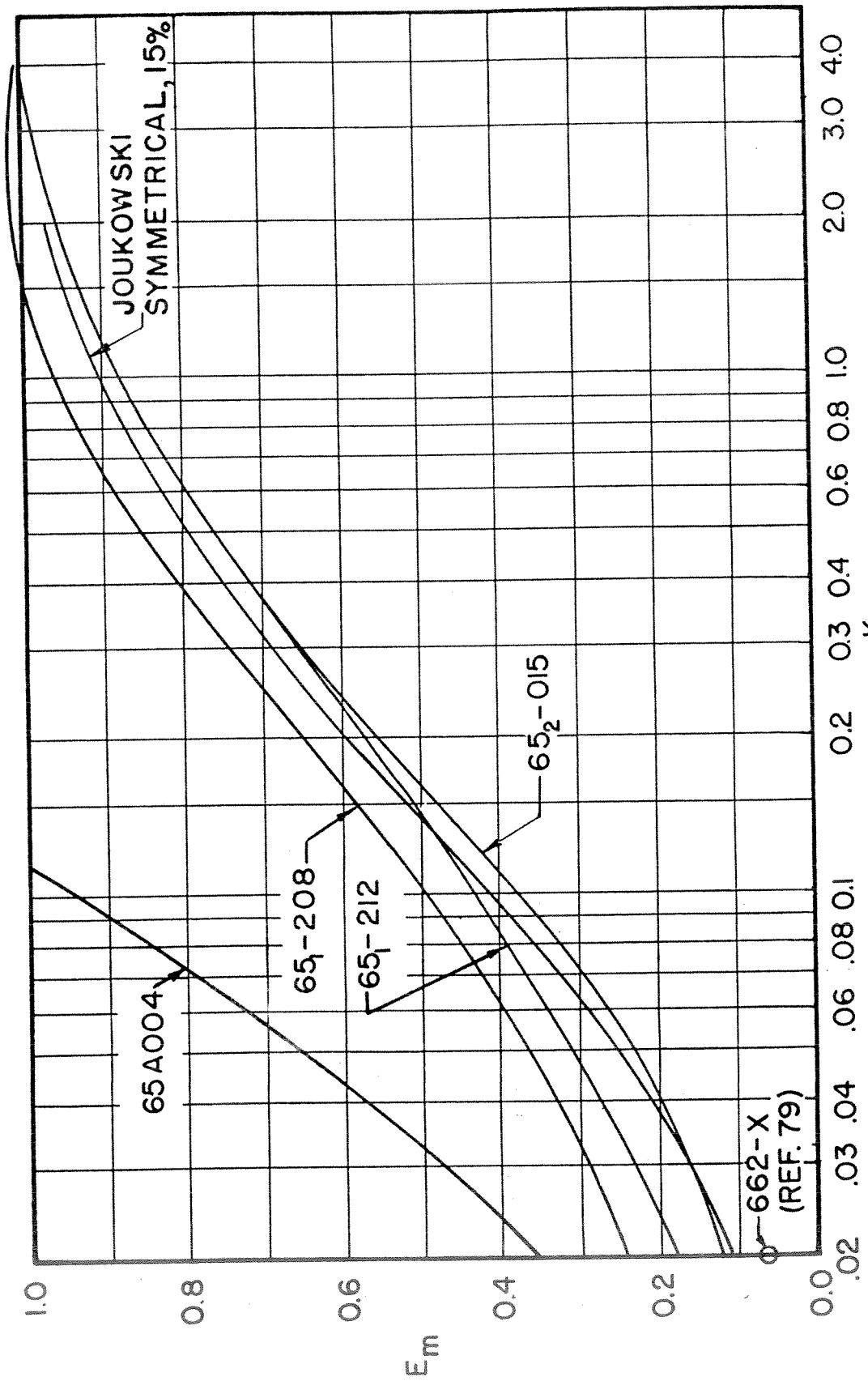

FIG. 3-56 TOTAL COLLECTION EFFICIENCY PLOTTED AGAINST K_s FOR VARIOUS AIRFOILS AT 4° ANGLE OF ATTACK

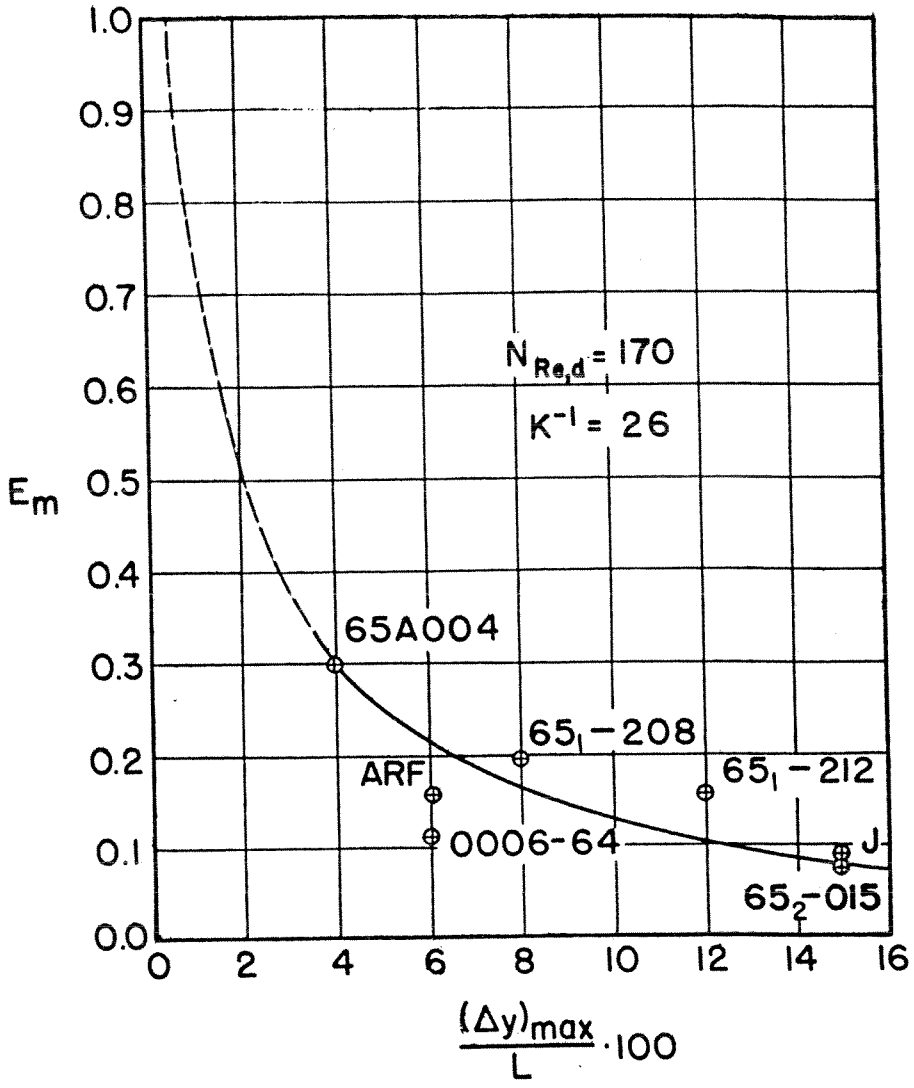

FIG. 3-57 TOTAL COLLECTION EFFICIENCY PLOTTED AGAINST THICKNESS OF AIRFOIL AT 4° ANGLE OF ATTACK

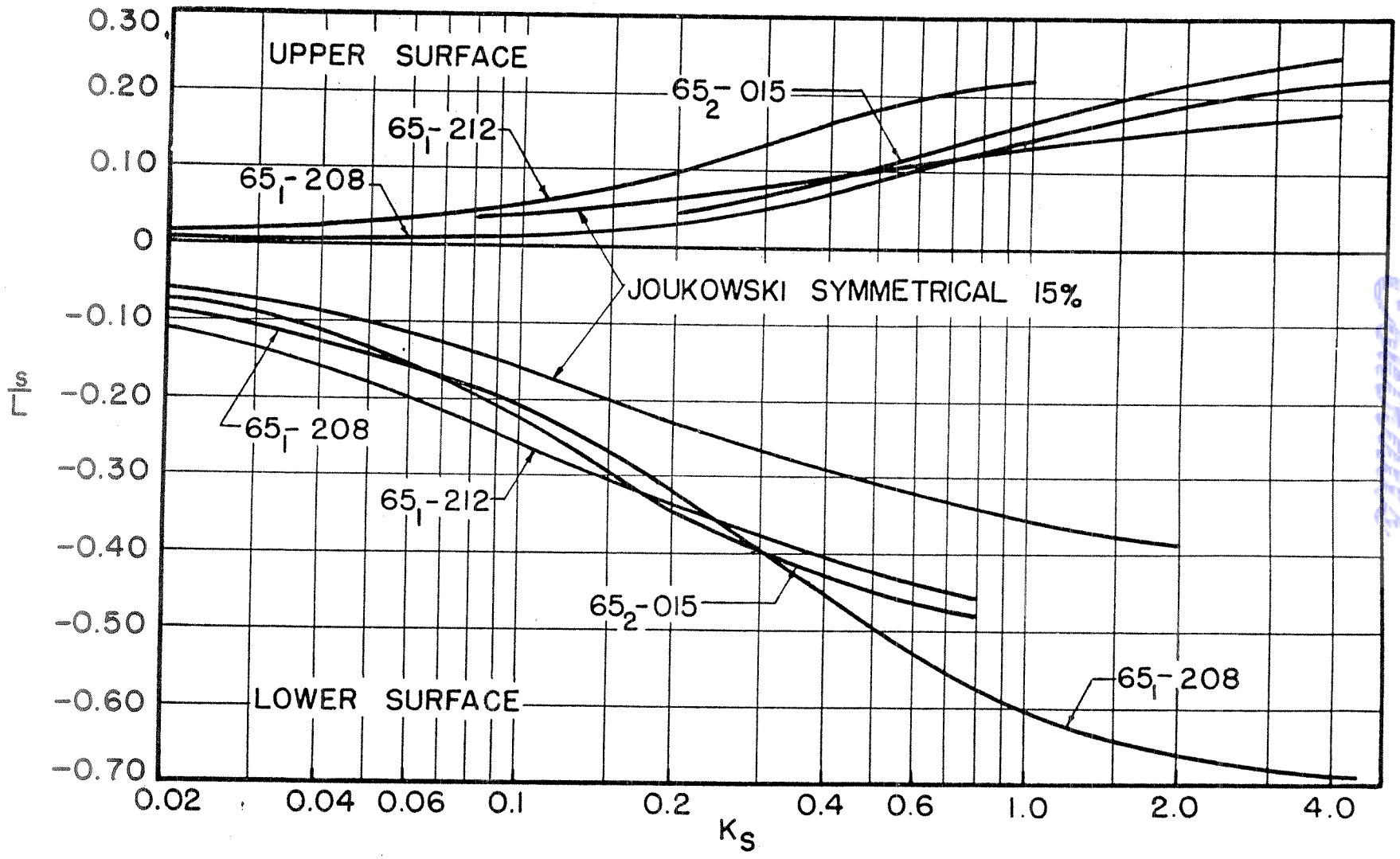

FIG. 3-58 IMPINGEMENT AREA VERSUS K_S FOR VARIOUS AIRFOILS AT 4° ANGLE OF ATTACK.

ratio decreases, the limit of impingement increases appreciably in cases where $K^{-1} \leq 1$. But for $K^{-1} \geq 10$ the impingement area increases only slightly. In general, a decrease in thickness ratio will result in less total water being spread over a larger area of the lower surface.

3-7 Tapered Wings

Some remarks regarding tapered wings have already been made in Section 3-3.2. In addition, it might be observed that the rate of catch is greater outboard for small droplets than it is inboard and that the reverse is true for large droplets. The explanation is that although E_m increases with decreasing chord length, the projected area of the wing in a plane normal to the main flow decreases. Beyond a certain value of droplet diameter, a further increase in droplet diameter and decrease in projected area produces relatively small increase in E_m.

3-8 Compressibility Effect in Subsonic Flight

Brun, Serafini, and Gallagher (Ref. 26) evaluated the effect of compressibility of air on the water impingement. They found that for a cylinder, it was negligible up to the flight critical Mach number. Their calculation revealed that the greatest effect of compressibility on the water impingement occurs at $K = 5$ and $\phi = 50{,}000$ with a decrease of collection efficiency of less than 3 per cent.

The extension of the results obtained with a cylinder to an airfoil is justifiable, because the incompressible flow fields of cylinders and airfoils are similarly altered by compressibility. Furthermore, the flow field around the nose section of the airfoil, where impingement occurs, is not affected to a significant degree by compressibility.

Aerodynamic considerations show that a change of the airflow field which might be caused by placing the airfoil at an angle of attack, would tend to shift the location of the maximum difference between the compressible and incompressible flows toward the leading edge of the upper surface and toward the tail on the lower surface. However, the same change also shifts the area of impingement in the same fashion; therefore, the area of

impingement would remain in the region where the effect of compressibility is of no practical consequence, and it appears that for airfoils as well as cylinders the effect of compressibility is negligible up to the critical Mach number.

3-9 Swept Wings in Subsonic Flight

Dorsch and Brun (Ref. 35) have discussed the general effect of wing sweep on cloud droplet trajectories and swept wings of high aspect ratios moving at subsonic speed. They proposed a method to extend the impingement data of non-swept wings to swept wings.

They show that for swept wings of high aspect ratio and small taper, it is possible to obtain the x,y-projection of the droplet trajectories around it from two-dimensional trajectory data by using the component of the free stream velocity and the angle of attack in the plane normal to the leading edge when evaluating the various dimensionless parameters. The spanwise displacement of the droplets causes a small spanwise shift of the impingement point. For droplets not of uniform size, each size will be shifted spanwise a slightly different amount, but the net chordwise impingement in the normal plane at each spanwise station will be the same as the net chordwise impingement calculated from the x,y-component of the trajectories when the given droplet-size distribution is used.

3-10 Water Impingement in Supersonic Flight

It appears that if the ambient temperatures are 0°F or higher (which includes 90 to 95 per cent of recorded icing conditions) icing will not occur at supersonic speeds. If all possible icing conditions are considered, very high speeds would be necessary to prevent icing by aerodynamic heating.

Callaghan and Serafini (Ref. 30 and 31) performed an analytical investigation with experimental confirmation on icing of a diamond (double wedge) airfoil at flight Mach numbers as high as 1.4. Because of the limited interest in these extreme conditions this problem will not be considered any further in this manual.

3-11 Distribution of Droplet Size in Clouds

In the preceding analysis droplets of uniform size were assumed. Actually, droplets of different sizes are usually present in the same cloud. It has been a common practice to use the mean-effective droplet diameter in calculating impingement data. For increased accuracy, however, a weighted sum corresponding to the specific droplet-size distribution pattern should be used. In particular, area of impingement is determined by the largest diameter rather than the mean-effective droplet diameter.

For convenience, Langmuir and Blodgett (Ref. 81) defined five different droplet-size distribution patterns as shown in Table 3-5. The size is expressed as the ratio of the average droplet radius a in each size group to the mean effective droplet radius a_o.

Table 3-5 WATER DROPLET DISTRIBUTIONS

Droplets in each size group (per cent)	a/a_o Distributions				
	A	B	C	D	E
5	1.00	0.56	0.42	0.31	0.23
10	1.00	0.72	0.61	0.52	0.44
20	1.00	0.84	0.77	0.71	0.65
30	1.00	1.00	1.00	1.00	1.00
20	1.00	1.17	1.26	1.37	1.48
10	1.00	1.32	1.51	1.74	2.00
5	1.00	1.49	1.81	2.22	2.71

A complete analysis requires that the impingement rate be calculated for each droplet size. The rates of catch are then summed in proportion to the amounts of water present in each size group. For ordinary design purposes this idea of distribution need not be used. It is usually found necessary in a testing program when it is desired to bring results from experiments and the theory into good agreement.

3-12 Miscellaneous Remarks on Water Impingement

It will be assumed in the following chapters that all the water impinging on the airfoil according to the trajectory data will have to be removed from the heated surfaces by evaporation. The assumption may be somewhat conservative because there are mechanisms which decrease the rate of impingement before the water reaches the airfoil or remove the water after it has collected on the airfoil surface.

3-12.1 Pre-Evaporation

So far it has been supposed that the water droplets do not change size as they approach the airfoil. The fact is that as a droplet moves toward the stagnation region of an airfoil, particularly at high speed, its size diminishes by evaporation. Lowell (Ref. 85) investigated such droplets analytically and came to the conclusion that evaporative losses may be several per cent of the droplet mass. A small droplet approaching along a stagnation line may even evaporate completely and never reach the airfoil.

3-12.2 Bounce-Off

Langmuir (Ref. 80) suggested that droplets may bounce off a surface. This problem was further studied by Schaefer (Ref. 113). He found that when droplets of 100 microns diameter or larger would impinge on a clean surface of a thick water layer they would not merge with the water but instead would bounce or "skate" a distance of 50 centimeters or more. The skating stops when the surface becomes even slightly contaminated, and the droplets enter the water upon initial contact with the surface. The skating stops, also, when the depth of the water layer is reduced to a fraction of a millimeter.

No direct experiments to evaluate the effect of bounce-off during flight seem to be available. However, the experimental results found by Gelder and Lewis (Ref. 45) on heat transfer are in better agreement with analysis if it is assumed that no bounce-off occurs.

3-12.3 Blowoff

Hardy (Ref. 54) has suggested that some water may be lifted or blown off a wet surface. However, experimentation reported on by Tribus (Ref. 124) indicates no blowoff. In that investigation, which was performed by T. B. Gardner, all water pumped out through the leading edge of an airfoil was collected downstream; the mass balance showed that no water was torn from the surface. Boelter et al (Ref. 16) analyzed the forces which might act to remove a drop from a surface. They found no net force to which they could attribute its being blown away.

4-1 Internal and External Heat Transfer

Heat is transferred directly from the hot air in the double-skin passages to the outer skin by convection; some is transferred indirectly by conduction through the inner skin. A part of the heat leaves the outside surface of the airfoil by convection, another part by evaporation; both these processes occur on the exterior surfaces within the narrow region of the boundary layer and are closely related.

The reader should take care to observe whether he is considering a local or a mean coefficient of heat transfer. Local rates of heat transfer are used to analyze the performance of a given anti-icing system. Average rates are employed in preliminary design calculations.

In this chapter, equations for calculating the coefficients are presented. In Chapter 6, the rates of heat transfer are calculated.

4-1.1 Convection of Heat at Low Speeds

The rate of convection from unit area of heated surfaces in a low-speed air stream is

$$q''_c = h(T_s - T_o) \qquad (4\text{-}1)$$

where h denotes the local coefficient of heat transfer.[1] Subscripts s and o refer to the surface and free stream, respectively, and T_s is the local absolute temperature of the surface at profile distance s from the stagnation point.

The coefficient h depends mainly on the local air speed and the distance from the leading edge. It also depends on the air properties.

---

[1] The quantity h is sometimes called the point unit conductance; a mean value is then said to be the average unit conductance. The units are B/hr ft^2 F.

4-1.2 Convection of Heat at High Speeds

At high speeds frictional or aerodynamic heating has an important effect and Eq. 4-1 must be modified to become applicable. The frictional heating reduces the rate of heat transfer by convection. It has been found (Ref. 39 and 40) that the following modification or generalization of Eq. 4-1 accurately gives the net rate of heat transfer by convection:

$$q_c'' = h\left(T_s - T_1 - \eta_r \cdot \frac{U_1^2}{2g\,J\,c_{p,a}}\right) = h\,(T_s - T_{aw}) \qquad (4\text{-}2)$$

where η_r is the local recovery factor (Section 4-2) and T_{aw}, defined by this equation, is known as adiabatic wall temperature. Subscript 1 refers to the local conditions at the outer edge of the boundary layer, which are discussed in Section 4-3. In Eq. 4-2, employing $[U_1]$ = ft/sec, g = 32.17 ft/sec^2, J = 778 ft lb/B, and $c_{p,a}$ = 0.240 B/lb F, the product $2gJc_{p,a}$ = 2,010 ft^2/sec^2 F. At low speeds the last term in the parentheses is relatively small and can be neglected, T_1 is hardly any different from T_s, and Eq. 4-2 reduces to Eq. 4-1. A particularly interesting feature of Eq. 4-2 is that the coefficient h can be evaluated from data of low-speed experiments in which Eq. 4-1 is used as a definition of h.

2 Local Recovery Factor η_r

The quantity η_r is found by both experiment and theory (Ref. 39 65) to depend upon whether the flow in the boundary layer is laminar turbulent and on the Prandtl number of air ($N_{Pr} \equiv \mu c_p/k$).

For the range of temperatures encountered in the present application, Prandtl number of air may be taken to be constant at the average value (see Table A-2).

1 Evaluation of η_r for the Laminar Boundary Layer

In the case of laminar heat heat transfer,

$$\eta_r = N_{Pr}^{1/2} = 0.84 \qquad (4\text{-}3)$$

R 54-313

4-2.2 Evaluation of η_r for the Turbulent Boundary Layer

In this case,

$$\eta_r = N_{Pr}^{1/3} = 0.89 \qquad (4\text{-}4)$$

4-3 Evaluation of Air Properties at the Outer Edge of the Boundary Layer

In order to use Eq. 4-2 and some subsequent equations, the local static absolute pressure p_1, the local static absolute temperature T_1, and the local velocity U_1 will have to be evaluated. For this purpose flow along the outer edge of the boundary layer is assumed to be isentropic. Also, the free stream Mach mumber M_o is assumed to be below the critical value so that the flow is either incompressible or subsonic, without shock.[1]

4-3.1 Preliminary Evaluation of p_1 and T_1

Since p_1 and T_1 depend upon the free-stream absolute static pressure p_o and temperature T_o, which are arbitrary design parameters, exact evaluation of p_1 and T_1 is not always necessary. For a preliminary calculation satisfactory results are obtained by placing $p_1 = p_o$ and $T_1 = T_o$, the pressure p_o being found opposite the given pressure altitude in a table of the Properties of the Standard Atmosphere (Table A-1).

4-3.2 Incompressible Flow

For $M_o < 0.3$ the flow may be assumed incompressible, so that $\rho \equiv \rho_o$. It follows that $T_1 \equiv T_o$ and that from Bernoulli's equation

$$p_1 = \frac{\rho_o U_o^2}{2}\left[1 - \left(\frac{U_1}{U_o}\right)^2\right] + p_o \qquad (4\text{-}5)$$

[1] The free stream Mach number M_o is the ratio of the free stream velocity U_o to the velocity of sound a_o in the free stream. Since atmospheric air can be considered an ideal gas, the velocity of sound in air depends only on the temperature. Tables A-1 and -2 give the velocity of sound in air as a function of the temperature. The chart of Fig. A-2 may be used to evaluate Mach numbers for a given speed and temperature.

In this equation $[p] = lb/ft^2$ when $[\rho_o] = slug/ft^3$ and $[U] = ft/sec$. To convert from lb/ft^2 to in.-mercury see Table A-4. In Ref. 1, ratios (U_1/U_o) and $(U_1/U_o)^2$ are tabulated as a function of chordwise distance for several airfoils of basic thickness form (symmetrical airfoils). The authors show by example how their tabulated values can be modified to allow for finite camber and angle of attack. Thus, U_1/U_o and p_1 can be calculated as a function of s/L.

In numerous other references dealing with properties of airfoils, the pressure coefficient,

$$C_{p,1} \equiv \frac{p_1 - p_o}{\rho_o U_o^2/2} \qquad (4\text{-}6)$$

is given as a function of chordwise distance in graphical or tabular form.

For some preliminary calculations it will be found convenient to employ the following mean velocity and to assume it is uniform over the entire heated surface (Ref. 89 and 117):

$$U_m \equiv U_o \left(1 \pm \frac{C_L}{4 \cos \alpha}\right) \qquad (4\text{-}7)$$

The positive sign is for the upper surface and the negative sign for the lower; C_L is the lift coefficient and α is the angle of attack.

4-3.3 Compressible Flow

If $M_o > 0.4$ more accurate results will be obtained by considering that the flow is compressible; then the density ρ is not uniform and $T_1 \neq T_o$.

At high subsonic velocities of the free stream, the local velocity U_1 at any points may reach the local velocity of sound. The corresponding value of the free stream Mach number is called the critical Mach number. Below the critical Mach number the flow is said to be subsonic. The present discussion has been limited to flow in this region, for at higher speeds aerodynamic heating becomes an increasingly significant quantity, reducing the thermal energy required from the anti-icing system. Information

regarding heat transfer calculations in the cases of transonic and supersonic flows around airfoils can be found in Ref. 65.

The distribution of the pressure coefficient C_p for subsonic speeds at any point on an airfoil may be found in terms of the pressure coefficient for incompressible flow $C_{p,i}$. The following equation, due to Kármán, is in good agreement with experimental results on the forward regions where separation does not occur and gives a good approximation up to the critical Mach number for most airfoils (Ref. 62).

$$C_p = \frac{C_{p,i}}{\beta + \frac{1}{2} C_{p,i} (1 - \beta)} \tag{4-8}$$

where

$$\beta = (1 - M_o^2)^{0.5} \tag{4-9}$$[1]

With given free stream Mach number and the distribution of C_p the properties at the outer edge of the boundary layer may be calculated by means of the following equations (Ref. 65, Section II):

$$\frac{p_1}{p_o} = 0.702 \cdot M_o^2 C_p + 1 \tag{4-10}$$

$$\frac{T_1}{T_o} = \left(\frac{p_1}{p_o}\right)^{0.288} \tag{4-11}$$

$$\frac{U_1}{U_o} = \left[1 + \frac{4.94}{M_o^2}\left(1 - \frac{T_1}{T_o}\right)\right]^{1/2} \tag{4-12}$$

and

$$\frac{\rho_1}{\rho_o} = \left(\frac{p_1}{p_o}\right)^{0.712} \tag{4-13}$$

Figures 4-1, -2, -3, and -4, reproduced from Ref. 65, may be used as aids in the calculations. The equations and figures are based on the value $\kappa = 1.405$ for the ratio of specific heats.

[1] Alternatively, for subsonic flow $\beta = \cos \sin^{-1} M_o$.

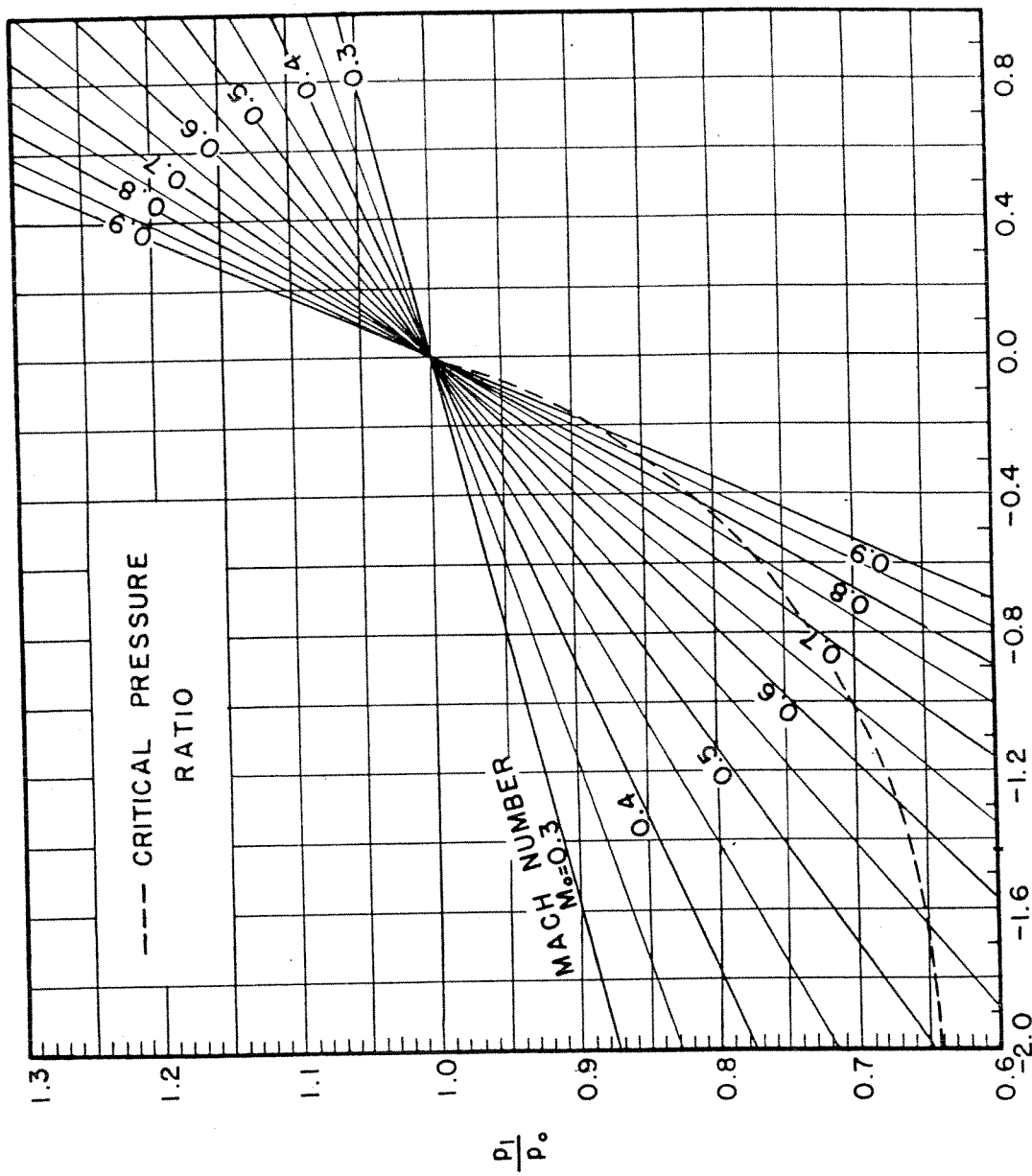

FIG. 4-1 ISENTROPIC PRESSURE RELATIONSHIP

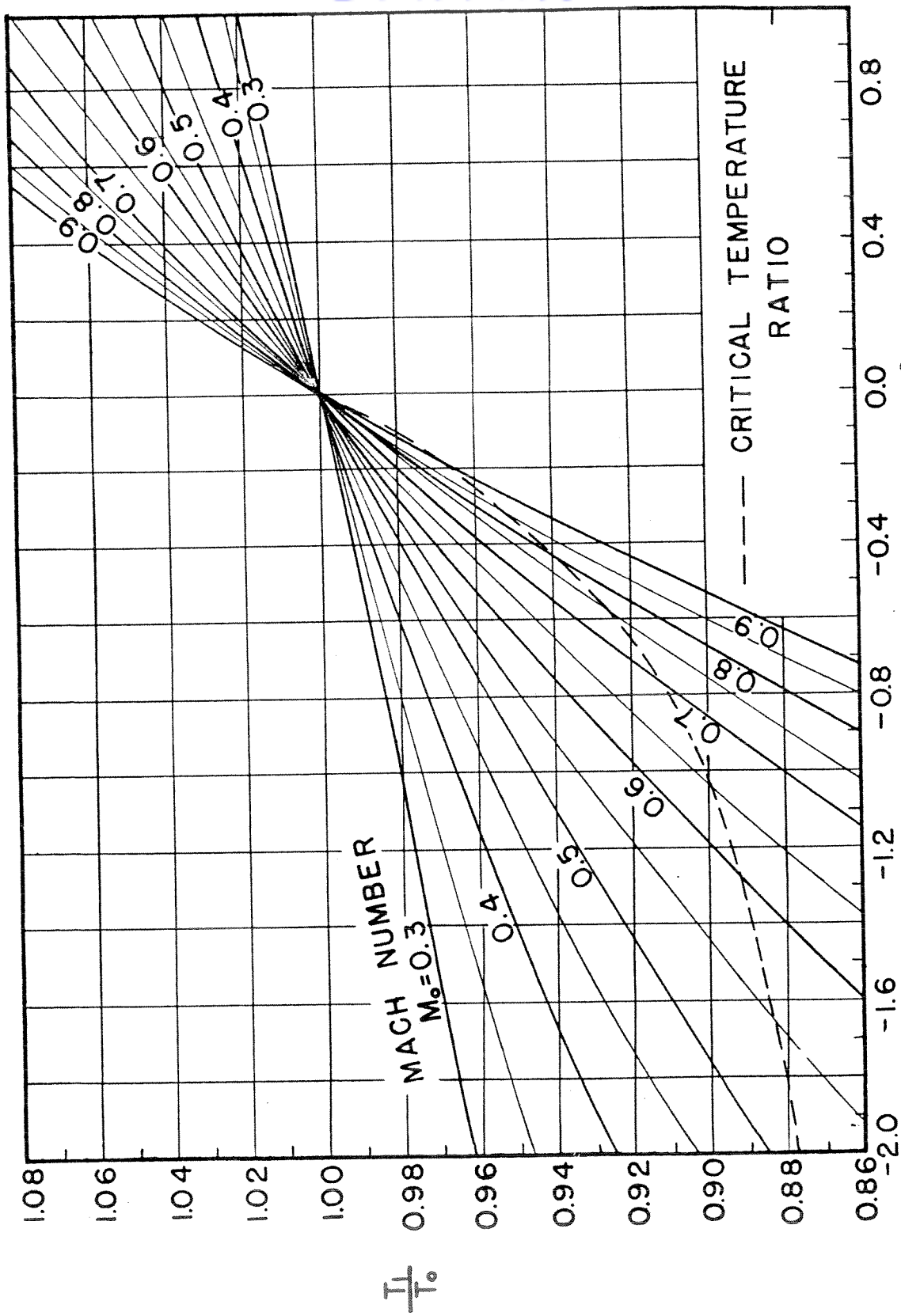

FIG. 4-2 ISENTROPIC TEMPERATURE, RELATIONSHIP

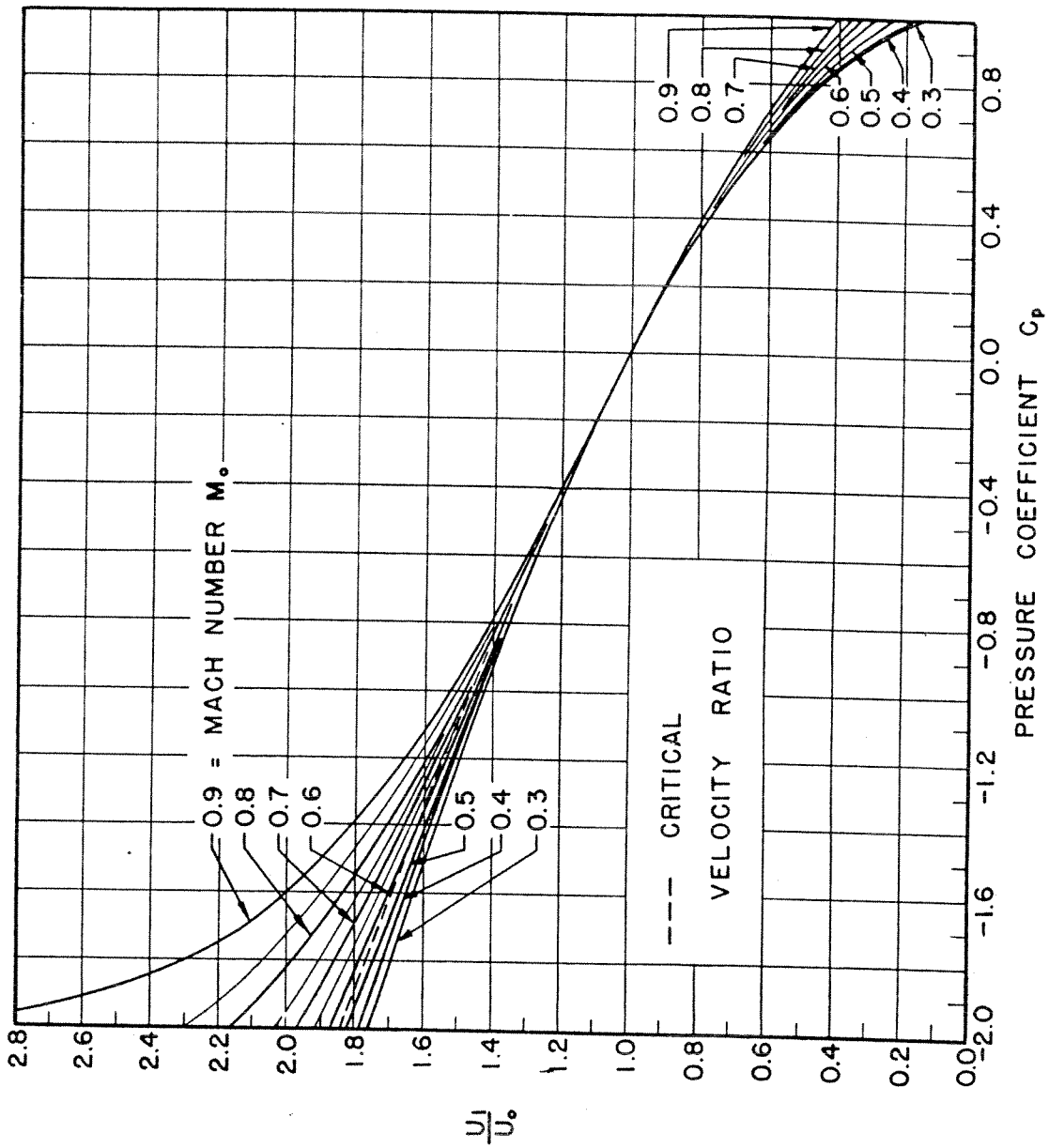

FIG. 4-3 ISENTROPIC VELOCITY RELATIONSHIP

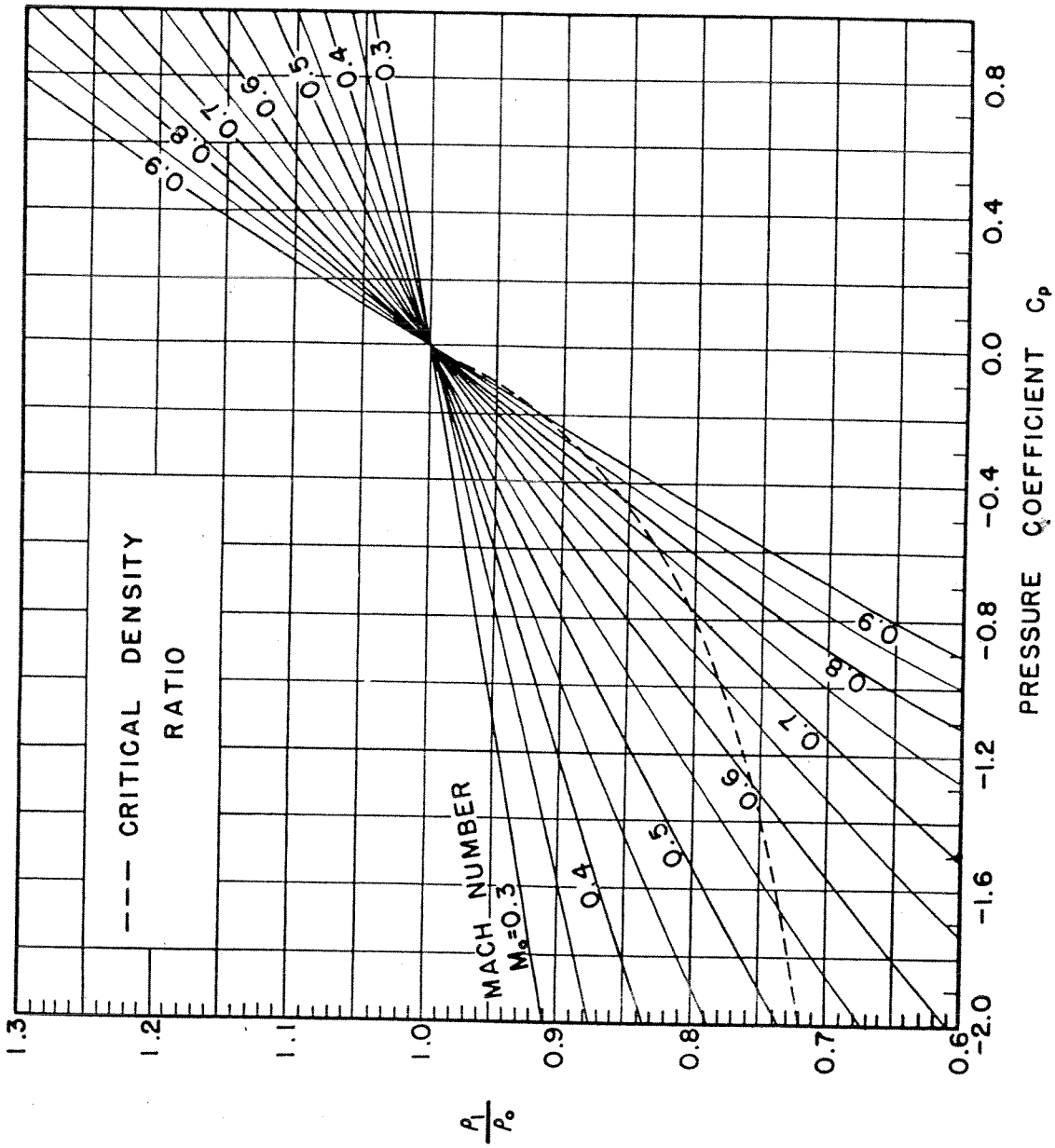

FIG. 4-4 ISENTROPIC DENSITY RELATIONSHIP

In some references on airfoil data the pressure coefficient C_p is not given and, instead, the ratio p_1/H_o is plotted against the chordwise distance. Here p_1 is the local pressure as before, and H_o is the free stream stagnation or total pressure:

$$H_o \equiv p_o + F_o \cdot \frac{1}{2} \rho_o U_o^2 \qquad (4\text{-}14)$$

where

$$F_o = 1 + \frac{1}{4} M_o^2 + \frac{1}{40} M_o^4 + \cdots \qquad (4\text{-}15)$$

which is plotted on the abscissa of the chart in Fig. A-3. The relationship between the pressure coefficient $C_{p,1}$ and the ratio p_1/H_o is

$$C_{p,1} = \frac{\frac{p_1}{H_o}\left(1 + \frac{\kappa - 1}{2} \cdot M_o^2\right)^{\frac{\kappa}{\kappa - 1}} - 1}{\frac{1}{2} \kappa M_o^2} \qquad (4\text{-}16)$$

4-4 Calculation of Profile Distances

In order to calculate certain quantities regarding rates of heat transfer and mass transfer, and to relate impingement areas to chordwise distance, profile distances from the geometric leading edge of the airfoil are needed. Profile coordinates can usually be found tabulated in the literature. For example, Ref. 1 contains tabulations of the profiles of many of the low-drag airfoils. Employing those data, one can lay out the airfoil to large scale and measure dimensionless distances s/L along the profile using dividers and scale. Or, the distances can be calculated in an approximative way suggested by Falkner (Ref. 42). This method is summarized below. A tabulation of the x,y-coordinates of the profile is required to start the calculation.

Falkner's method is based on the idea that circular arcs passing through successive sets of three points can be used to approximate the profile. The profile lengths are taken to be equal to the summation of the circular arc lengths. Figure 4-5 facilitates the calculations. In the following steps all distances are ratios of the chord length L.

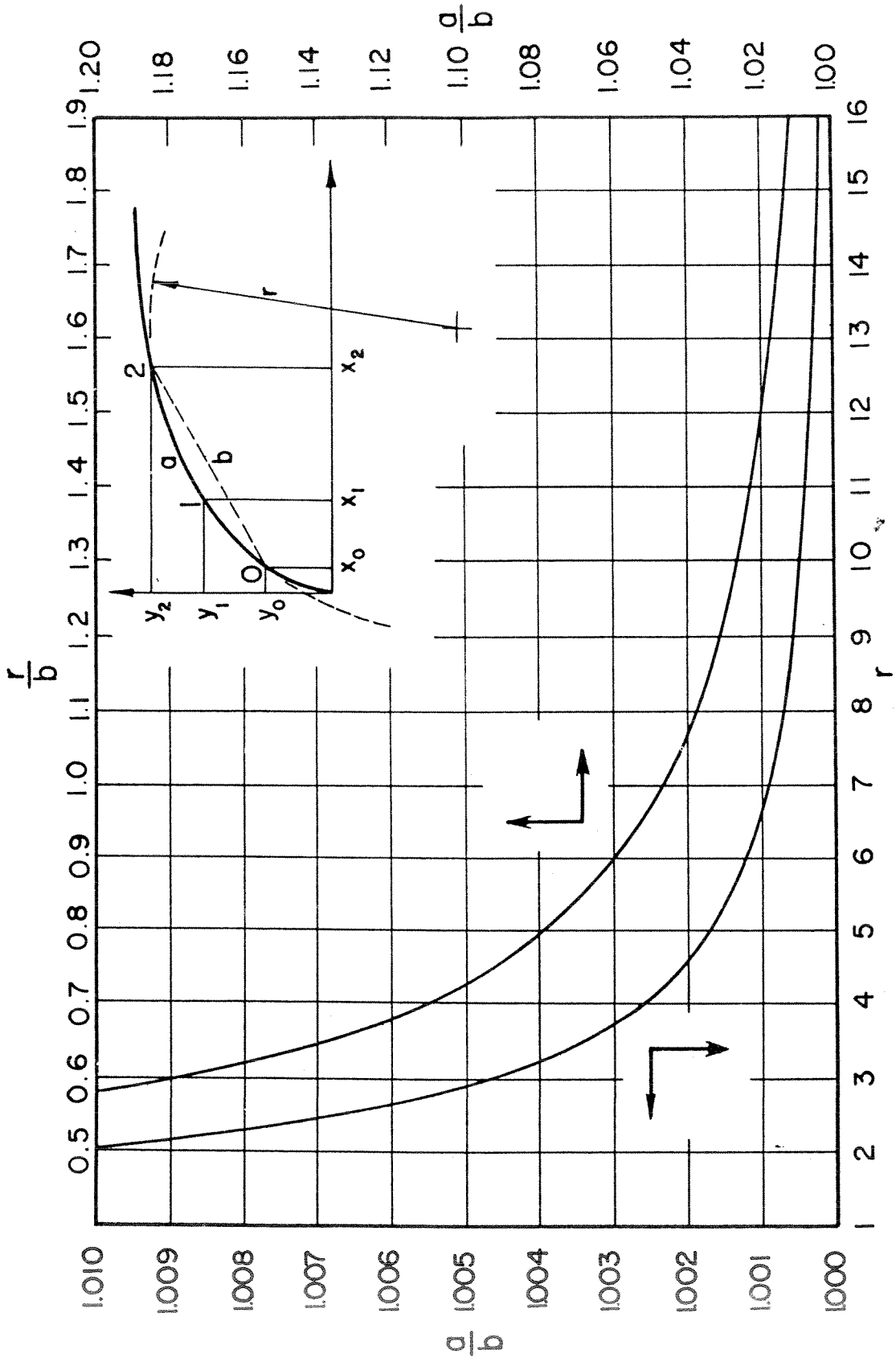

FIG. 4-5 CHART FOR CALCULATION OF PROFILE DISTANCES

ep 1. Let three successive points be (x_o,y_o); (x_1,y_1); and (x_2,y_2). e the upper right-hand corner of Fig. 4-5. Calculate $\Delta x_1 \equiv x_1 - x_o$, $x_2 \equiv x_2 - x_1$, $\Delta y_1 \equiv y_1 - y_o$, and $\Delta y_2 \equiv y_2 - y_1$.

ep 2. Calculate the ratio,

$$\frac{r}{b} = \frac{\text{radius of arc}}{\text{chord of arc}}$$

$$= \frac{\left[(\Delta x_1)^2 + (\Delta y_1)^2\right]^{1/2} \left[(\Delta x_2)^2 + (\Delta y_2)^2\right]^{1/2}}{2\left|\Delta x_1 \cdot \Delta y_2 - \Delta x_2 \cdot \Delta y_1\right|} \qquad (4\text{-}17)$$

p 3. Entering Fig. 4-5 with the ratio found in Step 2 find a/b, the io of the circular arc length $\overset{\frown}{012}$ to the chord $\overline{02}$ of the arc.

p 4. Calculate b, the chord of the arc.

$$b = \left[(\Delta x_1 + \Delta x_2)^2 + (\Delta y_1 + \Delta y_2)^2\right]^{1/2} \qquad (4\text{-}18)$$

s is the rectilinear distance from Point 0 to Point 2.

p 5. Multiply the results of Steps 3 and 4 to obtain a, the circular length from Point 0 to Point 2.

p 6. Repeat Steps 1 to 5 using the next three points: (x_2,y_2); (x_3,y_3); (x_4,y_4). And so forth.

p 7. The sum of the a's is approximately $\sum \Delta s = s$. Any profile ance s can then be found from a graph of s plotted against the dwise distance x.

Evaluation of the Coefficients of Heat Transfer on the Exterior Surface of an Airfoil

In the following presentation all distances s are measured along the ile from the geometric leading edge (point of intersection of the chord and the profile). The equations are based upon the assumptions that

the surface temperature T_s is uniform and that the flow is incompressible. Unless otherwise stated, fluid properties are evaluated at the temperature,

$$t_f = (t_s + t_o)/2 \qquad (4\text{-}19)$$

Finally, no distinction is made between the coefficients of heat transfer on dry and wet surfaces, and the influence of the presence of moisture, which has little effect on most air properties, is neglected. Deviations from some of these restrictions are considered in Sections 4-9 and -12.

Two methods of calculating the coefficient of heat transfer are presented: the "flat plate" approximation and the "wedge flow" approximation. The latter appears to be generally more accurate but requires more time. For thin airfoils, results from the flat plate approximation appear to be satisfactory.

4-6 Flat Plate Approximation

First approximations, which may be sufficiently accurate for most purposes, can be easily obtained by replacing the leading edge with a cylinder and the afterbody with a flat plate (Ref. 15 and 89). The best accuracy appears to be obtained for full-scale, thin airfoils in high-speed flow with long heated lengths.

4-6.1 Heat Transfer from the Leading Edge Region

Measurements of the local coefficient at angle ϕ from the point of stagnation on a heated cylinder (Ref. 115) have been represented by means of the equation,

$$N_{Nu,D} = 1.14\, N_{Re,D}^{0.5} \cdot N_{Pr}^{0.4} \left(1 - \left|\frac{\phi}{90}\right|^3\right) \qquad (4\text{-}20)$$

where $N_{Nu,D} \equiv \frac{hD}{k}$, $N_{Re,D} \equiv \frac{U_o D \rho}{\mu}$, and $0 \leq \phi \leq 90°$. In application to an airfoil, the leading edge having radius of curvature $D/2$ is replaced by the cylinder of diameter D. Customarily, this diameter is expressed as the ratio D/L where L is the chord length. Also,

$$\phi = \frac{360}{\pi} \frac{s}{D} \tag{4-21}$$

Placing $N_{Pr} \approx 0.71$, eliminating ϕ from Eq. 4-20 and -21, and introducing the chord length L instead of the leading edge diameter, as characteristic length in the Nusselt and Reynolds numbers,

$$N_{Nu,L} = 1.00\ N_{Re,L}^{0.5} \cdot G\left(\frac{s}{L}, \frac{L}{D}\right) \tag{4-22}$$

where $N_{Re,L} \equiv U_o L \rho / \mu$ and the factor

$$G\left(\frac{s}{L}, \frac{L}{D}\right) \equiv \left[\left(\frac{L}{D}\right)^{0.5} - 2.06 \left(\frac{L}{D}\right)^{3.5} \left(\frac{s}{L}\right)^{3}\right] \tag{4-23}$$

may be evaluated by means of Fig. 4-6. In this chart the leading edge radius, expressed as per cent of the chord length, replaces the parameter L/D. The charts of Fig. A-4 and -5 taken from Ref. 3 may be found convenient to calculate the Reynolds number $N_{Re} \equiv U_o L \rho_o / \mu_o$, when the Mach number M_o is known. Also, the charts of Fig. 4-7 and -8 can be used for 15°F icing atmosphere at 10,000 and 20,000 ft pressure altitude, respectively. After the Nusselt number hL/k has been calculated, the coefficient h may be found for 15°F atmosphere (k = 0.01352 B/hr ft F), using Fig. 4-9.

The product of the powers of the fluid properties in Eq. 4-22, excluding the density, has been expressed as a function of the temperature T_f with the result that it may be written in the dimensional form,

$$h = 0.185\ T_f^{0.5} \left(\frac{U_o \rho}{L}\right)^{0.5} G\left(\frac{s}{L}, \frac{L}{D}\right) \tag{4-24}$$

where $[h]$ = B/hr ft^2 F; $[U_o]$ = ft/sec; $[\rho]$ = lb/ft^3; $[L]$ = ft; and $[T_f]$ = °R. Based on the thermal properties of air in Table A-2, Eq. 4-24 represents Eq. 4-22 within ± 1 per cent in the range of temperature from 0 to 140°F.

4-6.2 Heat Transfer from the After Region — Laminar Regime

In the simplified treatment (Ref. 89) the airfoil shape downstream of the cylindrical part is treated as a flat plate. Whereas the velocity

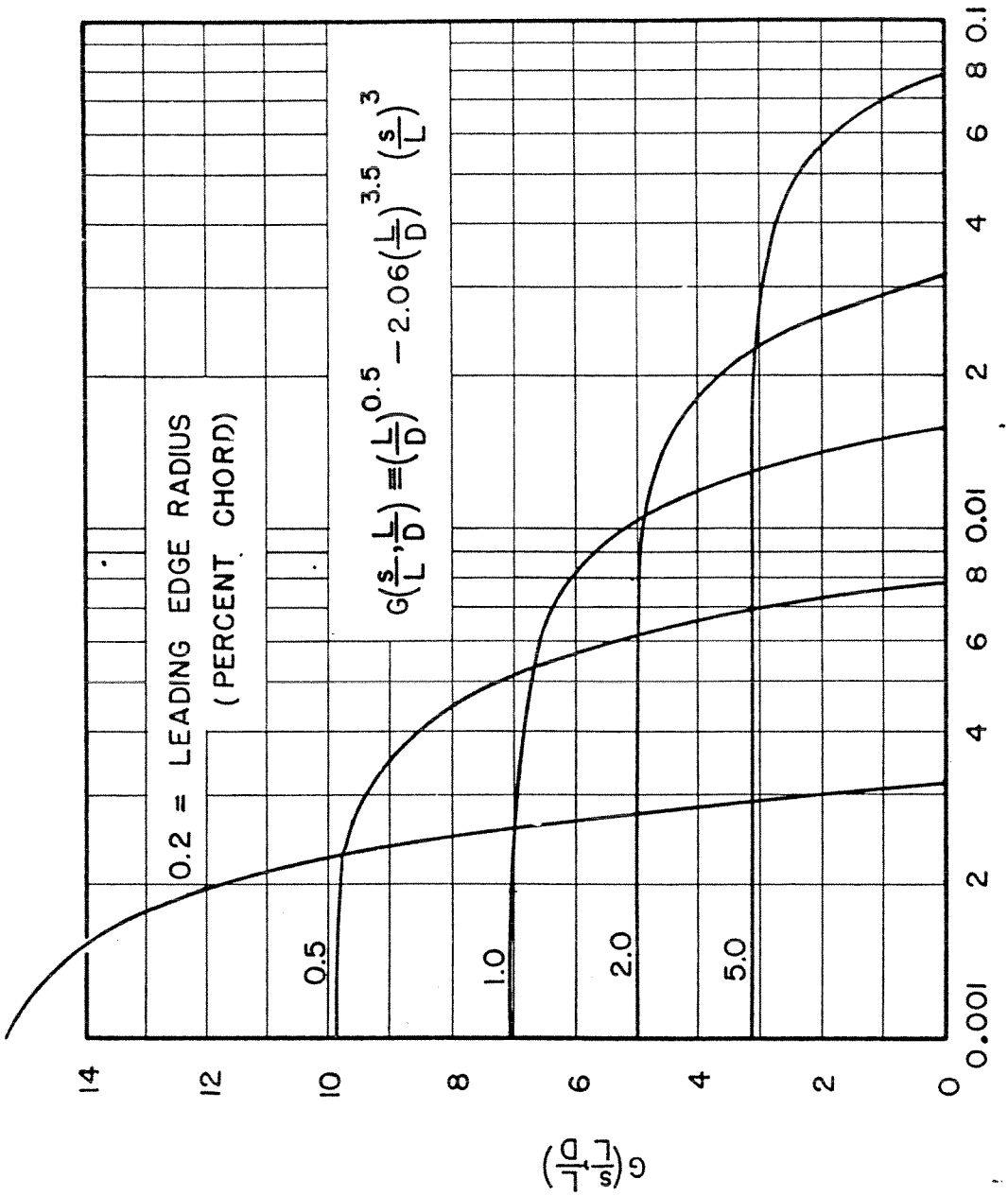

FIG. 4-6 FACTOR $G(\frac{s}{L},\frac{L}{D})$ FOR USE WITH EQUATION 4-22

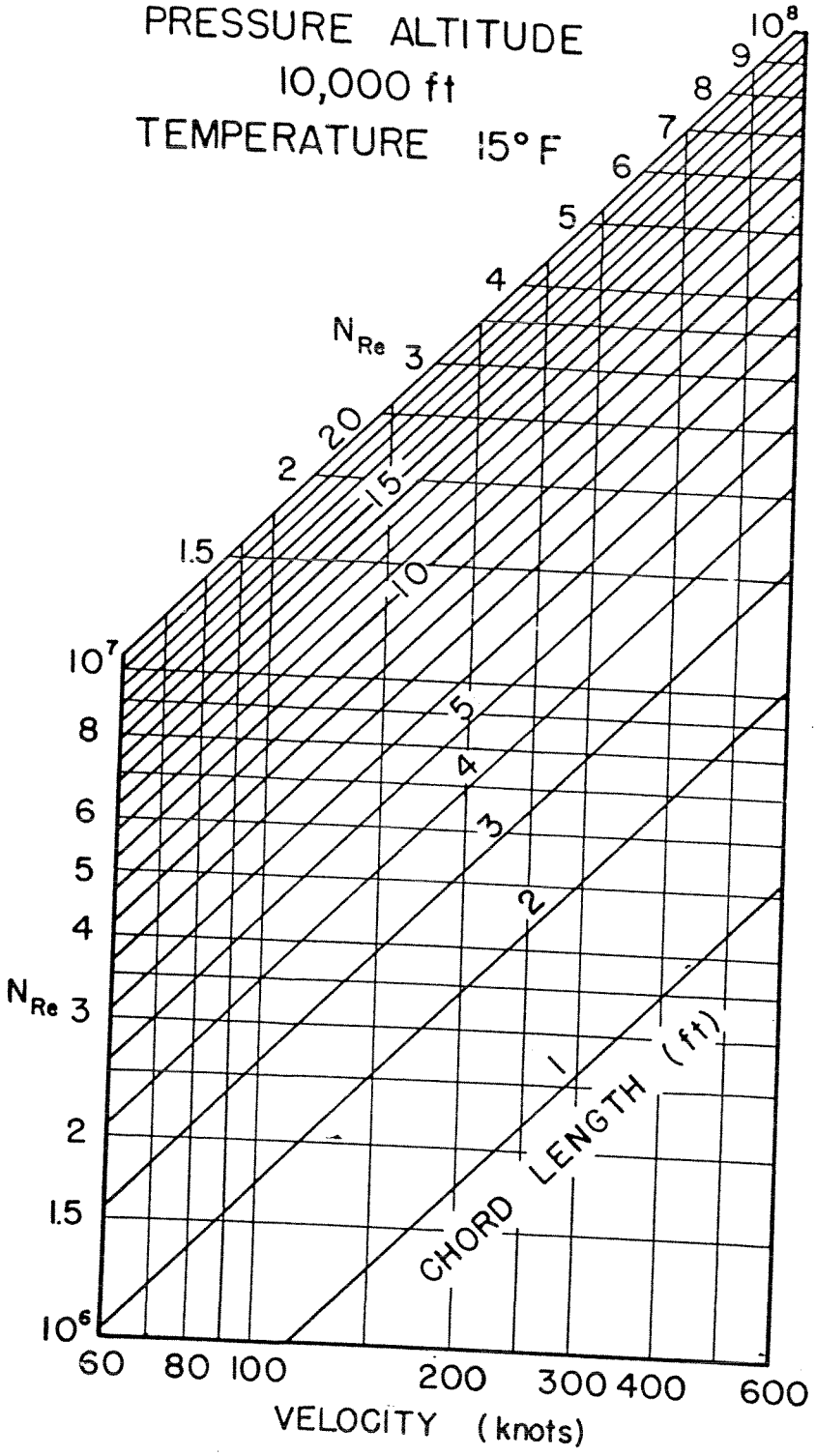

FIG. 4-7 CHART OF REYNOLDS NUMBER FOR 10,000 ft AND 15° F

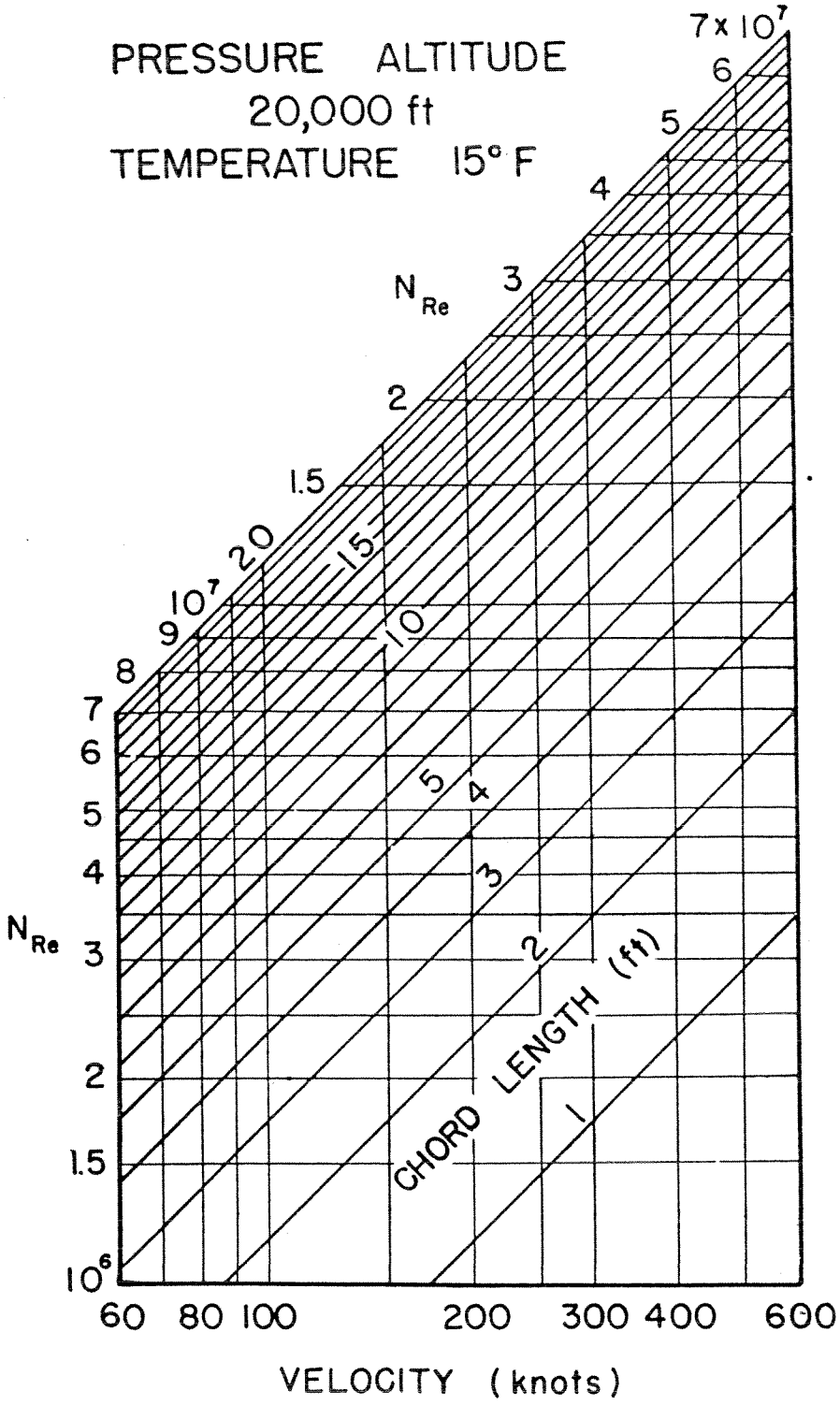

FIG. 4-8 CHART OF REYNOLDS NUMBER FOR 20,000 ft AND 15° F

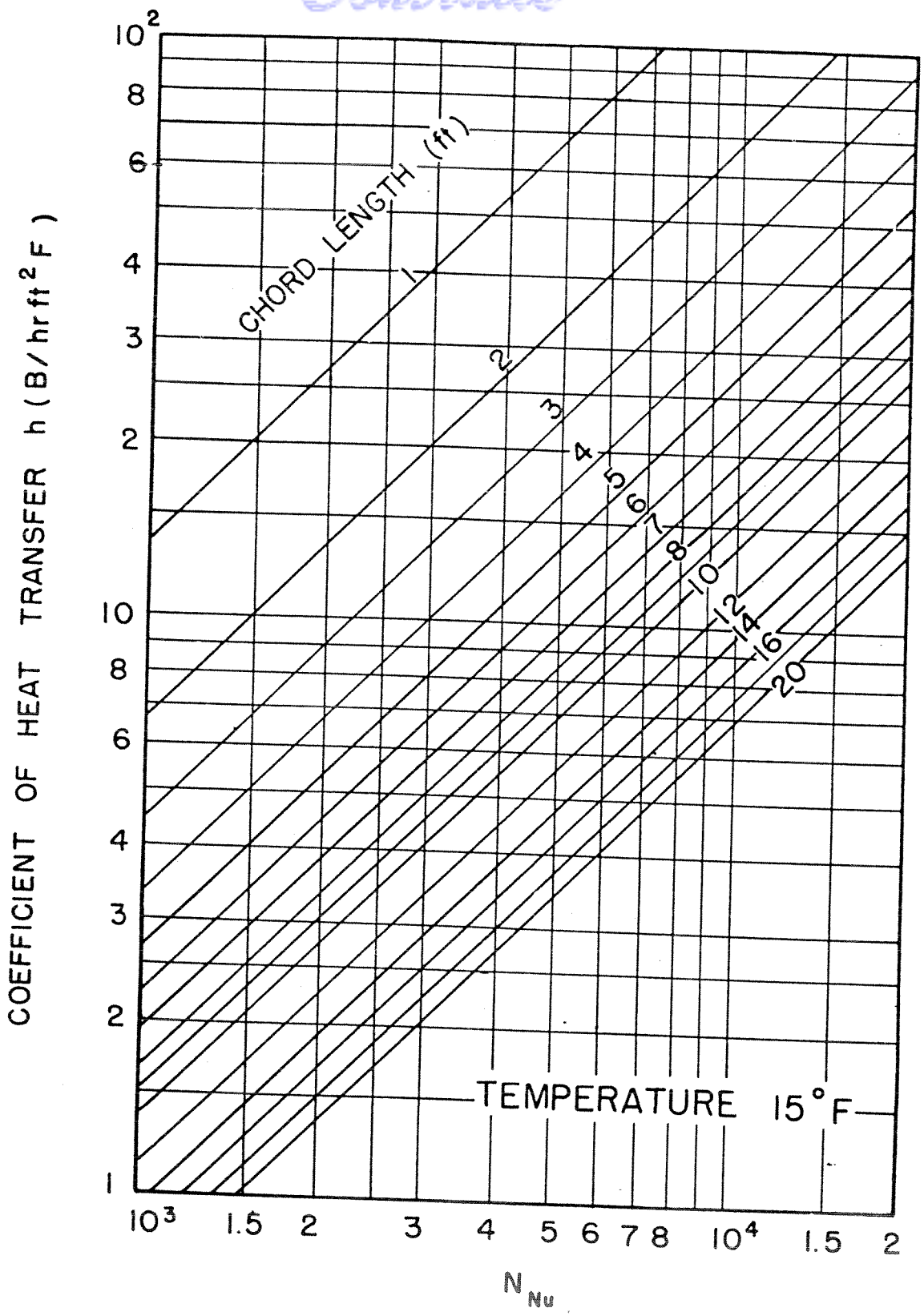

FIG. 4-9 CHART OF NUSSELT NUMBER FOR AIR AT 15 °F

outside the boundary layer is uniform on a flat plate, it is variable on the airfoil. In the present and the next sections, calculations are made under the assumption that the local heat transfer coefficient at distance s, where the local velocity outside the boundary layer on the airfoil is U_1, equals the local heat transfer coefficient at distance s from the leading edge of a flat plate in a uniform stream of velocity U_1.

In the laminar regime the local coefficient of heat transfer on a flat plate in a uniform stream of velocity U_1 is given by

$$\frac{hs}{k} = 0.332\, N_{Pr}^{1/3} \cdot \left(\frac{U_1 s \rho}{\mu}\right)^{0.5} \qquad (4\text{-}25)$$

Accordingly, on an airfoil

$$N_{Nu,L} = 0.286\, N_{Re,L}^{0.5} \cdot \sqrt{\frac{U_1}{U_o}} \cdot \sqrt{\frac{L}{s}} \qquad (4\text{-}26)$$

Similarly, as with Eq. 4-22 and -24, the following dimensional equation has been obtained:

$$h = 0.0530\, T_f^{0.5} \left(\frac{U_1 \rho}{L}\right)^{0.5} \cdot \left(\frac{L}{s}\right)^{0.5} \qquad (4\text{-}27)$$

4-6.3 Heat Transfer from the After Region — Turbulent Regime

In the turbulent regime the local coefficient of heat transfer on a flat plate in a uniform stream of velocity U_1 is given by:

$$\frac{hs}{k} = 0.0296\, N_{Pr}^{1/3} \left(\frac{U_1 s \rho}{\mu}\right)^{0.8} \qquad (4\text{-}28)$$

Even though the turbulent boundary layer is preceded by a laminar boundary layer, the distance s is measured from the leading edge; this is in accordance with Prandtl's assumption regarding the influence of transition on the turbulent boundary layer. It follows that on an airfoil

$$N_{Nu,L} = 0.0264\, N_{Re,L}^{0.8} \left(\frac{U_1}{U_o}\right)^{0.8} \left(\frac{L}{s}\right)^{0.2} \qquad (4\text{-}29)$$

And again in the dimensional form,

$$h = 0.711\ T_f^{0.247}\left(\frac{U_1\rho}{L^{0.25}}\right)^{0.8}\left(\frac{L}{s}\right)^{0.2} \qquad (4\text{-}30)$$

4-7 Evaluation of Local Coefficients of Laminar Heat Transfer by means of Wedge Flow Approximations

Another method to calculate local coefficients of heat transfer in the entire laminar regime (including both the leading-edge region and the laminar region beyond) is based on so-called wedge flow approximations. Predicted results are reportedly in better agreement with exact solutions and with experiments than are the flat plate solutions, particularly with regard to thick airfoils. This method has the disadvantage of requiring auxiliary calculations and, therefore, should be used only when it is required to have accuracy greater than that provided by the flat plate solutions presented above.

The flow outside the boundary layer on a wedge may be represented by an equation of the type,

$$U_1 = C \cdot s^m \qquad (4\text{-}31)$$

where m is a constant known as the Euler number; it depends upon the angle included by the wedge. The quantity C is, also, a constant but does not enter the calculations.

Boundary-layer calculations for wedges are exact. The idea of the wedge flow approximative calculations is to replace the flow at each point on the airfoil with a corresponding exact solution on the wedge.

The first step is to determine a value of m for each point where the coefficient is desired. Employing Eq. 4-31 and expressing m in terms of U_1 and dU_1/ds,

$$m = \frac{\dfrac{d\left(\dfrac{U_1}{U_o}\right)}{d\left(\dfrac{s}{L}\right)} \cdot \dfrac{s}{L}}{\dfrac{U_1}{U_o}} \qquad (4\text{-}32)$$

Accordingly, U_1/U_o should be found as a function of s/L; the differentiation can be performed graphically or numerically.

The second step is to evaluate the quantity,

$$\frac{\frac{hL}{k_s}}{\sqrt{\frac{U_o \rho_o L}{\mu_s}}} \cdot \frac{\sqrt{\frac{s}{L}}}{\sqrt{\frac{U_1 \rho_s}{U_o \rho_o}}} \equiv \frac{\frac{hs}{k_s}}{\sqrt{\frac{U_1 \rho_s s}{\mu_s}}} \qquad (4\text{-}33)$$

by means of the chart (Ref. 20 and 41) in Fig. 4-10. The local coefficient can then be calculated. It may be noted that the conductivity and dynamic viscosity are evaluated at the surface temperature. But if the temperature difference is small, the properties of the free stream may be used. Further, if the speed is moderate, the ratio $\rho_s/\rho_o \approx 1$.

For a circular cylinder, this method yields coefficients which are within 15 per cent of experimental values. Greater accuracy is claimed for streamline bodies (Ref. 41).

A so-called "equivalent wedge-type flow" method has been brought to a convenient form for calculations (Ref. 41). A modification of the wedge-type solution, it accounts in an approximate way for the previous history of the boundary layer. It gives higher accuracy for more shapes than the simpler theory. However, each calculation requires the solution of a differential equation by a combination of charts and graphical constructions.

4-8 Influence of Temperature of the Air on Coefficients of Heat Transfer

Theoretically, thermal conductivity and viscosity should be evaluated at the surface temperature. However, this procedure has not always given the best possible correlations of experimental results. The main rule regarding fluid properties is to evaluate them at the temperature recommended for the particular theoretical or empirical equation being employed.

The influence of the air temperature on the coefficient of heat transfer, insofar as the fluid properties are affected by temperature, is

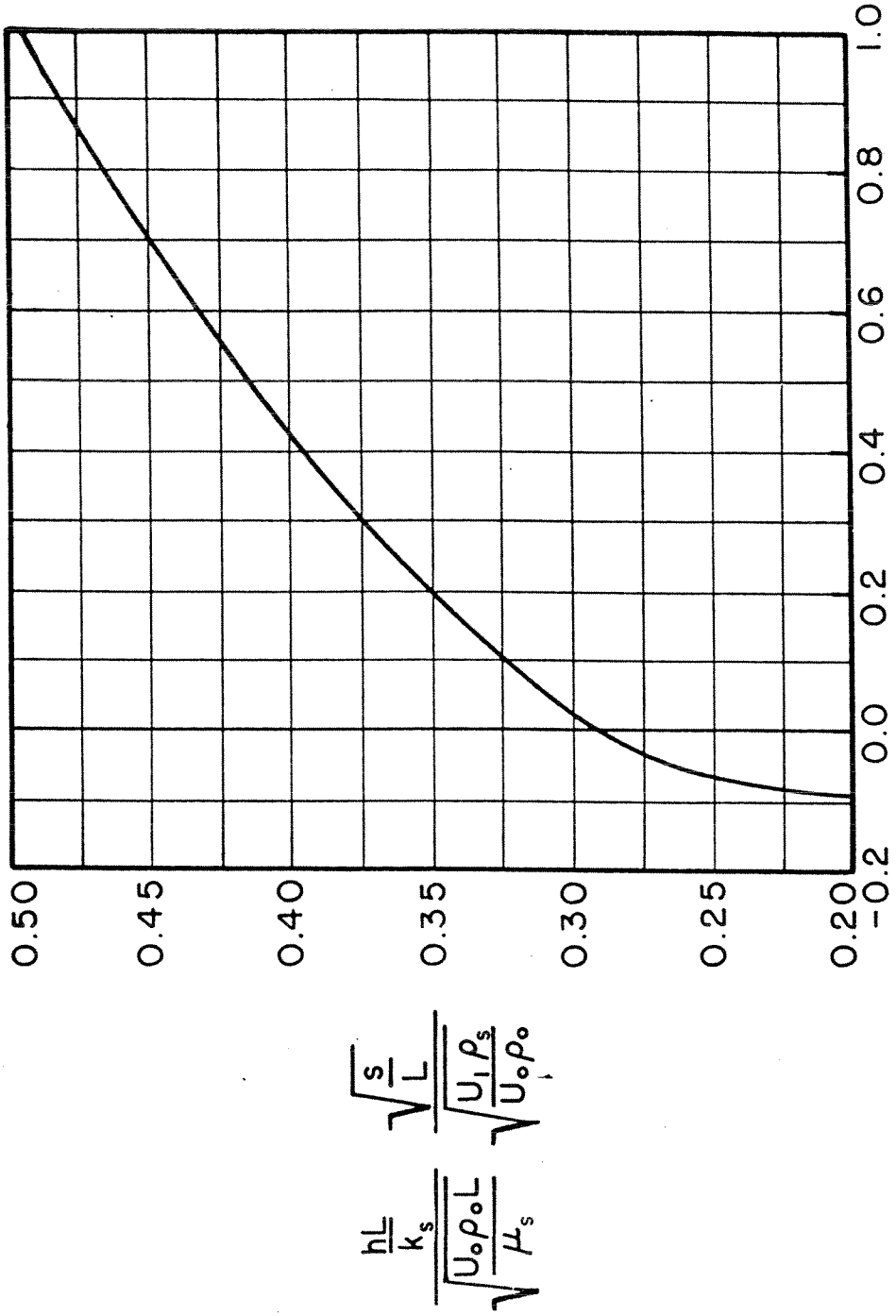

FIG. 4-10 CHART FOR WEDGE FLOW APPROXIMATIONS

relatively small in the present application. One reason is that within the range of temperature differences encountered in the present application, the fluid properties change relatively little.

Another reason is that the coefficient depends upon the fluid properties in a self-compensating manner. For example, in Eq. 4-24, since the density varies inversely with the absolute temperature T_f, the coefficient of heat transfer is virtually independent of the temperature. This is further exemplified by Eq. 4-27.

Equation 4-30, which is applicable to the turbulent boundary layer, shows by like reasoning that the coefficient of heat transfer varies inversely with the square root of the temperature. In an extreme case, if the surface temperature were 160°F and the main air temperature 0°F, the arithmetic mean absolute temperature would be 540°R. Evaluating the fluid properties at the free stream air temperature instead of the mean temperature, therefore, would give a value of the coefficient 6 per cent higher than the correctly calculated value. In most practical cases the difference would be much less.

Accordingly, for ease of calculation it is recommended that properties of the free stream be employed in evaluation of the coefficient of heat transfer. From the practical viewpoint of carrying out the calculations, this means that in Eq. 4-26 and -29, $N_{Re,L}$ (based on fluid properties evaluated at temperature t_f) may be replaced by N_{Re} (based on fluid properties evaluated at temperature t_o). For $t_o = 15°F$, N_{Re} may be obtained from Fig. 4-7 and -8 at 10,000 and 20,000 ft pressure altitude, respectively. When a second approximation is required, or when surface temperatures are quite high, the mean temperature t_f of the first approximation (dealt with in Chapter 6) should suffice to evaluate the fluid properties. Alternatively, by making reasonable estimates of the surface temperature and averaging this with the ambient plus 85 per cent of ram rise, the experienced designer can determine a temperature which will give values of the fluid properties that lie within 1 to 2 per cent of those computed using the actual mean temperature.

.9 Transition from the Laminar to the Turbulent Boundary Layer on the Exterior Surface

Accurate determination of the distribution of h along the exterior ırface requires that the point of transition be evaluated. This point, ›cated at distance s_{tr} from the leading edge, marks the end of the ıminar boundary layer. There the boundary layer begins to grow rapidly ıd to become turbulent. As a result the coefficient of heat transfer in-'eases very much. The growth may occur in a very short distance, in ıich case the transition is virtually abrupt. Or it may occur along a ›nsiderable distance before the boundary-layer turbulence becomes fully ›veloped. This interval of length is sometimes called the region of 'ansition. In this region the transition point is probably non-stationary.

The point of transition is allied to the stability of the laminar ›undary layer. The changing of factors which contribute to upset the ıminar qualities moves the point of transition upstream. Gazley (Ref. 44) ıs admirably summarized this subject.

On a flat plate high velocities, roughness, heated areas, evaporation, ıd external disturbances reduce s_{tr}. In addition, on an airfoil, ascend-ıg pressures reduce s_{tr}. Hence, a symmetrical airfoil at finite angle ' attack or a cambered airfoil will have a shorter laminar boundary layer ı the upper surface than on the lower surface. The disturbing effects of ırbulence in the main stream of a wind tunnel or of impinging water drop-ɛts move the point of transition forward. A major difference between ıll-scale flight and wind-tunnel model experiments is that the region of 'ansition in full-scale flight is relatively short. However, whereas ›rupt transition on a full-scale heated airfoil seems to occur in clear .r during free flight, a region of transition appears to occur in icing ›nditions.

A quantitative evaluation of all these factors is not possible. Tribus ıd Tessman (Ref. 127, p. 119) have performed calculations to learn the in-.uence of the nature of the boundary layer. If the surface is completely wet,

uncertainty of the distance s_{tr} will not affect the final design in a serious way; but, of course, the correct value should be used when it is known. To quote Tribus (Ref. 124, p. VI-14):

> "The reason...is that for a given airflow and air temperature inside the wing, an increased exterior [coefficient of heat transfer] results in a lower wing surface temperature, thus increasing the effectiveness with which the heat supply from the heaters may be used. The exponential variation of the vapor pressure with temperature tends to stabilize the evaporative system. A large [coefficient] combined with a low-vapor-pressure difference may evaporate as much water as a low [coefficient] combined with a high vapor-pressure difference. The size of air ducting and heaters may well be the same in the two cases, though the detailed behavior (surface temperatures, air outlet temperatures) may be radically different."

Further, in Ref. 89 it is shown that at high speeds the location of the point of transition has relatively small influence on the mean coefficient of heat transfer, particularly if the heated surface is quite long. Since the maximum average coefficient occurs when the point of transition is close to the leading edge it would seem that the design should be carried out for this position of the transition. In fact, in a preliminary calculation the entire boundary layer might be taken as turbulent.

Neel (Ref. 98) remarks that s_{tr} and the extent of the region of transition is the most uncertain factor influencing the convective heat transfer. A limited amount of data indicates that the transition starts at the end of the area of impingement (Ref. 45 and 99; also, see the next section). This appears to be a good approximation. Specifically, Neel suggests that the transition region be assumed to extend chordwise along the surface for a distance of about $0.75\, s_{tr}$ and that a linear variation of heat transfer coefficient with distance be taken.

4-10 Experimental Values of the Coefficient of Heat Transfer on Airfoils

Most experiments on airfoils have been performed on models in wind tunnels. Results from such tests are influenced considerably by the turbulence level. The transition region may extend over a larger percentage of the model than it would on a similar full-scale airfoil in flight.

4-10.1 Early Investigations

In Ref. 89 results of tests on four symmetrical models ranging from 6 to 24 in. chord length are summarized and compared with results predicted by means of Eq. 4-22, -26, and -29. In general, values of local coefficients predicted by the flat plate approximations are somewhat low along the forward 30 per cent, particularly on the upper surface at finite angle of attack.

Heat transfer investigations by the NACA on large-scale airfoils are reported in Ref. 4 and 40. Also, Tribus and Tessman (Ref. 127) and Hardy (Ref. 54) report on heat transfer measurements made during flight tests.

4-10.2 Recent NACA Investigation

Gelder and Lewis (Ref. 45) compared wind-tunnel and flight-test results under both dry and wet conditions and with various distributions of the heat supply. Their model was an NACA 65,2-016 at zero angle of attack. The chord length was 8 ft. They found local coefficients of heat transfer. The flight-test data were taken from Ref. 99.

The transition occurred at a lower Reynolds number in the wind tunnel than in free flight and its range on the surface was greater than in free flight, the transition in clear atmospheric conditions being practically abrupt. In most cases studied by the authors, the transition of the laminar heat transfer during icing conditions appears to occur at the impingement limit. The water in the air reduced the transition Reynolds number during both flight and wind-tunnel tests. Also, the wet air conditions effected a long transition range even in flight tests. For example, in one of the flight tests during icing weather, the transition region appeared to extend in the range of local Reynolds numbers from about $3 \cdot 10^5$ to $3 \cdot 10^6$. Further, results from some wind-tunnel tests indicate that the nature of the distribution of the surface temperature also affects the transition, for it appears that a non-uniform distribution gives a longer region of transition than does a uniform distribution.

A very small region of laminar heat transfer was found during flight conditions. The coefficients were about 15 per cent higher than those predicted by Eq. 4-26. Somewhat better agreement appeared to occur during icing conditions. During the wind-tunnel tests, in a region of local Reynolds

number usually considered to be laminar, coefficients were at least 75 per cent higher and usually nearly 100 per cent higher than the values predicted by Eq. 4-26. Turbulent heat transfer coefficients in flight were usually about 5 to 15 per cent higher than the values predicted by Eq. 4-29, depending upon icing and flight conditions. In general, the flat-plate approximations give low values according to the studies by Gelder and Lewis. This is not unusual since the theory is not strictly applicable to the curved surfaces. Further, the theory is for an aerodynamically smooth surface, and it is known that wing surfaces normally have minor imperfections that cause deviations from ideal conditions.

4-10.3 Recommendations regarding Modifications of Equations used to predict Heat Transfer Coefficients

The experimental evidence available so far has been obtained by surmounting numerous difficulties. Uncertainties in the measurements have occurred, and additional experimentation is needed. The influence of non-uniformity of surface temperature has not always been accounted for. Therefore, the following recommendations are made with a reservation pending further experimental checks. It appears from the experiments and from the calculations performed so far that for airfoils, the laminar and turbulent heat transfer coefficients calculated by means of flat plate equations should be increased about 10 per cent. Then the equations for laminar heat transfer on wings become

$$N_{Nu,L} = 0.315\, N_{Re,L}^{0.5} \sqrt{\frac{U_1}{U_o}} \cdot \sqrt{\frac{L}{s}} \qquad (4\text{-}26a)$$

or

$$h = 0.0584\, T_f^{0.5} \left(\frac{U_1 \rho}{s}\right)^{0.5} \qquad (4\text{-}27a)$$

And for turbulent heat transfer they become

$$N_{Nu,L} = 0.29\, N_{Re,L}^{0.8} \left(\frac{U_1}{U_o}\right)^{0.8} \left(\frac{L}{s}\right)^{0.2} \qquad (4\text{-}29a)$$

or

$$h = 0.782\, T_f^{0.247} \left(U_1 \rho\right)^{0.8} \left(\frac{1}{s}\right)^{0.2} \qquad (4\text{-}30a)$$

Nomographs for solving Eq. 4-27a and -30a appear on Fig. A-6 and -7 in the appendix at the end of this report.

4-11 Turbulent Heat Transfer with a Temperature Step

In light icing conditions, the size of the heated area may possibly exceed the wetted area. In such a case the dry heated region will not be cooled by evaporation and a rather steep rise of surface temperature may occur where the wetted area ends and the dry area begins. Neglecting the influence of conductivity in the outer skin, which smooths out the temperature distribution (Ref. 16), we may assume that the change is abrupt. Then we find that the coefficient of heat transfer may change significantly where the discontinuity of the temperature occurs. Since this will usually happen in the turbulent range, the influence on only turbulent heat transfer is considered.

One of the particular solutions that Rubesin (Ref. 110) deals with may be dealt with referring to the diagram of Fig. 4-11. From $s = 0$ to $s = s_1$, the surface temperature is $t_s = t_{s,1}$, which is greater than the air temperature t_o. For $s \geq s_1$, the surface temperature has the uniform value $t_{s,2}$.

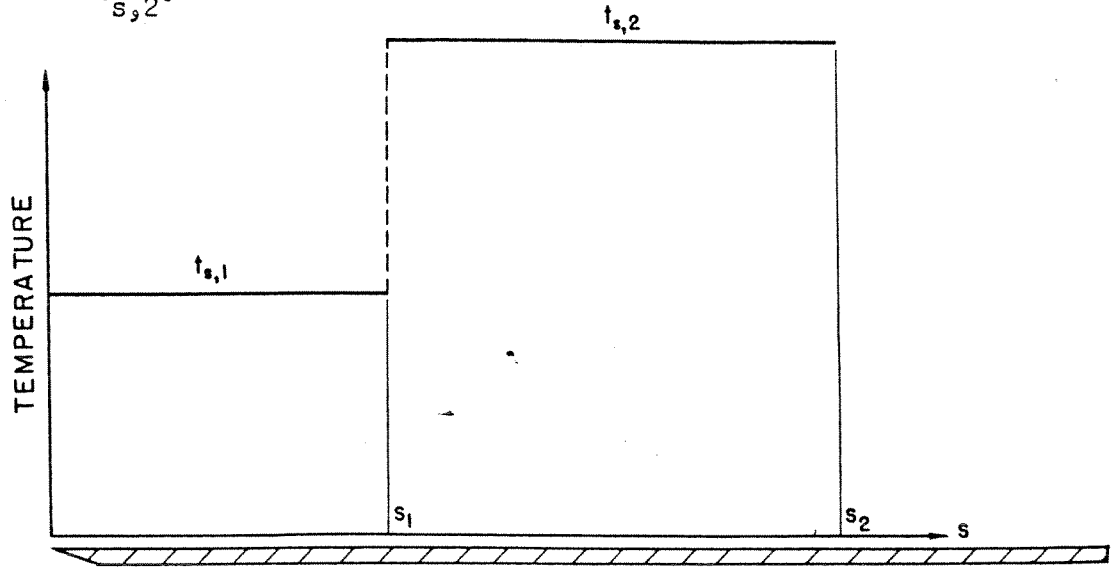

FIG. 4-11 STEPWISE TEMPERATURE DISTRIBUTION ON A FLAT PLATE

The coefficient of heat transfer at any point is denoted by $h(s,s_1)$. The first quantity in parentheses denotes the distance from the leading edge

to the point in question and the second quantity the distance from the leading edge to the position where the abrupt change of surface temperature occurs. Thus, $h(s,0)$ denotes the coefficient of heat transfer for a surface of just one uniform temperature, without a stepwise change. The author shows that the local coefficient in the range $s > s_1$, is

$$h(s,s_1) = h(s,0)\left\{\frac{t_{s,1} - t_o}{t_{s,2} - t_o} + \frac{t_{s,2} - t_{s,1}}{t_{s,2} - t_o}\left[1 - \left(\frac{s_1}{s}\right)^{39/40}\right]^{-7/39}\right\} \quad (4\text{-}34)$$

Rubesin also presents an equation and graphs to determine an average value of the coefficient in the range from s_1 to s_2. These results can be applied directly to an airfoil. Usually an iterative technique will be necessary to find the proper value of $t_{s,2}$.

4-12 Influence of Variable Surface Temperature on the Coefficient of Heat Transfer

It is highly improbable that the surface temperature of an airfoil will be uniform, as assumed in previous sections. Several analytical investigations, which are based on generalizations of the stepwise distributions described in the preceding section, have shown that non-uniformity of the surface temperature may significantly influence the coefficient of heat transfer in both the laminar and turbulent regimes. Klein and Tribus (Ref. 74) review and discuss the subject of heat transfer from the non-isothermal surfaces in considerable detail and present a comprehensive bibliography. Also, Scesa and Levy (Ref. 112) give a method to calculate laminar heat transfer coefficients for wedge flows with arbitrary variations of the surface temperature.

Where the heat transfer coefficient is used to evaluate the distribution of temperature on an airfoil surface for design purposes, it seems adequate to employ the coefficients calculated in the preceding sections. However, if further refinement will be required, an iterative procedure in the calculations will be needed; such a procedure has not yet been well developed.

4-13 Rate of Evaporation and a Coefficient of Mass Transfer

The evaporation from the surface of a heated, wet airfoil is a diffusional process which occurs within a thin boundary layer of air on the surface of the airfoil. At any point of the interface between the water film and the boundary layer the vapor on the surface is assumed to be in equilibrium with the water.[1] Accordingly, the vapor pressure at a point on the surface is the pressure of saturated steam corresponding to the temperature of the water[2] at that point. At the moderate temperatures encountered in the present application, the concentration, or vapor density, is proportional to the vapor pressure. The diffusional process occurs because the concentration on the heated, wet surface exceeds the concentration anywhere else in the boundary layer, the vapor in the boundary layer being convected away by the air.

If the temperature distribution across the boundary layer is uniform, or nearly uniform, a local coefficient of mass transfer may be defined by the equation,

$$m'' = b(\rho_{v,s} - \rho_{v,l}) \qquad (4\text{-}35)$$

where $[m''] = lb/hr\ ft^2$, $[b] = ft/hr$, and $[\rho_v] = lb/ft^3$. Subscript v is for the vapor, and subscripts s and l refer, respectively, to the interface with the water film and the outer edge of the boundary layer. Equation 4-35 is further discussed in Section 5-7. At present, only the evaluation of the coefficient b is of interest.

---

[1] In fact, there is a small difference (Ref. 114).

[2] Throughout this manual it is assumed that the water film temperature along any normal to the surface is uniform. Therefore, this temperature is equal to the local skin temperature and is referred to as the surface temperature. The assumption is justified by the facts that most of the water film is thin, that it is well stirred where it is thickest (in the area of impingement), and that the conductivity of water is fairly high.

4-14 Relationships between Heat Transfer and Mass Transfer Coefficients

Like a coefficient of heat transfer, the coefficient of mass transfer depends upon many factors. However, the amount of experimentation on mass transfer coefficients is relatively meager. Basic experiments on evaporation from the surface of a body with internal heat sources seem to have been performed only by Powell and Griffith (Ref. 108). Basic experiments on evaporation in high-speed air streams were reported to be nonexistent as late as April, 1953 (Ref. 95). Recently, Coles and Ruggeri (Ref. 33) performed sublimation experiments using ice in high-speed streams. An extensive bibliography with abstracts on various aspects of this subject appears in Ref. 64.

Fortunately, the principle of similarity has provided useful relationships between heat and mass transfer. While they still require further experimental verification, particularly for high-speed flow, results of their application in the present design problem, as well as in others, have shown that these relationships have considerable merit. They are presented here in brief; additional information can be found in the works of Mickley (Ref. 95), of Jakob (Ref. 63), and of Howarth (Ref. 62).

4-14.1 The Stanton Number and a Modified Stanton Number

The dimensionless group formed by dividing the Nusselt number by the product of the Reynolds and Prandtl numbers is called the Stanton number:[1]

$$N_{St} \equiv \frac{h}{U_o \rho c_p} \tag{4-36}$$

This number is very often used to correlate coefficients of heat transfer as a function of the Reynolds and Prandtl numbers. For example, Eq. 4-26 can be written in the form,

---

[1] This is the dimensionless coefficient employed in the present application by Hardy (Ref. 54) and others. Hardy denotes it by k_h.

$$N_{St} = 0.332\, N_{Re,L}^{-0.5} \cdot N_{Pr}^{-2/3} \cdot \left(\frac{s}{L}\right)^{-0.5} \left(\frac{U_1}{U_o}\right)^{0.5} \qquad (4\text{-}37)$$

A similar dimensionless group, which so far has no standard name, arises in mass transfer problems. In this manual it will be called the modified Stanton number:

$$(N_{St})_{mod} \equiv \frac{b}{U_o} \qquad (4\text{-}38)^1$$

4-14.2 Application of the Principle of Similarity

The principle of similarity, which is the root of all model experiments and analog techniques, simply expresses the fact that correlations of experimental results of any two phenomena that can be mathematically described by the same differential equations with the same boundary conditions, coincide in a system of corresponding coordinates. In general, the differential equations descriptive of heat and of mass diffusion differ considerably (Ref. 95); also, the boundary conditions are somewhat different. However, it happens that when water evaporates into an air stream relatively simple expressions can be introduced as good approximations to the true variables. Further, the difference of boundary conditions is insignificant in most cases, so that the principle of similarity may be employed. Experience so far has indicated that for practical purposes in engineering the inexactness is negligibly small, and the two phenomena, namely, heat transfer from a dry surface and evaporation of water, are treated as though they are physically similar processes.

The importance of this is that the Stanton number and modified Stanton number of two geometrically similar airfoils in physically similar conditions of flow[2] have a simple relationship, which is expressed here in the form,

---

[1] If the quantity $h/\rho c_p$ in Eq. 4-36 were replaced by a one-letter symbol, say, a, the similarity would perhaps be more apparent.

[2] That is, the same airfoil shape, the same angle of attack, the same Reynolds number, and so forth.

$$(N_{St})_{mod} = I \cdot N_{St} \qquad (4\text{-}39)$$

where I is a dimensionless quantity to be evaluated in the next two sections. Further, it appears that since temperatures and temperature differences in the present application are not excessively large, Eq. 4-39 may be employed even though both heat and mass transfer occur simultaneously on one airfoil.

4-14.3 Evaluation of I_{lam}

In accordance with the principle of similarity Eq. 4-26 written for evaporation becomes

$$(N_{St})_{mod} = 0.332\, N_{Re}^{-0.5} \cdot N_{Sc}^{-2/3} \cdot \sqrt{\frac{L}{s}} \cdot \sqrt{\frac{U_1}{U_o}} \qquad (4\text{-}40)$$

where N_{Sc}, the Schmidt number, replaces the Prandtl number. Just as the Prandtl number is the ratio of the kinematic viscosity to the thermal diffusivity $(k/\rho c_p)$, so the Schmidt number is the ratio of the kinematic viscosity to the mutual mechanical diffusivity D of water vapor in air. It follows from Eq. 4-37, -39, and -40 that

$$I_{lam} = \left(\frac{N_{Pr}}{N_{Sc}}\right)^{2/3} \qquad (4\text{-}41)$$

Now, $N_{Pr} = 0.71$; the value of N_{Sc} usually employed is 0.60, which seems to be based on a value of D given by the International Critical Tables, and this value seems to be due to Mache (Ref. 86). It follows from Eq. 4-41 that $I_{lam} = 1.12$. Jakob (Ref. 63, p. 591) gives 1.06, and Hausen (Ref. 54, p. 422) gives 1.04 for the value of I_{lam}.

However, more recent experiments on the diffusivity of water vapor in air were performed by Schirmer (Ref. 114) and Summerhays (Ref. 122). Their values, found in quite dissimilar ways, are in good agreement with each other and are higher than the values of Mache. Schirmer correlated his results by means of the equation,

$$D = 0.865\, \left(\frac{29.92}{p}\right)\left(\frac{T}{460}\right)^{1.81} \qquad (4\text{-}42)$$

where $[D] = ft^2/hr$; $[p]$ = in.-mercury; and $[T] = °R$. The pressure p is the total pressure of the mixture of air and water vapor. When the diffusivity is calculated according to Eq. 4-42 and the kinematic viscosity is taken from Table A-2, the value of the Schmidt number (ν/D) is found to be 0.525, independent of the pressure and virtually constant in the range of temperature from 32 to 140°F. Substituting this value of the Schmidt number into Eq. 4-48, we find that $I_{lam} = 1.22$, a value considerably higher than any of the above-mentioned values. Obviously, further checks on the relationships of heat transfer on wet and dry surfaces, including experimentation on the diffusivity of water vapor, are needed.

At the present time a compromise value is recommended: $I_{lam} = 1.1$. Hence, from Eq. 4-39 and the definitions of the Stanton number and the modified Stanton number,

$$b_{lam} = 1.1 \frac{h_{lam}}{\rho c_p} \qquad (4\text{-}43)$$

where ρc_p is the average heat capacity of the air per unit volume.

4-14.4 Evaluation of I_{turb}

In the turbulent boundary layer, unlike the laminar boundary layer, the ratio $(N_{St})_{mod}/N_{St}$ depends slightly on the Reynolds number. Callaghan (Ref. 29) recently studied the turbulent boundary on a flat plate in an approximative way, using a modification of the Prandtl conception of the turbulent boundary layer. He concluded that in a wide range of Reynolds numbers, I_{turb} decreases somewhat as the Reynolds number increases. Based on $N_{Sc} = 0.60$, the quantity I_{turb} has the approximate average value 1.05.

Had he employed $N_{Sc} = 0.525$, he would have found that I_{turb} is about 1.08. Further, if he had employed the Kármán analogy instead of the Prandtl analogy, he would have found values of I_{turb} between 1.01 and 1.03, depending upon the Reynolds and the Schmidt numbers.

Coles and Ruggeri (Ref. 32), experimenting with ice deposited by condensation on a flat plate in a high-speed wind tunnel, also found that I_{turb} (for sublimation) decreases slightly as the Reynolds number increases. They found no influence of the Mach number up to $M_o = 1.3$. Their average value of I_{turb} was 0.90. However, the surfaces were rough and the absolute values of N_{St} and $(N_{St})_{mod}$ were considerably higher than the predicted values for smooth surfaces.

Spielman and Jakob (Ref. 121) performed evaporation experiments with porous stones arranged as a flat plate. If, as the authors remark in the closure of their discussion $N_{Nu} = 1.26 \cdot (N_{Nu})_{mod}$ and their correlation is modified so that $N_{Sc} = 0.525$ instead of 0.59, the value obtained for I_{turb} is 0.96. Again, the heat transfer coefficients were considerably higher than those expected on a smooth surface, and the roughness of the stones may have had an influence on the results. Maisel and Sherwood (Ref. 87) obtained similar experimental results in the same way.

In view of the semi-empirical nature of the Prandtl and Karman analogies, they cannot be expected to distinguish between a few per cent in the value of I_{turb}. The experimentally determined values of I_{turb} on flat plates have been obtained with considerable difficulty, and then only for apparently rough surfaces. Further, information is lacking about the influences of pressure and temperature gradients. For these reasons it is recommended that for an airfoil I_{turb} be taken equal to 1.0 until more accurate knowledge is obtained. It follows that

$$b_{turb} = 1.0 \frac{h_{turb}}{\rho c_p} \qquad (4\text{-}44)$$

This is the so-called Lewis relationship.

4-15 Evaluation of Mean Coefficients of Heat Transfer $\bar{h}$

Pointwise calculations require much time. Often it is sufficient to find approximate mean values of the surface temperature and the heat load. Mean coefficients of heat transfer are needed for such calculations.

Whenever it is possible to use an equation of the typical form,

$$h = C\, s^{-n} \tag{4-45}$$

for local coefficients, the mean coefficient of heat transfer along the length s, denoted by $\bar{h}(s)$, is related to the local coefficient h at the point distance s from the leading edge by

$$\bar{h}(s) \equiv \frac{1}{s} \int_0^s h\, ds = \frac{h}{1 - n} \tag{4-46}$$

Equations 4-26 and -29 would have the form of the typical Eq. 4-45 if U_1 were uniform. It is recommended (Ref. 89) that U_1 be replaced with the mean velocity U_m given by Eq. 4-7. The numerical coefficients of Eq. 4-25 to -30 can then be replaced with values determined by Eq. 4-46. These alternate numerical coefficients are given in Table 4-1.

Table 4-1 NUMERICAL COEFFICIENTS TO CALCULATE MEAN COEFFICIENTS OF HEAT TRANSFER

Equation No.	Coefficient
4-25	0.664
4-26	0.572
4-27	0.106
4-28	0.037
4-29	0.033
4-30	0.890

By direct integration of Eq. 4-46, taking h from Eq. 4-22, the mean value $\bar{h}(s_c)$ on the leading edge is given by the same expression as Eq. 4-22 with the exception that the coefficient 2.06 changes to 0.515 and s goes to s_c, subscript c referring to the profile distance treated as a cylinder. The distance s_c, or s_c/L, may be determined by the intersection of Eq. 4-22 and -26 in the N_{Nu}, s/L-plane or of Eq. 4-24 and -27 in the h, s/L-plane.

In general, the mean coefficient on the surface extending from $s = s_i$ to $s = s_j$ is

$$\bar{h}(s_{ij}) = \frac{s_j \bar{h}(s_j) - s_i \bar{h}(s_i)}{s_j - s_i} \qquad (4\text{-}47)$$

For example, assuming an abrupt transition at distance s_{tr}, the mean coefficient on the heated length s_H is

$$\bar{h}(s_H) = \left\{ s_c \bar{h}(s_c) + \left[s_{tr} \bar{h}_{lam}(s_{tr}) - s_c \bar{h}_{lam}(s_c) \right] + \left[s_H \bar{h}_{turb}(s_H) - s_{tr} \bar{h}_{turb}(s_{tr}) \right] \right\} \frac{1}{s_H} \qquad (4\text{-}48)$$

where subscripts "lam" and "turb" mean that the expressions for the laminar and turbulent boundary layers, respectively, should be employed. A similar expression can be written for a non-abrupt transition. It may happen that s_c is relatively short; then the first and third terms in the braces may be neglected and the calculations are further simplified. Further, if s_{tr} is short and the distance covered long, it will be satisfactory to assume that only turbulent heat transfer occurs.

Of course, if more accurate mean values are desired, Eq. 4-22, -26, and -29 or Eq. 4-24, -27, and -30 could be plotted and integrated by any numerical or graphical procedure. Often it will be desirable to have a plot of h versus s at hand; a planimeter may then be found most convenient.

4-16 Coefficients of Heat Transfer on Internal Surfaces of Ducts

In the next few sections the heat transfer in circular and non-circular ducts will be reviewed. Then some results of direct measurements on double-skin heaters will be discussed.

4-16.1 Circular Ducts — Fully Developed Turbulent Region

A large amount of experimental evidence shows that heat transfer in the fully established turbulent region ($N_{Re,D_d} > 10{,}000$; see Section 2-1.2) of long circular ducts ($L_d/D_d > 60$) is virtually uniform and can

be calculated by means of the equation,

$$N_{Nu,D_d} = 0.023 \cdot N_{Re,D_d}^{0.8} \cdot N_{Pr}^{0.4} \qquad (4\text{-}49)$$

where $N_{Nu,D_d} \equiv h_{turb} D_d / k$, $N_{Re,D_d} \equiv U \rho D_d / \mu$, and U is the mean velocity in the conduit. In this section the quantity h_{turb} represents the internal heat transfer coefficient in the region of fully developed turbulent flow, subscript d refers to the duct, and L_d denotes the duct length. Employing $N_{Pr} = 0.71$ as an average value, Eq. 4-49 becomes

$$N_{Nu,D_d} = 0.020 \cdot N_{Re,D_d}^{0.8} \qquad (4\text{-}50)$$

The influence of the temperature through its effect on fluid properties is small. Usually sufficient accuracy will be obtained if the fluid properties are evaluated at the mean bulk temperature

$$t_b = (t_{in} + t_{out})/2 \qquad (4\text{-}51)$$

If large temperature differences are encountered and greater accuracy is desired, the fluid properties should be evaluated at the mean film temperature

$$t_f = (t_b + \bar{t}_s)/2 \qquad (4\text{-}52)$$

where $\bar{t}_s$ is the mean surface temperature. In this case it is also necessary to employ the mean bulk velocity, which is the mass velocity divided by the density at the mean bulk temperature (Ref. 107).

When the product of the powers of the properties of air with exception of the density in Eq. 4-51 are expressed as a power function of the absolute temperature T_b, the equation takes the dimensional form (Ref. 17):

$$h_{turb} = 10^{-4} \cdot 5.4 \cdot T_b^{0.3} \cdot G^{0.8} \cdot D_d^{-0.2} \qquad (4\text{-}53)$$

where $G = U\rho = w/A_d$; $[h_{turb}]$ = B/hr ft^2 F, $[T_b]$ = °R, $[G]$ = lb/hr ft^2, and $[D_d]$ = ft.

4-16.2 Non-Circular Ducts — Fully Developed Turbulent Regime

The coefficient of heat transfer for air flowing inside non-circular ducts in the range of fully developed turbulence ($N_{Re,D_e} > 10,000$) also, may be calculated with good approximation by means of Eq. 4-50 or -53. It is only necessary to replace D_d by the equivalent diameter,

$$D_e = \frac{4 \times \text{cross-sectional area}}{\text{perimeter}} \qquad (4\text{-}54)$$

For a flat rectangular passage (high aspect ratio) the equivalent diameter is practically twice the length of the shorter side. In general, the inception of turbulence in non-circular ducts occurs at Reynolds numbers less than 2300.

Experiments by Washington and Marks (Ref. 130) on heating air in rectangular ducts are in good agreement with predicted values using the equivalent diameter when $N_{Re,D_e} > 15,000$. However, for ducts of high aspect ratio and $N_{Re,D_e} < 15,000$, values predicted by Eq. 4-55 are substantially higher than their experimental values. Kays (Ref. 69) performed experiments heating air in ducts of aspect ratio 5.85. In the range of N_{Re,D_e} from 3,000 to 10,000 the experimental values lay 24 per cent below the values predicted by Eq. 4-50. Similar results were found by Bailey and Cope (Ref. 5) in the range of N_{Re,D_e} from 3,500 to 27,000 with ducts of aspect ratio ranging from 1 to 7.9.

Drexel and McAdams (Ref. 38) correlated results from the literature and found that they deviated from the values of Eq. 4-50 by ± 10 per cent when the coefficient is changed to 0.021.

Pinkel (Ref. 107) reports on numerous tests performed with rectangular and triangular tubes. For $N_{Re,D_e} > 10,000$, Eq. 4-49 is in good agreement with the experimental results.

4-16.3 Average Internal Coefficients in Ducts

The duct length L_d has an effect on the mean coefficient of heat transfer because of the transition in the entrance region of the tube. The local coefficient decreases in this region, approaching the uniform value in the region of fully developed turbulence. The nature of the flow in the inlet depends upon the shape of the entrance, the Reynolds number N_{Re,D_d}, and the temperature distributions on the duct walls. Boelter, Young, and Iverson (Ref. 19) performed experiments to determine the mean coefficients of heat transfer in straight round tubes with various inlet conditions. Their results in the range of Reynolds numbers from 26,000 to 56,000 and for ratio $L_d/D_d > 10$ may be represented by an equation of the type,

$$h_m = h_{turb}\left(1 + C \cdot \frac{D_d}{L_d}\right) \qquad (4\text{-}55)$$

where h_m is the integrated mean coefficient with respect to the length, h_{turb} is the coefficient in the fully developed turbulent region, and C is a constant depending on the shape of the entrance. For a straight heated tube preceded by a bell mouth, $C = 0.7$. If the bell mouth is replaced by an unheated 90° bend, $C = 7.0$. It should be noted that ducts in aircraft are seldom straight; neglect of this effect is undoubtedly one of the reasons why measured distributions of duct air temperature have been consistently lower than the calculated distributions. Values of C for other shapes may be found in Ref. 19 and 91.

For a sharp-edge entry, and Reynolds number above 10,000 McAdams recommends

$$h_m = h_{turb}\left[1 + \left(\frac{D_d}{L_d}\right)^{0.7}\right] \qquad (4\text{-}56)$$

These mean coefficients of heat transfer should be employed with the logarithmic mean temperature difference. Thus, the rate of heat transfer to a duct of uniform cross section and of uniform surface temperature t_s is

$$q = h_m(\pi D_d L_d)(\Delta t_a)_m \qquad (4\text{-}57)$$

where

$$(\Delta t_a)_m = \frac{[t_{aA} - t_s] - [t_a(L_d) - t_s]}{\ln \dfrac{t_{aA} - t_s}{t_a(L_d) - t_s}} \qquad (4\text{-}58)$$

and the quantity t_{aA} is the air temperature at the inlet while $t_a(L_d)$ is the air temperature at the end of the duct of length L_d.

4-16.4 Heat Transfer in the Transition and Laminar Ranges

McAdams (Ref. 91) presents heat transfer data in the transition range for air flowing in round ducts. It will be noteced that when $L_d/D_d = 5$ the transition is very gradual. But when $L_d/D_d = 60$ the transition is rather abrupt. The dip in the correlation is less extreme for rectangular ducts (Ref. 38); also, the inception of turbulence occurs at a lower Reynolds number.

At very low Reynolds numbers the flow in a duct may be laminar. For a general discussion of this subject the reader may consult Ref. 63 and 91. This type of flow could possibly occur in extremely fine double-skin passages. However, all known test data on double-skin heat exchangers indicate that within the practical limits of the application the flow becomes turbulent within a relatively short distance from the inlet to the passageways.

4-17 Double-Skin Heat Exchangers

The hot air in the passages is in contact with only a part of the metal comprising the outer skin. The adjacent parts where the inner and outer skins are fastened receive heat by conduction from both the inner and outer skins. If the bond between the two skins has low thermal resistance, as should be the case, the inner skin serves as an extended surface like a fin and contributes to heating the outer surface.

Also, if the bond is good, some heat is transferred from the air in the distribution duct. If this heat transfer rate is high, it will be effective in keeping the outside surface warm. However, unless a separate supply duct is used, the air temperature may be reduced so that by the time the air reaches the tips of the wing its effectiveness in passing through the double-skin passages will be inadequate to prevent icing.

In discussing the heat transfer to the outer skin, an effective coefficient h_e based on the following equation will be employed:

$$q'' = h_e(t_a - t_s) \qquad (4\text{-}59)$$

where q'' is the rate of heat transfer per unit area of the outer skin, t_a is the local temperature of the air inside the double-skin passages, and

's is the local surface temperature. Thus, h_e is a coefficient based on nit area of the outer skin and includes all the effects of conduction through he metal skins and their joints. The true local coefficient of heat transfer nside the double skin based on unit surface area of the corrugated walls ill be denoted by h_a.

In the next two sections, the actual coefficient of heat transfer h_a nd the coefficient h_d inside the distribution duct are discussed. In fol- owing sections relationships between h_a and h_e are developed, because rather than h_a is needed in many of the subsequent calculations.

18 Evaluation of the Actual Coefficient h_a in Double-Skin Passages

Double-skin passages are non-circular and may be treated as outlined Section 4-16.2 The critical Reynolds number is reported (Ref. 16) to be ss than 2000, even as low as 1300 in trapezoidal passages (Ref. 18) and 00 in passages of the type shown in Fig. 1-2(g) (Ref. 127). These low itical values are probably due to the shapes of the passages and the igh, or sharp-edge, construction of their entrances.

Hardy and Morris (Ref. 55) performed experiments on the type of pas- es shown in Fig. 1-2(f). They found that local coefficients of heat nsfer decrease in the direction of the flow, approaching a constant value a distance of about 25 equivalent diameters from the inlet. Boelter, nson, and Sanders (Ref. 16) found a similar result for the passages shown Fig. 1-2(e) when the entrance to the passages was streamlined. The same of results was reported for several configurations tested by Boelter, g, and Iverson (Ref. 19).

Hardy and Morris correlated their data in two parts, the entrance region the fully developed turbulent region. The correlations are, respectively,

$$= 0.152 \left(\frac{G_a D_e}{\mu_f}\right)^{0.7} \left(\frac{s}{D_e}\right)^{-0.3} ; \quad h_a = 0.782\, T_f^{0.331}\, G_a^{0.7}\, s^{-0.3} \qquad (4\text{-}60,\ -60a)$$

$$= 0.025 \left(\frac{G_a D_e}{\mu_f}\right)^{0.8} ; \quad h_a = 0.614\, T_f^{0.262}\, G_a^{0.8}\, D_e^{-0.2} \qquad (4\text{-}61,\ -61a)$$

$[G_a] = \text{lb/sec ft}^2$ and $[s] = [D_e] = \text{ft}$. Charts for the solution of

these equations appear on Fig. A-8 and -9 in the appendix. It may be noticed that the coefficient in Eq. 4-61 is 25 per cent higher than the coefficient in Eq. 4-50. A reason for this difference may lie in the authors' analysis (Section 4-20.2) of the effect of the conduction in the inner skin and of the contact resistance between the two skins. The results reported by other investigators (Ref. 16 and 127), fall within about 15 per cent of the correlations by Hardy and Morris. Neel (Ref. 98) recommends that Eq. 4-60 and -61 be employed where data on shapes other than that of Fig. 1-2(f) are unavailable.

It may be assumed, without serious deviation from the value $s = 25D_e$ reported by Hardy and Morris, that fully established turbulence begins at values of s/D_e determined by the intersection of the lines of constant Reynolds number, according to Eq. 4-60 and -61, as plotted in Fig. 4-12. The intersection for different Reynolds numbers is shown by the dotted line. Based on this assumption, the beginning of fully established turbulence moves forward as the Reynolds number increases. The chart may be found convenient to evaluate h_a.

A comparative study by direct test of three kinds of double-skin heaters (Ref. 101), namely, the corrugated, spaced, and the dimpled types shown in Fig. 1-3, indicate that the highest rate of heat transfer can be obtained with the dimpled type. At a given rate of air flow, the heat transfer for the dimpled skin was 21.5 per cent higher than for the spaced type; at a given pressure drop it was 12 per cent less.

Finally, it should be remarked that the heat transfer in the double-skin passages depends upon the curvature of the airfoil profile, the temperature distribution on the walls of the passages, and the shape of the inlet. With the exception of the shape of the inlet they seem to be of secondary importance, and satisfactory results are obtained even if one neglects them. According to Ref. 16, a major effect of a sharp-edged entrance is to increase the heat transfer in the passages and to delay the establishment of a fully developed turbulent region, that is, to prevent the coefficient from attaining a uniform value. Inspection of Fig. 4-12 indicates that the heat transfer near the inlet is at least twice that of the section where the normal velocity profile is established. In heat exchanger design turbulence

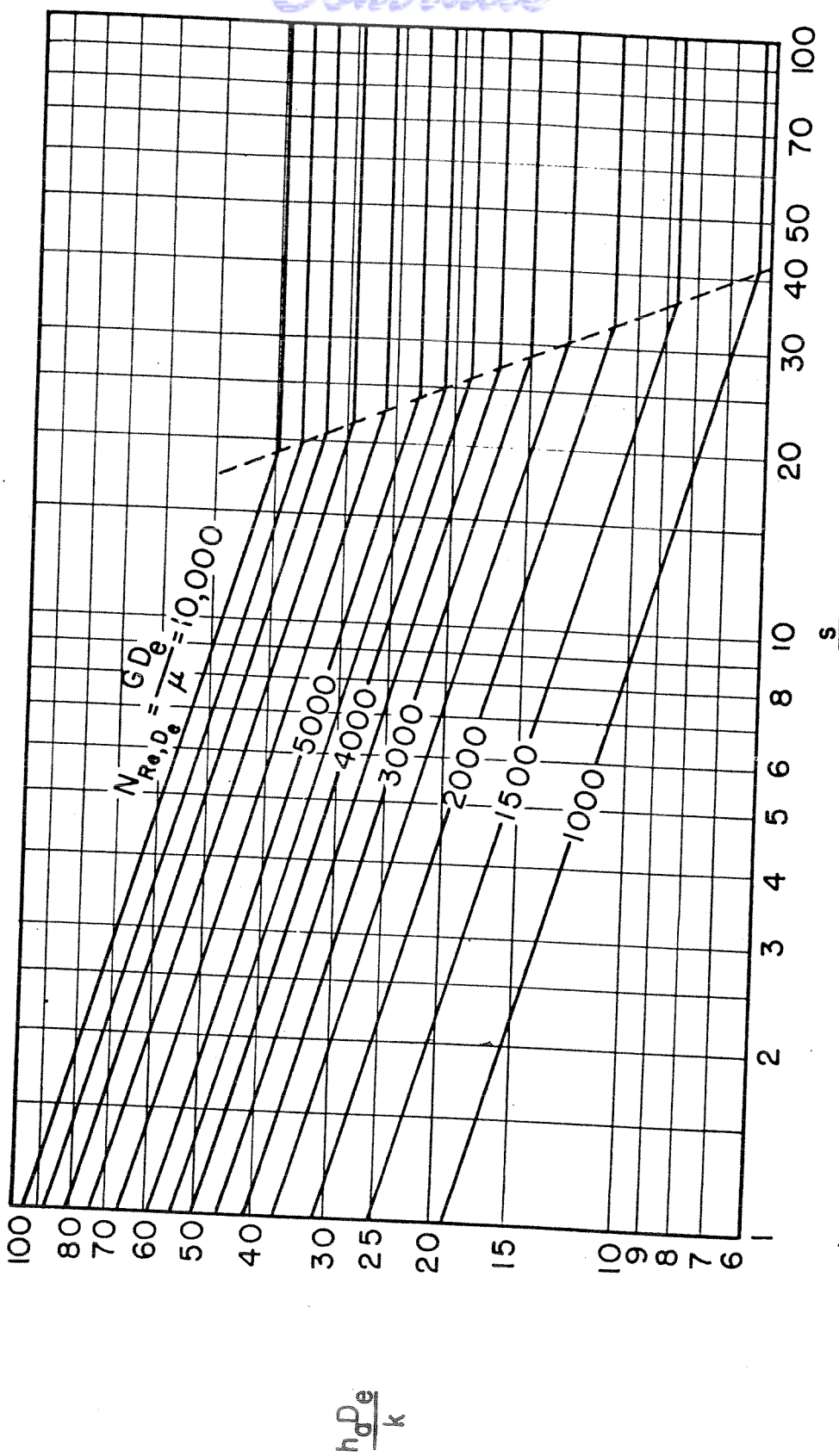

FIG. 4-12 LOCAL COEFFICIENTS OF HEAT TRANSFER IN DOUBLE-SKIN PASSAGES

inducers are used to maintain heat transfer coefficients equivalent to those at the entrance throughout the passage. The dimpled skin mentioned above is one approach to utilizing this phenomenon in double-skin passages. Greater exploitation of turbulence inducers in double-skin passages would appear to be well worth while even though specific tests to determine the effectiveness of the configuration would be required.

4-19 Heat Transfer Coefficients in the Distribution Duct

The air in the distribution or D duct shown in Fig. 1-1 loses heat by conduction through the false spar and the inner skin. Regarding the corrugations, Neel (Ref. 98) recommends using the following correlation which is based on the limited data of Ref. 55:

$$\frac{h_d D_e}{k} = 0.30 \left(\frac{G_d D_e}{\mu} \right)^{0.6} \qquad (4\text{-}62)$$

where D_e is the equivalent diameter of the duct. In the case of a smooth inner skin using spacer strips (Fig. 1-2(c)) or a duct liner (Fig. 1-2(a)), Eq. 4-50 may be employed.

4-20 Relationship between the Actual Coefficient h_a and the Effective Coefficient h_e

As already mentioned, on account of the spanwise conduction in the inner skin and the heat convection in the D duct, the effective coefficient h_e is different from h_a. The general relationship may be expressed by an equation of the type

$$h_e = F \cdot h_a \qquad (4\text{-}63)$$

where F is a dimensionless factor which depends upon the geometry of the skins, the metal, the contact resistance, and the coefficients of heat transfer on the exterior surface, inside the passages, and in the distribution duct. In Ref. 124 and 127, it is assumed that the heat transfer

area of the inside surface of the inner skin is practically as effective as the area of the outer skin in contact with the air in the passages, and the authors take $F = 2$. The test data presented in Ref. 127 correlate closer with predicted values when allowance is made for resistance to heat flow in the inner skin. The more conservative value of 1.5 was employed in Ref. 100 because it was found that the bond between the inner and outer skin was imperfect. To reduce the time of performing preliminary design calculations, it is recommended that a constant value of 1.5 be used. Where more accurate values may be required, one of the following expressions for F should be employed.

4-20.1 Approximations of h_e/h_a based on Extended Surface Calculations

Jonas (Ref. 66) developed an approximative solution for F by assuming that (1) the bond between the inner and outer skins is perfect, (2) the duct side of the inner skin is perfectly insulated, and (3) heat is conducted only spanwise in both the inner and outer skins. The first assumption is seldom satisfied in practice. The second assumption may be made if the coefficient h_d is small with respect to h_a or if an insulating type duct liner is used. The third assumption is employed so that the problem can be studied in two dimensions; but, in fact, Jonas uses a one-dimensional analysis. The results of his study indicate that for the types of corrugations ordinarily employed, the outer-skin conduction and convection play a minor role in determining F.

In the paragraphs that follow an analysis similar to Jonas' work is developed. It allows for an imperfect bond. Jonas' assumption that the duct side of the inner skin is perfectly insulated is retained. Use is made of his result that the heat transfer in and on the outer skin plays a minor role, and it is assumed that the skin temperature is uniform spanwise. It should be observed, however, that as the thermal resistance of the bond increases, spanwise conduction in the outer skin becomes of increasing importance. The following theory fails completely if the bond

allows no heat to pass through it, and it may be supposed that the joints will have been made with sufficient care so that their thermal resistance will not be excessively high.

Figure 4-13 shows the cross section of a rectangular corrugation and the nomenclature that will be employed. A trapezoidal or sinusoidal corrugation can be analyzed with appropriate definitions of a and b. Since the duct side is insulated, $h_d = 0$. The distance x_e is an equivalent thickness of air representing the thermal resistance of the bond (see Section 4-20.3).

In order to treat the corrugation as a one-dimensional fin, it is imagined that the outer skin is stretched and bent over as indicated by the dotted line in Fig. 4-14. Here, the inner skin is like an extended surface between two heat sinks at equal temperature t_s. However, unlike a true fin, the bond is imperfect so that the temperature t_c at the root is greater than t_s.

It is apparent in Fig. 4-13 that the heat transferred per unit area of the outer surface is

$$q'' = h_a \left[(t_a - t_s) \frac{a}{c} + \frac{q_c'}{h_a c} \right] \qquad (4\text{-}64)$$

where q_c' denotes the spanwise heat conduction on one corrugation, one foot in length chordwise.

If the fin in Fig. 4-14 were at a uniform temperature t_c, it would receive heat at the rate $h_a(a + 2b)(t_a - t_c)$. However, some parts of the fin are at temperatures higher than t_c, and so only a fraction of this heat is actually picked up. This fraction, denoted by η and called the fin effectiveness, may be evaluated by means of the equation (Ref. 63, p. 235),

FIG. 4-13 DOUBLE - SKIN CROSS SECTION AND NOMENCLATURE

FIG. 4-14 MODEL OF INNER SKIN FOR APPROXIMATE ANALYSIS

$$\eta = \frac{\tanh \frac{c}{2}\sqrt{\frac{h_a}{k_c Y}}\ \left(\frac{a}{c} + 2\,\frac{b}{c}\right)}{\frac{c}{2}\sqrt{\frac{h_a}{k_c Y}}\ \left(\frac{a}{c} + 2\,\frac{b}{c}\right)} \qquad (4\text{-}65)^1$$

where k_c is the thermal conductivity of the skin and Y its thickness. Hence,

$$q_c' = \eta \cdot h_a(a + 2b)(t_a - t_c) \qquad (4\text{-}66)$$

This heat must flow through the thin air layer representing the thermal resistance. Therefore,

$$q_c' = \frac{k_a(c - a)}{x_e}(t_c - t_s) \qquad (4\text{-}67)$$

where k_a is the conductivity of the air at an average temperature. Eliminating t_c from Eq. 4-66 and -67,

$$q_c' = \frac{t_a - t_s}{\frac{x_e}{k_a(c - a)} + \frac{1}{\eta h_a(a + 2b)}} \qquad (4\text{-}68)$$

Substituting this expression for q_c' into Eq. 4-64,

$$q'' = h_a\left[\frac{a}{c} + \frac{1}{\frac{h_a x_e}{k_a(1 - \frac{a}{c})} + \frac{1}{\eta(\frac{a}{c} + 2\,\frac{b}{c})}}\right] \qquad (4\text{-}69)$$

Comparing Eq. 4-59, -63, and -69,

$$F = \frac{a}{c} + \frac{1}{\frac{h_a x_e}{k_a(1 - \frac{a}{c})} + \frac{1}{\eta(\frac{a}{c} + 2\,\frac{b}{c})}} \qquad (4\text{-}70)$$

---

[1] The function $\tanh x \equiv (e^x - e^{-x})/(e^x + e^{-x})$. Its values can be found in almost any engineering handbook or ordinary collection of mathematical tables.

If the bond is perfect, $x_e = 0$ and

$$F = \frac{a}{c} + \eta\left(\frac{a}{c} + 2\frac{b}{c}\right) \qquad (4\text{-}71)$$

This equation is in good agreement with Jonas' results and is considerably easier to use. If the bond is a perfect insulator, $x_e = \infty$ and Eq. 4-70 fails to apply because it neglects to account for the fin effect of the outer skin. In this case it appears that if $a \geq 0.7\ c$, the value of F is at least 1.0.

The above analysis can be extended to the case where the duct side of the inner skin is uninsulated.[1] However, the result is rather clumsy to employ. The analysis of Hardy and Morris (Ref. 55), presented in the next section, accounts for the heat transfer from the air in the distribution duct in a simpler though less accurate manner.

4-20.2 Approximations of h_e/h_a based on Uniform Temperature of the Inner Skin

Hardy and Morris (Ref. 55) found from their measurements that the difference $t_c - t_s$ was virtually uniform for each rate of flow passing through the experimental heat exchanger. They based their calculations on the assumptions that the inner and outer skins reach uniform temperatures at average values t_c and t_s, respectively. It is as though they had assumed that the conductivity of the skin in the spanwise direction is infinitely great. Thus, with reference to Fig. 4-13, they come to the following four equations:[2]

The heat transferred directly to the outer skin is

$$q_1'' = h_a(t_a - t_s)\frac{a}{c} \qquad (4\text{-}72)$$

---

[1] Hauger (Ref. 56) has investigated the uninsulated case using an analog computer.

[2] It may be observed here as well as elsewhere that the thermal resistance of the metal in the transverse direction is relatively small and is neglected.

The heat transferred from the interior of the passage to the inner skin is

$$q_2'' = h_a(t_a - t_c)\left(\frac{a}{c} + 2\,\frac{b}{c}\right) \qquad (4\text{-}73)$$

The heat transferred from the distribution duct to the inner skin is

$$q_3'' = h_d(t_d - t_c)\left(1 + 2\,\frac{b}{c}\right) \qquad (4\text{-}74)$$

And the heat transferred through the bond between the two skins is

$$q_2'' + q_3'' = \frac{k_a}{x_e}(t_c - t_s)\left(1 - \frac{a}{c}\right) \qquad (4\text{-}75)$$

Each value of q'' is based on a square foot of the outside surface of the wing. Similar equations can be written for other shapes of passages. In this way four equations are obtained with the unknowns, q_1'', q_2'', q_3'', and t_c. The first equation can be solved directly for q_1'' and, therefore, only the last three need be solved simultaneously. The simplest procedure is to solve for t_c and then to evaluate q_2'' and q_3''. When Eq. 4-73, -74, and -75 are solved for t_c the result is

$$t_c = \frac{\frac{k_a}{x_e}\left(1 - \frac{a}{c}\right) t_s + h_a\left(\frac{a}{c} + 2\,\frac{b}{c}\right) t_a + h_d\left(1 + 2\,\frac{b}{c}\right) t_d}{\frac{k_a}{x_e}\left(1 - \frac{a}{c}\right) + h_a\left(\frac{a}{c} + 2\,\frac{b}{c}\right) + h_d\left(1 + 2\,\frac{b}{c}\right)} \qquad (4\text{-}76)$$

Finally, the ratio F can be evaluated using

$$F = \frac{q_1'' + q_2'' + q_3''}{h_a(t_a - t_s)} \qquad (4\text{-}77)$$

4-20.3 Values of the Equivalent Air Thickness x_e

As already suggested, the contact resistance of the bond between the inner and outer skins has come to be expressed in terms of the thickness of an air film which would have the same thermal resistance as the bond, assuming that the heat flows only by conduction through the film. In general, x_e depends on the design of the joints and the quality of the workmanship

Hauger (Ref. 56) performed interferometric tests on bonds between flat sheets of 0.051-in. dural and corrugated sheets of 0.016-in. 24ST aluminum. The equivalent air thicknesses which he measured are given in Table 4-2.

Table 4-2 EQUIVALENT AIR THICKNESS OF CONTACT RESISTANCES

Description of bond	Equivalent air thickness, x_e (in.)
1. Production riveted using rivet gun, rivets spaced 3 in. on center	0.0127
2. Production riveted using rivet gun, rivets spaced 1.5 in. on center	0.0058
3. Hand riveted, rivets spaced 3 in. on center	0.0072
4. Cemented, using EPON VI adhesive	0.00097
5. Spot welded, using overlapping spots	0.00086

The test panel used by Hardy and Morris (Ref. 55) consisted of two sheets of a light alloy fastened by rivets. The authors found values of k_a/x_e varying from 43 to 69 B/hr ft^2 F. This variation may be due partly to the approximative nature of their analysis, partly to the variation of the air flow through the gaps, and partly to the oversimplification of using an equivalent air resistance. Employing their average value, namely, 55 B/hr ft^2 F, the equivalent air thickness would be about 0.0035-in., which is in fair agreement with Hauger's values.

A recent investigation by Barzelay, Tong, and Hollo (Ref. 7) on thermal conductance of various aircraft joints indicates that the contact resistance in any one of them cannot be simply represented by the conduction across an air film. The reason is that the radiation, the metal-to-metal conduction, and the air-film conduction are interdependent. In particular, the radiation makes x_e dependent on the temperature level in

a manner which cannot be accounted for simply by the variation of k_a with temperature.

Accordingly, the values of x_e found in Ref. 55 and 56 should be regarded as qualitative, showing the relative thermal conductance of the various joints. It is believed, however, that calculated results based on those values will be satisfactory for the present purpose.

4-20.4 Recommendations regarding Evaluation of the Ratio h_e/h_a

There is insufficient evidence to say which of the several suggested methods is most accurate in evaluating the ratio F. It is believed that both methods described will give results which are satisfactory. The method by Hardy and Morris has the advantage that it estimates the rate of heat transferred from the air in the distribution duct.

Some calculations were carried out so that values of F could be compared. The basic data were the same as those employed by Jonas (Ref. 66, Fig. 2):

Temperature of exterior air	0°F
Local temperature of air in passages, t_a	350°F
Outer skin thickness	0.040 in.
Inner skin thickness, Y	0.020 in.
Outside local coefficient of heat transfer, h	15 B/hr ft^2 F
Local coefficient of heat transfer inside the passages, h_a	6 B/hr ft^2 F
Conductivity of the metal, k_c	120 B/hr ft F
Height of passage, b	0.125 in.

In addition, the following data were assumed:

Surface temperature, t_s	80°F
Local temperature of air in the duct, t_d	450°F
Coefficient of heat transfer in the duct, h_d	3 B/hr ft^2 F
Equivalent air thickness of contact resistance, x_e	0.006 in.
Conductivity of air at mean temperature of joint, k_a	0.020 B/hr ft F

Pitch of corrugations, c — 2.5 in.

Width of passage, a — 2 in.

The results are presented in Table 4-3.

Table 4-3 COMPARISON OF VALUES OF THE RATIO $F = h_e/h_a$

Source of calculation	Assumptions	F
(1) Jonas' graph (Ref. 66, Fig. 2)	Perfect bond; spanwise conduction in both skins; inner skin insulated on duct side.	1.60
(2) Eq. 4-71	Perfect bond; spanwise conduction in inner skin only; inner skin insulated on duct side.	1.63
(3) Eq. 4-70	Imperfect bond; spanwise conduction in inner skin only; inner skin insulated on duct side.	1.43
(4) Eq. 4-77	Imperfect bond; heat transfer from the air in the distribution duct.	1.63

With regard to the first and second results, the agreement is typical of the agreement obtained using other practical values of a and . This agreement may possibly be fortuitous on account of the particular passage height and coefficients of heat transfer that have been chosen.

The third result shows the influence of the imperfect bond.

It is undoubtedly circumstantial that the fourth result, which ncludes the influences of both the imperfect bond and the heat transfer rom the D duct, is in good agreement with the first and second and not ith the third result. However, even if the influence of the heat transer from the D duct had been included in the third calculation, the alue of F would have been increased from 1.43 to 1.46. Further, if e coefficient h_a had been calculated using the conventional Eq. 4-50 stead of Eq. 4-61 based on the data of Hardy and Morris, the third re- lt would have been 1.49.

It is obvious that since the method of Hardy and Morris neglects the effect of finite conductance of the inner skin, it will yield optimistic results. Before using this method the designer should perform some preliminary calculations to indicate the degree of optimism under conditions existing in the particular design and should apply a correction factor to compensate.

4-21 Heat Transfer on the Internal Stagnation Region

The shape of the entrance to the double-skin passages has a significant effect upon the heat transfer at the internal stagnation region. Since a great variety of entrance shapes is possible, a systematic investigation on the effects of several shape parameters is required. Only a relatively small amount of information on this subject is in the literature and generalization of this information must await further experimentation.

Tribus and Tessman (Ref. 127) report on measurements of an average coefficient of heat transfer at the internal stagnation region preceding the entrance to the passages shown in Fig. 1-2(g). The entrances had a round shape as shown in Fig. 1-1 and were located about 3/8 in. from the stagnation lines; the flow was evenly divided between the upper and lower heat exchangers. A rather small amount of data was obtained. The arithmetic mean of the air and surface temperatures was about 146°F. Introducing the influence of the temperature on the basis that the flow in the stagnation region is laminar and basing the correlation on half of the combined air flow in lb/hr ft-span of both the upper and the lower heat exchangers, the authors' correlation may be represented approximately by

$$h_{st} = 0.069\, T_f^{0.5}\, (\bar{w}'_a)^{0.55} \qquad (4\text{-}78)$$

Further generalization is not possible at the present time.

Boelter, Johnson, and Sanders (Ref. 16) measured average coefficients of heat transfer at the internal stagnation region of the same type of heat exchangers but with passages of the type shown in Fig. 1-2(e). The distance between the two lips of the rounded inlet was about 3/16 in. Experimental results may be represented by the equation

$$h_{st} = 0.11\, T_f^{0.5}\, (\bar{w}'_a)^{0.59} \qquad (4\text{-}79)$$

moving the round lips and measuring the coefficient for the sharp edges, ich were spaced about 3/4 in. apart, the authors obtained values 30 per nt lower than the values given by Eq. 4-79. However, the local coefficit in the passages with the sharp-edge inlets were about 10 per cent gher than those in the passages with round-edge inlets.

On account of the limited experimental set-ups employed, these equations ould be applied with caution to other than the configurations embraced by e investigations.

Chapter 5: MASS BALANCE OF WATER ON A HEATED AIRFOIL

5-1 Effective Operation

A thermal anti-icing system will be said to perform effectively when the rate at which water accumulates on the surface by impingement is equal to the rate at which the water leaves the surface by evaporation, no ice being present on the surface. This statement is the basis for the mass balance developed in the present chapter.

The heat required to evaporate the water comes from the double-skin heater and from aerodynamic heating. This subject, the heat balance, is dealt with in the next chapter.

5-2 Dry Anti-Icing

The area of impingement is considered to be completely covered with a film of water which usually is flowing aft at each point on the surface. If the rate of heating is high and the rate of impingement not too severe, it may happen that no water flows beyond the area of impingement. Under these conditions the anti-icing is said to be "dry", and a system designed for complete evaporation on the area of impingement is called a "dry anti-icing system".

The heat input required by a dry anti-icing system is quite sensitive to the rate of water impingement. These systems require high temperatures and high rates of heat transfer per unit span.

5-3 Runback and the Surface-Wetness Fraction

At high rates of impingement, some of the water in the surface film flows aft, out of the region of impingement. This flow, called runback, does not occur as a continuous sheet but in the form of thin rivulets. The water of the rivulets may evaporate if sufficient heat is conducted from the double-skin heater through the outer skin of the airfoil, or if the air speed is high enough to provide considerable aerodynamic heating, or if both these conditions prevail simultaneously. However, if the rate of impingement becomes more severe, the rivulets may flow farther aft to

a region where the amount of heat they receive is not sufficient either to evaporate them or to keep them in the liquid state, and there they may freeze.

Consider a long line drawn spanwise on the wet surface of a wing. The ratio of the wetted length to the total length is called the surface-wetness fraction ϵ. Of course, in the impingement region its value is 1.0; but in other regions it is less than 1.0. Averages of some typical values of ϵ obtained on a particular airfoil are shown in Fig. 5-1, which is taken from Ref. 98. Quantities s_u and s_l are the limits of impingement; hence, the abscissas are distances measured downstream from the end of the impingement area. It is believed that the values on this curve may be used to obtain satisfactory results for other airfoils. Notice that the runback falls off sharply reaching a value of about 0.2 at a distance of about half a foot beyond the limit of impingement. Therefore, it is important that a large part of the water be evaporated on the leading edge; otherwise, the runback may extend excessively far aft.

5-4 Wet Anti-Icing

The term, "wet anti-icing system", refers to a system designed on the basis that the surface temperature be at some preselected value greater than 32°F. This type of design is seldom employed today unless the air speed is sufficiently high so that aerodynamic heating provides a large amount of thermal energy and the shape and size of the object are such that heat can reach a large portion of its surface at a moderate rate per unit area. These systems are found to be more sensitive to the air temperature than to the rate of water impingement.

5-5 Evaporative Anti-Icing

A more rational approach to the problem is to consider a mass and heat balance on the entire surface or at each point on the surface. The latter procedure is the more accurate one; usually a compromise is reached by considering heat and mass balances on several divisions of the surface. Since dry or wet anti-icing systems can be considered as special cases, and

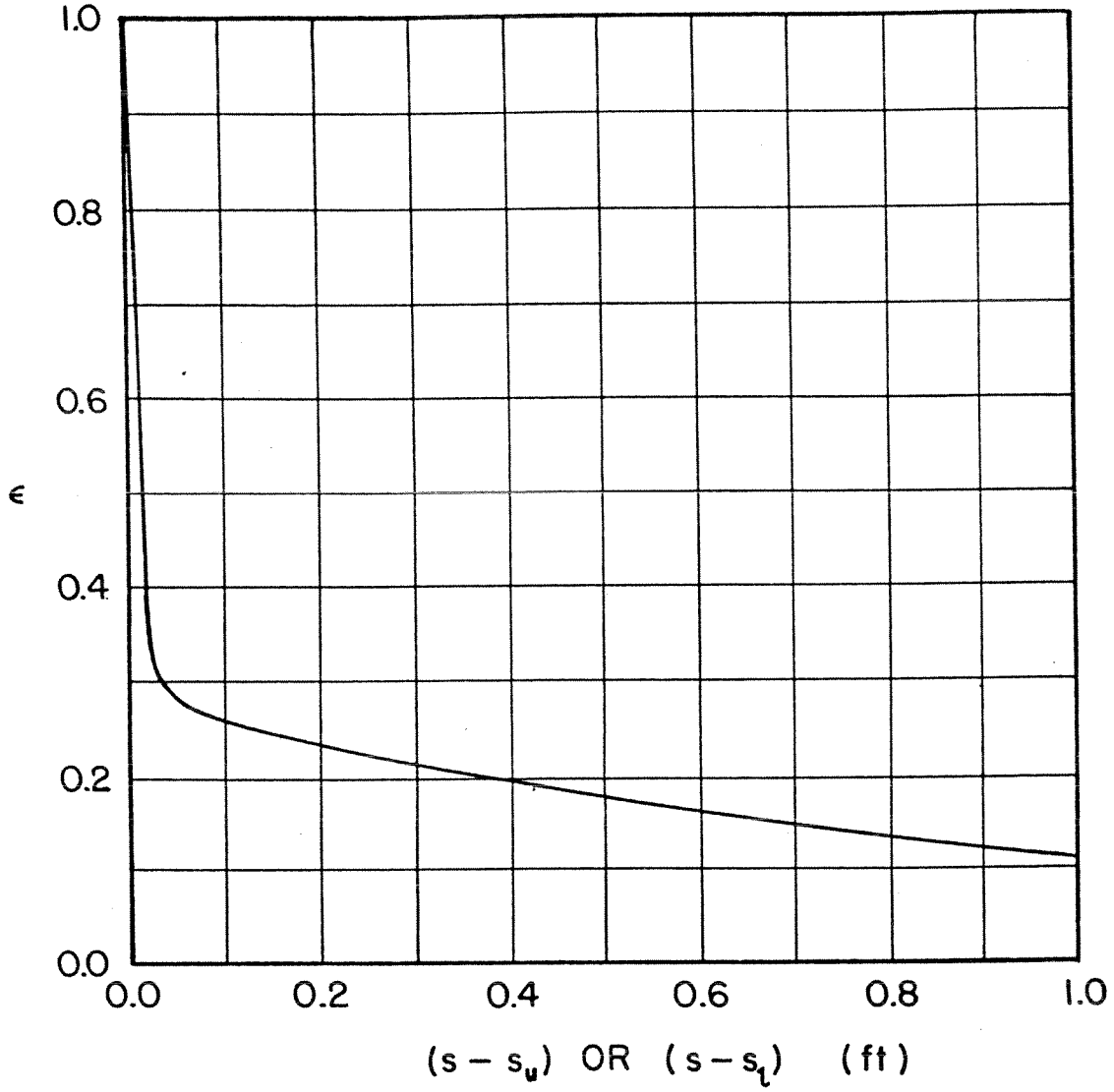

FIG. 5-1 SURFACE-WETNESS FRACTION BEYOND IMPINGEMENT AREA

since they can be analyzed by the same methods used in the analysis of evaporative systems, only evaporative systems will be considered in this manual.

It will be assumed that the chordwise heat conduction along the skin has no influence on any water that may run beyond the heated area. It will be necessary to consider whether aerodynamic friction alone, behind the double-skin area, is adequate to provide the heat necessary for evaporating the water. Accordingly, the chordwise heat conduction in the skin may be considered to provide, in a sense, a margin of safety.

5-6 Mass Balance on an Elemental Area of Profile Length Δs

A two-dimensional wet wing having a spanwise length of one foot is considered. On an elemental surface area of profile length Δs extending from s to $s + \Delta s$, as shown in Fig. 5-2, the rate of water impingement is $W'' \cdot (\Delta s \cdot 1)$. The rate of evaporation from the elemental area is $m'' \cdot (\Delta s \cdot 1) \cdot \epsilon$. Quantities W'', m'', and ϵ depend upon s. The quantity ϵ is the surface-wetness fraction discussed in Section 5-3; it is equal to 1 wherever $W'' > 0$. The methods for calculating W'' are treated in Chapter 3, and the evaluation of m'' is a subject of later sections in the present chapter.

It may be supposed that some water flows in the film along the surface. If the rate of flow per unit length of span at position s be denoted by w', then the rate of flow at position $s + \Delta s$ may be denoted by $w' + \frac{dw'}{ds} \cdot \Delta s$.

Equating the rate at which water comes to the elemental surface to the rate at which water leaves,

$$W'' \cdot \Delta s + w' = \epsilon\, m'' \cdot \Delta s + \left(w' + \frac{dw'}{ds} \cdot \Delta s\right)$$

Simplifying,

$$W'' - \epsilon\, m'' = \frac{dw'}{ds} \qquad (5\text{-}1)$$

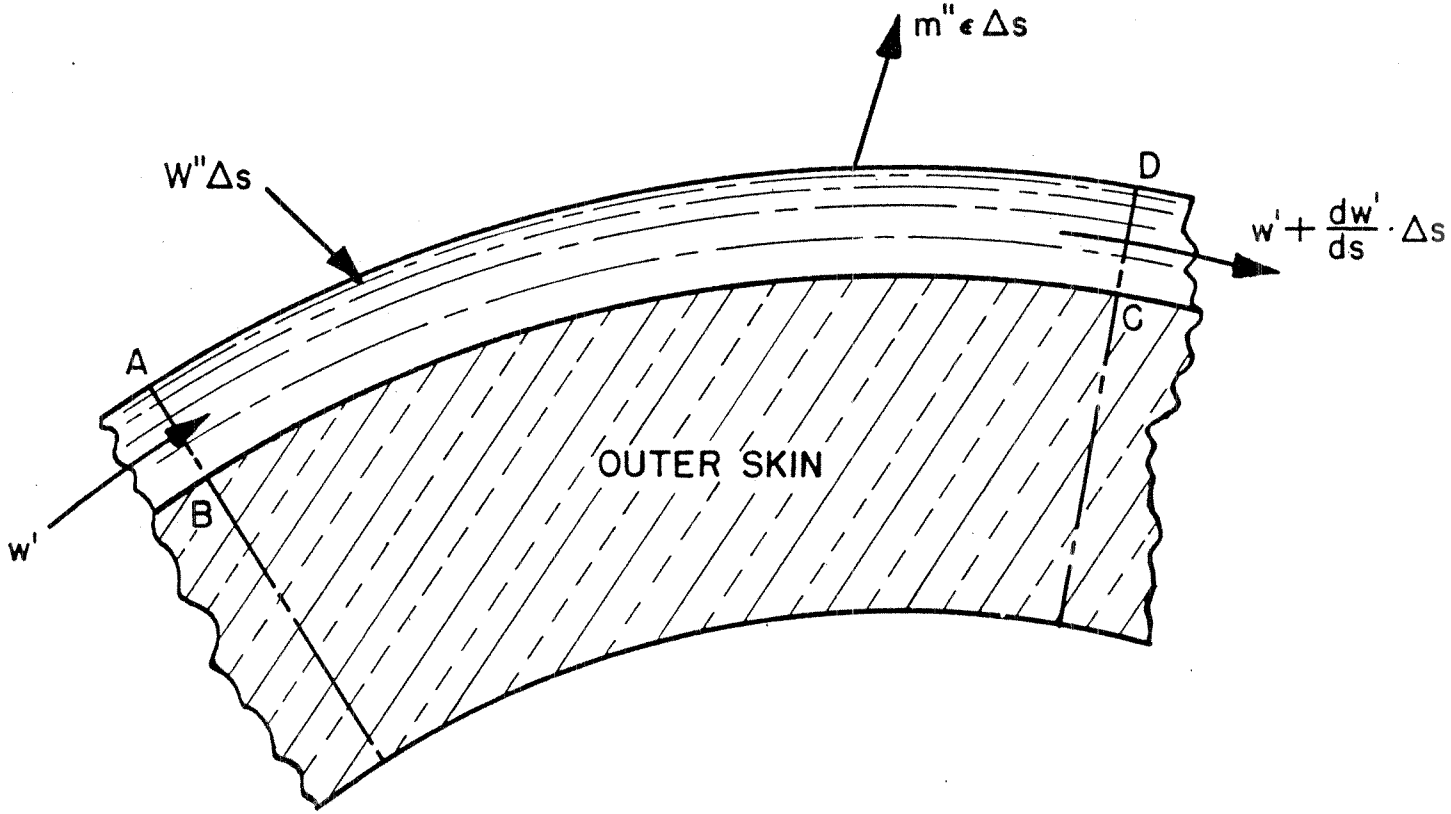

FIG. 5-2 DIAGRAM SHOWING MASS BALANCE ON ELEMENTAL SECTION OF A WET AIRFOIL

This equation shows how the rate of water accumulation with respect to distance along the surface depends on the local rates of impingement and evaporation. It is based on steady-state conditions; that is, icing and flight conditions are assumed to be steady, and the rate of flow and thickness of the film at every point are assumed to be independent of the time.

On the region of the surface near the forward stagnation point, W'' will usually substantially exceed m''; therefore, in this region the rate of water flowing in the film would increase with increasing length. Farther downstream there may be a region where $W'' = m''$; there w' remains uniform. Farther along the surface, the evaporation rate may exceed the rate of water interception, and the rate of flow in the water film diminishes. Beyond the area of impingement, $W'' = 0$ and w' decreases at the rate $-\epsilon m''$ until, finally $w' = 0$ and the film ends. Integrating Eq. 5-1 and taking $w'(o) = 0$,

$$w'(s) = \int_o^s (W'' - \epsilon m'')\, ds \qquad (5\text{-}2)$$

In a performance analysis of an anti-icing system to determine whether it is effective, the integration is carried out on the upper and lower surfaces until the values of s are reached where $w' = 0$. If icing is encountered along the way, the design must be modified.

5-7 Further Considerations of Evaporation Rates

In Section 4-13 a coefficient of mass transfer b was defined by the equation,

$$m'' = b(\rho_{v,s} - \rho_{v,l}) \qquad (4\text{-}35)$$

This equation is satisfactory at high total pressures of the air-water-vapor mixture and small temperature differences. To use the coefficient for other circumstances, however, Eq. 4-35 must be modified.

5-7.1 Evaporation Rate in Terms of Partial Pressures

Within the ranges of vapor pressures and temperatures encountered in the present application, it may be assumed that the water vapor behaves like a thermally perfect gas. This allows the thermodynamic properties of the vapor to be calculated as though the air were not present. It also allows $\rho_{v,s}$ and $\rho_{v,l}$ to be evaluated in terms of the partial pressures of the vapor:

$$\rho_v = \frac{p_v}{R_v T} \qquad (5\text{-}3)$$

where $R_v = 85.8$ ft lb/lb$_m$ F $= 1.213$ ft^3 in.-mercury/lb$_m$ F is the gas constant of water vapor and $[\rho_v] = \text{lb}_m/\text{ft}^3$. Hence, Eq. 4-35 may be written,

$$m'' = \frac{b}{R_v T}(p_{v,s} - p_{v,l}) \qquad (5\text{-}4)$$

This equation is satisfactory if the partial pressure of the vapor is very small compared with the local static pressure, that is, at low altitudes.

5-7.2 Influence of Induced Convection

The sum of the partial pressures of the air and vapor is virtually uniform across the boundary layer along any normal to the surface. Therefore, if the partial pressure of the vapor is decreasing, the partial pressure of the air is increasing, and the air diffuses toward the surface. But since the air cannot penetrate the surface, a counter convection of the air occurs which carries with it additional vapor. Analysis shows that Eq. 5-4 can be modified to allow for this additional transfer of mass:

$$m'' = \frac{b}{R_v T} \cdot \frac{p_{v,s} - p_{v,l}}{1 - \frac{p_{v,s}}{p_l}} \qquad (5\text{-}5)$$

When $p_{v,s}$ is much less than p_l, which usually happens at low altitudes, particularly when the surface temperature is low, Eq. 5-4 and -5 are practically identical.

The induced convection also influences the diffusion from the mathematical viewpoint, because it affects the boundary conditions which the solution of the differential equations of motion and diffusion must satisfy. However, in the case of the evaporation of water, as in the present application, the quantitative effect is minor; for this reason, the principle of similarity may be applied to calculate mass transfer rates from heat transfer rates as in Section 4-15.

The change of mechanical and thermal properties of the air due to the presence of the vapor is very small, and may be neglected in the present application.

5-7.3 Influence of Non-Uniform Temperature across the Boundary Layer.

When the temperature of the surface is much larger than the temperature at the outer edge of the boundary layer, as often happens in thermal anti-icing, Eq. 4-35 may possibly give unsatisfactory results.[1] Jakob (Ref. 63) has therefore recommended that Eq. 5-5 be modified by replacing T with the arithmetic mean film temperature T_f. The result is that

$$m'' = \frac{b}{R_v T_f} \cdot \frac{p_{v,s} - p_{v,l}}{1 - \frac{p_{v,s}}{p_l}} \qquad (5\text{-}6)$$

Equation 5-6 has yet to be checked by experiments on evaporation to an airstream from a wet surface heated from below. However, in the limiting cases of low pressure differences and small temperature gradients, it is in agreement with the simpler equations presented above, which have led to satisfactory predictions in the past, not only in anti-icing problems but in other fields as well. On account of this agreement and because it allows for deviations from those limiting cases, Eq. 5-6 will be employed as a basis for design and analysis. In Section 5-10, Eq. 5-6 is brought to a more convenient form to facilitate the calculations.

[1] This is an effect other than so-called "thermal diffusion", which is mentioned, for example, in Ref. 95.

5-8 Supersaturation and the Evaluation of $p_{v,l}$

With reference to Eq. 5-6, it has already been remarked that $p_{v,s}$ is the saturation pressure of steam at the temperature t_s. The vapor pressure $p_{v,l}$ could possibly be assumed to be the saturation pressure at the temperature t_l. However, a considerable amount of evidence indicates that an alternative procedure is required.

As the fog passes over the leading edge of the airfoil, its pressure decreases and the water vapor expands. The expansion may be considered isentropic. In an enthalpy-entropy diagram of the stream, the state point of the steam would start at the saturation line and descend into the region where the liquid and vapor would ordinarily be in thermodynamic equilibrium. If they were in equilibrium,[1] the droplets would grow by the process of condensation. The fact is that the water vapor does not condense; it seems that there is insufficient time for this process to occur. Experience shows that the vapor condenses when it reaches the so-called Wilson line. This is an experimentally determined characteristic of steam coinciding approximately with the line of 3.5 per cent moisture (Ref. 133) as shown in Fig. 5-3. This figure is a reproduction of a small part of the Mollier steam chart in Ref. 72 to which the Wilson line has been added. As can be seen in Fig. 5-3, relatively large isentropic pressure changes would be needed to reach the Wilson line from saturation. Since such changes usually lie beyond the range occurring in the present application, more vapor is expected during the expansion than is predicted by equilibrium calculations. The pressure of this so-called supersaturated vapor is somewhat in excess of the vapor pressure of saturated vapor at the temperature of the supersaturated vapor and the lines of constant pressure are disturbed from their equilibrium positions shown in the diagram.

Hence, it is assumed that no water condenses, that the constituents behave according to Dalton's law of partial pressures, and that the vapor pressure, like the pressure of any inert constituent, changes in proportion

---

[1] Calculations regarding fog in thermodynamic equilibrium can be conveniently carried out using the enthalpy-entropy diagram devised by Hensley (Ref. 60).

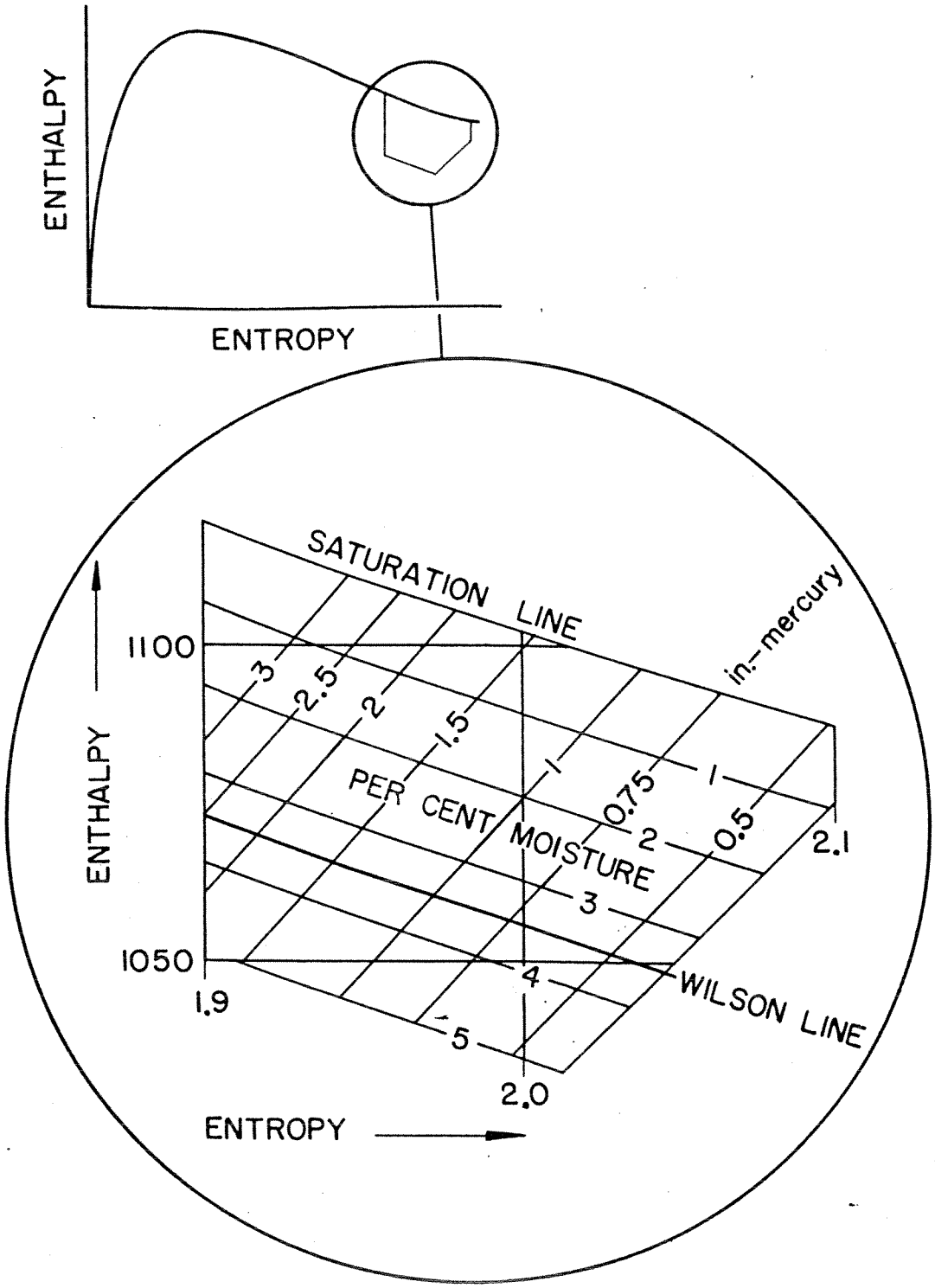

FIG. 5-3 WILSON LINE IN AN ENTHALPY-ENTROPY DIAGRAM OF STEAM

to the local absolute static pressure. Briefly,

$$p_{v,l} = \frac{p_l}{p_o} \cdot p_{v,o} \tag{5-7}$$

5-9 Specific Humidity or Humidity Ratio

The thermodynamic properties of a mixture of air[1] and water vapor are conveniently expressed in terms of the specific humidity, or the humidity ratio, which is the ratio of the vapor density to the air density. Also, rates of evaporation may be expressed in terms of the specific humidity. For all practical purposes the specific humidity may be evaluated by means of the relationship of state for thermally perfect gases and Dalton's law of partial pressures. Thus,

$$\omega \equiv \frac{\rho_v}{\rho_a} = \frac{R_a}{R_v} \cdot \frac{p_v}{p_a} \tag{5-8}$$

Since $p_a = p - p_v$ and $M_a R_a = M_v R_v$, Eq. 5-8 becomes

$$\omega = \frac{M_v}{M_a} \cdot \frac{p_v}{p - p_v} \tag{5-9}$$

Subscript a refers to the dry air and M denotes the molecular weight;[2] p denotes the sum of the partial pressures. Equation 5-9 may be used to calculate the specific humidity of a mixture when the vapor is either superheated, saturated, or supersaturated. Values of ω for saturated air are presented in the graph of Fig. 5-4 for absolute pressures from

---

[1] The term "air" used in the phrase "mixture of air and water vapor" always refers to the part of the mixture that is dry air. The term "saturated air" means a mixture of air and dry, saturated water vapor, or water vapor on the verge of condensing.

The liquid water in a cloud contributes very little to the value of the thermodynamic properties. Unless otherwise specified, the specific humidity of a cloud will include only the saturated vapor, the liquid water content being excluded. Of course, the liquid water content is very important in considering the rate of water impingement.

[2] Employing $M_v = 18.0160$ and $M_a = 28.966$ (Ref. 119), the ratio $M_v/M_a = 0.622$.

10 to 32 in.-mercury; also, values at pressure altitudes of 10,000 and 20,000 ft are plotted. Goodman (Ref. 48) has tabulated values of ω in the ranges 22(1)32 in.-mercury and -40(1)200°F. When a difference of ω corresponding to a small temperature difference is required, it may be necessary to use calculated values of ω instead of values from the graph.

5-10 Evaporation Rates in Terms of Specific Humidity

Employing the relationship $M_a R_a = M_v R_v$ and Eq. 5-7, Eq. 4-9 may be written in the form,

$$m'' = b \frac{p_1}{R_a T_f} \left[\frac{M_v}{M_a} \cdot \frac{p_{v,s}}{p_1 - p_{v,s}} - \frac{M_v}{M_a} \cdot \frac{p_{v,o}}{p_o} \cdot \frac{p_1}{p_1 - p_{v,s}} \right] \qquad (5\text{-}10)$$

The fraction ahead of the braces is the density of air in lb/ft^3 at pressure p_1 and temperature T_f; denote it by $(\rho_{a,1})_f$. Since the maximum static temperature of the main stream in the present application will be low, $p_{v,o} \ll p_o$, and the product $(M_v p_{v,o})/(M_a p_o)$ can be replaced by ω_o. Hence,

$$m'' = b(\rho_{a,1})_f \left[\omega_s - \omega_o \cdot \frac{p_1}{p_1 - p_{v,s}} \right] \qquad (5\text{-}11)$$

For low altitudes and small differences between temperatures T_s and T_1, Eq. 5-11 reduces to

$$m'' \approx b \rho_{a,1} \left[\omega_s - \omega_o \right] \qquad (5\text{-}12)$$

This is equivalent to the expression employed by most investigators.

In Section 4-14, it was shown that a coefficient of mass transfer could be written in terms of a corresponding coefficient of heat transfer. Eliminating b from Eq. 4-39 and 5-12 and noting that $\rho_a \approx (\rho_{a,1})_f$ (consistent with previous assumptions),

$$m'' = \frac{I}{c_{p,a}} \cdot h \left[\omega_s - \omega_o \cdot \frac{p_1}{p_1 - p_{v,s}} \right] \qquad (5\text{-}13)$$

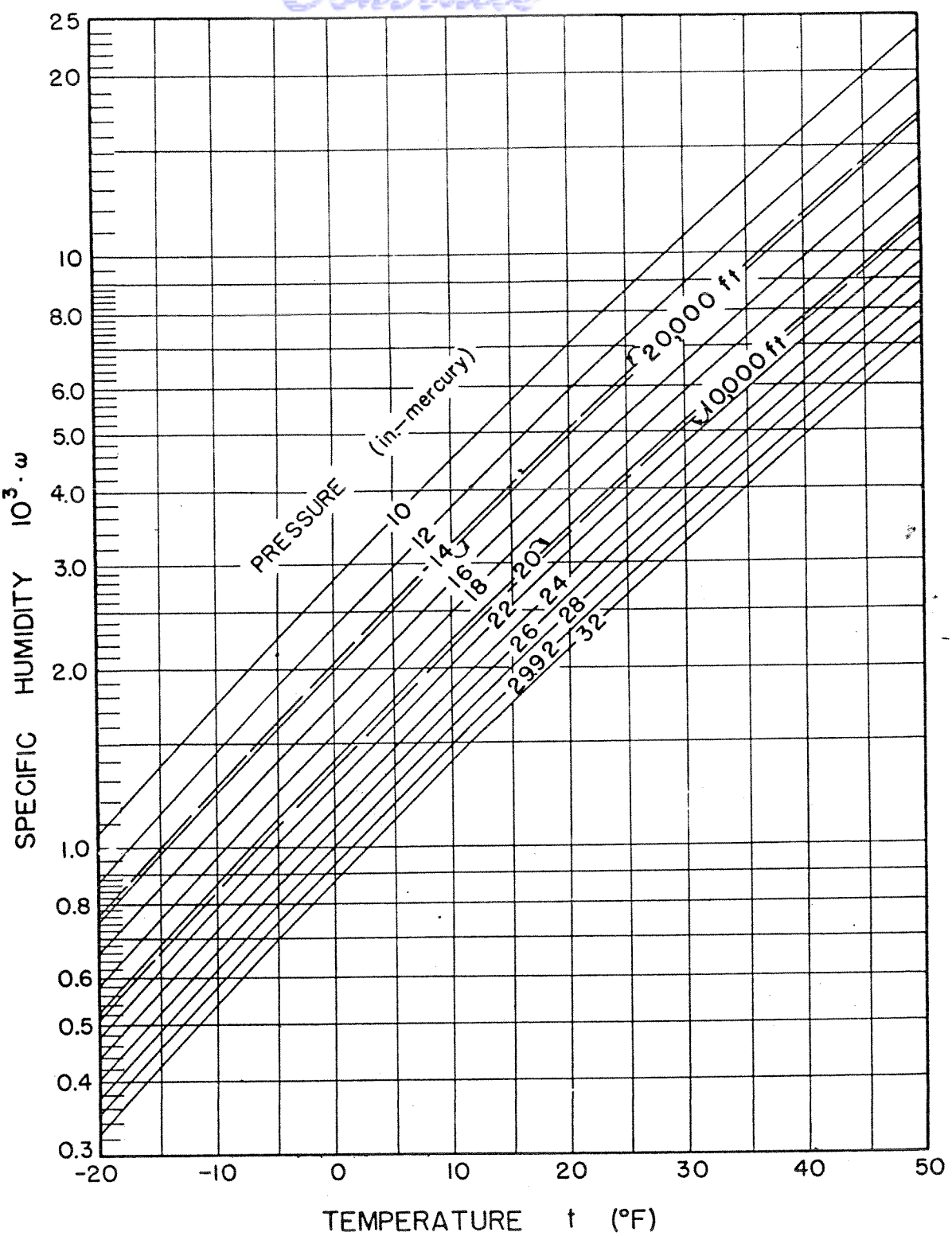

FIG. 5-4 SPECIFIC HUMIDITY OF SATURATED AIR

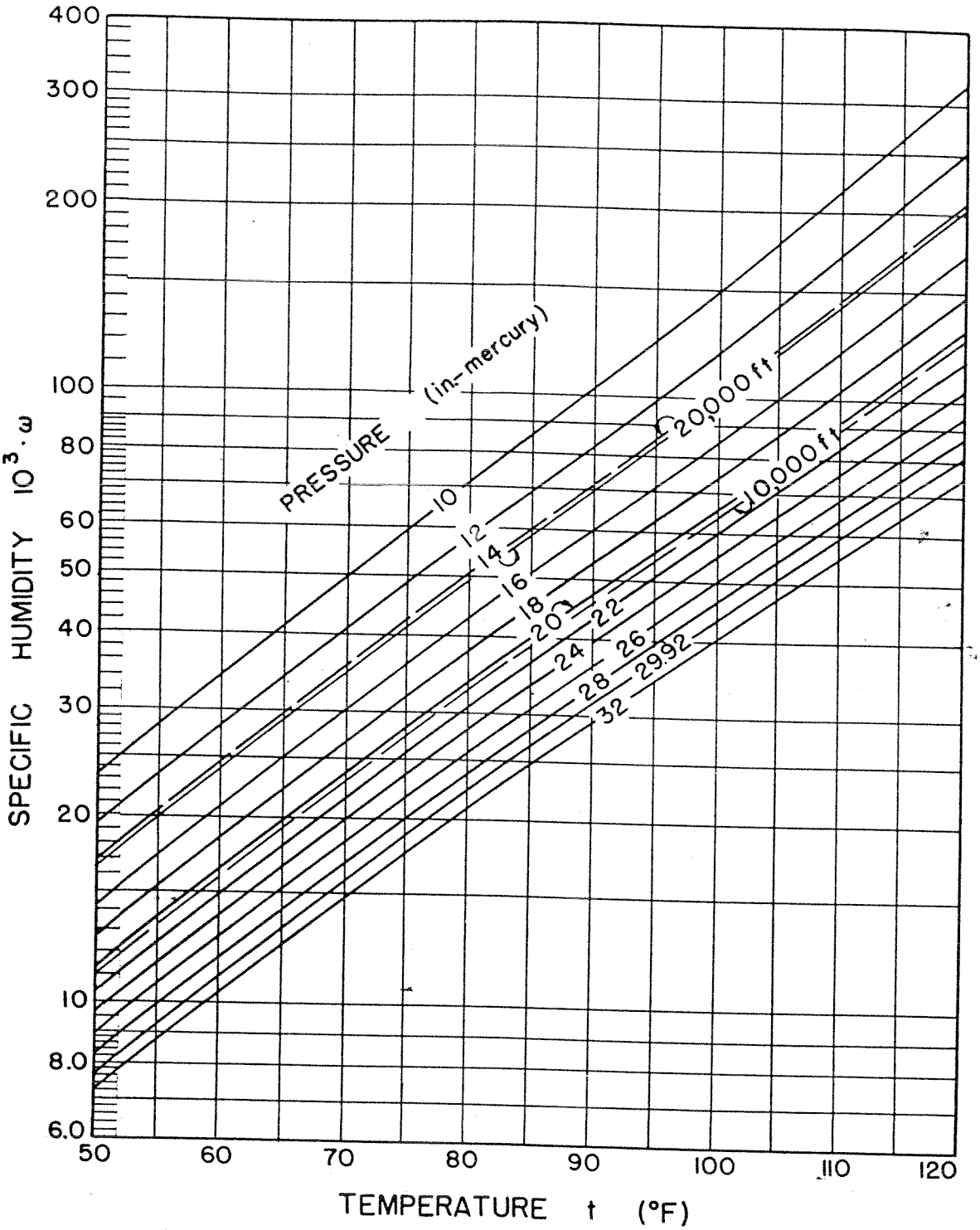

FIG. 5-4 (CONT.) SPECIFIC HUMIDITY OF SATURATED AIR

where I has been taken to be 1.1 and 1.0, respectively, for the laminar and turbulent boundary layers, and $c_{p,a} = 0.24$ B/lb F.

It is apparent that for any given icing and flight condition, the surface temperature T_s as well as the coefficient h must be known in order to determine m''. The next chapter shows how the distribution of the surface temperature T_s along the airfoil profile may be calculated.

6-1 Heat Balance on an Elemental Area

In order to determine the performance of a given thermal anti-icing system, a heat balance is required for each elemental area of the surface. It will be convenient to write the heat balance by applying the First Law of Thermodynamics to a typical elemental system comprised of the outer skin and the water film, represented by the region AEFD in Fig. 6-1. Being thin and of high conductivity, the metal skin and water film have high conductances compared to the inner and outer surface conductances. Therefore, it may be assumed that sections AE and DF are isothermal.

Thermal energy enters the element through the surface EF at the rate $q'' \cdot (\Delta s \cdot 1)$ by convection from the hot air in the heater. The water droplets impinging upon the surface AD come practically to rest and the thermal energy they bring with them enters the system at the rate $W''(i_{w,o})_{tot} \cdot (\Delta s \cdot 1)$. Subscript w,o refers to the water in the supercooled cloud at temperature t_o; subscript tot refers to the total or stagnation condition. Thus, $(i_{w,o})_{tot}$ is the sum of the static enthalpy of the water plus the thermal equivalent of the kinetic energy of the water droplets relative to the airfoil; the static enthalpy is referred to saturated water at 32°F.

Thermal energy is also carried into the system with the flow in the water film through the section AB; longitudinal conduction in the water is neglected since the film is relatively very thin. Assuming uniform temperature T_s through the depth of the film, the rate is $w' \cdot i_{w,s}$. Water leaving through the section DC carries energy at a rate which may be represented by $w' \cdot i_{w,s} + \frac{d}{ds}(w' \cdot i_{w,s}) \cdot \Delta s$.

Heat also is carried away from surface AD by convection in the boundary layer. The net rate in excess of the aerodynamic heating is denoted by $q''_c \cdot (\Delta s \cdot 1)$.

Thermal energy is carried away with the evaporating vapor from the surface AD at the rate $m'' i_{v,s}(\epsilon \cdot \Delta s \cdot 1)$ where ϵ is the surface-

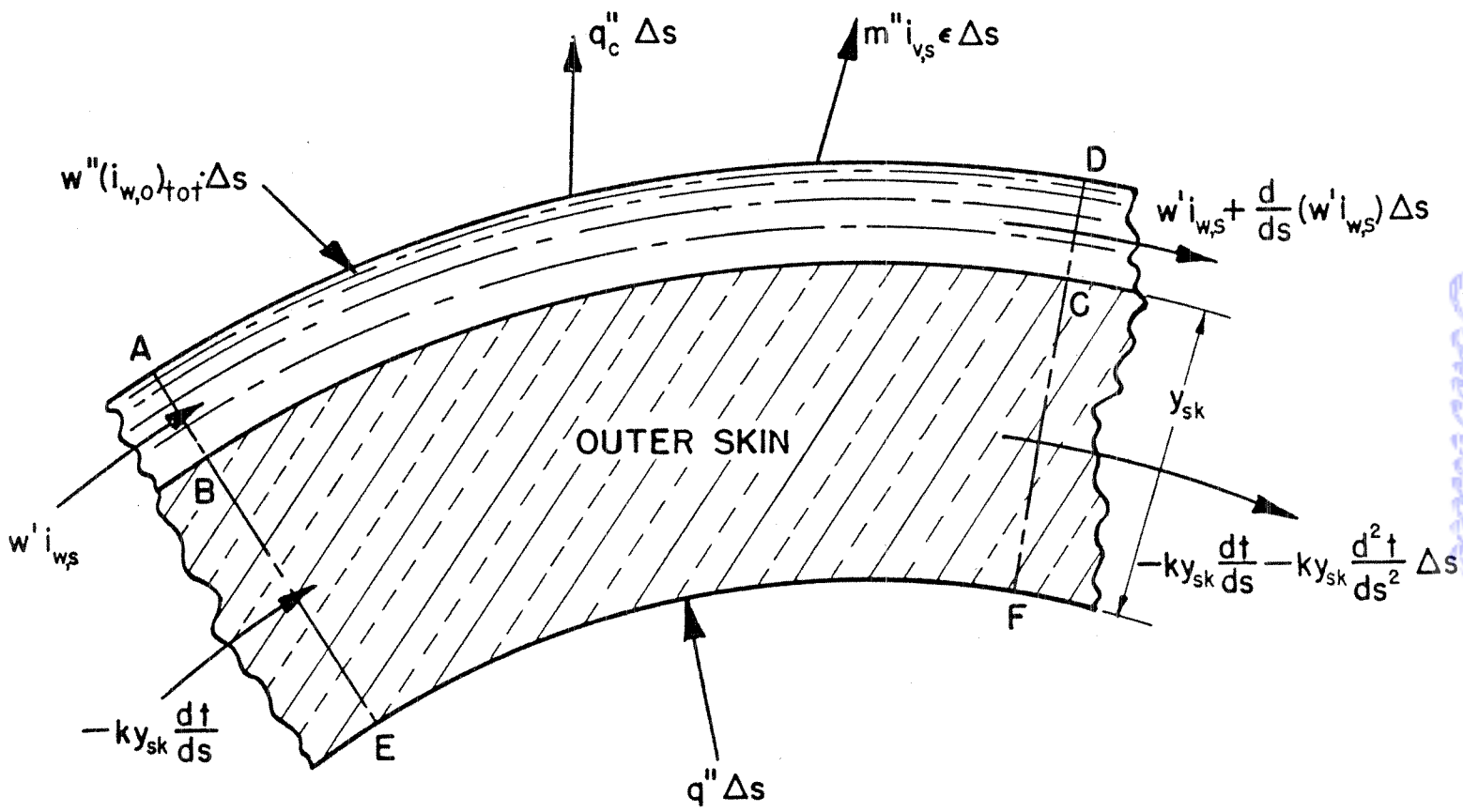

FIG. 6-1 DIAGRAM SHOWING HEAT BALANCE ON ELEMENTAL SECTION OF A WET AIRFOIL

wetness fraction defined in Section 5-3. The quantity $i_{v,s}$ is the enthalpy of saturated vapor at the temperature T_s.

The net rate of heat conducted longitudinally through the skin is $-k \cdot y_{sk} \frac{d^2t}{ds^2} \Delta s$.

Some heat leaves surface AD by radiation. However, the rate is relatively small because the temperature level is low. Therefore, this rate will not be considered any further in the heat balance.

Equating the sum of the rates of energy entering to the rates leaving our elemental system, simplifying, and solving for q",

$$q'' = q_c'' + \epsilon m'' i_{v,s} - W'' \cdot (i_{w,o})_{tot} + \frac{d}{ds}(w' \cdot i_{w,s}) + k \cdot y_{sk} \frac{d^2t}{ds^2} \tag{6-1}$$

Each of the terms will be evaluated, and Eq. 6-1 will be brought to a more convenient form for calculations. We begin with the next to the last term.

6-1.1 Evaluation of $\frac{d}{ds}(w' \cdot i_{w,s})$

The enthalpy of the water is conveniently represented by

$$i_{w,s} = c_{p,w}(T_s - 492) \tag{6-2}$$

where $c_{p,w} = 1$ B/lb F. It follows that

$$\frac{d}{ds}(w' \cdot i_{w,s}) = i_{w,s} \frac{dw'}{ds} + c_{p,w} w' \frac{dT_s}{ds} \tag{6-3}$$

Substituting for dw'/ds from Eq. 5-1,

$$\frac{d}{ds}(w' \cdot i_{w,s}) = W'' c_{p,w}(T_s - 492) - m'' \epsilon i_{v,s} + c_{p,w} w' \frac{dT_s}{ds} \tag{6-4}$$

6-1.2 Evaluation of $W'' \cdot (i_{w,o})_{tot}$

Evaluation of W'' is treated in Chapter 3. The stagnation enthalpy of the impinging water depends on the local velocity at which the droplets strike the surface. Those velocities can be determined from water droplet trajectories. For example, Ref. 81 presents the distribution of velocities on cylinders. However, distributions of impingement velocities on airfoils have not been published. Since the kinetic energy of the droplets is small compared with other quantities, the stagnation enthalpy can be conveniently expressed with sufficient accuracy for design purposes in terms of the free stream velocity. Accordingly,

$$(i_{w,o})_{tot} = c_{p,w}(T_o - 492) + \frac{U_o^2}{2gJ} \qquad (6\text{-}5)$$

When U_o is in ft/sec, $2gJ = 50{,}100$ ft^2 lb/sec^2 B.

6-1.3 Evaluation of $\epsilon m'' i_{v,s}$

Quantities ϵ and m'' have been considered in Chapter 5. The quantity $i_{v,s}$ depends only upon the temperature T_s.[1] In general,

$$i_{v,s} = i_{w,s} + \lambda_s \qquad (6\text{-}6)$$

where λ is the latent heat of vaporization and subscript s refers to the temperature T_s. Values of λ are tabulated by Goodman (Ref. 48) and Keenan and Keyes (Ref. 72). Goodman presents the following linear expression which represents the latent heat within 0.25 per cent in the range of temperatures from -40 to 140°F:

$$\lambda = 1093 - 0.55\ t \qquad (6\text{-}7)$$

6-1.4 Evaluation of q_c''

The net rate of heat transfer by forced convection is given by Eq. 4-2.

[1] The spanwise temperature is assumed to be uniform even in the region of runback where the airfoil is only partially wet. The low thermal resistance of the outer skin tends to keep the temperature uniform.

6-1.5 Simplification of Equation 6-1

Substituting from Eq. 6-2, -4, -5, -6, and 4-2 into Eq. 6-1 and collecting terms,

$$q'' = h\left(T_s - T_1 - \eta_r \frac{U_1^2}{2gJc_{p,a}}\right) + \epsilon m'' \lambda_s + W'' c_{p,w}(T_s - T_o) - W'' \frac{U_o^2}{2gJ} + w' c_{p,w} \frac{dT_s}{ds} - k y_{sk} \cdot \frac{d^2T}{ds^2} \qquad (6\text{-}8)$$

If the surface temperature is uniform the last two terms are zero. The assumption of uniform temperature has frequently been made to expedite the calculations and to arrive at a preliminary design. Measurements (Ref. 127) indicate that close to the stagnation region and in regions aft of the impingement area, the temperature gradient is practically zero. Between these two areas, w' is probably sufficiently small so that the next to the last term becomes relatively unimportant. In this manual the last two terms will be omitted from Eq. 6-8. However, it is possible that if they were retained their influence on the results could be accounted for by an iterative method of calculation. Such calculations are excessively time-consuming and unwarranted for ordinary design purposes.

In omitting the last term, the conduction in the skin is neglected. Boelter, Johnson, and Rubesin (Ref. 16) have performed calculations to make comparisons between solutions in which the conductivity is zero, finite, and infinite. They found that the solution for finite conductivity approaches the solution for no conduction, except where certain large changes of the coefficient of heat transfer occur or where a change of wing structure occurs. The procedure of the more exact solution is very tedious, and the authors recommend the assumption that the chordwise conductivity is zero. The assumption of infinite conductivity gives uniform chordwise temperature, but this result is not in good agreement with the more exact calculation.

Introducing the expression for m'' from Eq. 5-13 and omitting the last two terms from Eq. 6-8,

$$q'' = h\left(T_s - T_l - \eta_r \frac{U_l^2}{2gJc_{p,a}}\right) + \epsilon \frac{I}{c_{p,a}} h \lambda_s \left(\omega_s - \omega_o \cdot \frac{p_l}{p_l - p_{v,s}}\right)$$

$$+ W'' c_{p,w}(T_s - T_o) - W'' \frac{U_o^2}{2gJ} \qquad (6\text{-}9)$$

6-1.6 Further Simplification of the Heat-Balance Equation

Before continuing with the calculations it will be desirable to have Eq. 6-9 in a more suitable form. The form used here is patterned after that of Messinger (Ref. 94)[1] and Tribus (Ref. 124).[1]

It will be convenient to define a function,

$$f \equiv f(t,p,I) \equiv \omega \cdot F(t,I) \qquad (6\text{-}10)$$

where

$$F(t,I) = I \frac{\lambda}{c_{p,a}} \overline{T} \qquad (6\text{-}11)$$

These functions are both dimensionless. This coefficient is plotted against t with I as parameter, in Fig. 6-2. The function $f(t,p,1.1)$ is represented by the solid lines in Fig. 6-3. They cover the range from 10 to 32 in.-mercury; curves are also shown for pressure altitudes of 10,000 and 20,000 ft. The uppermost dotted line represents the function $f(t,10,1.05)$. The difference Δf is uniform. Curves for $I = 1.05$ at other pressures

---

[1] These authors give corresponding equations for subliming surfaces and for surfaces covered with ice-water mixtures, as well as wet surfaces. In particular, Messinger treats the unheated surface. Subliming surfaces are of little interest in anti-icing calculations; surfaces covered with ice-water mixtures may be of interest when analyzing an anti-icing system in operation under severe icing conditions. Since only "effective operation" (Section 5-1) is our goal the subliming surfaces and the surfaces covered with ice-water mixtures are not considered in the present manual.

Since the influence of the latent heat of fusion has been omitted from the derivation, Eq. 6-9 should not be employed unless $t_s > 32°F$. References 94 or 124 should be consulted if it is desired to study cases where t_s is less than or equal to 32°F.

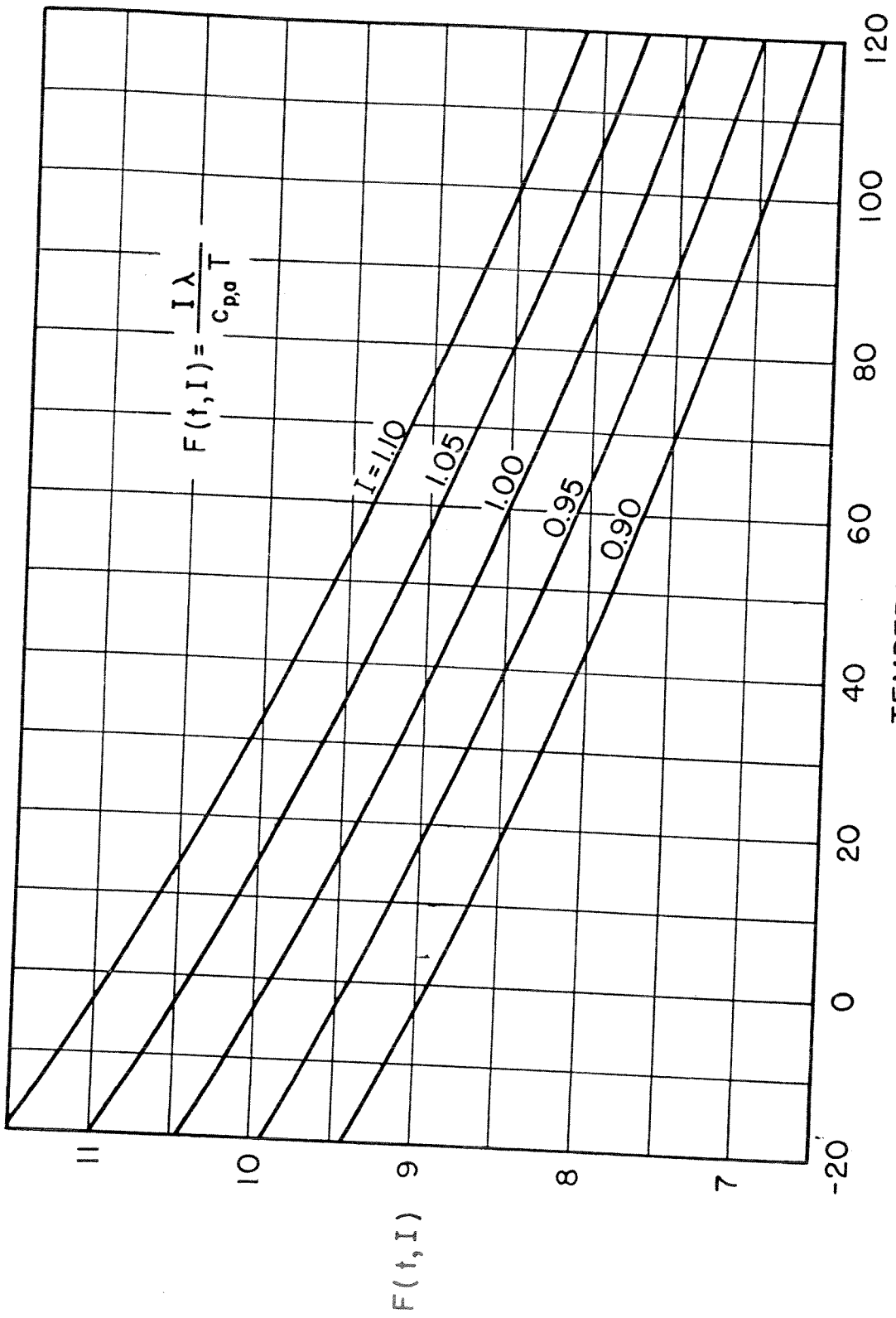

FIG. 6-2 FACTOR F(t,I) FOR USE WITH EQUATION 6-11

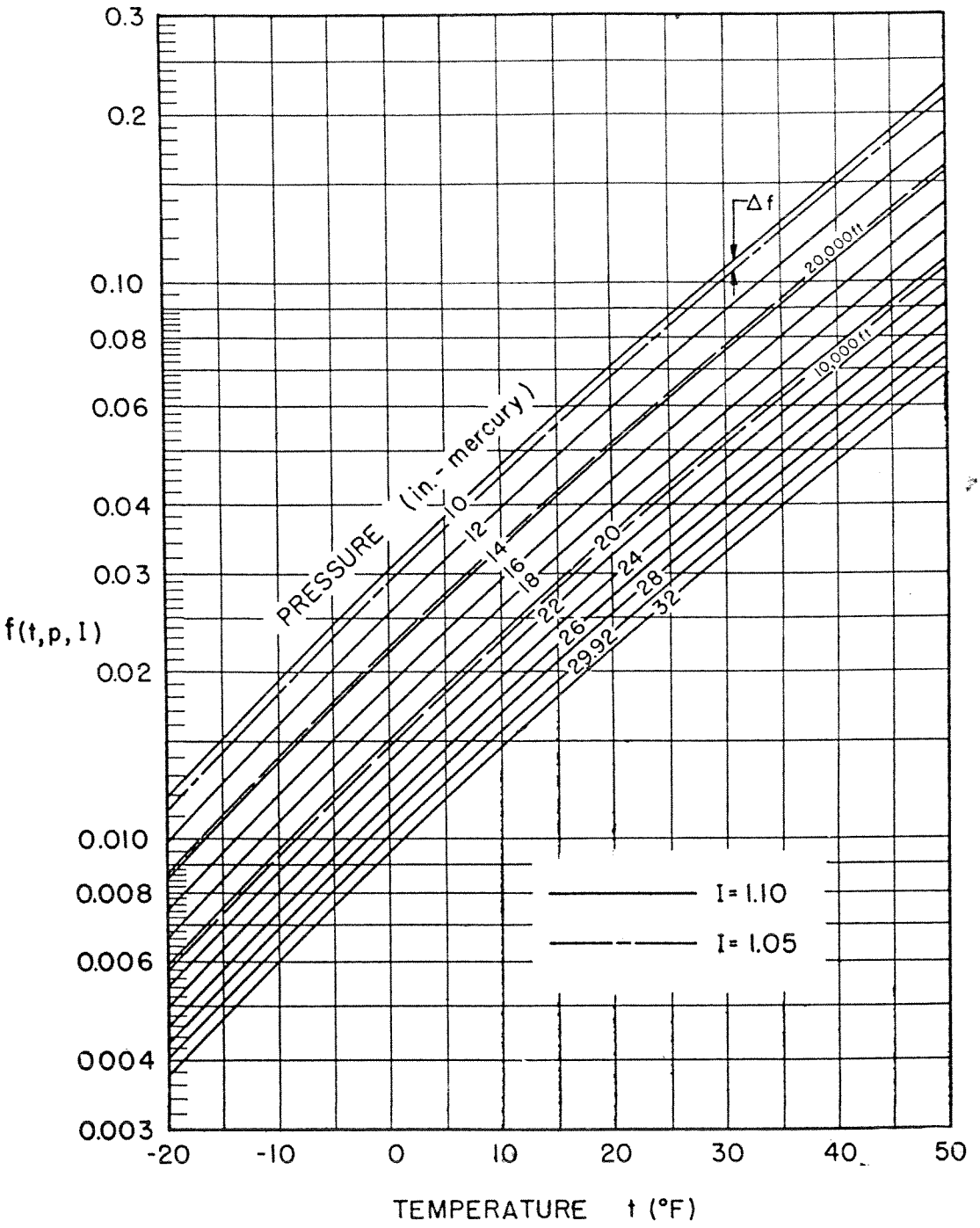

FIG. 6-3 CHART OF FUNCTION f(t,p,I)

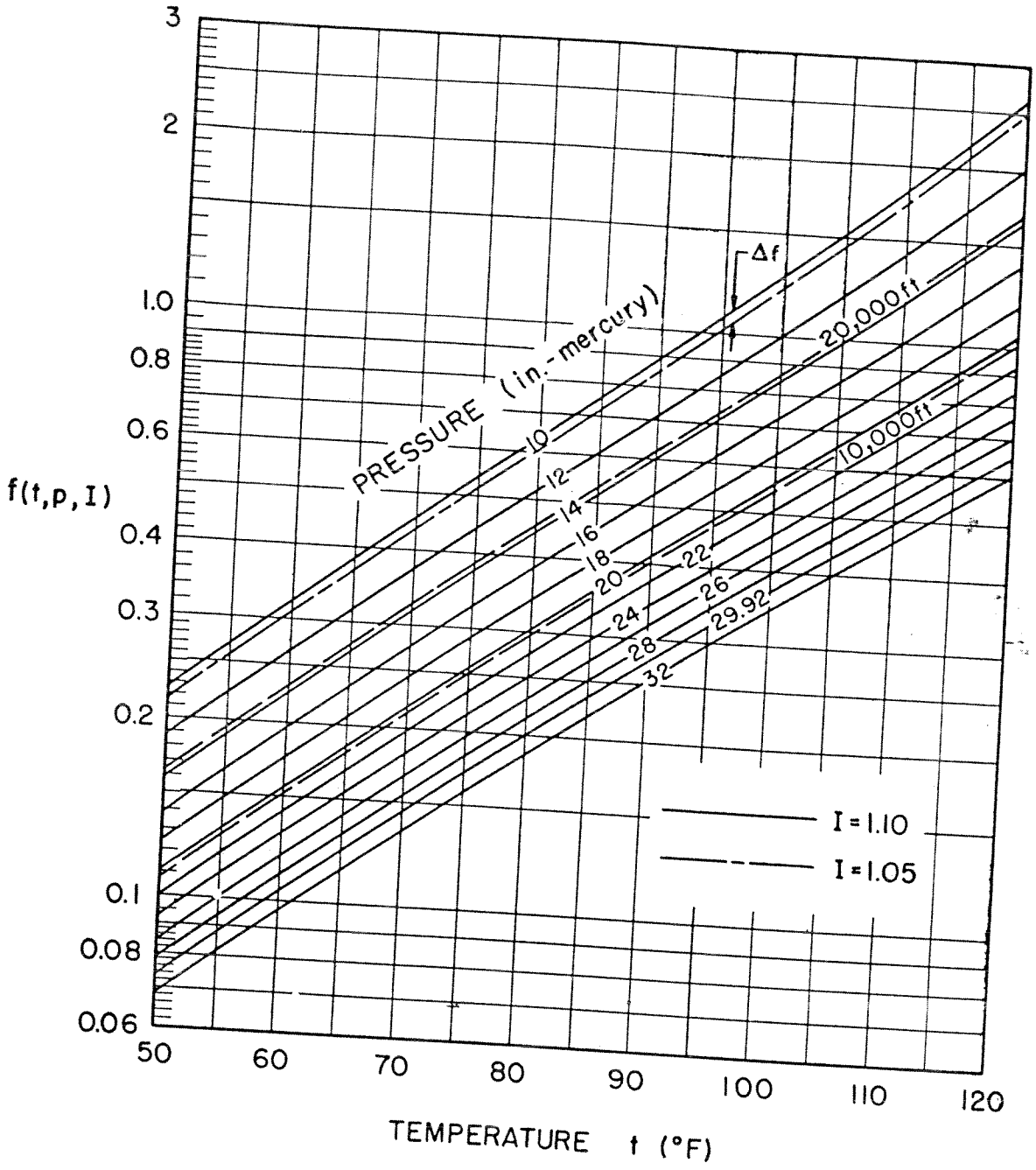

FIG. 6-3 (CONT.) CHART OF FUNCTION f(t,p,I)

would lie at equal distances Δf below the corresponding solid lines. They have been omitted to keep the diagram clear. Curves for $f(t,10,1.0)$ would lie at $2\,\Delta f$ below $f(t,10,1.1)$, and so forth.

Equation 6-9 may now be written in the following way after factoring h from all terms:

$$q'' = h\left\{T_s\left[1 + \left(\frac{W''c_{p,w}}{h}\right) + \epsilon\, f(t_s,p_1,I)\right] - T_o\left[\frac{T_1}{T_o} + \left(\frac{W''c_{p,w}}{h}\right) + \epsilon\, f(t_o,p_o,I)\,\frac{p_1}{p_1 - p_{v,s}} \cdot \frac{\lambda_s}{\lambda_o}\right] - \frac{U_o^2}{2gJc_{p,w}}\left[\eta_r\left(\frac{U_1}{U_o}\right)^2 \frac{c_{p,w}}{c_{p,a}} + \left(\frac{W''c_{p,w}}{h}\right)\right]\right\} \qquad (6\text{-}12)$$

Upon placing

$$z_s \equiv \left[1 + \left(\frac{W''c_{p,w}}{h}\right) + \epsilon \cdot f(t_s,p_1,I)\right] \qquad (6\text{-}13)$$

$$z_o \equiv \left[\frac{T_1}{T_o} + \left(\frac{W''c_{p,w}}{h}\right) + \epsilon \cdot f(t_o,p_o,I) \cdot \frac{p_1}{p_1 - p_{v,s}} \cdot \frac{\lambda_s}{\lambda_o}\right] \qquad (6\text{-}14)$$

and

$$\theta \equiv \frac{U_o^2}{2gJc_{p,w}}\left[\eta_r\left(\frac{U_1}{U_o}\right)^2 \frac{c_{p,w}}{c_{p,a}} + \left(\frac{W''c_{p,w}}{h}\right)\right] \qquad (6\text{-}15)$$

Eq. 6-12 may be written,

$$q'' = h(z_s T_s - z_o T_o - \theta) \qquad (6\text{-}16)$$

For most practical purposes, and particularly for low speed, low altitudes, and small temperature differences, it may be assumed that $\frac{p_1}{p_1 - p_s} \cdot \frac{\lambda_s}{\lambda_o} = 1$; then z_o becomes independent of t_s and assumes the same form as z_s.

6-2 Heat Transferred from the Double Skin

Equation 6-16 has two unknowns, t_s and q''. Therefore, another equation is needed. This is obtained by considering the air flowing through the double-skin heater. Having neglected conduction in the outer skin, we may write to a good approximation for small Δs,

$$\bar{q}'' \cdot \Delta s = \bar{h}_e \cdot \frac{1}{2} \left\{ \left[T_a(s) - T_s(s) \right] + \left[T_a(s+\Delta s) - T_s(s+\Delta s) \right] \right\} \cdot \Delta s \qquad (6\text{-}17)$$

where the bar designates the effective mean value in the interval from s to $s + \Delta s$, and subscript e refers to the effective coefficient discussed in Section 4-20. Since T_a also is unknown, another equation is needed. This is obtained from a heat balance on the air flowing from s to $s + \Delta s$:

$$\bar{q}'' \cdot \Delta s = w_a' \, c_{p,a} \left[T_a(s) - T_a(s+\Delta s) \right] + \bar{q}_d'' \cdot \Delta s \qquad (6\text{-}18)^1$$

Neel (Ref. 98) describes an electric analog calculater which solves Eq. 5-16, -17, and -18, or their equivalent, simultaneously. Gray (Ref. 49) has provided charts which also may be employed to obtain corresponding results. In the next section a stepwise numerical method is presented for desk-type calculations.

6-3 Numerical Calculation of q'', T_s, and T_a

The method presented here is a stepwise procedure. Figure 6-4 is a diagram of the upper or lower double-skin heater. A span 1 ft in length is considered. It is imagined to be stretched into a straight conduit. Also, it is supposed that coefficients of heat transfer on the inside and outside surfaces have been plotted according to the relationships presented in Chapter 4.

---

[1] If $\bar{h}_e$ in Eq. 6-17 includes the effect of convection from the distribution duct, $\bar{q}_d''$ may be evaluated using Eq. 4-74. If $\bar{h}_e$ is based on the assumption that the inner skin is insulated, $\bar{q}_d'' = 0$.

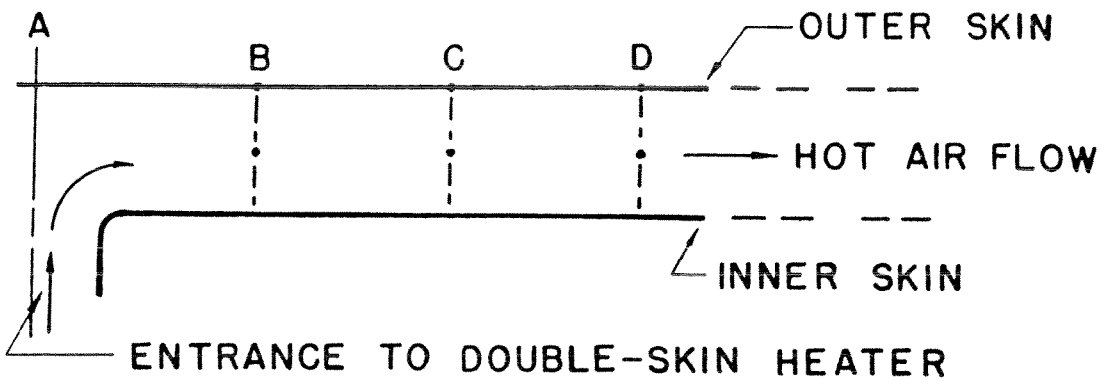

FIG. 6-4 DIVISIONS OF A DOUBLE-SKIN HEAT EXCHANGER

Starting with A the inner stagnation point (a point opposite the entrance to the double-skin passages) the chordwise length of the heater is divided into a number of sections AB, BC, etc, not necessarily equal. The number of sections is arbitrary, as will be mentioned later. As the number of divisions is increased, the calculation time is made longer and the accuracy is improved. A check of the accuracy can be made by increasing the number of divisions until no changes are found beyond an arbitrary allowable amount. The calculation starts with the stagnation point A.

6-3.1 The Starting Values

At the stagnation point the temperature T_{aA} is known;[1] it is the temperature of the air supplied to the passageways, at their entrances. Thus, T_{aA} is equal to the local spanwise temperature t_d in the distribution or supply duct. The local coefficients of heat transfer on the outside and inside surfaces are h_A and h_{aA}, respectively. From a heat

[1] Evaluation of T_{aA} is treated in Section 6-4.

balance at the Section A,

$$q''_A = h_A \left(z_{sA}\, T_{sA} - z_{oA}\, T_o - \Theta_A \right) \tag{6-19}$$

and

$$q''_A = h_{aA} \left(T_{aA} - T_{sA} \right) \tag{6-20}$$

Eliminating q''_A and solving for T_{sA},

$$T_{sA} = \frac{G_A\, T_{aA} + z_{oA}\, T_o + \Theta_A}{G_A + z_{sA}} \tag{6-21}$$

where

$$G_A = \frac{h_{a,A}}{h_A} \tag{6-22}$$

Equation 6-21 can be solved for T_{sA} by trial and error using the chart of Fig. 6-3 as another relationship between T_s and z_s. With T_{sA} known, the rest of the calculation proceeds in the manner described below.

6-3.2 Continuing the Calculation

Consider the division AB. Upon eliminating $\bar{q}'' \cdot \Delta s$ from Eq. 6-17 and -18, placing

$$H_{AB} = \frac{\bar{h}_{e,AB} \cdot \Delta s_{AB}}{2 w'_a\, c_{p,\bar{a}}} \tag{6-23}$$

where $\bar{h}_{e,AB}$ is an average coefficient along the inside surface area Δs_{AB}, and solving for T_{aB} in terms of T_{sB},

$$T_{aB} = \left(\frac{H_{AB}}{1 + H_{AB}}\, T_{sA} + \frac{1 - H_{AB}}{1 + H_{AB}}\, T_{aA} \right) + \left(\frac{H_{AB}}{1 + H_{AB}} \right) T_{sB} \tag{6-24}$$

This equation allows T_{aB} to be calculated when T_{sB} is known, the quantities in parentheses being known constants for the section AB. The above-mentioned restriction regarding the number of divisions is that Δs must

be chosen so that $H \leq 1$ in all intervals. Usually, it may be found most convenient to allow the divisions to terminate at the end of the laminar regime, the end of the transition, and so forth. Further, small intervals near the leading edge are needed in order to attain good accuracy.

Treating Point B in the same manner as Point A was treated in Section 6-3.1,

$$T_{sB} = \frac{G_B T_{aB} + z_{oB} T_o + \Theta_B}{G_B + z_{sB}} \tag{6-25}$$

Substituting for T_{aB} from Eq. 6-24 and solving for T_{sB},

$$T_{sB} = \frac{G_B \left(\frac{H_{AB}}{1 + H_{AB}} T_{sA} + \frac{1 - H_{AB}}{1 + H_{AB}} T_{aA} \right) + z_{oB} T_o + \Theta_B}{z_{sB} + \frac{G_B}{1 + H_{AB}}} \tag{6-26}$$

This equation is basically of the same type as Eq. 6-21 and may be solved, also, by trial and error. Only two or three trials are needed to find the solution.

Equations similar to Eq. 6-24 and -26 can be written for divisions BC, CD, etc, by permutation of the subscripts. By solving each set of equations in succession the distribution of temperatures T_s and T_a can be found. Finally, the rates of heat transfer can be obtained by means of Eq. 6-19 or -20. The integrated rate of heat transfer should be in agreement with

$$q'(s) = w'_a c_{p,a} \left[T_{aA} - T_a(s) \right] \tag{6-27}$$

at the end of each step.

6-3.3 Unheated Surface

Beyond the double skin, the air velocities along the inside surface are small and relatively little heat is transferred. It may be assumed that in this region $q'' = 0$. Then, from Eq. 6-16, for any point on the

unheated surface

$$T_s = \frac{z_o T_o + \theta}{z_s} \qquad (6\text{-}28)$$

6-3.4 Dry, Heated Surface

Simultaneously with the stepwise temperature calculations, it will be necessary to calculate $w'(s)$ by means of Eq. 5-2. This procedure shows whether all the water is evaporating.

If all the water is evaporated before the end of the heated length is reached, a dry, heated region occurs and Eq. 6-26 reduces to a simple form. For example, if Point D lies in such a region, then

$$T_{sD} = \frac{G_D \left(\frac{H_{CD}}{1 + H_{CD}} T_{sC} + \frac{1 - H_{CD}}{1 + H_{CD}} T_{aC} \right) + T_{lD} + \theta_D}{1 + \frac{G_D}{1 + H_{CD}}} \qquad (6\text{-}29)$$

This equation gives T_{sD} directly, no trial and error solution being needed. It will be found that surface temperatures in this region will be relatively high on account of the lack of cooling by evaporation. It is important to investigate these temperatures because during light icing conditions they may possibly exceed the allowable skin temperature when the rate of air flow and inlet temperature are high.

6-4 Preliminary Calculations

The success of the anti-icing system depends upon the selection and control of the inlet temperature T_{aA} and the rate of flow per unit span w'_a. Before performing the stepwise calculations of the previous sections, these quantities should be estimated to reduce the time of calculation. For this purpose the following plan, based on an over-all mass and heat balance, is suggested. The calculation begins with a rough approximation of the average surface temperature required to evaporate the water before it runs back out of the effectively heated area. This average temperature

is later employed to estimate the over-all rates of heat loss and, consequently, the rate of heat input.

6-4.1 Average Surface Temperature $\bar{t}_s$

An average surface temperature may be calculated by means of Eq. 5-13 and Fig. 5-4. To simplify the calculation, the ratio of the pressures appearing in the second term of the brackets of Eq. 5-13 may be taken equal to 1.0. Then using average values,

$$\bar{\omega}_s = \frac{\bar{m}''}{\frac{I\bar{h}}{c_{p,a}}} + \omega_o \qquad (6\text{-}30)$$

The quantity $\bar{m}''$, the average rate of evaporation per unit area, is discussed in the next section. Entering Fig. 5-4 with the calculated value of $\bar{\omega}_s$ and the absolute static pressure of the flight altitude, $\bar{t}_s$ may be obtained from the abscissa of the chart.

As an alternate procedure Eq. 6-30 may be further approximated by means of the equation,

$$\bar{p}_{v,s} = \frac{\bar{m}''}{0.622\,\frac{I\bar{h}}{c_{p,a}}}\, p_o + p_{v,o} \qquad (6\text{-}31)$$

which is obtained by neglecting p_v in the denominator of Eq. 5-9. The approximations which have been made give least error at low altitudes. However, for the present purpose they will give adequate results at all altitudes, since these results are to be checked by the stepwise calculations. In Eq. 6-31 $[\bar{m}'']$ = lb/hr ft^2, $[\bar{h}]$ = B/hr ft^2 F, and $[p]$ = in.-mercury. When $\bar{p}_{v,s}$ has been calculated, $\bar{t}_s$ may be found in Table A-3.

Introducing $I = 1.12$ and $c_{p,a} = 0.24$, the factor $0.622\ I/c_{p,a} = 2.90$, as used by Messinger (Ref. 94). It is based on the assumption of laminar mass transfer, which is probably a good assumption for the lower surface in most cases. If the transfer is taken to be turbulent, the value 2.6 can be employed.

6-4.2 Evaluation of $\bar{m}''$

Since methods to calculate $\bar{h}$ are already treated in Chapter 4, it is necessary only to consider how to find $\bar{m}''$. Before proceeding, it is noted that $\bar{m}''$ could be regarded as the mean rate of evaporation per unit area on either the upper or the lower surface. Since the impingement on the lower surface is heaviest, the plan is to arrive at an estimate of the temperature T_{aA} and of the flow w_a' required for the lower surface. Then the heat requirements of the upper surface can be met with the same temperature T_{aA} but with a modified rate of flow. Accordingly, in the remainder of this chapter, $\bar{m}''$ and $\bar{h}$ are referred to the lower surface.

There are several methods to estimate $\bar{m}''$. One group of methods may be represented by an equation of the type,

$$\bar{m}'' = \frac{\alpha W'}{\beta s_H} \qquad (6\text{-}32)$$

where W' is the total rate of impingement on the lower surface and s_H is its heated length; α and β are arbitrary fractions which the designer may choose according to the intensity of anti-icing desired and to his experience with the results of the stepwise calculations. Some examples are given below:

(1) If $\alpha = 1$ and $\beta = s_1/s_H$, a dry system is planned in which all the water would be evaporated on the area of impingement. As mentioned previously, such a system would require high temperatures, high rates of flow, or both; ordinarily it would not be employed.

(2) If $\alpha = 1$ and $\beta = 1$, it is planned to evaporate all the water on the heated area.

(3) If $\alpha < 1$ and $\beta = 1$, it is planned to evaporate a fraction of the water on the heated area and to allow the remainder to be evaporated by aerodynamic heating. The same result is obtained by taking $\alpha = 1$ and $\beta > 1$, which would mean that it is planned to evaporate all the water on an area somewhat larger than the heated area. In these cases the ratio α/β should probably be 0.8 or 0.9.

Other methods may be used which are modifications of those presented. For example, the influence of the partially wetted surface could be included. Another group of methods has been based on assumptions regarding the surface temperature; the length of the heated area is subsequently adjusted. Whatever the method adopted, as the preliminary design procedure is made more complex, it takes longer time. Since any final configuration should be analyzed by means of the stepwise calculation, it is recommended to keep the procedure as simple as possible. If the results of the preliminary calculations are found to provide excessive or inadequate heating, the stepwise calculations will show what adjustment is needed to improve the performance of the system. Modifications of the performance calculations required by the adjustment can be made with little difficulty, using the results of those calculations as a guide.

6-4.3 Total Rate of Heat Transfer

With the average surface temperature $\bar{t}_s$ known, the total heat loss from the wing may be calculated. This loss is made up of three main parts, namely, (1) the sensible heat loss to the water, (2) the rate of heat loss by evaporation, and (3) the net rate of heat transfer by convection. They will be denoted for a unit span by q_1', q_2', and q_3', respectively. The third item accounts for the aerodynamic heating. The kinetic gain from the impinging droplets can be neglected from the preliminary calculation because it is relatively small. Accordingly, the total rate of heat transfer per unit span is

$$q' = q_1' + q_2' + q_3' \tag{6-33}$$

These items are evaluated in the next three sections.

6-4.4 Sensible Heat Transfer to the Water

The rate of sensible heat transfer per unit span to the impinging water is

$$q' = W' c_{p,w} (\bar{t}_s - t_o) \tag{6-34}$$

Of course, $c_{p,w} = 1$ B/lb F, and t_o is the ambient air temperature.

6-4.5 Heat Loss by Evaporation

The rate of heat loss by evaporation per unit span is

$$q_2' = \bar{m}'' \lambda_s \cdot \left(\frac{\beta}{\alpha}\right) \cdot s_H \qquad (6\text{-}35)$$

where λ_s is the latent heat of evaporation at the average surface temperature $\bar{t}_s$. It is satisfactory to employ $\lambda_s = 1050$ B/lb as an average value over the temperature range encountered in the present application.

6-4.6 Net Heat Loss by Convection

Neglecting any change of temperature outside the boundary layer, the net heat loss by convection per unit span is

$$q_3' = \bar{h}\, s_H \left(\bar{t}_s - t_o - \eta_r \cdot \frac{U_o^2}{2gJc_{p,a}} \right) \qquad (6\text{-}36)$$

where U_o is the airplane speed in ft/sec; however, if an average speed is used to calculate $\bar{h}$, then the same average value may be used instead of U_o. A convenient rule of thumb to calculate the last term in the parentheses of Eq. 6-36 is to double the square of the speed in knots divided by 100; the result uses $\eta_r = 0.844$ as a basis and has the unit, Fahrenheit degrees.

6-4.7 Determination of T_{aA} and w_a'

The final step in the preliminary calculation is to select a desirable or allowable value of either $\bar{w}_a'$ or T_{aA} and to determine the corresponding value of the other quantity. The following relationships exist between them. The heat transferred per unit span is

$$q_a' = w_a' c_{p,a} \left[T_{aA} - T_a(s_H) \right] \qquad (6\text{-}37)$$

where $T_a(s_H)$ is the temperature of the air at the end of the heat exchanger. Also, since the surface temperature is assumed uniform,

$$q'_a = \bar{h}_e \, s_H \cdot \frac{T_{aA} - T_a(s_H)}{\ln \dfrac{T_{aA} - \bar{T}_s}{T_a(s_H) - \bar{T}_s}} \qquad (6\text{-}38)$$

The difference between q' in Eq. 6-33 and q'_a in Eq. 6-37 and -38 is the heat transferred from the air in the distribution duct. In many cases the difference is relatively small and may be neglected so that q'_a may be placed equal to q'. Further, $\bar{h}_e$ represents an average effective heat transfer coefficient based only on the heat transferred inside the passages. As already suggested, for the present purpose it may be assumed that on account of the fin effect of the inner skin, the effective coefficient is about 50 per cent higher than the true coefficient $\bar{h}_a$ (cf. Section 4-20). Eliminating $T_a(s_H)$ from Eq. 6-37 and -38,

$$q'_a = w'_a \, c_{p,a} (T_{aA} - \bar{T}_s)(1 - e^{-Z}) \qquad (6\text{-}39)$$

where

$$Z = \frac{\bar{h}_e \, s_H}{w'_a \, c_{p,a}} \qquad (6\text{-}40)$$

From Eq. 6-39 and -40, w'_a can be calculated if T_{aA} is known or T_{aA} can be found if w'_a is known. In selecting w'_a, due regard must be given the pressures available to meet the resistances of the passages.

In selecting T_{aA}, which is essentially the local distribution-duct or supply-duct temperature, an allowance must be made for any heat losses from the ducts. In systems like that shown in Fig. 1-3(c) and -3(d), the duct losses are minor. However, in systems such as those in Fig. 1-3(a) and -3(b), the temperature drop along the ducts may be significant, and an estimate of the spanwise temperature distribution is required. This estimate could be obtained from heat and mass balances on successive parts of the distribution system.

In many cases, the heat lost from the distribution system finds its way to the wet surface, for example, by conduction through structural members or partitions. That heat, of course, is not "lost"; it merely

alters the distribution of the total heat supplied. Since the effects of these losses on the wet surfaces usually would not be appreciable and since their distribution is difficult to calculate, it is recommended to consider them as a margin of safety, provided that allowance is made for the spanwise temperature distribution in the duct.

6-5 General Remarks

The procedures outlined above are based on a unit span of a typical wing section. Therefore, the performance of three or more airfoil sections of each wing should be analyzed. In this way the required distribution of hot air through the system can be calculated.

Having found the system to protect the airplane against specified icing conditions, the designer may then proceed to study the performance in other icing conditions, at other altitudes and temperatures, and for other speeds.

Finally, he will have to consider the controls necessary to provide the proper rates of air flow and to prevent structural overheating. Some instrumentation, also, may be needed for ground and flight tests as well as for routine flying.

BIBLIOGRAPHY

[1] Abbott, I. H., A. E. von Doenhoff, and L. S. Stivers, Jr. A Summary of Airfoil Data. NACA Rept. 824, 1945.

[2] Abramovich, G. Fluid Motion in Curved Channels. From collections of Reports on Industrial Aerodynamics and Fan Construction. Rept. 211. Transactions Central Aero-Hyrodyn. Institute (Moscow) 1935, pp. 97-151.

[3] Aiken, W. S., Jr. Standard Nomenclature for Airspeeds with Tables and Charts for Use in Calculation of Airspeed. NACA Rept. 837, 1946.

[4] Allen, H. J. and B. C. Look. A Method for Calculating Heat Transfer in the Laminar Flow Region of Bodies. NACA Rept. 764, 1943.

[5] Bailey, A. and W. F. Cope. ARC Tech. Rept. 43, 1933, p. 199.

[6] Barton, B. E. and L. J. DeKostor. A Preliminary Investigation of the Characteristics of Air Scoops on a Fuselage. NACA WR L-275, 1942.

[7] Barzelay, M. E., K. N. Tong, and G. Hollo. Thermal Conductance of Contacts in Aircraft Joints. NACA Tech. Note 3167, 1954.

[8] Bauchayer, M. A. The Loss of Energy in Duct Elbows and Branches. Hydroelectr. Kongress Grenable, 1925; Engineering 2, 1925, p. 241.

[9] Becker, J. V. Wind-Tunnel Tests of Air Inlet and Outlet Openings on a Streamline Body. NACA WR L-300, 1940.

[10] Beij, H. K. Pressure Losses for Fluid Flow in 90 Degree Bends, National Bureau of Standards Journal of Research, Research Paper 1110, 21, 1938.

[11] Bergrun, N. R. A Method for Numerically Calculating the Area and Distribution of Water Impingement on the Leading Edge of an Airfoil in a Cloud. NACA Tech. Note 1397, 1947.

[12] Bergrun, N. R. An Empirical Method of Permitting Rapid Determination of the Area, Rate, and Distribution of Water Drop Impingement on an Airfoil of Arbitrary Cross-section at Subsonic Speeds. NACA Tech. Note 2476, 1951.

[13] Bergrun, N. R. An Empirically Derived Basis for Calculating the Area, Rate, and Distribution of Water-Drop Impingement on Airfoils. NACA Rept. 1107, 1952.

[14] Berry, C. H. Flow and Fan. The Industrial Press, New York, 1954.

[15] Boelter, L. M. K., L. M. Grossman, R. C. Martinelli, and E. H. Morrin. An Investigation of Aircraft Heaters. XXIX - Comparison of Several Methods of Calculating Heat Losses from Airfoils. NACA Tech. Note 1453, 1948.

[16] Boelter, L. M. K., H. A. Johnson, V. D. Sanders, and M. W. Rubesin. Icing Report by the University of California, Fiscal Year 1946. AAF Tech. Rept. 5529, 1946.

[17] Boelter, L. M. K, E. H. Morrin, R. C. Martinelli, and H. F. Poppendiek. An Investigation of Aircraft Heaters XIV - An Air and Heat Flow Analysis of a Ram-Operators Heater and Duct System. NACA ARR No. 4001, 1944.

[18] Boelter, L. M. K., V. D. Sanders, and F. E. Romie. An Investigation of Aircraft Heaters. XXVIII - Determination of Thermal Performance of Rectangular- and Trapezoidal-Shaped Inner-Skin Passages for Anti-Icing Systems. NACA Tech. Note 2524, 1951.

[19] Boelter, L. M. K., G. Young, and H. W. Iverson. An Investigation of Aircraft Heaters. XXVII - Distribution of Heat Transfer Rate in the Entrance Section of a Circular Tube. NACA Tech. Note 1451, 1948.

[20] Brown. W. B. Exact Solutions of the Laminar Boundary Layer Equations for a Porous Plate with Variable Fluid Properties and a Pressure Gradient in the Main Stream. Proceedings of the First U. S. National Congress of Applied Mechanics, 1952, pp. 843-852.

[21] Brun, E. The Mechanics of Suspensions. Airplane Icing Information Course, Lecture 2, Univ. of Michigan, 1953.

[22] Brun, E. and R. Caron. A Method for Determining the Trajectories of Particles in Suspension in a Fluid. Univ. of Michigan, Engineering Research Institute, Contract AF 18(600)-51, 1953.

[23] Brun, R. J., H. M. Gallagher, and D. E. Vogt. Impingement of Water Droplets on NACA 65-208 and 65-212 Airfoils at 4° Angle of Attack. NACA Tech. Note 2952, 1953.

[24] Brun, R. J., H. M. Gallagher, and D. E. Vogt. Impingement of Water Droplets on NACA 65A004 Airfoil and Effect of Change in Airfoil Thickness from 12 to 4 Per Cent at 4° Angle of Attack. NACA Tech. Note 3047, 1953.

[25] Brun, R. J., H. M. Gallagher, and D. E. Vogt. Impingement of Water Droplets on NACA 65A004 Airfoil at 8° Angle of Attack. NACA Tech. Note 3155, 1954.

[26] Brun, R. J., J. S. Serafini, and H. M. Gallagher. Impingement of Cloud Droplets on Aerodynamic Bodies as Affected by Compressibility of Air Flow Around the Body. NACA Tech. Note 2903, 1953.

[27] Brun, R. J., J. S. Serafini, and G. J. Moshos. Impingement of Water Droplets on an NACA 65_1-212 Airfoil at an Angle of Attack of 4°. NACA RM E52B12, 1952.

[28] Budenholzer, R. A. et al. A Study of Use of High Temperature, High Pressure Air for Flight Surface Anti-Icing Systems. Armour Research Foundation of Illinois Institute of Technology, Contract AF 18(600)-195, 1953.

[29] Callaghan, E. E. Analogy between Mass and Heat Transfer with Turbulent Flow. NACA Tech. Note 3045, 1953.

[30] Callaghan, E. E. and J. S. Serafini. Analytical Investigation of Icing Limit for Diamond-Shaped Airfoil in Transonic and Supersonic Flow. NACA Tech. Note 2861, 1953.

[31] Callaghan, E. E. and J. S. Serafini. A Method for Rapid Determination of the Icing Limit of a Body in Terms of the Stream Conditions. NACA Tech. Note 2914, 1953.

[32] Coles, W. D. and R. S. Ruggeri. Experimental Investigation of Sublimation of Ice at Subsonic and Supersonic Speeds and Its Relation to Heat Transfer. NACA Tech. Note 3104, 1954.

[33] Dannenberg, R. E. A Design Study of Leading-Edge Inlets for Unswept Wings. NACA RM A9K02b, 1950.

[34] Dearborn, C. H. and A. Silverstein. Drag Analysis of Single-Engine Military Airplanes Tested in the NACA Full-Scale Wind Tunnel. NACA ACR L-489, 1940.

[35] Dorsch, R. G. and R. J. Brun. A Method for Determining Cloud Droplet Impingement on Swept Wings. NACA Tech. Note 2931, 1953.

[36] Dorsch, R. G. and P. T. Hacker. Photomicrographic Investigation of Spontaneous Freezing Temperature of Supercooled Water Droplets. NACA Tech. Note 2142, 1951.

[37] Douglas Aircraft Company, Inc. Air Conditioning Manual, 1945.

[38] Drexel, R. E. and W. H. McAdams. Heat-Transfer Coefficients for Air Flowing in Round Tubes, in Rectangular Ducts, and around Finned Cylinders. NACA ARR 4F28 (WR W-108), 1945.

[39] Eckert, E. R. G. Introduction to the Transfer of Heat and Mass, First Edition. McGraw-Hill Book Co., New York, 1950.

[40] Eckert, E. R. G. and O. Drewitz. The Heat Transfer to a Plate in Flow at High Speed. NACA Tech. Memorandum 1045 (original paper in German, 1940).

[41] Eckert, E. R. G. and J. N. B. Livingood. Method for Calculation of Heat Transfer in Laminar Region of Air Flow Around Cylinders of Arbitrary Cross Section (Including Large Temperature Differences and Transpiration Cooling). NACA Tech. Note 2733, 1952.

[42] Falkner, V. M. The Length of Aerofoil Curved Surfaces. Aircraft Engineering, 25, 1953, p. 72.

[43] Frick, C. W., Jr. and G. B. McCullough. A Method for Determining the Rate of Heat Transfer from a Wing or Streamline Body. NACA Rept. 830, 1945.

[44] Gazley, C., Jr. Boundary-Layer Stability and Transition in Subsonic and Supersonic Flow - A Review of Available Information with New Data in the Supersonic Range. J. Aero. Sci, 20, 1953, pp. 19-28.

[45] Gelder, T. F. and J. P. Lewis. Comparison of Heat Transfer from Airfoil in Natural and Simulated Icing Conditions. NACA Tech. Note 2480, 1951.

[46] Gibson, A. H. Hydraulics and Its Applications. Van Nostrand, New York, 1912.

[47] Glauert, M. A Method of Constructing the Paths of Raindrops of Different Diameters moving in the Neighborhood of (1) A Circular Cylinder, (2) An Aerofoil, Placed in a Uniform Stream of Air; and A Determination of the Rate of Deposit of the Drops on the Surface and the Percentage of Drops Caught. Br. ARC R&M 2025, 1940.

[48] Goodman, W. Air Conditioning Analysis. The Macmillan Company, New York, 1943.

[49] Gray, V. H. Simple Graphical Solution of Heat Transfer and Evaporation from Surface Heated to Prevent Icing. NACA Tech. Note 2799, 1952.

[50] Guibert, A. G. and W. C. Hurty. Impingement of Waterdrops on Various Airfoils from Trajectories Obtained on the Differential Analyzer-Addendum I. Univ. of California, Contract NAw 5677, 1949.

[51] Guibert, A. G., E. Janssen, and W. M. Robbins. Determination of Rate, Area, and Distribution of Impingement of Water Drops on Various Airfoils from Trajectories Obtained on the Differential Analyzer. NACA RM 9A05, 1949.

[52] Hacker, P. T. and R. G. Dorsch. A Summary of Meteorological Conditions Associated with Aircraft Icing and a Proposed Method of Selecting Design Criterions for Ice-Protection Equipment. NACA Tech. Note 2569, 1951.

[53] Hall, N. A. Thermodynamics of Fluid Flow. Prentice-Hall, New York, 1951.

[54] Hardy, J. K. An Analysis of the Dissipation of Heat in Conditions of Icing from a Section of the Wing of the C-46 Airplane. NACA Rept. 831, 1945.

[55] Hardy, J. K. and R. Morris. Transfer of Heat Internally in a Heated Wing. RAE Rept. Mech. Eng. 4, 1948.

[56] Hauger, H. H., Jr. Design of Air Heated Intermittent De-Icer. Airplane Icing Information Course, Lecture 9, Univ. of Michigan, 1953.

[57] Hausen, H. Waermeuebertragung in Gegenstrom, Gleichstrom und Kreuzstrom. Springer-Verlag, Berlin, 1950.

[58] Heating Ventilating Air Conditioning Guide 1953. Vol. 31, ASHVE, New York.

[59] Henry, J. R. Design of Power-Plant Installations Pressure-Loss Characteristics of Duct Components. NACA ARR L4F26 (WR L-208), 1944.

[60] Hensley, R. V. Mollier Diagrams for Air Saturated with Water Vapor at Low Temperatures. NACA Tech. Note 1715, 1948.

[61] Hoffman, A. The Energy Loss around 90° Bends in Tubes of Uniform Cross-Section. Mitteilungen des Hydraul. Instit. der Technischen Hochschule, Muenchen, Heft 3, 1929, 45.

[62] Howarth, L. Modern Developments in Fluid Dynamics -- High Speed Flow, Vol. II. Oxford Univ. Press, London, 1953.

[63] Jakob, M. Heat Transfer, Vol. I. John Wiley, New York, 1949.

[64] Jakob, M., S. P. Kezios, and W. J. Christian. Heat Transfer and Mass Transfer of Water from an Airfoil Model at Mach Numbers 0.5 to 0.9. Summary Rept., Contract AF 18(600)-153, 1954.

[65] Johnson, H. A. A Design Manual for Determining the Thermal Characteristics of High Speed Aircraft. AAF Tech. Rept. 5632, 1947.

[66] Jonas, J. Thermal Fin Effect in Heat Anti-Icing Corrugations. J. Aero. Sci, 15, 1948, pp. 163-166.

[67] Jones, A. R. and W. Lewis. Recommended Values of Meteorological Factors to be Considered in the Design of Aircraft Ice-Prevention Equipment. NACA Tech. Note 1855, 1949.

[68] Kantrowitz, A. Aerodynamic Heating and the Deflection of Drops by an Obstacle in an Air Stream in Relation to Aircraft Icing. NACA Tech. Note 779, 1940.

[69] Kays, W. M. Tech. Rept. 14, NR-035-104, Dept. of Mech. Eng., Stanford University, 1951.

[70] Kays, W. M. Loss Coefficients for Abrupt Changes in Flow Cross Section with Low Reynolds Number Flow in Single and Multiple-Tube Systems. Transactions ASME, 72, 1950, pp. 1067-1074.

[71] Kays, W. M. and A. L. London. Heat Transfer and Flow Friction Characteristics of Some Compact Heat Exchanger Surfaces. Part I - Test System and Procedure. Part II - Design Data for Thirteen Surfaces. Transactions ASME, 72, 1950, pp. 1075-1097.

[72] Keenan, J. H. and F. G. Keyes. Thermodynamic Properties of Steam. John Wiley, New York, 1936.

[73] Kirchbach, H. Energy Loss in Elbows. Mitteilungen des Hydraul. Institut. der Technischen Hochschule, Muenchen, Heft 3, 1929, 68.

[74] Klein, J. and M. Tribus. Forced Convection from Nonisothermal Surfaces. Presented at the ASME Semi-Annual Meeting, Los Angeles, 1953, Paper No. 53-SA-46.

[75] Klein, G. J., K. F. Tripper, and J. J. Green. The Design of Corners in Fluid Channels, Canadian Journal of Research, 3, 1930.

[76] Korst, H. H., N. A. Buckley, S. Konzo, and R. W. Roose. Fitting Losses for Extended-Plenum Forced Air System. Transactions ASHVE, 56, 1950, pp. 259-276.

[77] Kroeber, G. Guide Vanes for Deflecting Fluid Currents with Small Loss of Energy. NACA Tech. Memorandum 722, 1933.

[78] Kuechemann, D. and J. Weber. Aerodynamics of Propulsion, McGraw-Hill, New York, 1953.

[79] Lal, S. Icing of Low-Drag Wing Sections, I and II. J. Aero. Soc. India, 3, No. 1 and 2, 1951.

[80] Langmuir, I. Final Report on Icing Research up to July 1, 1945. G. E. Research Laboratory, Contract W33-038-AC-951(14006), 1945.

[81] Langmuir, I. and K. B. Blodgett. A Mathematical Investigation of Water Droplet Trajectories. AAF Tech. Rept. 5418, 1946.

[82] Levine, J. Statistical Explanation of Spontaneous Freezing of Water Droplets. NACA Tech. Note 2234, 1950.

[83] Lewis, W. and N. R. Bergrun. A Probability Analysis of the Meteorological Factors Conducive to Aircraft Icing in the United States. NACA Tech. Note 2738, 1952.

[84] Locklin, W. D. Energy Losses in 90-degree Duct and Elbows. Survey and Analysis of Available Information. Research Rept. 1405, Transactions ASHVE, 56, 1950.

[85] Lowell, H. H. Maximum Evaporation Rates of Water Droplets approaching Obstacles in the Atmosphere under Icing Conditions. NACA Tech. Note 3024, 1953.

[86] Mache, H. Sitzungsber. d. Kais. Akad. d. Wiss. Wien, math-naturwiss. Klasse 119, 1910, p. 1417.

[87] Maisel, D. S. and T. K. Sherwood. Evaporation of Liquids into Turbulent Gas Streams. Chem. Eng. Progress, 46, 1950, p. 131.

[88] Marks, L. S. Mechanical Engineers' Handbook, Fourth Edition. McGraw-Hill, New York, 1941.

[89] Martinelli, R. C., A. G. Guibert, E. H. Morrin, and L. M. K. Boelter. An Investigation of Aircraft Heaters. VIII - A Simplified Method for the Calculation of the Unit Thermal Conductance over Wings. NACA ARR (WR W-14), 1943.

[90] Martinelli, R. C., E. B. Weinberg, E. H. Morrin, and L. M. K. Boelter. An Investigation of Aircraft Heaters III - Measured and Predicted Performance of Double Tube Heat Exchangers. ARR W-98, 1942.

[91] McAdams, W. H. Heat Transmission. McGraw-Hill, New York, Second Edition, 1942; Third Edition, 1954.

[92] McGann, R. A Method for Compressible Flow Analysis. Special publication of Northrop Aircraft, 1951.

[93] McLellan, H. and W. A. Bartlett, Jr. Investigation of Air Flow in Right-Angle Elbows. NACA ARR, 1941.

[94] Messinger, B. L. Equilibrium Temperature of an Unheated Icing Surface as a Function of Air Speed. J. Aero. Sci, 20, 1953, pp. 29-42.

[95] Mickley, H. S. Mass Transfer at High Velocities. Airplane Icing Information Course, Lecture 5, Univ. of Michigan, 1953.

[96] Moody, L. F. Friction Factor for Pipe Flow. Transactions ASME, 66, 1944, pp. 671-678.

[97] Morton, A. O. An Investigation of an Experimental Technique for Determining the Trajectory of a Water Droplet in an Airstream. Univ. of Michigan, Eng. Research Institute, Contract AF 18(600)-51, 1952

[98] Neel, C. B., Jr. The Design of Air-Heated Thermal Ice-Prevention Systems. Airplane Icing Information Course, Lecture 7, Univ. of Michigan, 1953; also, A Procedure for the Design of Air-Heated Ice-Prevention Systems. NACA Tech. Note 3130, 1954.

[99] Neel, C. B., Jr., N. R. Bergrun, D. Jukoff, and B. A. Schlaff. The Calculation of the Heat Required for Wing Thermal Ice Prevention in Specified Icing Conditions. NACA Tech. Note 1472, 1947.

[100] North American Aviation, Inc. Design Analysis of the Thermal Anti-Icing System for the Model P-82E Airplane. Rept. NA-46-1027, 1948.

[101] North American Aviation, Inc. Thermal Transfer Tests of Wing Double Skin Designs Applicable to the F-86D Airplane. Rept. NA-50-340, Contract W33-038-AF-9211, 1951.

[102] Northrop Aircraft, Inc. Preliminary Report on the Computation of Water Drop Trajectories about a 6 Per Cent Airfoil. TDM 67, 1952.

[103] Orr, J. L. Electro-Thermal De-Icing Systems, Their Design and Control. Airplane Icing Information Course, Lecture 8, Univ. of Michigan, 1953.

[104] Patterson, G. N. Note on the Design of Corner in Duct System. ARC Reports and Memoranda 1773, 1937.

[105] Patterson, G. N. Modern Diffuser Design. Aircraft Engineering, 10, 1938, pp. 267-273.

[106] Pigott, R. J. S. Pressure Losses in Tubing, Pipe and Fitting. Prepared for Presentation at the Petroleum Engineering Conference, Oklahoma City, 1949. (Gulf Research and Development Co. Research Report KL 11-2).

[107] Pinkel, B. A Summary of NACA Research on Heat Transfer and Friction for Air Flowing through Tube with Large Temperature Difference. Presented at the ASME Semi-Annual Meeting, Los Angeles, 1953. Paper No. 53-SA-34.

[108] Powell, R. W. and E. Griffith. The Evaporation of Water from Plane and Cylindrical Surfaces. Transactions Institution of Chemical Engineers, 13, 1935, 175.

[109] Rogallo, F. M. Internal-Flow Systems for Aircraft. NACA Rept. 713, 1941.

[110] Rubesin, M. W. Effect of an Arbitrary Surface Temperature Variation along a Flat Plate on the Convective Heat Transfer in an Incompressible Turbulent Boundary Layer. NACA Tech. Note 2345, 1951.

[111] SAE. Airplane Heating and Ventilating Equipment, Engineering Data, Fluid Dynamics. SAE Aeronautical Information Report No. 23, Society of Automotive Engineers, New York, 1951.

[112] Scesa, S. and S. Levy. Heat Transfer to Constant-Property Laminar Boundary-Layer Wedge Flows with Stepwise and Arbitrary Wall-Temperature Variation. Transactions ASME, 76, 1954, 279-286.

[113] Schaefer, V. J. Final Report on Icing Research by General Electric Company, Fiscal Year 1946. AAF Tech. Rept. 5539, 1947.

[114] Schirmer, R. Die Diffusionszahl von Wasserdampf-Luft-Gemischen und die Verdampfungsgeschwindigkeit. Zeitschrift Ver. Deut. Ing., Beiheft Verfahrens-technik, 1938, pp. 170-177.

[115] Schmidt, E. and K. Wenner. Heat Transfer over the Circumference of a Heated Cylinder in Transverse Flow. NACA Tech. Memorandum 1050, 1943 (original paper in German, 1941).

[116] Schubart, W. Energy Loss in Smooth- and Rough-Surfaced Bends and Curves in Pipw Lines. Mitteilungen des Hydraul. Instit. der Technischen Hochschule, Muenchen, Heft 3, 1929, 81.

[117] Seibert, O. Heat Transfer of Airfoils and Plates. NACA Tech. Memorandum 1044, 1944 (original paper in German, 1938).

[118] Serafini, J. S. Impingement of Water Droplets on Wedges and Diamond Airfoils at Supersonic Speeds. NACA Tech. Note 2971, 1953.

[119] Sheppard, P. A. The Physical Properties of Air with Reference to Meteorological Practice and the Air Conditioning Engineer. Transactions ASME, 71, 1949, 915-919.

[120] Sherman, P., J. S. Klein, and M. Tribus. Determination of Drop Trajectories by Means of an Extension of Stokes' Law. Univ. of Michigan, Engineering Research Institute, Contract AF 18(600)-51, 1952.

[121] Spielman, M. and M. Jakob. Local Coefficients of Mass Transfer by Evaporation of Water into an Air Jet. Transactions ASME, 75, 1953, 385-394.

[122] Summerhays, W. E. A Determination of the Coefficient of Diffusion of Water Vapour. Proc. Phys. Soc. (London) 42, 1930, pp. 218-225.

[123] Thomson, W. R. The Thermodynamics of Frictional Resisted Adiabatic Flow of Gases through Ducts of Constant and Varying Cross Section. National Gas Turbine Establishment, Rept. R. 119, 1952.

[124] Tribus, M. Modern Icing Technology. Univ. of Michigan, Engineering Research Institute, Contract AF 18(600)-51, 1952.

[125] Tribus, M. and A. Guibert. Impingement of Spherical Water Droplets on a Wedge at Supersonic Speeds in Air. J. Aero. Sci., 19, 1952, 391-394.

[126] Tribus, M. and L. L. Rauch. A New Method for Calculating Water Droplet Trajectories about Streamlined Bodies. Univ. of Michigan, Engineering Research Institute, Contract AF 18(600)-51, 1951.

[127] Tribus, M. and J. R. Tessman. Report on the Development and Application of Heated Wings, Addendum I. AAF Tech. Rept. 4972, Addendum I, 1946.

[128] Vazsonyi, A. Pressure Loss in Elbows and Duct Branches. Transactions ASME, 66, 1944, p. 178.

[129] Vonnegut, B. Supercooled Clouds. Airplane Icing Information Course, Lecture 5, Univ. of Michigan, 1953.

[130] Washington, L. and W. M. Marks. Ind. Eng. Chem., 29, 1937, pp. 337-345.

[131] Weske, J. R. Pressure Loss in Ducts with Compound Elbows. NACA WR W-39, 1943.

[132] Wirt, L. Pressure Loss in Elbows and Ducts Systems. Gen. Elect. Rev., 30, 1927, pp. 286-296.

[133] Yellot, J. I., Jr. Supersaturated Steam. Transactions ASME, 56, 1934, 411-430.

APPENDIX

Tables

Figures

TABLE A-1

PROPERTIES OF THE STANDARD ATMOSPHERE

ALTITUDE	PRESSURE			DENSITY	TEMPERATURE		SPEED OF SOUND		DYNAMIC VISCOSITY	KINEMATIC VISCOSITY	THERMAL CONDUCTIVITY
	p			$\rho \times 10^3$	t	T	a		$\mu \times 10^7$	$\nu \times 10^4$	$k \times 10^2$
(ft)	(lb/ft^2)	(in.-water)	(in.-mercury)	$\left(\frac{slugs}{ft^3}\right)$	(^oF)	(^oR)	(ft/sec)	(knots)	$\left(\frac{slug}{ft\ sec}\right)$	$\left(\frac{ft^2}{sec}\right)$	$\left(\frac{B}{hr\ ft\ F}\right)$
0	2116	407.1	29.92	2.378	59.0	518.7	1116	660.5	3.725	1.566	1.462
500	2078	399.8	29.38	2.343	57.2	516.9	1114	659.3	3.716	1.586	1.457
1,000	2041	392.6	28.86	2.309	55.4	515.1	1112	658.2	3.705	1.604	1.453
1,500	2004	385.5	28.33	2.275	53.6	513.3	1110	657.1	3.695	1.624	1.449
2,000	1968	378.5	27.82	2.242	51.8	511.5	1108	655.9	3.685	1.644	1.444
2,500	1932	371.6	27.31	2.209	50.1	509.8	1106	654.7	3.674	1.663	1.440
3,000	1896	364.8	26.81	2.176	48.3	508.0	1104	653.6	3.664	1.684	1.434
3,500	1862	358.2	26.32	2.144	46.5	506.2	1102	652.5	3.654	1.704	1.430
4,000	1828	351.6	25.84	2.112	44.7	504.4	1101	651.3	3.644	1.725	1.426
4,500	1794	345.1	25.36	2.080	43.0	502.7	1099	650.2	3.633	1.747	1.422
5,000	1760	338.7	24.89	2.049	41.2	500.9	1097	649.0	3.623	1.768	1.417
5,500	1728	332.4	24.43	2.018	39.4	499.1	1095	647.9	3.612	1.790	1.412
6,000	1696	326.2	23.98	1.988	37.6	497.3	1093	646.7	3.602	1.812	1.408
6,500	1664	320.1	23.53	1.957	35.8	495.5	1091	645.5	3.592	1.835	1.403
7,000	1633	314.1	23.09	1.928	34.0	493.7	1089	644.3	3.581	1.857	1.398
7,500	1602	308.2	22.65	1.898	32.3	492.0	1087	643.2	3.571	1.881	1.394
8,000	1572	302.4	22.22	1.869	30.5	490.2	1085	642.1	3.561	1.905	1.389
8,500	1542	296.6	21.80	1.840	28.7	488.4	1083	640.8	3.550	1.929	1.384
9,000	1512	291.0	21.38	1.812	26.9	486.6	1081	639.7	3.540	1.954	1.380
9,500	1483	285.4	20.98	1.784	25.1	484.8	1079	638.5	3.529	1.978	1.376
10,000	1455	279.9	20.58	1.756	23.3	483.0	1077	637.4	3.519	2.004	1.372
10,500	1427	274.5	20.18	1.728	21.6	481.3	1075	636.2	3.508	2.030	1.367
11,000	1399	269.2	19.79	1.702	19.8	479.5	1073	635.0	3.498	2.055	1.363
11,500	1372	264.0	19.40	1.675	18.0	477.7	1071	633.8	3.487	2.082	1.358
12,000	1346	258.9	19.03	1.648	16.2	475.9	1069	632.6	3.476	2.109	1.353
12,500	1319	253.8	18.65	1.622	14.3	474.1	1067	631.5	3.466	2.137	1.349
13,000	1293	248.8	18.29	1.596	12.6	472.3	1065	630.3	3.455	2.165	1.344
13,500	1268	243.9	17.93	1.570	10.9	470.6	1063	629.0	3.445	2.194	1.339
14,000	1243	239.1	17.57	1.545	9.1	468.8	1061	627.9	3.434	2.223	1.335
14,500	1218	234.4	17.22	1.520	7.3	467.0	1059	626.7	3.423	2.252	1.330
15,000	1194	229.7	16.88	1.496	5.5	465.2	1057	625.5	3.413	2.281	1.326
15,500	1170	225.1	16.54	1.472	3.7	463.4	1055	624.3	3.402	2.311	1.321
16,000	1146	220.6	16.21	1.448	1.9	461.6	1053	623.1	3.391	2.342	1.316
16,500	1123	216.1	15.89	1.424	-0.4	459.9	1051	621.8	3.380	2.374	1.312
17,000	1101	211.8	15.56	1.401	-2.2	458.1	1049	620.6	3.370	2.405	1.307
17,500	1078	207.5	15.25	1.378	-4.0	456.3	1047	619.4	3.359	2.438	1.303
18,000	1056	203.2	14.94	1.355	-5.8	454.5	1045	618.2	3.348	2.471	1.298
18,500	1035	199.1	14.63	1.333	-7.6	452.7	1043	617.0	3.337	2.503	1.293
19,000	1014	195.0	14.33	1.311	-9.4	450.9	1040	615.8	3.326	2.537	1.288
19,500	992.6	191.0	14.04	1.289	-11.1	449.2	1038	614.5	3.316	2.572	1.284
20,000	972.1	187.0	13.75	1.267	-12.9	447.4	1036	613.3	3.305	2.608	1.279
20,500	951.9	183.1	13.46	1.246	-14.7	445.6	1034	612.1	3.294	2.644	1.275
21,000	932.0	179.3	13.18	1.225	-16.5	443.8	1032	610.9	3.283	2.680	1.270
21,500	912.5	175.6	12.90	1.204	-18.3	442.0	1030	609.7	3.272	2.718	1.265
22,000	893.3	171.9	12.63	1.183	-20.1	440.2	1028	608.5	3.261	2.756	1.260
22,500	874.4	168.2	12.36	1.163	-21.8	438.5	1026	607.3	3.250	2.794	1.256
23,000	855.9	164.7	12.10	1.143	-23.6	436.7	1024	606.0	3.239	2.834	1.251
23,500	837.7	161.2	11.84	1.123	-25.4	434.9	1022	604.7	3.228	2.874	1.246
24,000	819.8	157.7	11.59	1.103	-27.2	433.1	1020	603.5	3.217	2.916	1.242
24,500	802.2	154.3	11.34	1.085	-29.0	431.3	1018	602.2	3.206	2.955	1.237
25,000	784.9	151.0	11.10	1.065	-30.8	429.5	1016	601.0	3.195	3.000	1.232
25,500	767.9	147.7	10.86	1.046	-32.5	427.8	1013	599.8	3.184	3.044	1.228
26,000	751.2	144.5	10.62	1.028	-34.3	426.0	1011	598.5	3.173	3.086	1.223
26,500	734.8	141.4	10.39	1.010	-36.1	424.2	1009	597.3	3.162	3.131	1.218
27,000	718.7	138.3	10.16	0.992	-37.9	422.4	1007	596.0	3.150	3.175	1.213
27,500	702.9	135.2	9.939	0.974	-39.7	420.6	1005	594.8	3.139	3.223	1.208
28,000	687.4	132.2	9.720	0.957	-41.5	418.8	1003	593.5	3.128	3.268	1.204
28,500	672.1	129.3	9.504	0.940	-43.2	417.1	1001	592.2	3.117	3.316	1.199
29,000	657.1	126.4	9.293	0.922	-45.0	415.3	998.5	590.9	3.106	3.369	1.194
29,500	642.4	123.6	9.085	0.906	-47.8	413.5	996.3	589.6	3.094	3.415	1.190

TABLE A-I (CONT'D)

PROPERTIES OF THE STANDARD ATMOSPHERE

ALTITUDE	PRESSURE			DENSITY	TEMPERATURE		SPEED OF SOUND		DYNAMIC VISCOSITY	KINEMATIC VISCOSITY	THERMAL CONDUCTIVITY
	p			$\rho \times 10^3$	t	T	a		$\mu \times 10^7$	$\nu \times 10^4$	$k \times 10^2$
(ft)	(lb/ft^2)	(in.-water)	(in.-mercury)	($\frac{slugs}{ft^3}$)	(^oF)	(^oR)	(ft/sec)	(knots)	($\frac{slug}{ft\ sec}$)	($\frac{ft^2}{sec}$)	($\frac{B}{hr\ ft\ F}$)
30,000	628.0	120.8	8.880	0.889	-48.6	411.7	994.3	588.4	3.083	3.468	1.185
30,500	613.8	118.0	8.680	0.873	-50.4	409.9	992.1	587.1	3.072	3.519	1.180
31,000	599.9	115.4	8.483	0.857	-52.2	408.1	989.9	585.8	3.060	3.570	1.175
31,500	586.3	112.8	8.290	0.842	-53.9	406.4	987.7	584.5	3.049	3.621	1.170
32,000	572.9	110.2	8.101	0.826	-55.7	404.6	985.6	583.3	3.038	3.678	1.166
32,500	559.7	107.6	7.915	0.810	-57.5	402.8	983.4	582.0	3.026	3.736	1.161
33,000	546.8	105.2	7.732	0.795	-59.3	401.0	981.2	580.7	3.015	3.792	1.156
33,500	534.1	102.8	7.554	0.780	-61.0	399.3	979.0	579.4	3.004	3.851	1.151
34,000	521.7	100.4	7.377	0.765	-62.8	397.5	976.8	578.1	2.992	3.911	1.147
34,500	509.5	98.03	7.205	0.750	-64.6	395.7	974.6	576.8	2.981	3.975	1.142
35,000	497.6	95.75	7.036	0.736	-66.4	393.9	972.4	575.4	2.969	4.034	1.137
35,332	489.8	94.24	6.926	0.727	-67.6	392.7	970.9	574.6	2.962	4.073	1.134
35,500	485.8	93.51	6.873	0.721	-67.6	392.7	970.9	574.6	2.962	4.105	1.134
36,000	474.4	91.31	6.711	0.705	-67.6	392.7	970.9	574.6	2.962	4.204	1.134
36,500	463.2	89.15	6.552	0.688	-67.6	392.7	970.9	574.6	2.962	4.306	1.134
37,000	452.2	87.04	6.397	0.672	-67.6	392.7	970.9	574.6	2.962	4.410	1.134
37,500	441.6	85.00	6.247	0.656	-67.6	392.7	970.9	574.6	2.962	4.516	1.134
38,000	431.1	82.97	6.098	0.640	-67.6	392.7	970.9	574.6	2.962	4.625	1.134
38,500	421.0	81.01	5.954	0.625	-67.6	392.7	970.9	574.6	2.962	4.737	1.134
39,000	411.0	79.10	5.813	0.610	-67.6	392.7	970.9	574.6	2.962	4.852	1.134
39,500	401.3	77.23	5.676	0.596	-67.6	392.7	970.9	574.6	2.962	4.969	1.134
40,000	391.9	75.44	5.544	0.582	-67.6	392.7	970.9	574.6	2.962	5.089	1.134
40,500	382.6	73.64	5.412	0.568	-67.6	392.7	970.9	574.6	2.962	5.212	1.134
41,000	373.6	71.89	5.284	0.555	-67.6	392.7	970.9	574.6	2.962	5.338	1.134
41,500	364.8	70.18	5.158	0.542	-67.6	392.7	970.9	574.6	2.962	5.467	1.134
42,000	356.2	68.56	5.038	0.529	-67.6	392.7	970.9	574.6	2.962	5.599	1.134
42,500	347.8	66.93	4.919	0.516	-67.6	392.7	970.9	574.6	2.962	5.735	1.134
43,000	339.6	65.34	4.802	0.504	-67.6	392.7	970.9	574.6	2.962	5.873	1.134
43,500	331.5	63.79	4.688	0.492	-67.6	392.7	970.9	574.6	2.962	6.015	1.134
44,000	323.7	62.29	4.578	0.480	-67.6	392.7	970.9	574.6	2.962	6.161	1.134
44,500	316.1	60.82	4.470	0.469	-67.6	392.7	970.9	574.6	2.962	6.310	1.134
45,000	308.6	59.40	4.365	0.458	-67.6	392.7	970.9	574.6	2.962	6.462	1.134

TABLE A-2

PROPERTIES OF AIR AT 29.92 INCH - MERCURY

TEMPERATURE	VELOCITY OF SOUND		DENSITY		DYNAMIC VISCOSITY		KINEMATIC VISCOSITY		SPECIFIC HEAT	CONDUCTIVITY	PRANDTL NUMBER
t	a		ρ		$\mu \times 10^7$	μ	$\nu \times 10^4$	ν	c_p	k	N_{Pr}
^oF	ft/sec	knots	slug/ft^3	lb/ft^3	slug/ft sec	lb/ft hr	ft^2/sec	ft^2/hr	B/lb F	B/hr ft F	–
-100	930.1	550.6	0.003428	0.1103	2.77	0.0321	0.808	0.291	0.2393	0.01045	0.739
-80	955.6	565.7	3248	1045	2.90	336	0.894	.322	.2393	1100	.736
-60	980.1	580.2	3084	0.09924	3.03	351	0.983	.354	.2393	1154	.731
-40	1005	595.0	0.002938	0.09452	3.16	0.0366	1.074	0.387	.2393	0.01208	.728
-35	1010	597.9	2903	9341	3.19	369	1.098	.395	.2393	1221	.726
-30	1016	601.5	2869	9232	3.22	373	1.122	.404	.2394	1234	.725
-25	1022	605.0	2836	9126	3.25	376	1.145	.412	.2394	1247	.725
-20	1028	608.6	2804	9022	3.28	380	1.170	.421	.2394	1261	.724
-15	1034	612.1	2773	8921	3.31	383	1.194	.429	.2394	1274	.723
-10	1040	615.7	2742	8821	3.34	387	1.218	.439	.2394	1287	.722
-5	1045	618.6	2712	8724	3.37	390	1.243	.447	.2394	1300	.721
0	1051	622.2	2682	8630	3.40	394	1.268	.457	.2394	1313	.720
+5	1057	625.7	2653	8537	3.43	397	1.292	.465	.2395	1326	.719
10	1062	628.7	2625	8446	3.46	401	1.317	.475	.2395	1339	.719
15	1068	632.3	2597	8357	3.49	404	1.343	.483	.2395	1352	.718
20	1074	635.8	2570	8270	3.52	408	1.368	.493	.2395	1365	.717
25	1080	639.4	2544	8184	3.55	411	1.394	.502	.2396	1378	.716
30	1085	642.3	2518	8101	3.57	414	1.420	.511	.2396	1390	.715
32	1087	643.5	2508	8070	3.58	415	1.431	.514	.2396	1396	.715
35	1090	645.3	0.002492	0.08019	3.60	0.0417	1.444	0.520	0.2396	0.01403	0.714
40	1096	648.8	2469	7939	3.63	420	1.473	.529	.2396	1416	.714
45	1101	652.1	2440	7851	3.66	424	1.499	.540	.2396	1428	.713
50	1107	655.3	2412	7761	3.69	427	1.526	.550	.2397	1441	.712
55	1112	658.5	2394	7703	3.71	431	1.553	.559	.2397	1454	.711
60	1118	661.7	2372	7633	3.74	434	1.580	.569	.2397	1467	.710
65	1123	664.9	2342	7536	3.77	437	1.607	.579	.2398	1479	.710
70	1128	668.1	2331	7501	3.80	441	1.634	.588	.2398	1492	.709
75	1134	671.2	2307	7423	3.83	444	1.661	.598	.2398	1504	.708
80	1139	674.3	2284	7349	3.86	447	1.688	.608	.2399	1516	.708
85	1144	677.5	2256	7259	3.88	450	1.717	.619	.2399	1529	.707
90	1150	680.6	2247	7230	3.91	453	1.744	.627	.2399	1541	.707
95	1155	683.7	2226	7163	3.94	456	1.720	.637	.2400	1553	.706
100	1160	686.7	2203	7089	3.96	459	1.800	.648	.2400	1565	.706
105	1165	689.8	2180	7015	3.99	462	1.828	.659	.2400	1578	.705
110	1170	692.8	2156	6937	4.01	465	1.857	.670	.2401	1590	.704
115	1175	695.9	2149	6915	4.04	468	1.886	.677	.2401	1603	.704
120	1180	699.1	2127	6844	4.07	471	1.914	.688	.2401	1615	.703
140	1201	711.0	0.002056	0.06615	4.19	0.0483	2.03	0.730	0.2403	0.01663	0.700
160	1220	722.2	1989	6401	4.28	496	2.15	.775	.2405	1711	.698
180	1235	731.1	1927	6201	4.38	507	2.27	.818	.2408	1759	.696
200	1254	742.4	1869	6013	4.48	519	2.40	.863	.2410	1807	.694
220	1273	753.6	1814	5836	4.58	530	2.52	.908	.2413	1853	.691
240	1292	764.9	1762	5670	4.68	542	2.66	.956	.2416	1900	.690
260	1311	776.1	1713	5512	4.77	552	2.78	1.004	.2419	1945	.689
280	1334	789.7	1667	5363	4.87	564	2.92	1.052	.2422	1990	.688
300	1346	796.8	1623	5222	4.96	574	3.06	1.101	.2426	2035	.686
320	1364	807.5	1581	5088	5.05	585	3.19	1.151	.2430	2079	.685
340	1382	818.1	1546	4973	5.14	595	3.33	1.202	.2434	2122	.684
360	1399	828.2	1504	4840	5.23	606	3.47	1.254	.2439	2166	.683
380	1416	838.3	1468	4724	5.32	616	3.61	1.306	.2444	2209	.682
400	1438	851.3	1434	4614	5.41	627	3.78	1.358	.2449	2252	.681
500	1519	899.2	0.001285	0.04134	5.83	0.0675	4.53	1.635	0.2475	0.02457	0.680
600	1596	944.8	1164	3744	6.23	722	5.36	1.930	.2504	2655	.680
700	1669	988.0	1063	3421	6.60	764	6.19	2.237	.2535	2844	.682
800	1740	1080.	9787	3149	6.96	806	7.11	2.562	.2566	3026	.684

TABLE A-3

PRESSURE OF WATER VAPOR IN EQUILIBRIUM WITH WATER

t	p_v	t	p_v	t	p_v	t	p_v	t	p_v
°F	in.-mercury	°F	in.-mercury	°F	in.-mercury	°F	in.-mercury	°F	in.-mercury
- 40	0.0055880	- 4	0.037120	32	0.1803	68	0.6903	104	2.1775
- 39	.0059204	- 3	.038940	33	.1878	69	.7144	105	2.2429
- 38	.0062686	- 2	.040827	34	.1955	70	.7392	106	2.3099
- 37	.0066379	- 1	.042809	35	.2035	71	.7648	107	2.3786
- 36	.0070235	0	.044862	36	.2118	72	.7912	108	2.4491
- 35	.0074320	+ 1	.047017	37	.2203	73	.8183	109	2.5214
- 34	.0078594	2	.049250	38	.2292	74	.8462	110	2.5955
- 33	.0083118	3	.051593	39	.2383	75	.8750	111	2.6715
- 32	.0087844	4	.054018	40	.2478	76	.9046	112	2.7494
- 31	.0092844	5	.056562	41	.2576	77	.9352	113	2.8293
- 30	.0098099	6	.059213	42	.2677	78	.9666	114	2.9111
- 29	.010359	7	.061954	43	.2782	79	.9989	115	2.9948
- 28	.010938	8	.064829	44	.2891	80	1.0321	116	3.0806
- 27	.011544	9	.067800	45	.3004	81	1.0664	117	3.1687
- 26	.012183	10	.070915	46	.3120	82	1.1016	118	3.2589
- 25	.012849	11	.074133	47	.3240	83	1.1378	119	3.3512
- 24	.013553	12	.077506	48	.3364	84	1.1750	120	3.4458
- 23	.014287	13	.080989	49	.3493	85	1.2133	121	3.5427
- 22	.015061	14	.084636	50	.3626	86	1.2527	122	3.6420
- 21	.015873	15	.088430	51	.3764	87	1.2931	123	3.7436
- 20	.016718	16	.092347	52	.3906	88	1.3347	124	3.8475
- 19	.017609	17	.096447	53	.4052	89	1.3775	125	3.9539
- 18	.018537	18	.10068	54	.4203	90	1.4215	126	4.0629
- 17	.019515	19	.10510	55	.4359	91	1.4667	127	4.1745
- 16	.020532	20	.10967	56	.4520	92	1.5131	128	4.2887
- 15	.021604	21	.11444	57	.4686	93	1.5608	129	4.4055
- 14	.022718	22	.11936	58	.4858	94	1.6097	130	4.5251
- 13	.023892	23	.12451	59	.5035	95	1.6600	131	4.6474
- 12	.025119	24	.12986	60	.5218	96	1.7117	132	4.7725
- 11	.026395	25	.13536	61	.5407	97	1.7647	133	4.9005
- 10	.027737	26	.14112	62	.5601	98	1.8192	134	5.0314
- 9	.029130	27	.14705	63	.5802	99	1.8751	135	5.1653
- 8	.030596	28	.15324	64	.6009	100	1.9325	136	5.3022
- 7	.032117	29	.15961	65	.6222	101	1.9915	137	5.4421
- 6	.033717	30	.16627	66	.6442	102	2.0519	138	5.5852
- 5	.035376	31	.17313	67	.6669	103	2.1138	139	5.7316
								140	5.8812

TABLE A-4

CONVERSION FACTORS

To convert	from the number of	to the number of	multiply by
length	inch	cm	2.540
length	ft	cm	30.48
length	statute mile	ft	5280
length	international nautical mile	ft	6076.1
droplet diameter	microns	ft	10^{-6} · 3.281
droplet diameter	microns	10^{-3} · in.	10^{-3} · 39.37
speed	mph	ft/sec	1.467
speed	knot	ft/sec	1.688
speed	ft/sec	knot	0.5925
speed	mph	knot	0.8690
speed	knot	mph	1.151
mass	grams	lb_m	0.002205
mass	lb_m	gram	453.6
mass;density	slug; $slug/ft^3$	lb_m; lb_m/ft^3	32.17
mass;density	lb_m; lb_m/ft^3	slug; $slug/ft^3$	0.0311
liquid water content	gram/cu meter	lb/ft^3	10^{-6} · 62.430
liquid water content	lb/ft^3	gram/cu meter	16018
pressure	lb/ft^2	in.-mercury	0.01414
pressure	in.-mercury	lb/ft^2	70.73
pressure	lb/ft^2	in.-water	0.1924
pressure	in.-water	lb/ft^2	5.198
pressure	in.-mercury	lb/sq in.	0.49115
viscosity, dynamic	slug/ft sec	lb_m/ft hr	115830
viscosity, dynamic	slug/ft sec	lb_f sec/ft^2	1
viscosity, kinematic	cm^2/sec	ft^2/hr	3.874
mutual diffusivity	cm^2/sec	ft^2/hr	3.874
heat flow	B/hr	watt	0.293
heat flow	watt	B/hr	3.413
heat flow per unit area	B/hr ft^2	$watt/cm^2$	10^{-3} · 0.3155
heat flow per unit area	B/hr ft^2	watt/sq in.	10^{-3} · 2.035
heat flow per unit area	$watt/in^2$	B/hr ft^2	491
conductivity	watt/cm C	B/hr ft F	57.79
conductivity	B/hr ft F	watt/cm C	0.0173
coefficient of heat transfer	$watt/cm^2$ C	B/hr ft^2 F	1761
coefficient of heat transfer	B/hr ft^2 F	$watt/cm^2$ C	10^{-3} · 0.5679

Acceleration constant $g = 32.17\ ft/sec^2 = 10^6 \cdot 417.0\ ft/hr^2$

Mechanical equivalent of heat $J = 778.3$ ft lb/B

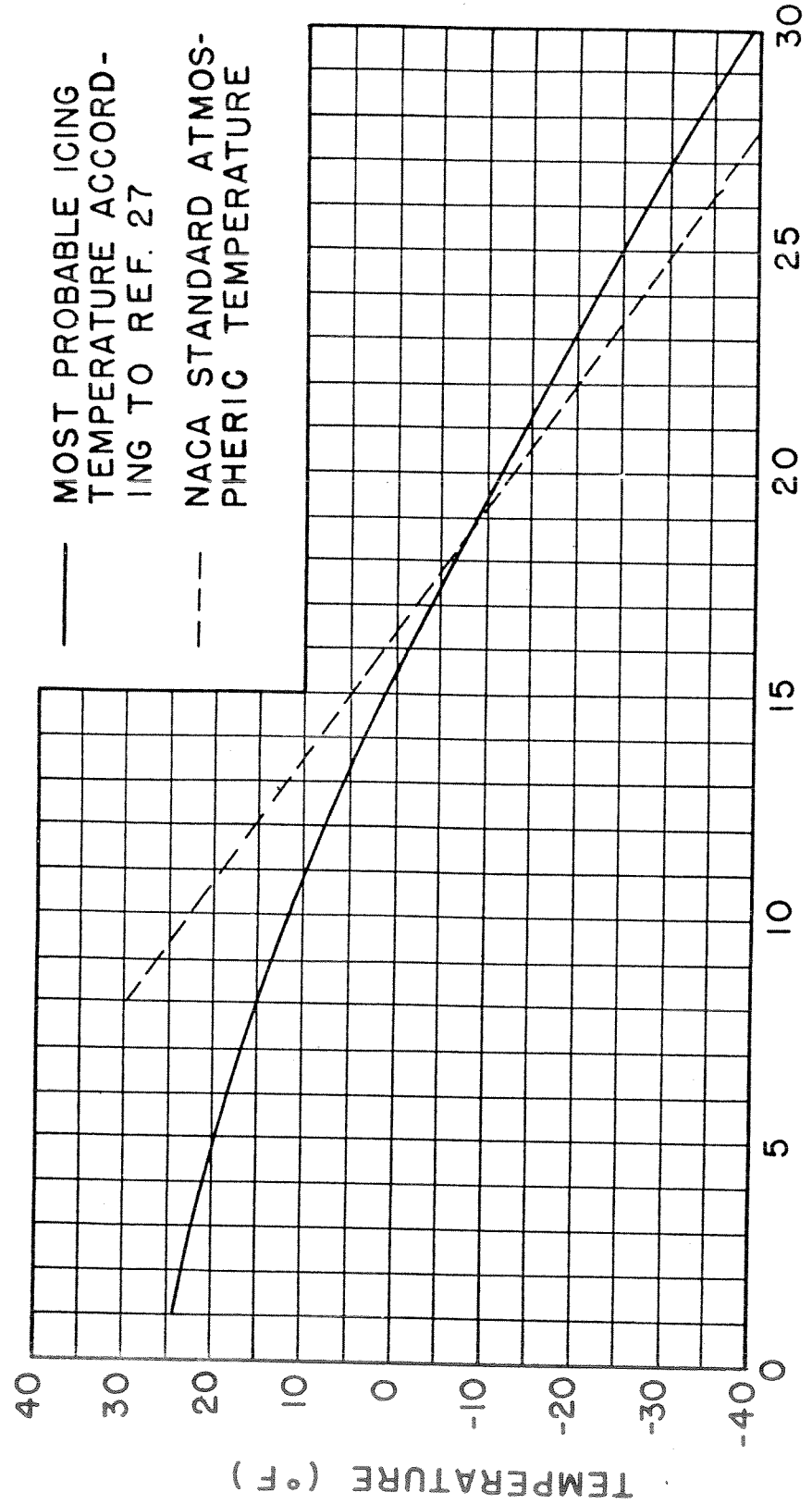

FIG. A-1 COMPARISON OF MOST PROBABLE ICING AND STANDARD ATMOSPHERIC TEMPERATURES

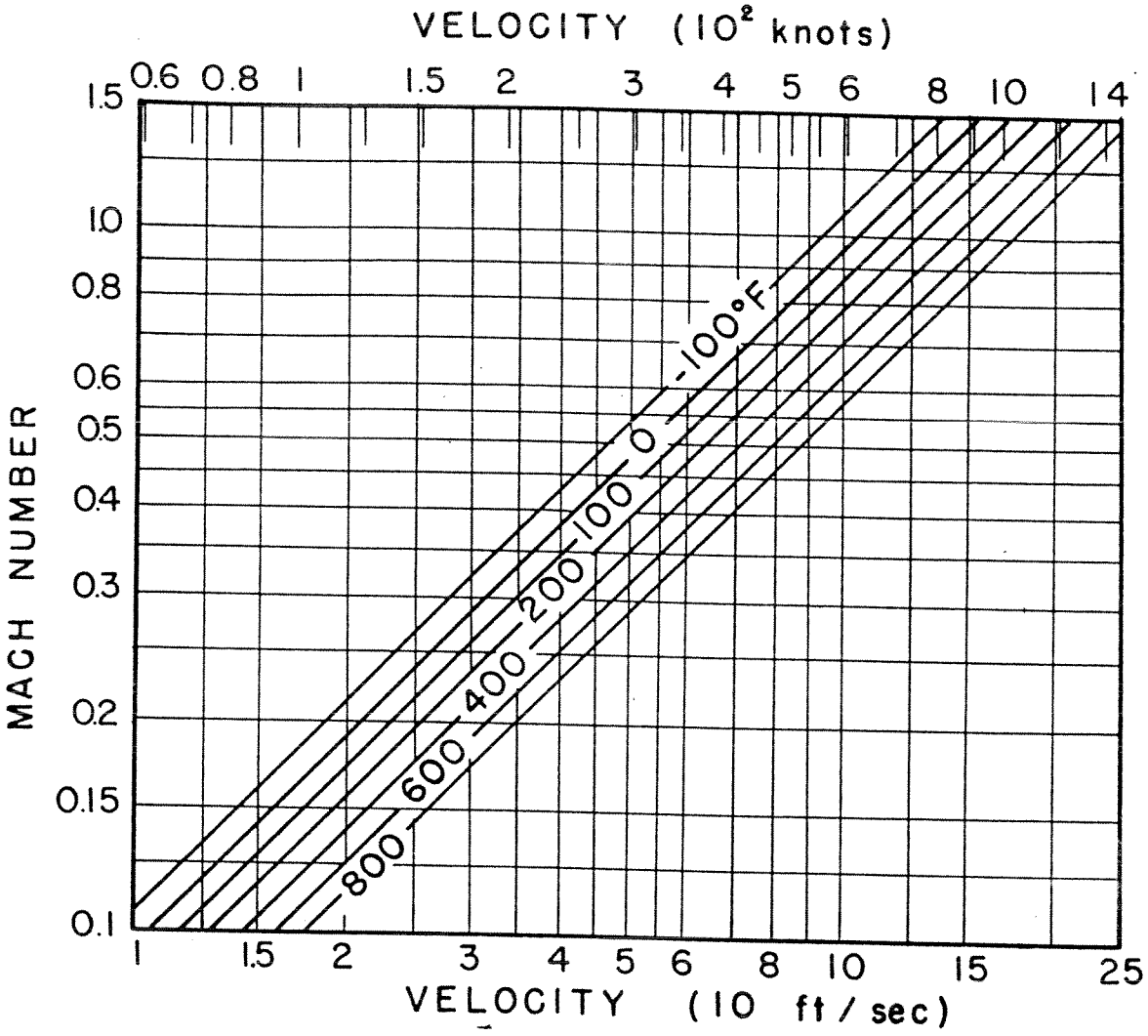

FIG. A-2 MACH NUMBER AS A FUNCTION OF AIR SPEED AND TEMPERATURE

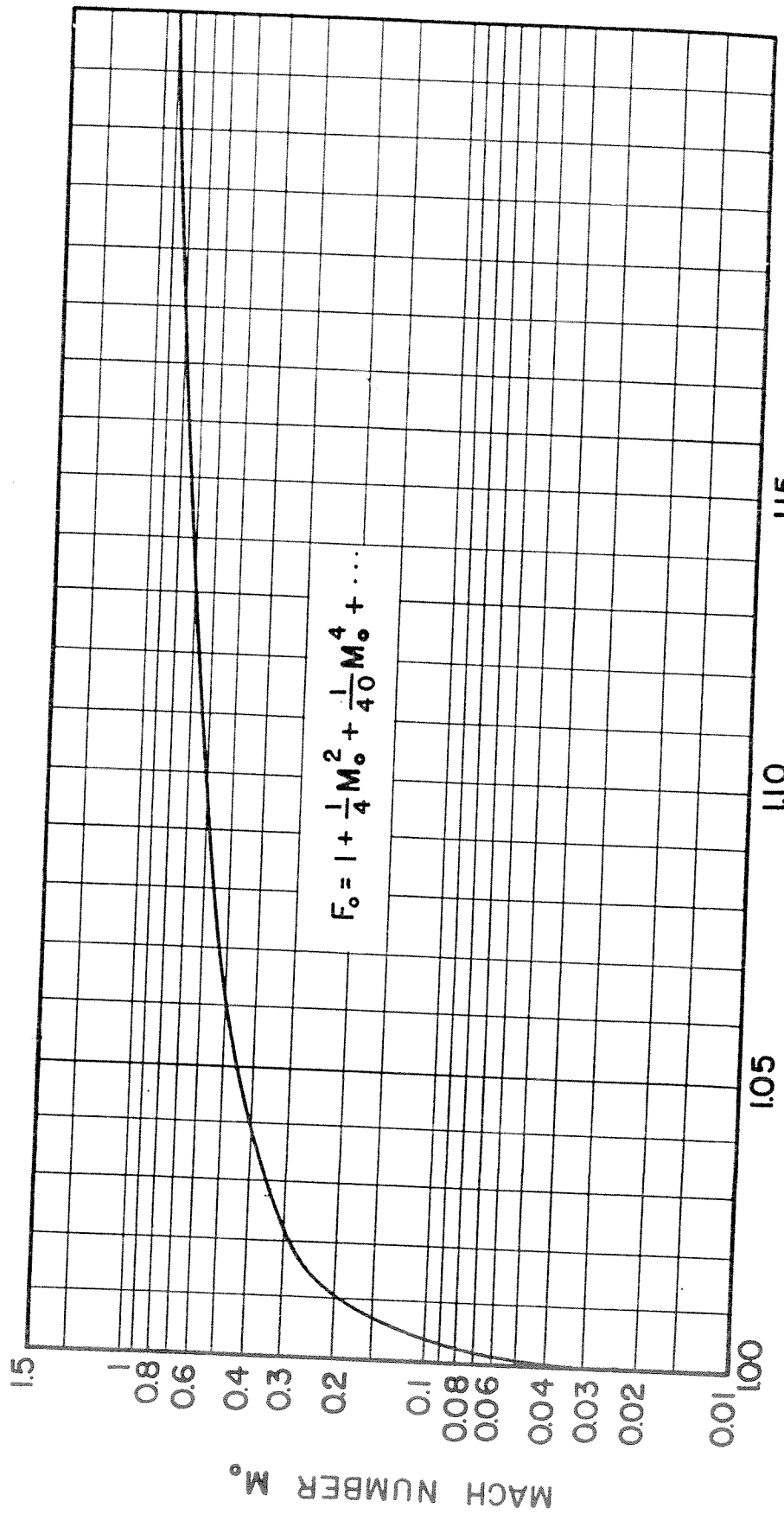

FIG. A-3 COMPRESSIBILITY FACTOR AS FUNCTION OF MACH NUMBER

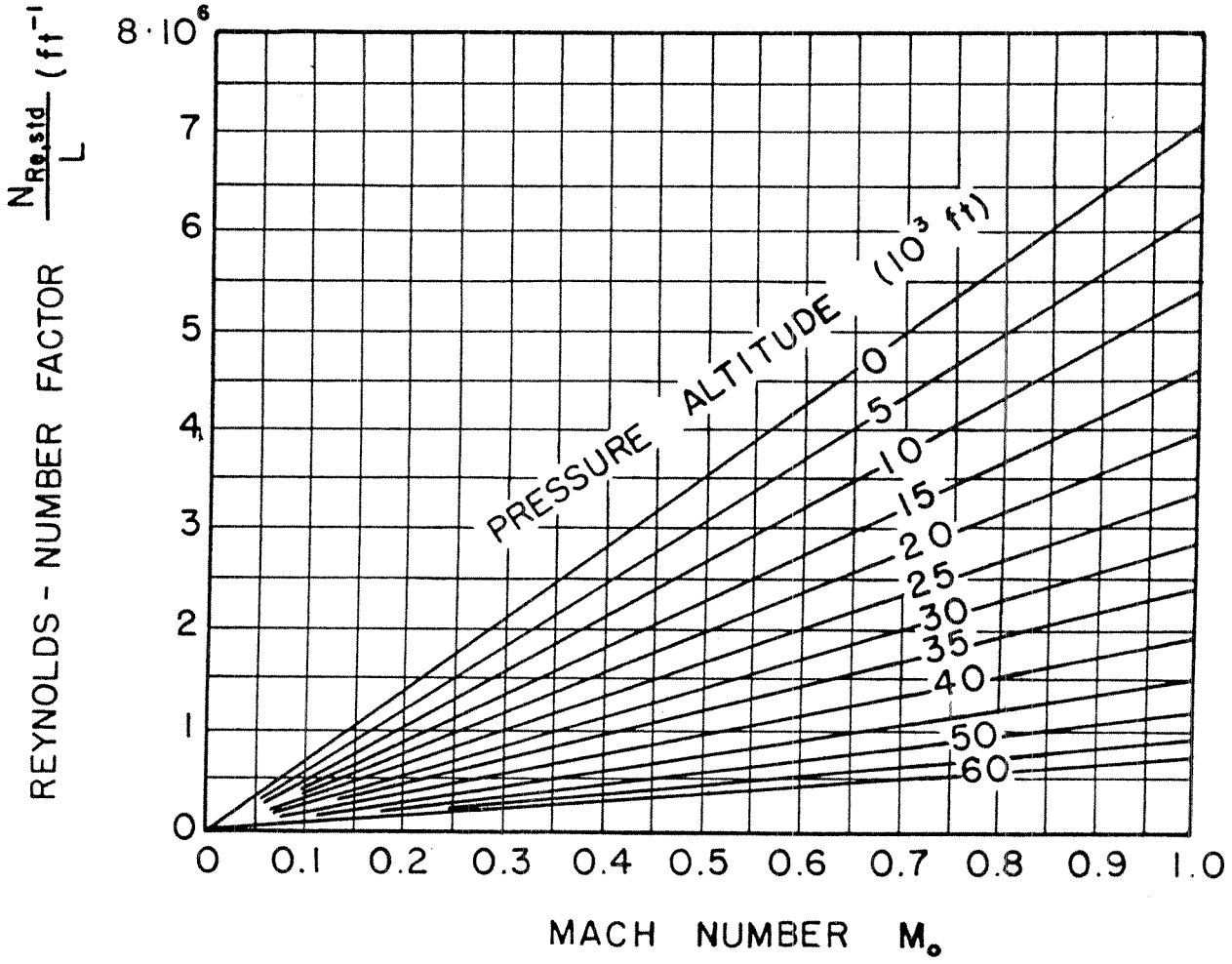

FIG. A-4 REYNOLDS-NUMBER FACTOR U_0/ν_0 VERSUS MACH NUMBER M_o IN THE STANDARD ATMOSPHERE

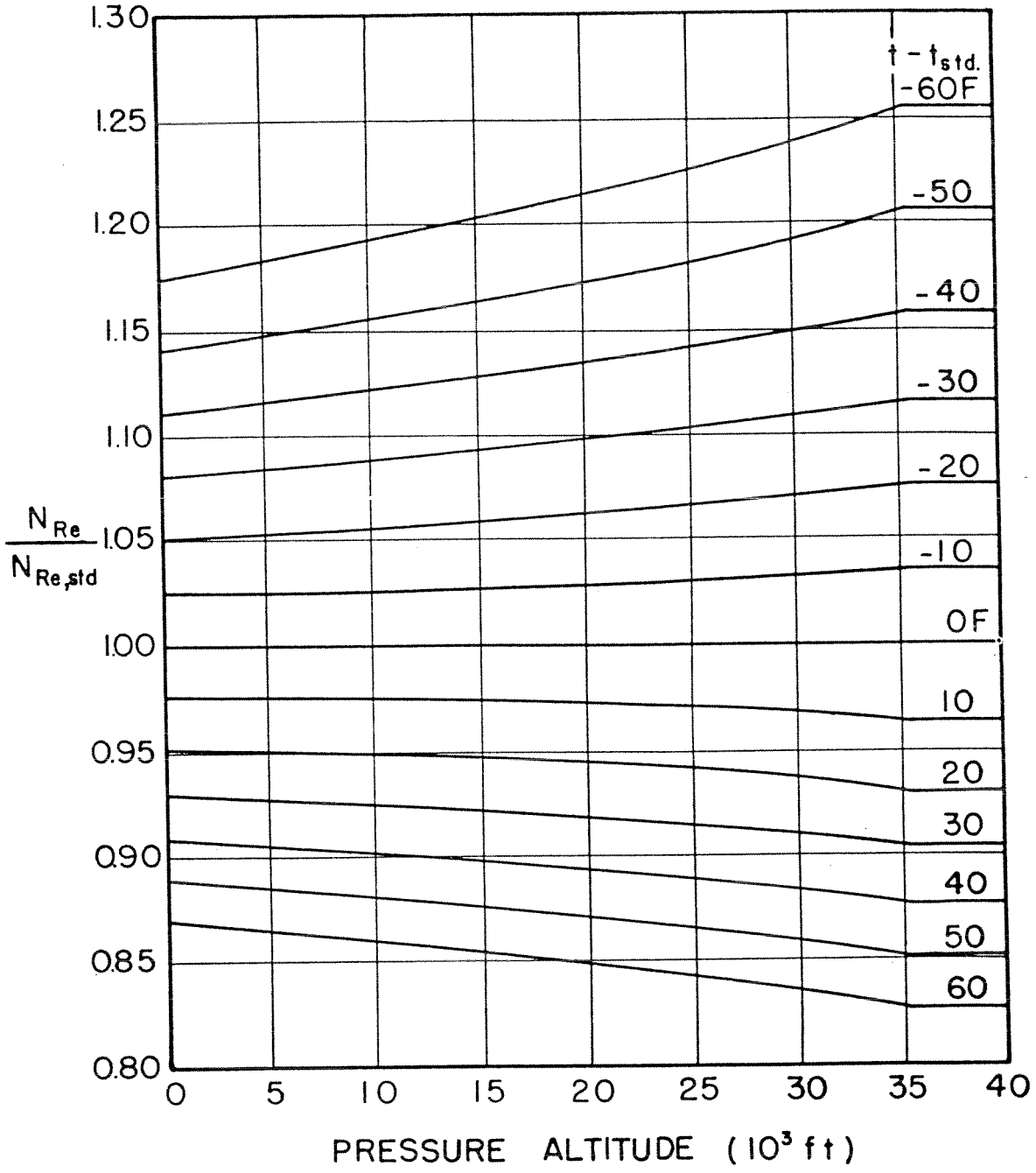

FIG. A-5 REYNOLDS - NUMBER CORRECTION FACTORS FOR NON-STANDARD TEMPERATURES

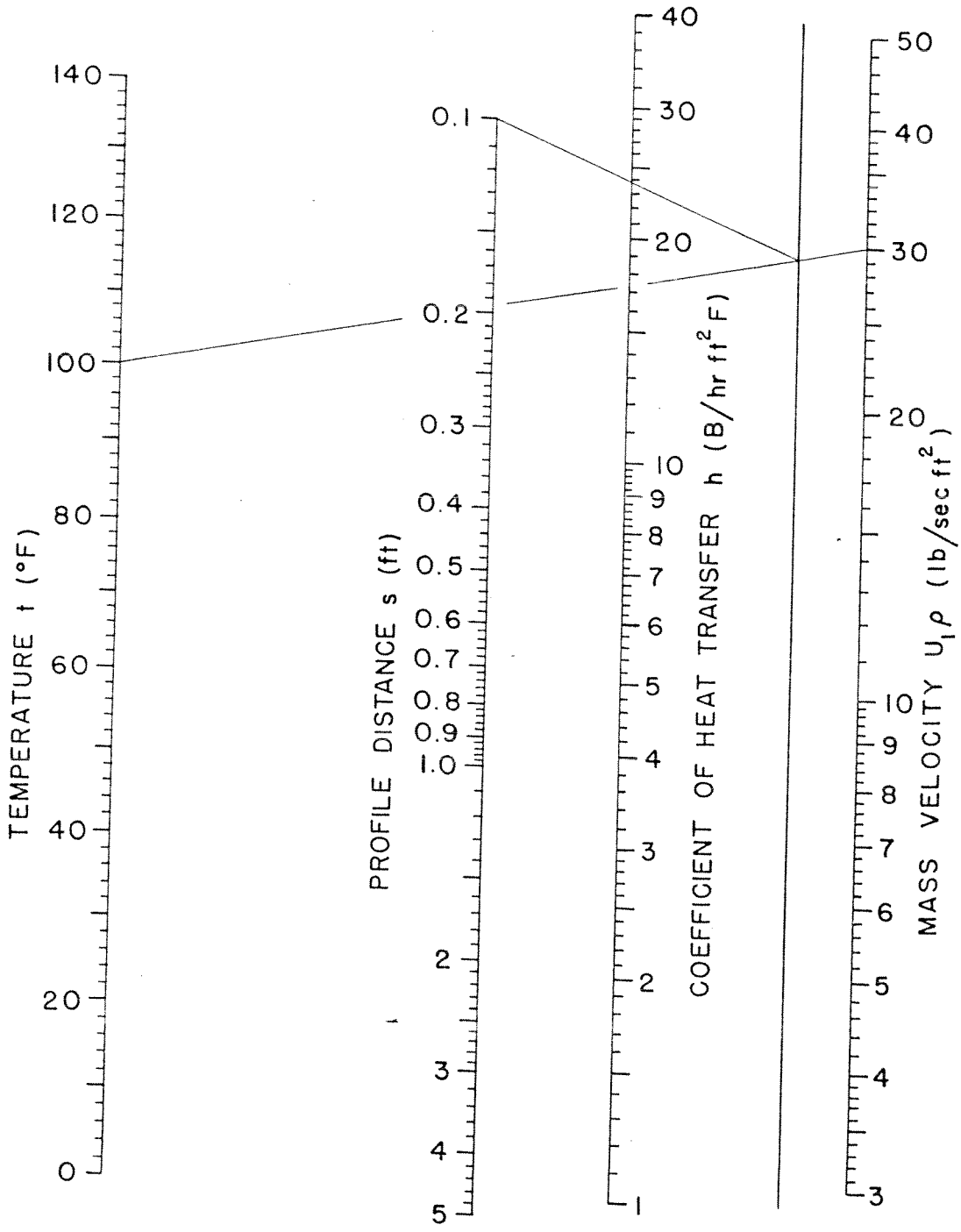

$$h = 0.0584\, T_f^{0.5} (U_1\rho)^{0.5} s^{-0.5} \quad \text{(EQ. 4-27a)}$$

FIG. A-6 NOMOGRAPH FOR LAMINAR HEAT TRANSFER ON AN AIRFOIL

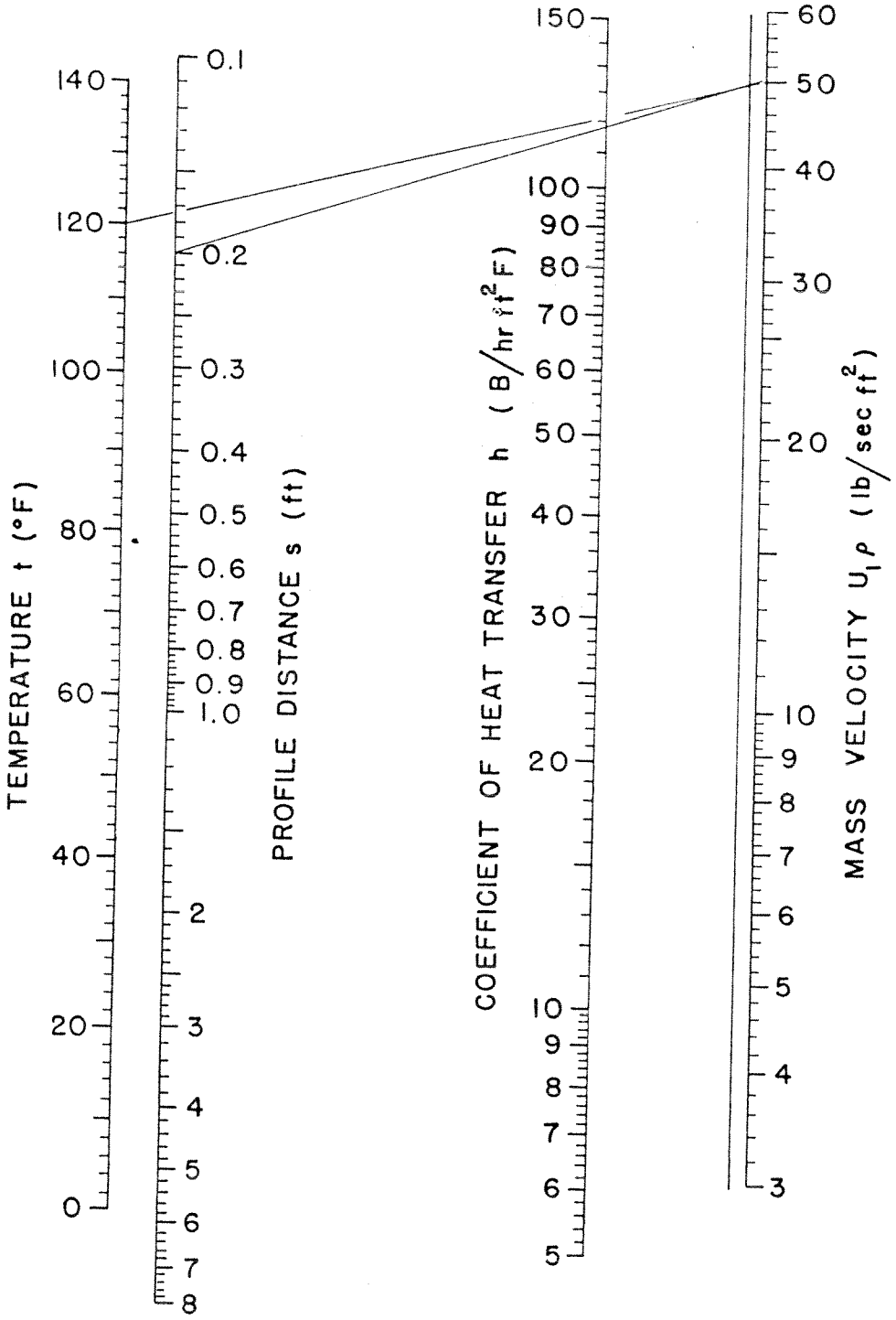

$$h = 0.782\, T_f^{0.247} (U_1 \rho)^{0.8} s^{-0.2} \quad \text{(EQ. 4-30a)}$$

FIG. A-7 NOMOGRAPH FOR TURBULENT HEAT TRANSFER ON AN AIRFOIL

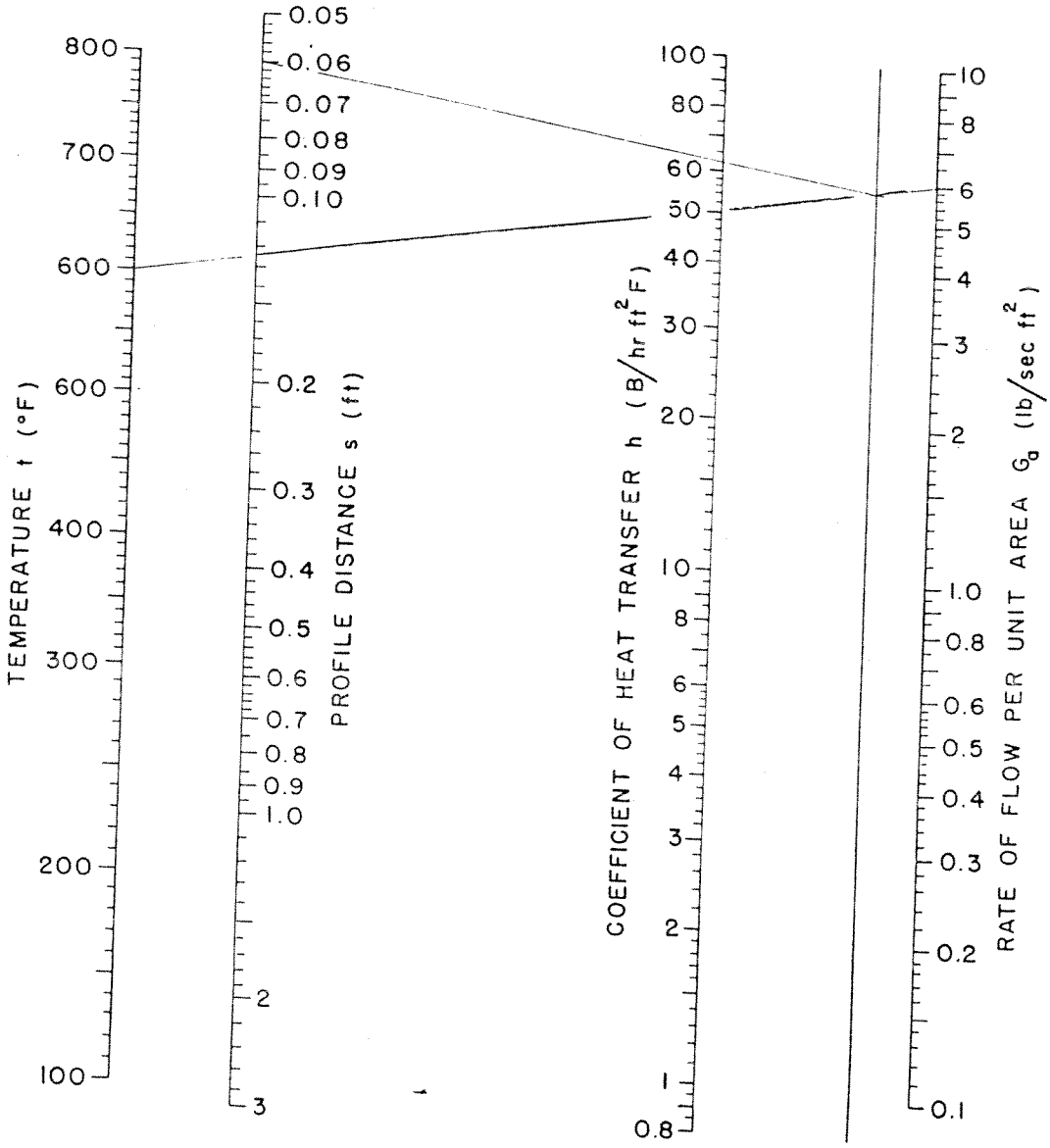

$$h = 0.782\, T_f^{0.331}\, G_a^{0.7}\, s^{-0.3} \qquad \text{(EQ. 4-60a)}$$

FIG. A-8 NOMOGRAPH FOR HEAT TRANSFER IN THE ENTRANCE REGION OF A DOUBLE-SKIN PASSAGE

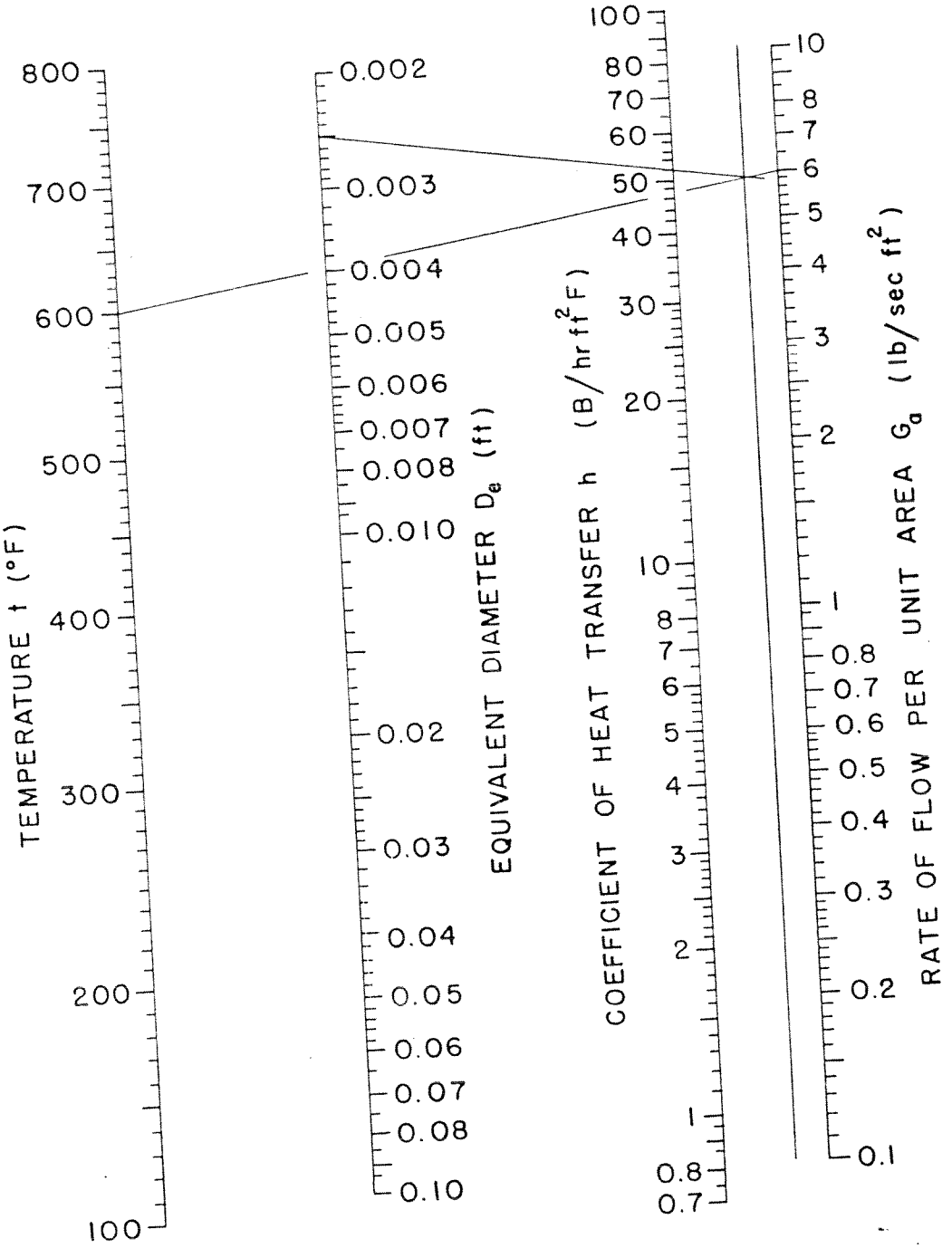

$$h_a = 0.614\, T_f^{0.262}\, G_a^{0.8}\, D_e^{-0.2} \quad \text{(EQ. 4-61a)}$$

FIG. A-9 NOMOGRAPH FOR HEAT TRANSFER IN THE FULLY DEVELOPED TURBULENT REGION OF A DOUBLE-SKIN PASSAGE

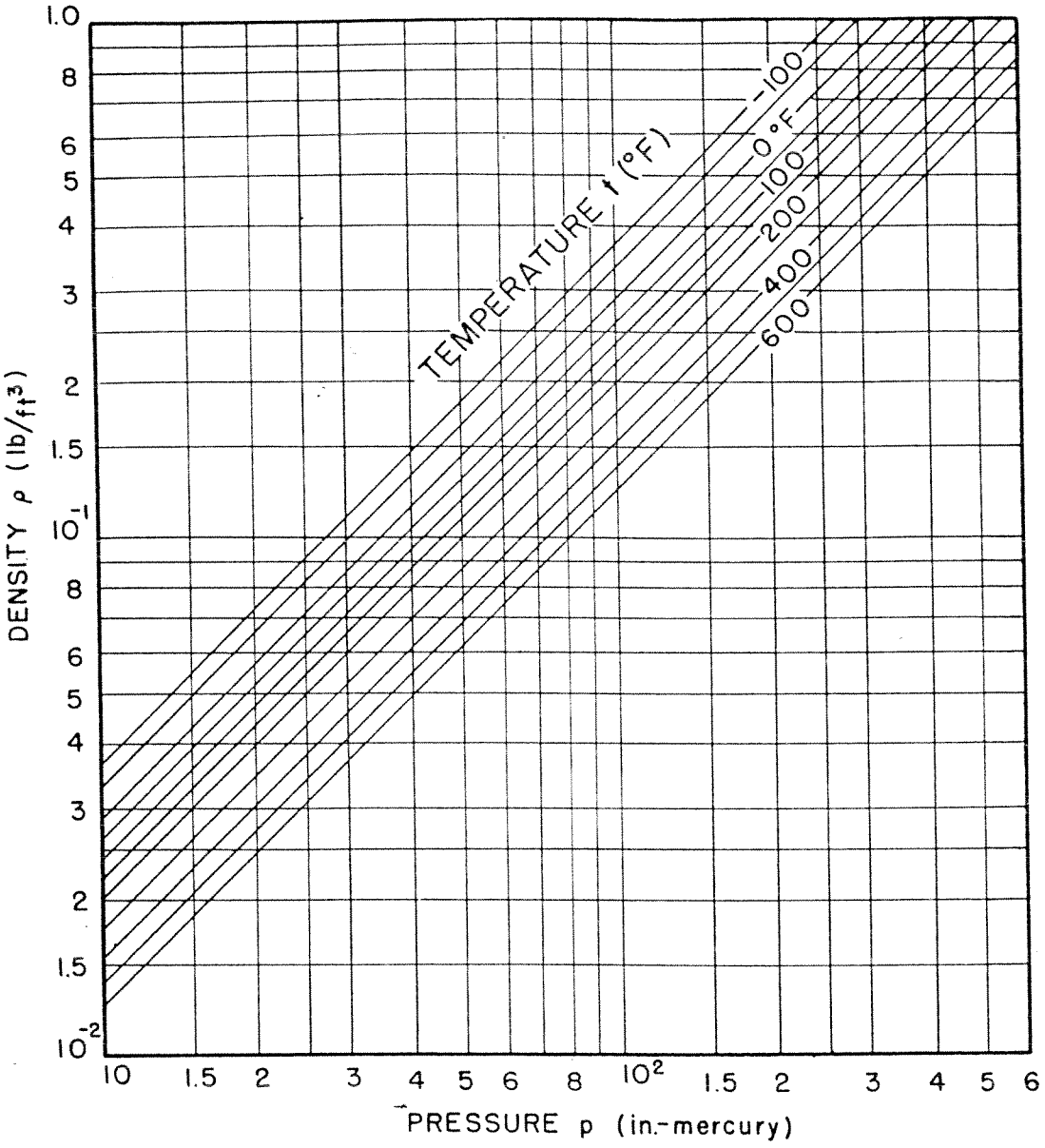

FIG. A-10 DENSITY OF DRY AIR

AFTERWORD

This work was submitted in December, 1954, to the Equipment Laboratory, WADC, for technical approval. On January 4, 1955, Dr. Max Jakob died. Since that time administrative duties related to this work were performed by Mr. Stothe P. Kezios, Acting Director, Heat Transfer Laboratory, IIT. Some minor revisions of the manuscript have been made, and the nomographs in the appendix, which were constructed by Mr. Kamal-Eldin Hassan, have been added.